Advanced and Accurate Discretization Schemes for Relevant PDEs in Finance

Le Floch, Fabien

DOI
Publication date
2020
Document Version
Final published version
Citation (APA)

Important note
To cite this publication, please use the final published version (if applicable).
Please check the document version above.

ADVANCED AND ACCURATE DISCRETIZATION SCHEMES FOR RELEVANT PDES IN FINANCE

ADVANCED AND ACCURATE DISCRETIZATION SCHEMES FOR RELEVANT PDES IN FINANCE

Proefschrift

ter verkrijging van de graad van doctor
aan de Technische Universiteit Delft,
op gezag van de Rector Magnificus prof. dr. ir. T. H. J. J. van der Hagen,
voorzitter van het College voor Promoties,
in het openbaar te verdedigen op dinsdag 21 januari 2020 om 12:30 uur

door

Fabien LE FLOC'H

Ingénieur, École supérieure d'électricité (CentraleSupélec), Gif-sur-Yvette, France,
geboren te Fontenay-sous-bois, France.

Dit proefschrift is goedgekeurd door de promotor:

Prof. dr. ir. C. W. Oosterlee.

Samenstelling promotiecommissie:

Rector Magnificus,	voorzitter
Prof. dr. ir. C. W. Oosterlee,	Technische Universiteit Delft, promotor
Dr. ir. L. A. Grzelak,	Technische Universiteit Delft, copromotor

Onafhankelijke leden:

Prof. dr. ir. C. Vuik	Technische Universiteit Delft
Prof. dr. L. von Sydow	Uppsala Universitet (Sweden)
Prof. dr. K. In't Hout	University of Antwerp (Belgium)
Prof. dr. B.D. Kandhai	University of Amsterdam
Prof. dr. ir. A.W. Heemink	Technische Universiteit Delft

Ce qu'il y a souvent de plus difficile à apprécier et à comprendre, c'est ce qui se passe sous nos yeux.

What is often most difficult to appreciate and understand is what takes place directly under our own eyes.

Alexis de Tocqueville

SUMMARY

This thesis studies advanced and accurate discretization schemes for relevant partial differential equations (PDEs) in finance. We start with techniques which may be particularly useful for the pricing of so-called *vanilla* financial options, European or American, and then move on to more complex models for the pricing of exotic options.

The most popular model used to price options in finance is the Black-Scholes model which consists in assuming that the underlying asset follows a geometrical Brownian motion. Under the pure Black-Scholes model, European vanilla options can be priced and hedged with a simple analytical formula. This is one of the key reasons of the success of the Black-Scholes model. On the market, vanilla options on single stocks are very regularly traded in their *American* variety, for example on the Chicago Board Options Exchange. In contrast with an European option, the holder of an American option can exercise his right at any time prior to the maturity date. This small change in the contract translates the problem of pricing an option into a non-linear optimization problem. In Chapter 2, we apply the Trapezoidal Rule with a Second Order Backward Difference Formula (TR-BDF2) finite difference scheme on the Black-Scholes-Merton PDE. American option convergence and Greeks stability are both studied against popular alternatives, namely Crank-Nicolson and Rannacher time-marching schemes. We then show that the TR-BDF2 scheme can be applied to other, more complex non-linear PDEs arising in finance such as the Hamilton-Jacobi-Bellman PDE of the uncertain volatility model.

The Black-Scholes-Merton framework assumes a constant volatility parameter across option strikes and maturities. In reality, the volatility implied by the market option prices is far from constant and arbitrage-free models are needed to capture the shape of the implied volatilities, known as *smile* by practitioners. In the interest rates derivatives market, practitioners use the stochastic alpha beta rho (SABR) model of Hagan et al., which captures the swaptions implied volatility smile with a flexible dynamic. In the current low rates environment, the classic SABR formula, used to compute the swaptions Black-Scholes implied volatilities, leads to arbitrage. Hagan et al. recently proposed a new arbitrage-free SABR solution, based on a finite difference discretization of an expansion of the probability density. They rely on a Crank-Nicolson discretization, which can create undesirable oscillations in the option price. In Chapter 4, we apply a variety of second-order finite difference schemes to the SABR arbitrage-free density problem and explore alternative formulations. It is found that the TR-BDF2 and Lawson-Swayne schemes stand out on this problem in terms of stability and speed. A PDE is also derived for the so-called free-boundary SABR model, which allows for negative interest rates without any additional shift parameter, leading to a new arbitrage-free solution for this model. Finally, the free-boundary model behavior is analyzed. For many other stochastic volatility models, it is possible to find an expansion of the marginal probability density which follows a one-dimensional Fokker-Planck PDE. In order to keep the arbitrage-free property numerically, it is particularly important to use a positivity preserving finite difference scheme. With a discontinuous initial condition like a Dirac delta function, many

schemes will produce oscillations or negative densities. By looking at the density located at the Dirac point in time, we give, in Chapter 3, simple conditions on the discretization grid to preserve positivity for a few schemes related to backward Euler, namely the BDF2, Lawson-Morris and Lawson-Swayne schemes applied to the specific problem of a diffusion with Dirac initial condition.

The four parameters of the SABR model don't always allow to capture accurately the implied volatility smile of equity or equity index options, as the market may quote the prices for more than a hundred option strikes per maturity. In Chapters 5 and 6, we explain how to apply the stochastic collocation technique to obtain a smooth and arbitrage-free representation of the market option prices, with either a specific monotonic polynomial or a monotonic B-spline parameterization, which preserves the first moment of the implied distribution exactly. The technique also allows for a fast joint calibration of the constant maturity swap (CMS) convexity adjustment with the market swaptions prices, as the CMS convexity adjustment has then a simple closed-form expression. Similarly, it also allows for a simple joint calibration of variance swap prices and vanilla option prices.

A smooth and arbitrage-free representation is also the key ingredient of the Dupire local volatility model. While the local volatility model solves the inconsistency of the Black-Scholes model with regards to the implied volatility smile, it suffers however from an unrealistic dynamic of the smile in time. In practice this means that forward starting options are mispriced under this model. A different approach is to assume that the volatility is stochastic. Several stochastic volatility models that retain some analytical and numerical tractability have been explored over the years, the most popular being the model from Heston. They all suffer from similar issues: they don't allow to match the implied volatility smile for short maturities very well and they may be challenging to calibrate. A fix for the former issue is to mix stochastic and local volatilities together at the cost of increasing the computational complexity. Grzelak proposes another alternative with the collocating volatility model (CLV), where the model prices are calibrated to the market options with the stochastic collocation technique, used as a convenient representation of the terminal distribution. A specific dynamic is added in the form of a stochastic driver process, which allows more control over the prices of forward starting options. This is reminiscent of the Markov functional models. Grzelak uses a single factor Ornstein-Uhlenbeck process as the driver for the CLV model, and Fries a single factor Wiener process with time-dependent volatility in his equity Markov functional model. Van der Stoep et al. consider a Heston stochastic volatility driver process and show it offers more flexibility to capture the forward smile in the context of foreign exchange options. In Chapters 7 and 8, we discuss all aspects of derivative pricing under the Heston-CLV model: calibration with an efficient Fourier method, a Monte-Carlo simulation with second-order convergence and accurate PDE pricing through implicit and explicit finite difference methods.

With the work in this thesis, one is able to use new techniques to price and hedge vanilla options under simple one-factor models, as well as exotic options under more complex multi-factor models, with a focus on stability and efficiency. Most of the work developed in this thesis is based on journal articles, which have either been published or are submitted for publication.

Samenvatting

Dit proefschrift bestudeert geavanceerde en nauwkeurige discretisatieschema's voor relevante partiële differentiaalvergelijkingen (PDE's) in financiële wiskunde. We beginnen met technieken die met name nuttig kunnen zijn voor de prijsstelling van zogenaamde *vanilla* financiële opties, Europees of Amerikaans, en gaan vervolgens over op complexere modellen voor de prijsstelling van exotische opties.

Het meest populaire model dat wordt gebruikt om opties in de financiële sector te prijzen, is het Black-Scholes model dat erin bestaat aan te nemen dat de onderliggende waarde een geometrische Brownse beweging volgt. Onder het pure Black-Scholes model kunnen Europese vanille-opties worden geprijsd en afgedekt met een eenvoudige analytische formule. Dit is een van de belangrijkste redenen voor het succes van het Black-Scholes model. Op de markt worden vanille-opties op afzonderlijke aandelen zeer regelmatig verhandeld in hun *Amerikaanse* variëteit, bijvoorbeeld op de Chicago Board Options Exchange. In tegenstelling tot een Europese optie kan de houder van een Amerikaanse optie zijn recht op elk moment vóór de vervaldatum uitoefenen. Deze kleine wijziging in het optiecontract vertaalt het probleem van de prijsbepaling van een optie in een niet-lineair optimalisatieprobleem.

In Hoofdstuk 2 passen we de trapeziumregel met een eindig differentieschema van de tweede orde, de achterwaartse differentieformule (TR-BDF2) toe op de Black-Scholes-Merton PDV. Convergentie van de Amerikaanse optie en stabiliteit van berekende afgeleiden worden beiden bestudeerd en vergeleken met populaire alternatieven, namelijk de Crank-Nicolson en Rannacher tijdsdiscretisatie schema's. Vervolgens laten we zien dat het TR-BDF2-schema kan worden toegepast op andere, meer complexe niet-lineaire PDV's die in de financiële sector voorkomen, zoals de Hamilton-Jacobi-Bellman PDV voor het onzekere volatiliteitsmodel.

Het Black-Scholes-Merton raamwerk gaat uit van een constante volatiliteitsparameter voor verschillende uitoefenprijzen en looptijden van opties. In werkelijkheid is de volatiliteit die wordt geïmpliceerd door de marktoptieprij-zen verre van constant en zijn betere arbitragevrije modellen nodig om de vorm van de impliciete volatiliteit vast te leggen, door professionals bekend als *volatility smile*. Op de markt voor rentederivaten gebruiken experts het stochastische alpha beta rho (SABR) model van Hagan et al., dat de *swaptions implicit volatility smile* vastlegt met een flexibele dynamica. Echter, in het huidige renteklimaat met lage rentes leidt de klassieke SABR-formule, die wordt gebruikt om de Black-Scholes swaptions impliciete volatiliteit te berekenen, tot arbitrage. Hagan et al. stelde onlangs een nieuwe, arbitrage-vrije SABR oplossing voor, gebaseerd op een eindige differentiediscretisatie van een uitbreiding van de PDV voor de bijbehorende kansdichtheid. Ze baseren op een Crank-Nicolson discretisatie, die ongewenste schommelingen in de optieprijs kan veroorzaken. In Hoofdstuk 4 passen we een aantal eindige differentieschema's van de tweede orde toe op het SABR arbitragevrije PDV probleem en onderzoeken we alternatieve formuleringen. Het blijkt dat de TR-BDF2 en Lawson-Swayne schema's positief opvallen voor dit probleem in termen van stabiliteit en snel-

heid.

Een PDV wordt ook afgeleid voor een alternatief SABR model, dat negatieve rentetarieven mogelijk maakt zonder enige extra parameters. Dit leidt tot een nieuwe arbitragevrije oplossing voor dit model. Ten slotte wordt het gedrag van dit alternatieve model geanalyseerd. Voor veel andere stochastische volatiliteitsmodellen is het mogelijk om een uitbreiding van de marginale kansdichtheid te vinden die volgt uit een een-dimensionale Fokker-Planck PDV. Om de arbitrage-vrije eigenschap numeriek te behouden, is het bijzonder belangrijk om een differentieschema met positiviteit voor te stellen. Met een discontinue initiële toestand zoals een Dirac delta-functie, zullen veel schema's oscillaties of negatieve dichtheden produceren. Door te kijken naar de dichtheid die zich op het Dirac-punt bevindt, geven we, in Hoofdstuk 3, eenvoudige voorwaarden voor het discretisatierooster om de positiviteit te behouden voor een paar schema's gebaseerd op het achterwaartse Euler schema, namelijk de BDF2, Lawson-Morris en Lawson-Swayne schema's toegepast op het specifieke probleem van een diffusie met een Dirac initiële toestand.

De vier parameters van het SABR model laten niet altijd toe om de *implied volatility smile* van aandelen- of aandelenindexopties nauwkeurig vast te leggen, aangezien de markt de prijzen voor meer dan honderd uitoefenprijzen per looptijd kan citeren. In de Hoofdstukken 5 en 6 leggen we uit hoe de stochastische collocatietechniek kan worden toegepast om een soepele en arbitrage-vrije weergave van de marktoptieprijzen te verkrijgen, met een specifiek monotoon polynoom of een monotone B-spline parameterisering, waardoor het eerste moment van de impliciete verdeling exact behouden blijft. De techniek maakt ook een snelle gezamenlijke kalibratie mogelijk van een convexiteitsaanpassing van een constante maturiteitsswap (CMS) met de prijzen van markt swaptions, omdat de convexiteitsaanpassing van de CMS dan een eenvoudige uitdrukking in gesloten vorm heeft. Evenzo maakt het ook een eenvoudige gezamenlijke kalibratie van variantie swapprijzen en vanille optieprijzen mogelijk.

Een flexibele en arbitrage-vrije weergave is ook het belangrijkste ingrediënt van het lokale volatiliteitsmodel van Dupire. Hoewel het lokale volatiliteitsmodel de inconsistentie van het Black-Scholes model met betrekking tot de *implied volatility smile* oplost, lijdt het echter aan een onrealistische dynamica van de smile in de tijd. In de praktijk betekent dit dat zogenaamde voorwaartse startopties onder dit model verkeerd worden geprijsd. Een andere benadering is gebaseerd op de aanname dat de volatiliteit stochastisch is. Verschillende stochastische volatiliteitsmodellen, die enige analytische en numerieke traceerbaarheid behouden, zijn in de loop der jaren onderzocht, de meest populaire is het model van Heston. Deze modellen hebben allemaal dezelfde problemen: ze laten niet toe om de implied volatility smile vanuit de marktobservaties voor korte optielooptijden goed te reproduceren en ze kunnen een uitdaging zijn om te kalibreren. Een oplossing is het combineren van stochastische en lokale volatiliteit, echter ten koste van het verhogen van de computationele complexiteit.

Lech Grzelak stelt een alternatief voor met het zogeheten collocating volatility model (CLV), waarbij de modelprijzen worden gekalibreerd naar de marktopties met behulp van de stochastische collocatietechniek, die wordt gebruikt als een nauwkeurige weergave van de distributie op de eindtijd van de optie. Een specifieke dynamica wordt toegevoegd in de vorm van een stochastisch stuurproces, dat meer controle mogelijk

maakt over de prijzen van de voorwaartse startopties. Dit doet denken aan de functionele modellen van Markov. Grzelak gebruikt een Ornstein-Uhlenbeck proces met één factor als basis voor het CLV model, en Christian Fries een Wiener-proces met één factor met tijdsafhankelijke volatiliteit in zijn functionele Markov model. Van der Stoep et al. overwegen een Heston stochastisch volatiliteitsstuurproces en laten zien dat het meer flexibiliteit biedt om de voorwaartse smile vast te leggen in de context van wisselkoersopties.

In de Hoofdstukken 7 en 8 bespreken we alle aspecten van derivaten prijzen volgens het Heston-CLV model: kalibratie met een efficiënte Fourier-methode, een Monte-Carlo simulatie met tweede-orde convergentie en nauwkeurige PDV-prijsstelling door impliciete en expliciete eindige differentiemethoden.

Met het werk in dit proefschrift is het mogelijk om nieuwe technieken te gebruiken om vanilla opties te prijzen en te hedgen onder eenvoudige één-factor modellen, evenals exotische opties onder meer complexe multi-factor modellen, met een focus op stabiliteit en efficiëntie. Het grootste deel van het werk dat in dit proefschrift is ontwikkeld, is gebaseerd op tijdschriftartikelen, die zijn gepubliceerd of worden ingediend voor publicatie.

CONTENTS

1

INTRODUCTION

1.1. VANILLA OPTIONS

A *European* vanilla option is a financial instrument that gives the holder the right, but not the obligation, to buy (call) or sell (put) an asset S at a specific price, known as the strike price K, on a specified date T, the maturity date. In exchange for this right, the buyer of the option pays a fixed amount, the premium, usually a few days after the contract start date, while the settlement of the option payoff occurs a few days after the maturity date. In some markets, the premium may be settled a few days after the maturity date. The buyer of a call option would normally choose to exercise his right if the asset price is higher than the strike price at maturity, as the option payoff, $\max(S - K, 0)$, is then strictly positive. When the underlying asset is a stock, the option may be settled in cash or physically. When cash-settled, the closing price of the underlying stock is most often chosen to compute the settlement amount.

We define the price of an option at a given valuation date as the theoretical price one would pay at the valuation date to buy the option. In the Black-Scholes-Merton model, the underlying asset follows a lognormal distribution. The corresponding stochastic differential equation reads

$$dS(t) = \bar{\mu}(t)S(t)\,dt + \sigma(t)S(t)\,dW(t). \tag{1.1}$$

where we allow for time-varying drift $\bar{\mu}$ and volatility σ. Under the risk-neutral measure, we have $\bar{\mu}(t) = \mu(t) = r_g(t) - q(t)$, where r_g is the deterministic growth short rate and q is the instantaneous dividend yield. Note that in practice, a stock grows at the repurchase agreement contract (repo) rate r_g, which is typically lower than the risk-free interest rate r, and derivative contracts on the asset S may be discounted with the agreed overnight rate r_c paid on collateral among dealers under a so-called credit support annex agreement (CSA), when fully collateralized [170]. In order to simplify the equations in this thesis, we will not make the distinction between the various interest rates involved and consider $r = r_g = r_c$. We will however keep distinct the discounting part, so that the reader may deduce the correct interest rate to use.

Let $V(t, S)$ be the price of a financial derivative contract depending on the price of the asset S at a set of dates up to the maturity date of the contract. Let $B(0, t)$ be the deterministic discount process defined by $B(0, t) = e^{-\int_0^t r(s)\,ds}$. According to the risk-neutral pricing formula [180, Equation (5.2.31), p.218], $B(0, t)V(t, S(t))$ is a martingale under the risk-neutral measure $\mathbb{Q}$ and we thus have

$$B(0, t)V(t, S(t)) = \mathbb{E}_{\mathbb{Q}}\left[B(0, T)V(T, S(T))\right]. \tag{1.2}$$

1

Let us recall the Feynman-Kaç theorem [180, Theorem 6.4.1, p.268], which establishes the link between stochastic differential equations and partial differential equations.

Theorem 1.1.1 (Feynman-Kaç)**.** *Consider the stochastic differential equation*

$$\mathrm{d}S(u) = \beta(u, S(u))\,\mathrm{d}u + \gamma(u, S(u))\,\mathrm{d}W(u).$$

where $\beta(u, s), \gamma(u, s)$ are given functions. Let $h(y)$ be a Borel-measurable function. Fix $T > 0$ and let $t \in [0, T]$ be given. Define the function

$$g(t, s) = \mathbb{E}[\,h(S(T))\,|\,S(t) = s]$$

Assuming $\mathbb{E}[\,|h(S(T))|\,|\,S(t) = s] < \infty$ for all t and s, then $g(t, s)$ satisfies the partial differential equation

$$\frac{\partial g}{\partial t}(t, s) + \beta(t, s)\frac{\partial g}{\partial s}(t, s) + \frac{1}{2}\gamma^2(t, s)\frac{\partial^2 g}{\partial s^2}(t, s) = 0,$$

and the terminal condition $g(T, x) = h(x)$ for all x.

An application of the Feynman-Kaç theorem with $g(t, S) = B(0, t)V(t, S)$ leads to the Black-Scholes PDE

$$\frac{\partial V}{\partial t} + \frac{1}{2}\sigma^2(t)S^2\frac{\partial^2 V}{\partial S^2} + \mu(t)S\frac{\partial V}{\partial S} - r(t)V = 0. \tag{1.3}$$

For a European vanilla call or put option, the terminal condition is respectively $V(T, S) = \max(S - K, 0)$ and $V(T, S) = \max(K - S, 0)$. The solution to the PDE is then known explicitly and reads

$$V(t) = \eta B(t, T)\left[F(t, T)\Phi\left(\eta d_1\right) - K\Phi\left(\eta d_2\right)\right], \tag{1.4}$$

where $\eta = 1$ for a call option, $\eta = -1$ for a put option, Φ is the cumulative normal distribution function, and d_1 and d_2 are defined by

$$d_1 = \frac{\ln\frac{F(t,T)}{K} + \frac{1}{2}\bar{\sigma}^2(T - t)}{\bar{\sigma}\sqrt{T - t}}, \quad d_2 = d_1 - \bar{\sigma}\sqrt{T - t},$$

with $\bar{\sigma} = \sqrt{\frac{1}{T-t}\int_t^T \sigma^2(u)\,\mathrm{d}u}$. Under deterministic rates, the discount factor is $B(t, T) = e^{-\int_t^T r(s)ds}$ and the forward price is $F(t, T) = S(t)e^{\int_t^T \mu(s)ds}$. In order to simplify the equations, we ignored the payment lag, in reality, the discounting is from the valuation date to the settlement date, which is typically one business day after the maturity date.

The *implied volatility* of a vanilla option is the value $\bar{\sigma}$ used in Equation (1.4) in order for the Black-Scholes-Merton option price to be equal to the market price.

On the market, vanilla options on single stocks are also very regularly traded in their *American* variety, for example on the Chicago Board Options Exchange. In contrast with the European option, the holder of an American option can exercise its right at any time prior to the maturity date. This small change in the contract translates the problem of

pricing an option into a non-linear optimization problem. The price of an American option satisfies the following linear complementarity problem [111, 122]

$$
\left.\begin{array}{r}
\dfrac{\partial V}{\partial t} + \mu(t)S\dfrac{\partial V}{\partial S} + \dfrac{1}{2}\sigma(t)^2 S^2 \dfrac{\partial^2 V}{\partial S^2} - r(t)V \leq 0 \\[2mm]
V - h \geq 0 \\[2mm]
\left(\dfrac{\partial V}{\partial t} + \mu(t)S\dfrac{\partial V}{\partial S} + \dfrac{1}{2}\sigma(t)^2 S^2 \dfrac{\partial^2 V}{\partial S^2}(t) - r(t)V(t)\right)(V - h) = 0
\end{array}\right\} \tag{1.5}
$$

with $h(S) = \max\big(\eta(S - K), 0\big)$.

1.2. BEYOND BLACK-SCHOLES DYNAMICS

In Chapter 2, we will apply the Trapezoidal Rule with second-order Backward Difference Formula (TR-BDF2) finite difference scheme to the more general PDE problem

$$
\left.\begin{array}{r}
\dfrac{\partial V}{\partial t} + \mu(S,t)S\dfrac{\partial V}{\partial S} + \dfrac{1}{2}\sigma(S,t)^2 S^2 \dfrac{\partial^2 V}{\partial S^2} - r(S,t)V \leq 0 \\[2mm]
V - h \geq 0 \\[2mm]
\left(\dfrac{\partial V}{\partial t} + \mu(S,t)S\dfrac{\partial V}{\partial S} + \dfrac{1}{2}\sigma(S,t)^2 S^2 \dfrac{\partial^2 V}{\partial S^2}(S,t) - r(S,t)V(t)\right)(V - h) = 0
\end{array}\right\} \tag{1.6}
$$

where we let μ, r, σ depend also on the asset price. This encompasses models beyond Black-Scholes-Merton, such as the Dupire *local volatility* model [55], which allows to capture the *smile* shape of the market implied volatilities, as well as various single factor short rate models when S represents an interest short rate. The TR-BDF2 scheme possesses several characteristics that makes it particularly attractive:

- it is second-order accurate,

- it is *L*-stable, which means that rapid transients in the solution will be damped in a single time step,

- it consists of two-stages, but is a single-step scheme, as opposed to traditional multi-step schemes such as the second-order backward difference (BDF2) scheme.

We will also apply the TR-BDF2 scheme to the non-linear Hamilton-Jacobi-Bellman (HJB) PDE corresponding to the *uncertain volatility* model developed in [17]. This model supposes that the volatility is uncertain but bounded between a minimum volatility $\sigma_{\min}$ and a maximum volatility $\sigma_{\max}$. Under this model one can find the prices of a derivative product for a worst long strategy or a best long strategy. The corresponding PDE is

$$
\frac{\partial V}{\partial t} - \sup_{\sigma \in \{\sigma_{\min}, \sigma_{\max}\}} \left\{ \mu(t)S\frac{\partial V}{\partial S} + \frac{1}{2}\sigma^2 S^2 \frac{\partial^2 V}{\partial S^2} - r(t)V \right\} = 0. \tag{1.7}
$$

It is shown in [171] that the Crank-Nicolson scheme does not necessarily converge to the correct solution, when applied to this problem. In Chapter 2, we show, that, on the same example, the TR-BDF2 scheme has no such issue.

1.3. SMILES, SWAPTIONS AND THE SABR MODEL

Let F be the stochastic process of the underlying forward price, A is the volatility process eventually correlated to F and L is a function of F which may be used to define a specific dynamic, and is often taken to be $L(F) = F^\beta$ with some $\beta \in \mathbb{R}$. For example, in the SABR model, the underlying forward price follows

$$\mathrm{d}F = AL(F)\,\mathrm{d}W_1\,, \tag{1.8a}$$

$$\mathrm{d}A = \nu A\,\mathrm{d}W_2\,, \tag{1.8b}$$

with initial volatility $A(0) = \alpha$ and where ν is the volatility of volatility parameter (vol-of-vol), W_1, W_2 are two correlated Brownian motions with correlation ρ.

In many popular stochastic volatility models, including generalized versions of the SABR [85] and Heston [91] models, the marginal density Q satisfies an effective forward equation of the form [86]

$$\frac{\partial Q}{\partial T} = \frac{1}{2}\alpha^2 \sigma^2(T)\frac{\partial^2}{\partial F^2}\left[\left(1 + \frac{2b(T)z}{\alpha} + \frac{c(T)z^2}{\alpha^2}\right)L^2(F)Q\right]\,, \tag{1.9}$$

with initial condition

$$\lim_{T \to 0} Q(T,F) = \delta(F - f)\,,$$

where

$$z = \int_f^F \frac{\mathrm{d}u}{L(u)}\,.$$

The marginal density is defined by

$$Q(T,F) = \int_0^\infty p(0,f,\alpha,T,F,A)\,\mathrm{d}A\,, \tag{1.10}$$

where p is the probability density at $F(T)$, $A(T)$ and time T, given that $F(0) = f$, $A(0) = \alpha$. The coefficients $\sigma(T), b(T), c(T)$ are determined from the model parameters by singular perturbation analysis, with the constant α chosen so that $\sigma(0) = 1$. In particular, for the standard SABR model (Equation 1.8), we have [84]

$$\sigma(T) = e^{\frac{1}{2}\rho\nu\alpha L'(f)T}\,, \quad b(T) = \rho\nu\,, \quad c(T) = \nu^2\,.$$

Once the effective forward equation (1.9) is solved, for example with a finite difference method, European option prices are obtained by a simple one-dimensional integration over the marginal density. In comparison, the straightforward approach to compute the European option prices for a set of strike prices would instead involve either the solution of the two-dimensional backward PDE resulting from the application of the multi-dimensional Feynman-Kaç theorem for each option strike, or the solution of the two-dimensional forward Komolgorov PDE for to the given stochastic volatility model. The expansion of the marginal density thus allows to calibrate efficiently any stochastic volatility model (eventually with parametric local volatility component) to European option prices.

A positive valued numerical marginal density is however a prerequisite to obtain an arbitrage-free representation in practice. With a discontinuous initial condition like a Dirac delta function, many schemes will produce oscillations or negative densities. By looking at the density located at the Dirac in time, we give in Chapter 3 simple conditions on the discretization grid to preserve positivity for a few schemes related to the backward Euler scheme, namely the BDF2, Lawson-Morris and Lawson-Swayne schemes on the specific problem of a diffusion with a Dirac delta initial condition. We also derive an equivalence relation between the TR-BDF2 and the Lawson-Swayne schemes in the presence of constant coefficients.

In order to price and hedge interest rate swaptions, the market practice is to use the SABR model of Hagan et al. [85], as it gives a satisfactory representation of the implied volatility smile, and is flexible enough to capture the implied volatility dynamics in time. The SABR formula[1] for the Black-Scholes implied volatility of a swaption with strike price K and maturity τ_{ex} reads

$$\sigma(K) = \frac{1}{x(\zeta(K))} \ln\left(\frac{f}{K}\right) \left[1 + \left(g(K) + \frac{1}{4}\rho v \alpha \beta f^{\frac{\beta-1}{2}} K^{\frac{\beta-1}{2}} + \frac{1}{24}(2 - 3\rho^2)v^2\right)\tau_{ex}\right], \quad (1.11)$$

with

$$g(K) = \frac{1}{24}(\beta - 1)^2 f^{\beta-1} K^{\beta-1} \alpha^2,$$

$$\zeta(K) = \frac{v}{\alpha(1 - \beta)}\left(f^{1-\beta} - K^{1-\beta}\right),$$

$$x(\zeta) = \frac{1}{v}\ln\left(\frac{\sqrt{1 - 2\rho\zeta + \zeta^2} - \rho + \zeta}{1 - \rho}\right),$$

and where f is the initial forward swap rate for the maturity τ_{ex}. At $t = 0$ we have $f = F(0)$. Under this representation, the marginal probability density of the forward rate F between $t = 0$ and $t = \tau_{ex}$ may be computed with the help of the undiscounted Black-Scholes vanilla option prices V with volatility $\sigma(K)$ via the identity [28]

$$Q(\tau_{ex}, K) = \frac{\partial^2 V}{\partial K^2}. \quad (1.12)$$

The above equation may also be directly derived by differentiating twice the risk-neutral pricing formula (1.2).

The SABR formula is not exact, but is based on a small volatility expansion, where both the initial volatility α and the "vol-of-vol" parameter v are considered small. With the advent of low interest rates, it was noticed that the classic Hagan expansion for implied volatilities in the SABR model often led to butterfly spread arbitrage, or equivalently to a negative probability density [84]. An example is given in Figure 1.1. Hagan et al. therefore propose to use the marginal density approach and solve the SABR PDE corresponding to Equation (1.9) in order to guarantee arbitrage-free option prices. In

---

[1] Equation 1.11 is not exactly the formula presented in [85], but the variation from Obloj [162], which has the advantage of being consistent when $\beta \to 1$. The negative density issue is shared by all popular SABR approximations.

1

Chapter 4, we will apply a variety of second-order finite difference schemes to this problem and explore alternative formulations. It is found that the TR-BDF2 and Lawson-Swayne schemes stand out on this problem in terms of stability and speed. A PDE is also derived for the so-called free-boundary SABR model, which allows for negative interest rates without any additional shift parameter, leading to a new arbitrage-free solution for this model. Finally, the free-boundary model behaviour is analyzed.
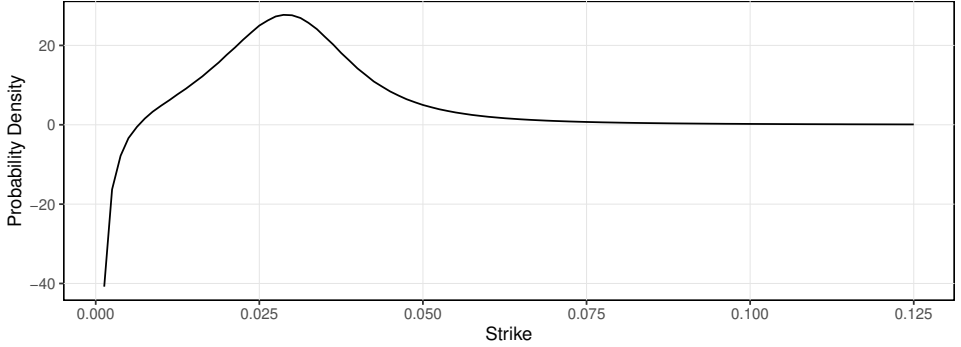
Figure 1.1: Probability density implied by the Hagan formula (1.11) using the SABR parameters of Andreasen and Huge [13]: $\alpha = 0.0873, \beta = 0.7, \rho = -0.48, \nu = 0.47$ with an initial forward swap rate $f = 0.025$ and a maturity $\tau_{ex} = 10.0$.

1.4. ARBITRAGE-FREE STOCHASTIC COLLOCATION METHOD

The financial markets provide option prices for a discrete set of strike prices and maturity dates. In order to price over-the-counter vanilla options with different strikes, or to hedge complex derivatives with vanilla options, it is useful to have a continuous arbitrage-free representation of the option prices or, equivalently, of their implied volatilities.

A rudimentary, but popular representation is to interpolate market implied volatilities with a cubic spline across option strikes. Unfortunately this may not be arbitrage-free as it does not preserve the convexity of option prices in general. Convex interpolations of the call option prices by quadratic splines or rational splines are also not satisfactory in general since they may generate unrealistic oscillations in the corresponding implied volatilities, as evidenced in [109]. Kahale [116] designs an arbitrage-free interpolation of the call prices, which however requires convex input quotes, employs two embedded non-linear minimizations, and it is not proven that the algorithm for the C^2 interpolation function converges. In reality, it is often not desirable to strictly interpolate option prices as those fluctuate within a bid-ask spread. As per Equation (1.12), a direct interpolation will lead to a noisy estimate of the probability density.

More recently, Andreasen and Huge [12] have proposed to calibrate the discrete piecewise constant local volatility corresponding to a single-step finite difference discretization of the forward Dupire equation. In their representation of the local volatility, the authors use as many constants as the number of market option strikes for an optimal fit.

It is thus sometimes considered to be "non-parametric". Their technique works well but often yields a noisy probability density estimate, as the prices are typically over-fitted. Furthermore, the output of their technique is a discrete set of option prices, which, while relatively dense, must still be interpolated carefully to obtain the price of options whose strike falls in between nodes.

An alternative is to rely on a richer underlying stochastic model, which allows for some flexibility in the implied volatility smile, such as the Heston or SABR stochastic volatility models. While semi-analytic representations of the call option price exist for the Heston model [91], the model itself does not allow to represent short maturity smiles accurately. The SABR model is better suited for this, but has only closed-form approximations for the call option price, which can lead to arbitrage (Figure 1.1). Furthermore, the small number of parameters of such models is not always adequate to represent volatility surfaces, particularly for liquid equity or equity index options.

Grzelak and Oosterlee [78] use stochastic collocation to fix the Hagan SABR approximation formula defects and produces arbitrage-free option prices starting from the Hagan SABR formula. Collocation methods are commonly used to solve ordinary or partial differential equations [138]. The underlying principle is to solve the equations in a specific finite dimensional space of solutions, such as polynomials up to a certain degree. In contrast, the stochastic collocation method [151] consists in mapping a physical random variable Y to a point X in an artificial stochastic space. Collocation points x_i are used to approximate the function mapping X to Y, $\Phi_X^{-1} \circ \Phi_Y$, typically by a polynomial, where Φ_X, Φ_Y are respectively the cumulative distribution functions (CDF) of X and Y. Thus only a small number of inversions of Y (and evaluations of Φ_Y) are used. This allows the problem to be solved in the "cheaper" artificial space. Using a Gaussian distribution for X, European option prices are obtained by a simple closed-form formula, for any strike. A necessary condition for the prices to be free of arbitrage, is for the mapping to be monotonic, otherwise the collocated CDF may decrease. This is, a priori, not guaranteed with the approach of Grzelak [78], where a Lagrange polynomial on Gauss-Hermite nodes is used.

Chapter 5 explores how to calibrate the stochastic collocation polynomial directly to market prices, without going through an intermediate model. A specific isotonic parameterization is used to ensure the monotonicity of the collocation polynomial as well as the conservation of the zero-th and first moments transparently during the optimization, guaranteeing the absence of arbitrage.

The isotonic polynomial stochastic collocation leads to a smooth, implied probability density, without any artificial peak, even with a high degree of the collocation polynomial. The technique may also be applied to interest rate derivatives, as it leads to a closed-form formula for CMS convexity adjustments, which can thus be easily calibrated jointly with interest rate swaptions.

The stochastic collocation technique is of particular interest to the richer Heston collocated local volatility (*Heston-CLV*) model, which allows to price exotic options through Monte-Carlo or finite difference methods [77]. In this model, the financial asset S follows

1

$$S(t) = g(t, X(t)),\tag{1.13a}$$

$$\mathrm{d}X(t) = (r(t) - q(t))X(t)\,\mathrm{d}t + \sqrt{V(t)}\,X(t)\,\mathrm{d}W_X(t),\tag{1.13b}$$

$$\mathrm{d}V(t) = \kappa\,(\theta - V(t)) + \sigma\sqrt{V(t)}\,\mathrm{d}W_V(t),\tag{1.13c}$$

with W_X and W_V being two Brownian motions with correlation ρ, r, q the instantaneous growth and dividend rates, and $g(t, x)$ a collocation function. According to Equations (1.13b) and (1.13c), the driver process X follows the Heston stochastic volatility model [91]. The collocation function g is typically a polynomial or a spline, which will be calibrated to the market using the stochastic collocation technique. Robust and efficient pricing of vanilla options is obtained by applying the adaptive Filon quadrature of Chapter 7 on a specific payoff.

1.4.1. SPLINES
The use of a polynomial may however be problematic as the (lognormal) Heston model suffers from moment explosions [8]. The moment $\mathbb{E}[S(t)^m]$ for $m \geq 1$ may become infinite after some finite time. In those cases, which are quite common when the Heston model is calibrated to the market, the first moment of the Heston-CLV model is not defined. While it is always possible to constrain the Heston parameters to a region where the moments are well defined, such a constraint places a severe limitation on the Heston model quality of fit (see, for examples, Figures 8.3.1a and 8.3.1b). This has potential consequences on the martingale conservation properties of the Heston-CLV model.

A known deficiency of Markov functional models is that they do not respect the martingale property [30, 108]. The Heston-CLV model is similar to a Markov functional model: the collocation function only captures the terminal distribution at each maturity date and is then applied at different dates independently, without taking into account any joint distribution between the dates. Yet, the driver is a calibrated Heston model, whose joint distribution is close to the market distribution. We may thus expect the collocation function to provide a second-order correction and the martingale property to be reasonably well preserved. This is confirmed on our example calibration towards SX5E options as of February 26, 2016 (Table 8.4.2 and Figure 8.4.3b). The measured drift is an order of magnitude smaller than with one-dimensional Markov functional models.

Another drawback of the use of polynomials in the stochastic collocation technique, independently of the Heston-CLV model, relates to their difficulties in capturing multi-modal distributions. Although, theoretically, as proven in Chapter 5, we can always find a polynomial to capture multi-modal distributions, such a polynomial may be required to be of a prohibitively high degree to match accurately the distribution, which renders the technique not practical.

Instead of collocating on a polynomial, Chapter 6 explores various ways to use a monotonic spline, including B-spline parametrizations which preserve the first moment exactly. This allows for a richer representation, with as many parameters as there are market option strikes.

A first consequence is the ability to capture more complex implied probability distributions such as multi-modal distributions. Over-fitting is avoided by adding an ap-

propriate regularization, whose optimal value may be found with the *L-curve* method of Hansen [88]. This is reminiscent of the penalized B-spline technique for volatility modelling of Corlay [38], where a B-spline parameterization of the Radon-Nikodym derivative of the underlying's risk-neutral probability density with respect to a roughly calibrated base model is used. Concretely, Corlay's method translates to an explicit probability density representation where the probability density is a spline multiplied by a base probability density function, such as the lognormal or normal probability density function. Corlay's technique however seriously restricts the implied volatility shapes allowed, and often requires the use of a more elaborate base probability density function, such as the one stemming from the SVI parameterization of Gatheral [72], to properly fit the market in practice. The stochastic collocation on a spline is more flexible and can fit the market accurately when collocating to a simple Gaussian variable.

A second consequence of the use of splines is to remove the restrictions on the Heston parameters with regards to the first moment explosion in the Heston-CLV model: with a linear extrapolation, there will be no first moment explosion.

1.4.2. PRICING UNDER THE HESTON-CLV MODEL

The Monte-Carlo simulation of the Heston-CLV model is straightforward: we use a good discretization scheme for the Heston model in order to discretize the X process; then we obtain the value of S on each path by applying directly the collocation function to each path of X (Equation 8.1a). Unlike the case of the stochastic local volatility model, there is no need to use very small time-steps. The discretization error is entirely due to the Heston process discretization. The quadratic exponential (QE) scheme of Andersen [6] is widely used to discretize the Heston process. Its convergence properties are however not known (on a concrete example, we measure a convergence order between 1.3 and 1.7). Instead, in Chapter 8, we present a minor modification of the DVSS2 scheme of Lenkšas and Mackevičius [135], which has a proven second-order convergence, and stays computationally efficient.

We also explore in Chapter 8 different ways of solving the Heston-CLV partial differential equation (PDE): directly through the L-stable second-order finite difference scheme of Lawson and Swayne [125], through an alternating direction explicit method, through the explicit Runge-Kutta-Legendre scheme, as well as with various alternating direction implicit (ADI) methods. When using the simpler Heston driver process coordinate, barrier options impose an implicitly defined time-varying boundary, which is then very challenging to take into account by second-order finite difference schemes, while keeping their order of convergence intact. We thus apply the various finite difference methods to the PDE in the asset coordinate. We then put in evidence the oscillations that may appear in the greeks, measure the order of convergence, accuracy and performance of each scheme on a practical example.

1.5. CONCLUSION

We propose, analyse and evaluate new, less well-known numerical techniques, and check their applicability and suitability for financial PDEs and for other financial equations. The financial PDE problems are not only the commonly well-known academic financial

1

PDEs, but also industrially relevant PDEs with features that are important for the financial industry. So, PDE techniques are evaluated regarding their suitability in industrial practice. At the same time, we aim to understand, and confirm the corresponding properties of the favourable schemes.

2

TR-BDF2 SCHEME FOR FAST STABLE AMERICAN OPTION PRICING

The Trapezoidal Rule with Second-Order Backward Difference Formula (TR-BDF2) finite difference scheme is applied to the Black-Scholes-Merton PDE on a non-uniform grid. American option convergence and Greeks stability is studied against popular alternatives, namely Crank-Nicolson and Rannacher time-marching.

Keywords: Finite Difference · American option · Crank-Nicolson · TR-BDF2 · Rannacher.

2.1. INTRODUCTION

It is well-known that discontinuities in the payoff function or its derivatives can cause inaccuracies for numerical schemes when financial contracts are priced. For a vanilla (or digital) option, to avoid discretization errors, several ad-hoc remedies can be applied, for example, placing the strike price on a grid node, or applying smoothing or projection techniques to the payoff [172, 188]. Additionally, the scheme itself can introduce unwelcomed inaccuracies. The Crank-Nicolson scheme can introduce spurious oscillations in the greeks [73]. Rannacher smoothing is a known fix for European options. However, we show here that it does not work as well for American (or Bermudan) options. In contrast, the Trapezoidal Rule with Second Order Backward Difference Formula (TR-BDF2) does not produce any spurious oscillations for European, Bermudan or American options, and is, like backward Euler (and unlike the Crank-Nicolson scheme), mathematically *L*-stable.

Estimating precisely the Gamma and Delta is key as those greeks are the most commonly used greeks for hedging.

2.1.1. WHERE IS TR-BDF2 BEING USED?

TR-BDF2 has been in use for more than 25 years in various domains. It was first used in electronics by Bank et al. to solve the coupled system of nonlinear partial differential equations that model the transient behavior of silicon VLSI device structures [19]. It remains a popular scheme in electronics [70] and has been studied extensively [149, 197]. In biology, Tyson et al. used the scheme to solve a chemotaxis model [193]. In mechanical engineering, Bathe studied its application for the transient response solution of structures when large deformations and long time durations are considered [21].

The author is unaware of any previous use of TR-BDF2 within computational finance.

2.1.2. A-STABILITY AND L-STABILITY

For a finite difference method, A-stability (or absolute stability) is defined using the simple test problem:

$$u'(t) = \lambda u(t), \tag{2.1}$$

where λ is a complex number. The application of a numerical scheme to this problem will lead to a condition on $z = k\lambda$, where k is the time step, in order to ensure convergence [137]. For the forward Euler scheme, the discretization leads to $u_{j+1} = (1 + k\lambda)u_j$, its stability region will be defined by $|1 + z| \leq 1$. When the stability region contains the whole left half plane, the method is said to be A-stable. Backward Euler is A-stable, but forward Euler is not: its stability region is a disc of radius 1 around the point 1.

L-stability is a stronger requirement than A-stability: a numerical method is L-stable if, for the same simple problem (2.1), it is A-stable and $\frac{u_{j+1}}{u_j} \to 0$ as $|z| \to \infty$ [137]. With L-stability, rapid transients in the solution will be damped in a single time step.

2.2. TR-BDF2 SCHEME

2.2.1. WHAT IS TR-BDF2?

The Trapezoidal Rule with second-order Backward Difference Formula (TR-BDF2) is a second-order accurate fully implicit Runge Kutta method.

For a time discretization defined by $(t_j)_{j\in\{0,..,n\}}$, $k_j = t_j - t_{j-1}$, where t_0 is typically the valuation time and t_n the option expiry, there are two stages at each time step: the first stage is the trapezoidal method (Crank-Nicolson) applied from t_j to $t_{j-\alpha} = t_j - \alpha k_j$; the second stage is the two-step BDF method applied to the first stage output and the initial data, and will give the value at t_{j-1}. Let $\mathscr{L}$ be the Black-Scholes-Merton operator defined by:

$$\mathscr{L}(v(x,t),x,t)) = -\mu(x,t)x\frac{\partial v}{\partial x} - \frac{1}{2}\sigma(x,t)^2x^2\frac{\partial^2 v}{\partial x^2} + r(x,t)v(x,t), \tag{2.2}$$

where x is the underlying price, μ is the underlying drift, σ its volatility and r the interest rate, and $V(x) = v(x,t_n)$ the option payoff at maturity.

The Black-Scholes-Merton equation is:

$$\frac{\partial v}{\partial t}(x,t) = \mathscr{L}(v(x,t),x,t). \tag{2.3}$$

The TR-BDF2 method, backward in time, can be written as [137]:

$$v^* = v_n + \frac{\alpha k_n}{2}\left(\mathscr{L}(v_n) + \mathscr{L}(v^*)\right), \tag{2.4}$$

$$v_{n-1} = \frac{1}{2-\alpha}\left(\frac{1}{\alpha}v^* - \frac{(1-\alpha)^2}{\alpha}v_n + (1-\alpha)k_n\mathscr{L}(v_{n-1})\right). \tag{2.5}$$

Even though there are two stages, this is still a one-step method. Any full step only depends on the previous full step. This is an important difference with the standard second-order backward difference scheme (BDF2) that depends on the two previous time steps and can lose its accuracy [199] with variable time steps and linear complementarity problems. This scheme does not suffer from such drawbacks.

Using the simple problem (2.1), the TR-BDF2 stability region is defined by [19]:

$$\left| \frac{(1+(1-\alpha)^2)z + 2(2-\alpha)}{\alpha(1-\alpha)z^2 + (\alpha^2-2)z + 2(2-\alpha)} \right| \leq 1. \tag{2.6}$$

It is unconditionally A-stable: its stability region includes the whole imaginary plane. It is also L-stable while the Crank-Nicolson scheme is only A-stable [47]. In practice, the non L-stability manifests itself by spurious oscillations in the first and second spatial derivatives with Crank-Nicolson. This phenomenon will not appear with TR-BDF2 or with Backward Euler (which is also L-stable).
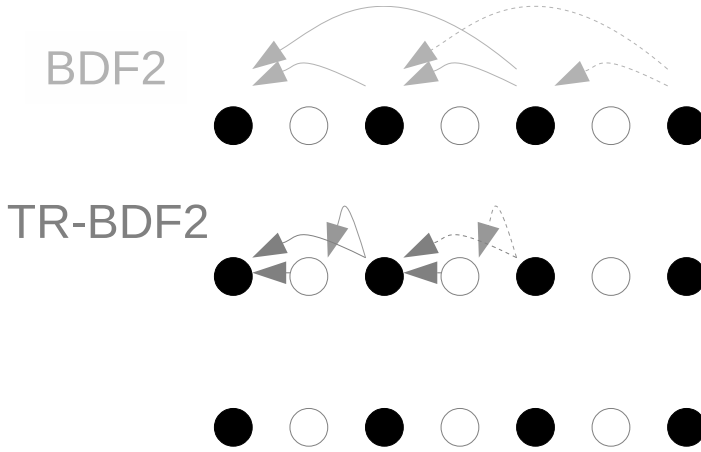
Figure 2.1: BDF2 has overlapping input over different time steps while TR-BDF2 has not

2.2.2. CHOICE OF α

There are two popular choices for α:

$$\alpha = \frac{1}{2},$$
$$\alpha = 2 - \sqrt{2}.$$

The choice of $\alpha = \frac{1}{2}$ makes the first stage to be the Crank-Nicolson scheme [137], while the choice of $\alpha = 2 - \sqrt{2}$ is known to give the least truncation error among all α, proportional linear systems [19], and the largest stability region [48]. With proportional linear systems the underlying algorithm can be faster and is simpler to implement.

In practice, we did not find any significant difference in accuracy between the two when TR-BDF2 is applied to the Black-Scholes PDE. We will therefore use $\alpha = 2 - \sqrt{2}$.

2.2.3. DISCRETIZATION OF THE BLACK-SCHOLES PDE

For a space discretization defined by $(x_i)_{i \in \{0,...,m\}}$, $h_i = x_i - x_{i-1}$ The central difference operator $\mathscr{D}_x$ is defined as:

$$\mathscr{D}_x v_{i,j} = \frac{v_{i+1,j} - v_{i-1,j}}{h_{i+1} + h_i}. \tag{2.7}$$

The central second difference operator $\mathscr{D}_x^2$ is defined as:

$$\mathscr{D}_x^2 v_{i,j} = 2 \frac{h_i v_{i+1,j} - (h_{i+1} + h_i) v_{i,j} + h_{i+1} v_{i-1,j}}{h_i h_{i+1} (h_{i+1} + h_i)}. \tag{2.8}$$

For $i \in \{1, ..., m-1\}$, $j \in \{1, ..., n\}$, let $\mathscr{L}_{i,j} = (r_{i,j} I - \mu_{i,j} x_i \mathscr{D}_x - \frac{1}{2} \sigma_{i,j}^2 x_i^2 \mathscr{D}_x^2)$ be the discrete differential operator where $\mu_{i,j}$ is the drift, $\sigma_{i,j}$ the volatility and $r_{i,j}$ the interest rate on the interval $[t_{j-1}, t_j]$. The various rates are only taken at the initial grid points, and not at the $t_{j-\alpha}$. This allows to keep the proportional same left-hand side linear system for each stage.

The Trapezoidal stage is given by

$$\frac{v_{i,j-\alpha} - v_{i,j}}{-\alpha k_j} = \frac{1}{2} (\mathscr{L}_{i,j} v_{i,j} + \mathscr{L}_{i,j} v_{i,j-\alpha}). \tag{2.9}$$

This leads to the following tridiagonal system for the unknown $v_{i,j-\alpha}$:

$$a_{i,j} v_{i-1,j-\alpha} + b_{i,j} v_{i,j-\alpha} + c_{i,j} v_{i+1,j-\alpha} = -a_{i,j} v_{i-1,j} + b_{i,j}^* v_{i,j} - c_{i,j} v_{i+1,j},$$

with

$$a_{i,j} = \frac{\alpha k_j}{2(h_{i+1} + h_i)} \left(\mu_{i,j} x_i - \frac{\sigma_{i,j}^2 x_i^2}{h_i} \right), \tag{2.10}$$

$$b_{i,j} = 1 + \frac{\alpha k_j}{2} \left(r_{i,j} + \frac{\sigma_{i,j}^2 x_i^2}{h_i h_{i+1}} \right), \tag{2.11}$$

$$c_{i,j} = -\frac{\alpha k_j}{2(h_{i+1} + h_i)} \left(\mu_{i,j} x_i + \frac{\sigma_{i,j}^2 x_i^2}{h_{i+1}} \right), \tag{2.12}$$

$$b_{i,j}^* = 1 - \frac{\alpha k_j}{2} \left(r_{i,j} + \frac{\sigma_{i,j}^2 x_i^2}{h_i h_{i+1}} \right). \tag{2.13}$$

The BDF2 stage reads

$$(2 - \alpha) v_{i,j-1} - \frac{1}{\alpha} v_{i,j-\alpha} + \frac{(1-\alpha)^2}{\alpha} v_{i,j} = -(1-\alpha) k_j \mathscr{L}_{i,j} v_{i,j-1}. \tag{2.14}$$

The approximation $v_{i,j-\alpha}$ is the result of the first stage. For the second stage we have the following tridiagonal system:

$$a_{i,j} v_{i-1,j-1} + b_{i,j} v_{i,j-1} + c_{i,j} v_{i+1,j-1} = \frac{1}{2-\alpha} \left(\frac{1}{\alpha} v_{i,j-\alpha} - \frac{(1-\alpha)^2}{\alpha} v_{i,j} \right),$$

using the same $a_{i,j}$, $b_{i,j}$ and $c_{i,j}$ as above, because we have imposed $\alpha = 2 - \sqrt{2}$. The left-hand side tridiagonal matrix can be reused. We have found that in practice, this leads to an important performance improvement as a good portion of the overall time is spent to just build the matrices.

2.2.4. BOUNDARY CONDITIONS

We consider here the boundary condition, where we assume that $\frac{\partial^2 v}{\partial x^2} = 0$ at the boundaries. This is true for all payoffs linear at the boundaries, which is a reasonable assumption for most payoffs [200]. The Black-Scholes equation becomes:

$$\frac{\partial v}{\partial t}(x,t) + \mu(x,t) x \frac{\partial v}{\partial x}(x,t) = r(x,t) v(x,t). \tag{2.15}$$

We will discretize the derivative by an order-1 approximation in x. This is reasonable because the first-order error in x is proportional to the Gamma, which we assumed to be 0:

$$\mathscr{D}_x^+ v_{i,j} = \frac{v_{i+1,j} - v_{i,j}}{h_{i+1}}. \tag{2.16}$$

With our choice of α, the boundaries are the same for both stages.

LOWER BOUNDARY

For the lower boundary, we find

$$\frac{v_{0,j-\alpha} - v_{0,j}}{\alpha k_j} = \frac{1}{2} \left(\mathscr{L}_{0,j} v_{i,j} + \mathscr{L}_{0,j} v_{0,j-\alpha} \right), \tag{2.17}$$

$$b_{0,j} v_{0,j-\alpha} + c_{0,j} v_{1,j-\alpha} = b_{0,j}^* v_{0,j} - c_{0,j} v_{1,j},$$

with

$$b_{0,j} = 1 + \frac{\alpha k_j}{2} \left(r_{0,j} + \frac{\mu_{0,j} x_0}{h_1} \right), \tag{2.18}$$

$$b_{0,j}^* = 1 - \frac{\alpha k_j}{2} \left(r_{0,j} + \frac{\mu_{0,j} x_0}{h_1} \right), \tag{2.19}$$

$$c_{0,j} = -\alpha k_j \frac{\mu_{0,j} x_0}{2 h_1}. \tag{2.20}$$

UPPER BOUNDARY

For the upper boundary, we have

$$a_{m,j} v_{m-1,j-\alpha} + b_{m,j} v_{m,j-\alpha} = -a_{m,j} v_{m-1,j} + b_{m,j}^* v_{m,j},$$

with:

$$a_{m,j} = \alpha k_j \frac{\mu_{m,j} x_m}{2 h_m}, \tag{2.21}$$

$$b_{m,j} = 1 + \frac{\alpha k_j}{2} \left(r_{m,j} - \frac{\mu_{m,j} x_m}{h_m} \right), \tag{2.22}$$

$$b_{m,j}^* = 1 - \frac{\alpha k_j}{2} \left(r_{m,j} - \frac{\mu_{m,j} x_m}{h_m} \right). \tag{2.23}$$

2.3. AMERICAN OPTION SPECIFICS

The early-exercise feature of the option adds a free boundary on top of the Black-Scholes partial differential equation. Let v be the option price, the following system of partial differential inequalities should be satified [122]:

$$\left.\begin{aligned}
\frac{\partial v}{\partial t}(x,t) + \mu(x,t)x\frac{\partial v}{\partial x}(x,t) + \frac{1}{2}\sigma(x,t)^2 x^2 \frac{\partial^2 v}{\partial x^2}(x,t) &\leq r(x,t)v(x,t) \\
\left(\frac{\partial v}{\partial t}(x,t) + \mu(x,t)x\frac{\partial v}{\partial x}(x,t) + \frac{1}{2}\sigma(x,t)^2 x^2 \frac{\partial^2 v}{\partial x^2}(x,t) - r(x,t)v(x,t)\right)(v-V) &= 0 \\
v &\geq V
\end{aligned}\right\} \tag{2.24}$$

Let M_j be the tridiagonal matrix with lower diagonal $a_{i,j}$ for $i \in \{1,...,m\}$, upper diagonal $c_{i,j}$ for $i \in \{0,...,m-1\}$ and main diagonal $b_{i,j}$ for $i \in \{0,...,m\}$, with $a_{i,j}$, $b_{i,j}$, $c_{i,j}$ defined by equations (2.10), (2.11), (2.12). Let us define $v_j = (v_{0,j},...,v_{m,j})$, $g_j = (g_{0,j},...,g_{m,j})$ with

$$g_{i,j} = -a_{i,j}v_{i-1,j} + b_{i,j}^* v_{i,j} - c_{i,j}v_{i+1,j},$$

and $h_j = (h_{0,j},...,h_{m,j})$ with

$$h_{i,j} = \frac{1}{2-\alpha}\left(\frac{1}{\alpha}v_{i,j-\alpha} - \frac{(1-\alpha)^2}{\alpha}v_{i,j}\right).$$

We discretize the linear complementarity problem (2.24) with TR-BDF2 stage by stage, for $j = n,...,1$:

$$\left.\begin{aligned}
M_j v_{j-\alpha} &\geq g_j \\
v_{j-\alpha} &\geq V \\
\left(M_j v_{j-\alpha} - g_j\right)^\top (v_{j-\alpha} - F) &= 0
\end{aligned}\right\} \quad \text{Trapezoidal stage}, \tag{2.25}$$

$$\left.\begin{aligned}
M_j v_{j-1} &\geq h_j \\
v_{j-1} &\geq V \\
\left(M_j v_{j-1} - h_j\right)^\top (v_{j-1} - V) &= 0
\end{aligned}\right\} \quad \text{BDF2 stage}. \tag{2.26}$$

Alternatively, we could solve the linear complementarity problem only in the BDF2 stage (2.26). While it might improve speed a little, it would however result in a larger error.

There are many ways to solve (2.25) and (2.26), the most popular being the Brennan-Schwartz algorithm [29] (however, with known shortcomings [111] - it does not work on the following payoff $V(x) = |x-K|$), Front-Tracking [165], the Penalty Method [159], Operator Splitting [101], and Projected SOR [198].

The simplest way is to solve the tridiagonal system without considering the free boundary and to then apply the early-exercise condition through

$$v_{j-\alpha} = \max(V, v_{j-\alpha}), \quad v_{j-1} = \max(V, v_{j-1}).$$

While this keeps the second-order accuracy for the explicit scheme, it is only first-order accurate in time in general [164].

As a higher-order method, for the sake of simplicity, we will only consider the Brennan-Schwartz algorithm. The results are similar with other solution techniques. In particular, we evaluated SOR. SOR has the disadvantage of a slightly increased complexity due to two additional parameters: the relaxation factor ω and the global error acceptance.

The Brennan-Schwartz method is only valid if the matrix M_j has the following properties [111]:

- the lower and upper diagonals are negative: $a_{i,j} \leq 0$ and $c_{i,j} \leq 0$ for $i \in \{1, ..., m-1\}$, $c_{0,j} \leq 0$, $a_{m,j} \leq 0$,

- the main diagonal is dominant: $a_{i,j} + b_{i,j} + c_{i,j} \geq 0$ for $i \in \{1, ..., m-1\}$, $b_{0,j} + c_{0,j} \geq 0$, $a_{m,j} + b_{m,j} \geq 0$ and $b_{i,j} > 0$ for $i \in \{0, ..., m\}$.

In other terms, M_j must be an irreducible Minkowski matrix. For our TR-BDF2 discretization, this translates to, for $i \in \{1, ..., m-1\}$,

$$-\frac{\sigma_{i,j}^2 x_i}{h_{i+1}} \leq \mu_{i,j} \leq \frac{\sigma_{i,j}^2 x_i}{h_i}, \tag{2.27}$$

$$0 \leq 1 + \frac{\alpha k_j}{2} r_{i,j}, \tag{2.28}$$

and for the boundaries:

$$\mu_{0,j} \geq 0, \tag{2.29}$$
$$\mu_{m,j} \leq 0. \tag{2.30}$$

Except for the boundaries, those conditions are almost always verified in practice. Furthermore, one can always make h_i small enough so that (2.27) holds. The Crank-Nicolson and backward Euler schemes would need to verify almost the same conditions, the only difference being the factor in front of r in Equation (2.28), which is anyway always verified for $r \geq 0$. For the boundaries, a possible solution to produce a Minkowski matrix is to use a Dirichlet condition at $x = x_m$ or $x = x_0$ depending on the sign of $\mu_{0,j}$ or $\mu_{m,j}$. Indeed, a Dirichlet boundary at $x = x_0$ will result in $c_{0,j} = 0$ and $b_{0,j} = 1$, a Dirichlet boundary at $x = x_m$ will result in $a_{m,j} = 0$ and $b_{m,j} = 1$.

In practice, the $\frac{\partial^2 v}{\partial x^2} = 0$ boundary conditions can be used and it is commonly observed that the Brennan-Schwartz algorithm still works. We have found no discernable error when compared to a solution solved by SOR for the American put option using various parameters, not even on a small grid, where the boundaries play an important role.

In the case of Bermudan options, one would use the standard tridiagonal solver [37] for non-exercisable dates, or alternatively set the SOR or Brennan-Schwartz solver lower boundary for the price to 0 instead of the payoff at maturity V. As the exercisable dates will be among the t_i and the first stage result does not correspond to one of those, the first stage will always be solved without considering the linear complementarity problem.

2.4. GREEKS STABILITY

2.4.1. GAMMA FOR A BERMUDAN PUT

In order to better understand what is happening with the American put option gamma we first look at the simpler case of the Bermudan put option. It is well-known that the Crank-Nicolson scheme may distort the greeks because of oscillations in the scheme [73], especially as the payoff at maturity has a discontinuity in its first derivative at the strike price. TR-BDF2 does not have this issue.

As an example, we give the gamma of a one-year Bermudan put option of strike $K = 100$ with spot $S = 100$, 40% volatility, 5% interest rate that can be exercised in six months and in one year. We choose the following boundaries for the grid:

$$x_m = Se^{3\sigma\sqrt{T}},$$
$$x_0 = Se^{-3\sigma\sqrt{T}}.$$

It corresponds to 3 standard deviations up and down the spot price. We also make sure that the strike is on the grid by slightly shifting the grid if necessary. The free boundary problem is solved by Brennan-Schwartz algorithm.

(a) Crank-Nicolson   (b) Rannacher   (c) TR-BDF2
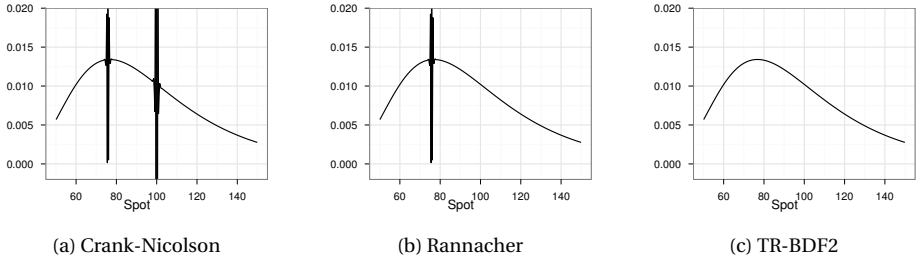
Figure 2.2: Gamma of an at-the-money Bermudan put option.

The Rannacher smoothing introduces two half steps of the backward Euler scheme at maturity, to smooth out the payoff function before the Crank-Nicolson time-marching scheme is employed[173]. When Rannacher smoothing is only applied at maturity, it does not fix all Crank-Nicolson oscillations. If we applied Rannacher smoothing at all Bermudan exercise dates, we would have a smooth gamma in a similar fashion to TR-BDF2. Contrary to TR-BDF2, for Bermudan options, the Rannacher smoothing requires the knowledge of the early-exercise dates to be efficient. D'Halluin et al. [46] observed the same phenomenon on callable bonds. This flexibility of TR-BDF2 can be important if one is required to solve other kinds of linear complementarity problems.

2.4.2. GAMMA FOR AN AMERICAN PUT

We compute the gamma of a one-year American put option of strike price $K = 160$ with spot value $S = 100$, 40% volatility, 5% interest rate on a grid composed of 500 space steps and 80 time steps. The option is therefore in the money. The boundary is set up the same way as in Subsection 2.4.1.

(a) Crank-Nicolson

(b) TR-BDF2

(c) Rannacher
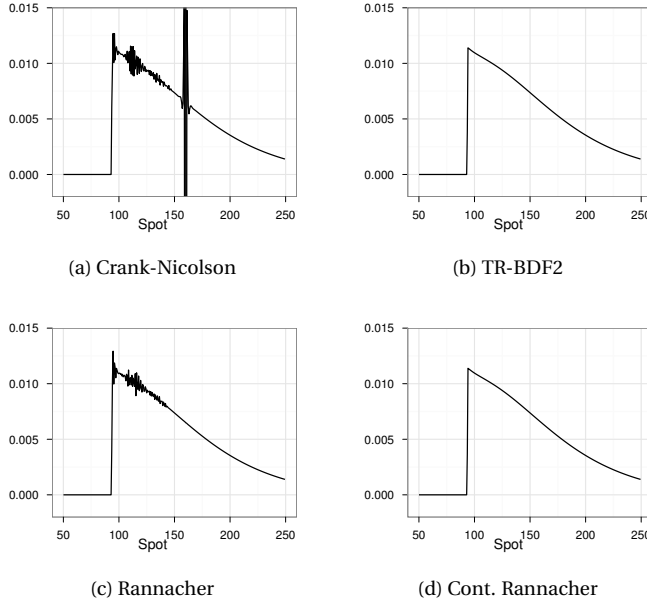
(d) Cont. Rannacher

Figure 2.3: Gamma of an In-The-Money American put option with strike at 160 and 80 time steps.

The gamma with TR-BDF2 is smooth while Crank-Nicolson presents oscillations at the payoff discontinuity.

The Rannacher smoothing works well for European options [73]: it produces smooth greeks and improves the convergence. However, this is not true for American (or Bermudan) options, as shown in Figures 2.2b and 2.3c.

If the Rannacher smoothing is only applied at maturity, some oscillations are left: the ones that correspond to the early-exercise boundary. In order to have smooth greeks for American options, one would need to add backward Euler steps after every potential discontinuity introduced by the early-exercise feature (see Figure 2.3d). We name this scheme *Continuous Rannacher*. The problem is that the *Continuous Rannacher* scheme loses one order of accuracy (see Figure 2.4).

2.5. CONVERGENCE

2.5.1. CONVERGENCE FOR A FIXED SPACE STEP

As O'Sullivan [164], we look at the convergence for a 1 year American put option of strike price $K = 100$ with a spot value $S = 100$, a discount rate of 5%, and a volatility of 20%. We fix the space step size at 1.0. This corresponds to 500 space steps. Note that this places the strike and the spot on the grid, which is important to avoid the introduction of additional errors from the payoff discretization in the grid [172].

We use the same theoretical value of 6.0874933186 as in their paper. We verified its

accuracy by an explicit scheme going progressively to 5 million time steps (6.087493609042786). Note that this is not the exact American option price because we have fixed the space step size. We compare the convergence of TR-BDF2 (named "TRBDF2"), Crank-Nicolson (named "CN") and Rannacher (named "RAN"), with the order-1 approximation of the free boundary as well as with the Brennan-Schwartz solver (named with prefix "BS_").

Finally, we also consider a simple Richardson extrapolation in time of the TR-BDF2 scheme solved by the order-1 method (named "RE_TRBDF2") in the spirit of [164].
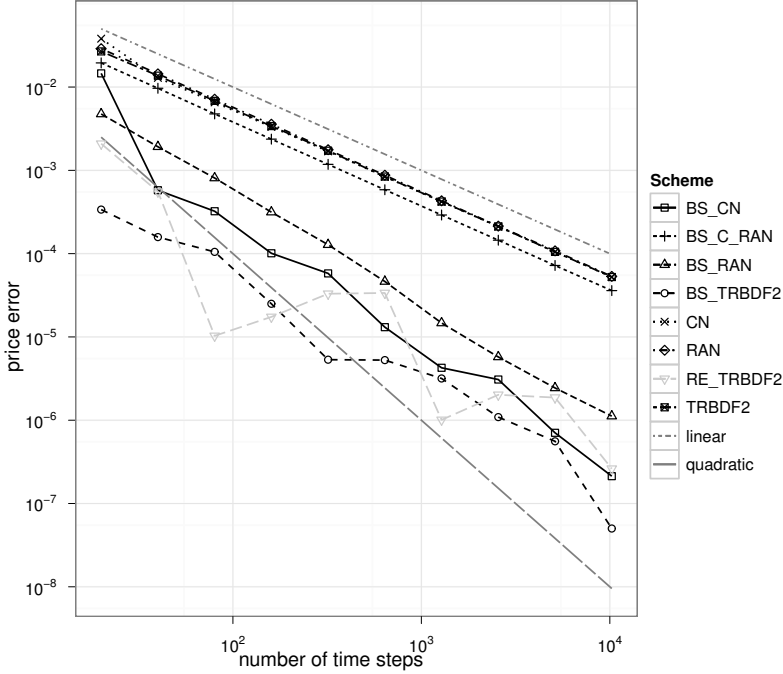
Figure 2.4: Convergence for an American put with a fixed space step. TR-BDF2 "TRBDF2", Crank-Nicolson "CN", Rannacher "RAN" and Continuous Rannacher "C_RAN", with the order-1 approximation of the free boundary as well as with the Brennan-Schwartz solver (with prefix "BS_").

From Table 2.A.1, we see that TR-BDF2 is about 1.5 times slower than Crank-Nicolson. This is because we have to solve a linear system twice per time step. However, it is always as accurate or more accurate than Crank-Nicolson. It is particularly more accurate than Crank-Nicolson and Rannacher when combined with a precise linear complementarity problem solver. The Richardson extrapolation allows to gain an order in magnitude for the convergence of the order-1 free boundary approximation method, although we can see some oscillations in the convergence.

2.5.2. ORDER OF CONVERGENCE

Like Forsyth and Vetzal [65], we look at the convergence on a successively refined grid in order to determine the global order of convergence. We use the same American option, with the same number of spacesteps and time steps as in [65]. The grid is uniform and varies in space from $x_0 = 0$ to $x_m = 350$. TR-BDF2 does not attain quadratic convergence but is not far from it: a quadratic convergence would correspond to a ratio of 4.0 in Table 2.1.

Spatial steps	Time steps	Value	Change	Ratio	Time(s)
		Rannacher with order-1 solver			
68	25	14.626460			2.82e-04
135	50	14.662090	3.56e-02		8.53e-04
269	100	14.672618	1.05e-02	3.4	2.40e-03
537	200	14.676338	3.72e-03	2.8	7.82e-03
1073	400	14.677771	1.43e-03	2.6	2.83e-02
		TR-BDF2 with order-1 solver			
68	25	14.631221			1.83e-03
135	50	14.663649	3.24e-02		6.76e-03
269	100	14.673209	9.56e-03	3.4	1.22e-02
537	200	14.676556	3.35e-03	2.9	1.00e-02
1073	400	14.677855	1.30e-03	2.6	3.80e-02
		Rannacher with Brennan-Schwartz solver			
68	25	14.635640			3.68e-04
135	50	14.667110	3.15e-02		7.82e-04
269	100	14.675363	8.25e-03	3.8	2.37e-03
537	200	14.677766	2.40e-03	3.4	8.48e-03
1073	400	14.678514	7.48e-04	3.2	4.00e-02
		TR-BDF2 with Brennan-Schwartz solver			
68	25	14.641161			3.09e-04
135	50	14.669421	2.83e-02		9.65e-04
269	100	14.676294	6.87e-03	4.1	3.16e-03
537	200	14.678149	1.85e-03	3.7	1.24e-02
1073	400	14.678668	5.19e-04	3.6	5.04e-02

Table 2.1: Value of an American put option, $T = .25$, $r = .10$, $K = 100$, $S = 100$. "Change" is the difference in the solution from the coarser grid. "Ratio" is the ratio of the changes on successive grids. Constant time steps. The strike is on the grid.

However, when the payoff at maturity is smoothed by averaging, as described in [172], the TR-BDF2 convergence decreases to nearly order $\frac{3}{2}$, even though the error is lower than without averaging (Table 2.A.2). This is likely because the error coming from the exercise boundary discontinuity dominates and is not quadratic. Still, even in this case, TR-BDF2 has better convergence than Rannacher time stepping.

We will see in the next section that the ratio of convergence also depends on the grid

geometry.

2.5.3. CONVERGENCE ON VARIOUS GRID GEOMETRIES

We now look at the convergence for a 1 year American put option of strike price $K = 100$ with a spot value $S = 100$, a discount rate of 5%, and a volatility of 40%. We use the same boundaries as in Subsection 2.4.1. Like Giles and Carter [73], on a log-uniform grid centered on the strike, we look at the maximum error in price and gamma as a function of the ratio $\lambda = \frac{m}{n}$ computed by TR-BDF2 and Rannacher, using the Brennan-Schwartz solver. The reference is an American option price obtained by an explicit scheme on a very fine grid (10K space steps and 10M time steps).

(a) Rannacher   (b) TR-BDF2
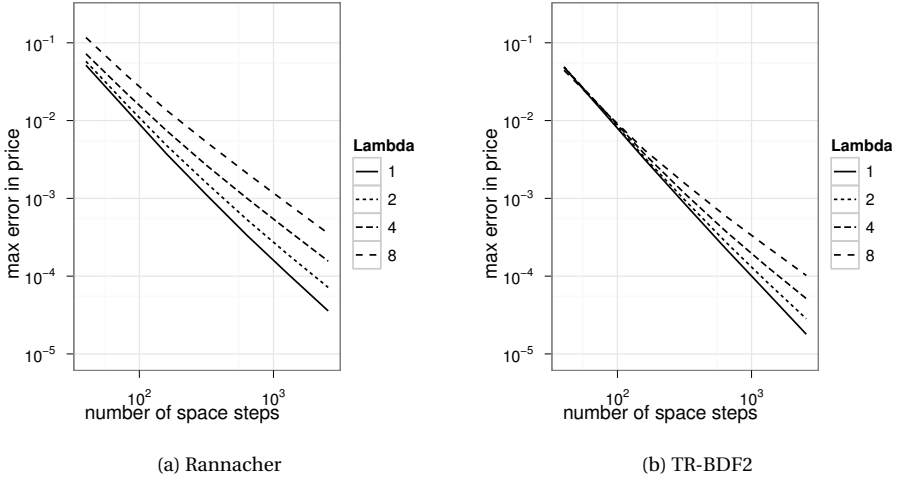
Figure 2.5: Maximum error in the price of an American put option with a fixed λ

The maximum price error is a little lower for the TR-BDF2 scheme, than for the Rannacher scheme (Figure 2.5). In both cases, the convergence decreases as λ increases, this is particularly clear in Table 2.A.3. It suggests that an adaptive time stepping strategy, like the one in [65] could be useful to restore quadratic convergence. Richardson extrapolation allows to increase the order of convergence, and is nearly quadratic even with the order-1 free boundary approximation and with smoothing of the payoff by averaging (see Table 2.A.4). It also is more effective for the TR-BDF2 scheme than for the Rannacher scheme.

The gamma graphs of Figure 2.6 reveal another important aspect of Rannacher time-stepping: the gamma computed with Rannacher smoothing does not converge when λ is high. In our settings this happens with a ratio $\lambda \geq 4$. This divergence corresponds to the oscillations related to the exercise boundary that we observed in Figure 2.3c. The maximum gamma error does not happen at the strike price, unlike the European option case.
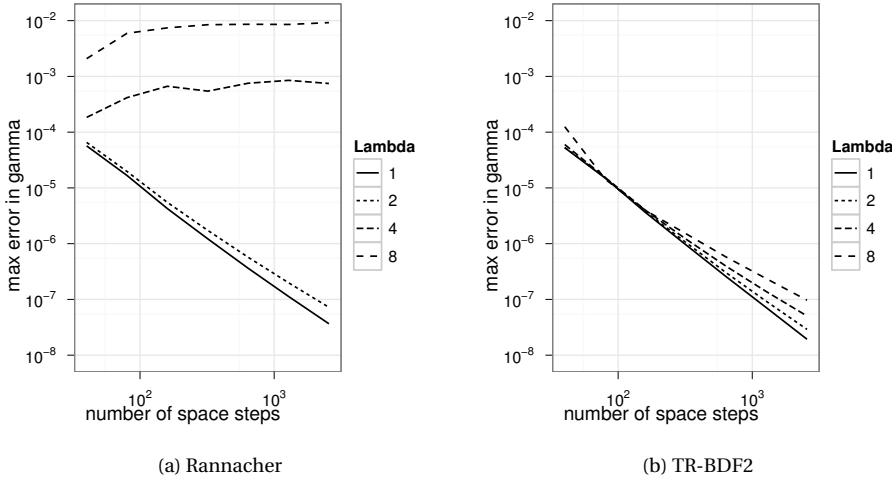
Figure 2.6: Maximum error in the gamma of an American put option with a fixed λ

In contrast, the gamma computed with TR-BDF2 always converges, independently of the grid ratio λ. This is because TR-BDF2 is L-Stable, while Rannacher time-stepping is only A-stable.

It is common for more complex payoffs to use a non-uniform grid with more points near the payoff discontinuities [188]: typically for a barrier option, a higher concentration of points around the barrier will speed up convergence significantly. With such a grid, Crank-Nicolson oscillations will be problematic and seriously impact the accuracy of the greeks as there will be regions where λ is high. TR-BDF2 does not have this defect.

2.6. WHEN BDF2 BREAKS
The second-order backward difference (BDF2) scheme, another popular L-stable scheme, while simpler than TR-BDF2 has been shown not to be a good candidate in option pricing in general [199]. We give the example of a simple Bermudan option, where BDF2 breaks down.

We consider a one-year Bermudan put option of strike price $K = 100$, with spot value $S = 100$, 40% volatility , 5% interest rate, which can be exercised in six months and in one year. The theoretical price of 13.386303 has been computed using an explicit finite difference scheme with more than 4 millions time steps and 5120 space steps. BDF2 is initialized with one backward Euler step.

Brennan-Schwartz and the order-1 free boundary approximation have the same convergence because there is only one date where the linear complementarity problem is solved.

BDF2 converges, but to a wrong price (13.506 instead of 13.386)! TR-BDF2 has no such issue and converges quadratically, like Crank-Nicolson, to the correct price. This

(a) TR-BDF2 vs BDF2

(b) Brennan-Schwartz vs order-1 free boundary approximation
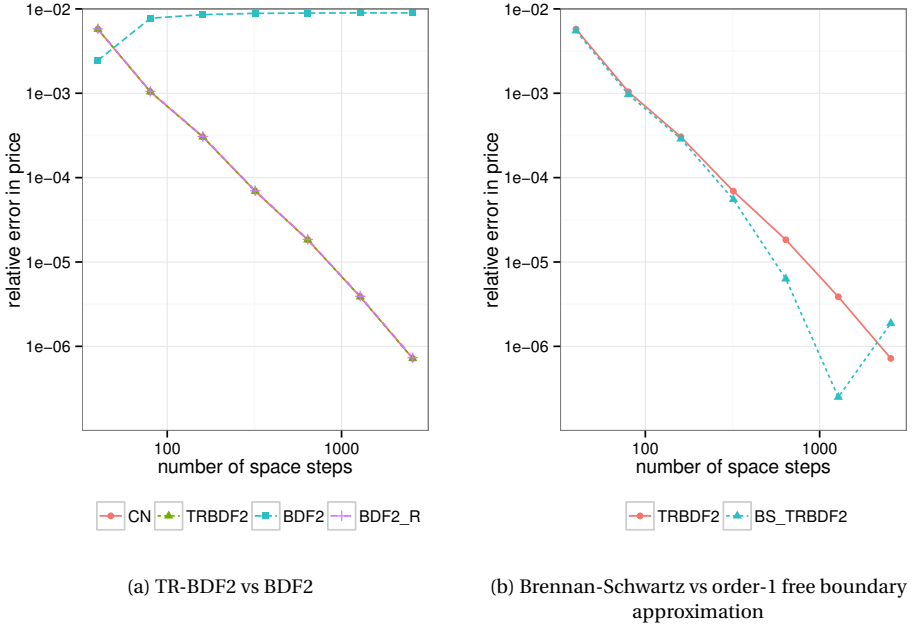
Figure 2.7: Relative error of the price of a Bermudan put option on a grid with $\Lambda = 0.5$

example shows a key difference between BDF2, a multistep scheme, and TR-BDF2, a 1-step scheme.

In this simple example, there is a simple fix for BDF2, one needs to restart BDF2 just before the early-exercise date, i.e. to apply a backward Euler step instead of a BDF2 step at this date. We call this scheme $BDF2_R$. Another similar example where naive BDF2 fails is the case of an American option with discrete dividends, as the exercise boundary is then discontinuous. The authors in [163] also fix this by restarting the scheme at each dividend date. All multistep schemes will suffer from these issues. For a standard American option, BDF2 will converge to the correct result, but with lower convergence than Crank-Nicolson or TR-BDF2.

In more complex cases like the shout option in [199], the fix for BDF2 might not be so trivial.

2.7. HAMILTON-JACOBI-BELLMAN PDE

Contrary to Backward Euler, TR-BDF2 is not a monotone scheme. In theory, this could be a problem when dealing with nonlinear Hamilton-Jacobi-Bellman (HJB) partial differential equations. The uncertain volatility model developed in [17] is an example of an HJB equation in finance. It supposes that the volatility is uncertain but bounded between a minimum volatility σ_{min} and a maximum volatility σ_{max}. Under this model one can find the prices of a derivative product for a worst long strategy or a best long strategy.

The optimal control problem is given by:

$$\frac{\partial v}{\partial t}(x,t) - \sup_{\sigma \in \hat{\sigma}}\{\mu(x,t)x\frac{\partial v}{\partial x} + \frac{1}{2}\sigma^2 x^2\frac{\partial^2 v}{\partial x^2} - r(x,t)v(x,t)\} = 0,, \tag{2.31}$$

where x is the underlying price, μ is the underlying drift, σ its volatility and r the interest rate, $\hat{\sigma} = \{\sigma_{min}, \sigma_{max}\}$ and $V(x) = v(x, t_n)$ the option payoff at maturity.

2

Spatial steps	Time steps	Value	Change	Ratio
		TR-BDF2		
60	25	2.299723		
120	50	2.303857	4.13e-03	
240	100	2.298947	-4.91e-03	-0.8
480	200	2.298005	-9.42e-04	5.2
960	400	2.297767	-2.37e-04	4.0
1920	800	2.297705	-6.21e-05	3.8
		Backward Euler		
60	25	2.362552		
120	50	2.333157	-2.94e-02	
240	100	2.313157	-2.00e-02	1.5
480	200	2.305099	-8.06e-03	2.5
960	400	2.301314	-3.78e-03	2.1
1920	800	2.299479	-1.83e-03	2.1

Table 2.2: Value of a butterfly spread option. "Change" is the difference in the solution from the coarser grid. "Ratio" is the ratio of the changes on successive grids. Constant time steps.
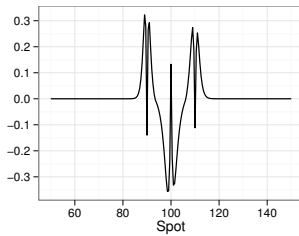
(a) Gamma after the first time step
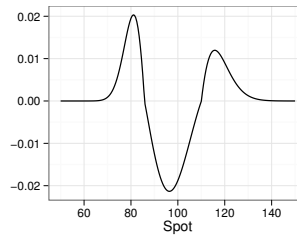
(b) Gamma at $t = 0$

Figure 2.8: Gamma of a butterfly spread option with $m = 400$ spacesteps and $n = 20$ time steps on a uniform grid from $x_0 = 0$ to $x_m = 200$

Like Pooley, Forsyth and Vetzal [171], we price a butterfly spread option under the uncertain volatility model using the same parameters and using a uniform grid in space from $x_0 = 0$ to $x_m = 300$ doubling the size in both the space dimension and the time

dimension in order to look at the convergence. A butterfly spread corresponds to a long position in 2 calls at strike K_1 and K_2 and a short position in 2 calls at strike $\frac{K_1+K_2}{2}$. Our butterfly spread option is defined with the strikes $K_1 = 90$ and $K_2 = 110$ expiring at $T = 0.25$ years. The interest rate is $r = 0.1$, and the volatility is between $\sigma_{min} = 0.15$ and $\sigma_{max} = 0.25$. We solve the HJB via the same Newton method as in [171], only replacing the scheme by TR-BDF2. This means that we solve the non-linearity in the same Newton iteration for the 2 stages. We limit the number of Newton iterations to 3 per time step, otherwise, because TR-BDF2 is not monotone, the Newton method might not converge when the time step is large.

Table 2.2 shows that in practice, TR-BDF2 converges. The price given in [171] for the worst long strategy of the same option is 2.29769. In this case, it converges better than the Backward Euler scheme, even if the gamma has major oscillations after the first time step (Figure 2.8a) when the ratio of time steps over spacesteps λ is high. This is because with time, the oscillations are quickly damped, in contrast to the Crank-Nicolson scheme.

2.8. EXACT CALIBRATION TO DISCOUNT BONDS AND FORWARD PRICES

Most academic papers and books use a constant drift when describing the valuation of financial derivatives. Andersen et al. considers the effect of non-constant rates and dividends in the theta finite difference method in the context of the local volatility model [7]. In particular, the authors show that one should not use the rates coming from the curves directly. In order to reproduce the bond and forward contract prices, the rates should be converted according to the chosen discretization for the finite difference scheme (in their case, the theta scheme) to take into account the effect of discretization.

2.8.1. EXACT BOND PRICE

Let $P_j = P(0, t_j)$ be the prices of zero-coupon bonds maturing at times t_j. They satisfy the Black-Scholes partial differential equation with terminal payoff $P(S) = \$1$. We consider at time step t_j the bond maturing at t_{j+1} of price:

$$P(t_j, t_{j+1}) = \frac{P(0, j+1)}{P(0, j)} = \frac{P_{j+1}}{P_j}. \tag{2.32}$$

At t_{j+1}, $P(t_{j+1}, t_{j+1}) = 1$. The bond price P is independent of the asset S.

A naive approach is to rely on the continuous PDE solution directly, leading to the inaccurate forward bond rate between t_j and t_{j+1}.:

$$r(t_j) = -\frac{1}{k_j} \ln\left(\frac{P_{j+1}}{P_j}\right), \tag{2.33}$$

where $k_j = t_j - t_{j-1}$ is the time step size between times t_{j-1} and t_j.

This however does not take the effect of the discretization on the bond prices into account. To achieve exact bond prices, we require that the bond prices satisfy the finite difference equations. For TR-BDF2, we wish the bond prices to follow the Equations (2.4)

and (2.5) corresponding to each stage, i.e.

$$\frac{P_{j+1}}{P^*} = 1 - \frac{\alpha k_j}{2}\left(r_j + r_j\frac{P_{j+1}}{P^*}\right), \tag{2.34}$$

and

$$\frac{P_{j+1}}{P_j} = \frac{1}{2-\alpha}\left(\frac{1}{\alpha}\frac{P_{j+1}}{P^*} - \frac{(1-\alpha)^2}{\alpha} - (1-\alpha)k_jr_j\frac{P_{j+1}}{P_j})\right). \tag{2.35}$$

Eliminating $P^* = \frac{1+\frac{1}{2}\alpha k_j r_j}{1-\frac{1}{2}\alpha k_j r_j}P_{j+1}$ leads to a quadratic equation in r_j:

$$\frac{1}{2}\alpha(1-\alpha)\frac{P_{j+1}}{P_j}k_j^2 r_j^2 + \frac{1}{2}\left((2-\alpha^2)\frac{P_{j+1}}{P_j} + 1 + (1-\alpha)^2\right)k_j r_j + (2-\alpha)\left(\frac{P_{j+1}}{P_j}-1\right) = 0.$$

Let $a = \frac{1}{2}\alpha(1-\alpha)\frac{P_{j+1}}{P_j}$, $b = \frac{1}{2}\left((2-\alpha^2)\frac{P_{j+1}}{P_j} + 1 + (1-\alpha)^2\right)$, and $c = (2-\alpha)\left(\frac{P_{j+1}}{P_j}-1\right)$, the unique positive solution is:

$$r_j = \frac{-b+\sqrt{b^2-4ac}}{2ak_j}. \tag{2.36}$$

With this choice of r_j, the value of a contract paying \$1 is exact at every node of the finite difference grid: the scheme is in a sense perfectly calibrated to the discount curve.

2.8.2. EXACT FORWARD PRICE

We consider here a contract at time t_j which pays out $v_{j+1}(S) = S$ at time t_{j+1}. The value of this contract at t_j is:

$$v_j(S) = SP(t_j, t_{j+1})e^{\int_{t_j}^{t_{j+1}}\mu(u)du} = S\frac{P_{j+1}}{P_j}\frac{F_{j+1}}{F_j}, \tag{2.37}$$

where $F_j(S) = Se^{\int_0^{t_j}\mu(u)du}$ is the forward to t_j. The derivatives of this contract are:

$$\frac{\partial^2 v_j}{\partial S^2}(S) = 0,$$

$$\frac{\partial v_j}{\partial S}(S) = \frac{P_{j+1}}{P_j}\frac{F_{j+1}}{F_j}.$$

Similarly to the bond case, a naive approach is to rely on the direct solution of the Black-Scholes PDE, leading to the growth rate:

$$\mu(t_j) = \frac{1}{k_j}\ln\left(\frac{F_{j+1}}{F_j}\right). \tag{2.38}$$

Instead, for the TR-BDF2 scheme, we wish the forward contract prices to satisfy both Equations (2.4) and (2.5), i.e.

$$v^* = v_{j+1} - \frac{\alpha k_j}{2}\left((r_j-\mu_j)v_{j+1} + (r_j-\mu_j)v^*\right), \tag{2.39}$$

and

$$v_j = \frac{1}{2-\alpha}\left(\frac{1}{\alpha}v^* - \frac{(1-\alpha)^2}{\alpha}v_{j+1} - (1-\alpha)k_j(r_j - \mu_j)v_j\right). \tag{2.40}$$

This leads to the same quadratic equation as for the bonds, but replacing $\frac{P_{j+1}}{P_j}$ by $\frac{v_j}{v_{j+1}}$ and r_j by $r_j - \mu_j$. The solution is:

$$r_j - \mu_j = \frac{-b' + \sqrt{b'^2 - 4a'c'}}{2a'k_j} \tag{2.41}$$

with $a' = \frac{1}{2}\alpha(1-\alpha)\frac{P_{j+1}}{P_j}\frac{F_{j+1}}{F_j}$, $b' = \frac{1}{2}\left((2-\alpha^2)\frac{P_{j+1}}{P_j}\frac{F_{j+1}}{F_j} + 1 + (1-\alpha)^2\right)$, and $c' = (2-\alpha)\left(\frac{P_{j+1}}{P_j}\frac{F_{j+1}}{F_j} - 1\right)$. Then

$$\mu_j = r_j - \frac{-b' + \sqrt{b'^2 - 4a'c'}}{2a'k_j}. \tag{2.42}$$

Table 2.3: Price for a forward of maturity 10 years of strike $k = 100$ under TR-BDF2 with constant rates on a logarithmic grid of 10 time steps and 50 points per time step. "Raw" denotes the direct use of the constant rates in the scheme discretization, and "Discrete" denote the use of the discrete rates r_j and μ_j.

r	μ	Spot	Price	Error
			Raw rates	
0.05	0.00	100	-3.8E-14	3.8E-14
0.05	0.00	110	6.064999	3.1E-4
0.05	0.02	100	13.431025	2.3E-3
0.05	0.02	110	20.839127	2.2E-3
			Discrete rates	
0.05	0.00	100	-4.6E-14	4.6E-14
0.05	0.00	110	6.0653066	8.5E-14
0.05	0.02	100	13.428756	2.4E-13
0.05	0.02	110	20.836938	3.4E-13

With this choice of μ_j and r_j, forward contract prices are exact at every node of the finite difference grid. This is confirmed by the numerical results presented in Table 2.3.

2.8.3. PUT-CALL PARITY

Let V_C^j, V_P^j be the solutions of the Equations (2.4) and (2.5) at time t_j with respective final payoffs $|S - K|^+$ and $|K - S|^+$. At maturity t_n, the put-call parity relation $V_C^n - V_P^n = S - K$ holds as long as the final payoffs are not smoothed so that at each node S_i, we have $|S_i - K|^+ - |K - S_i|^+ = S_i - K$. At t_{n-1}, by linearity of the operator $\mathscr{L}$, we have:

$$V_C^* - V_P^* = V_C^n - V_P^n - \frac{\alpha k_j}{2}\left(\mathscr{L}(V_C^n - V_P^n) + \mathscr{L}(V_C^* - V_P^*)\right), \tag{2.43}$$

$$V_C^{n-1} - V_P^{n-1} = \frac{1}{2-\alpha}\left(\frac{1}{\alpha}(V_C^* - V_P^*) - \frac{(1-\alpha)^2}{\alpha}(V_C^n - V_P^n) - (1-\alpha)k_{n-1}\mathcal{L}(V_C^{n-1} - V_P^{n-1})\right).$$
(2.44)

In other words, $V_C^{n-1} - V_P^{n-1}$ is the solution of (2.4) and (2.5) at time t_{n-1} with terminal payoff $K - S$. One can apply the same logic recursively to find that $V_C^0 - V_P^0$ is the solution of (2.4) and (2.5) at time t_0 with terminal payoff $K - S$. A forward contract of strike K and maturity t_n is solution the Black-Scholes PDE with the same terminal payoff. Therefore $V_C^0 - V_P^0$ is exactly the discretized forward contract price.

As the forward contract price is exactly preserved at each node by the TR-BDF2 discretization (Section (2.8.2)), $V_C^0 - V_P^0$ is exactly the forward contract price at t_0, and the put-call parity relation holds. Table 2.4 confirms that the put-call parity is preserved in

Table 2.4: Put-call parity for options of maturity 10 years of strike $k = 100$ under TR-BDF2 with constant rates $r = 0.05$ and $\mu = 0.02$ on a logarithmic grid of 10 time steps and 50 points per time step.

Spot	Call Price V_C	Put Price V_P	Parity $V_C - V_P$	Parity Error
90.0	18.990086	12.969512	6.020574	3.3E-13
100.0	24.241044	10.812288	13.428756	3.4E-13
120.0	35.824349	7.579229	28.245121	2.4E-13

practice on a non-uniform, shifted grid.

2.9. CONCLUSION

In this chapter, we have shown how the TR-BDF2 scheme can be applied to option pricing. It does not suffer from Crank-Nicolson oscillations problems, that are particularly visible in the greeks. It is more resilient to the grid geometry and to the underlying PDE in general. Moreover the Rannacher time-marching, while an interesting fix of the Crank-Nicolson discretization scheme for European options, does not work as well for American options.

2.A. REFERENCE VALUES

Steps	Scheme	Price	Error	Time(s)	Steps	Price	Error	Time(s)
20	CN	6.0494286	3.81e-02	0.00044	640	6.0866566	8.37e-04	0.01362
	RAN	6.0586066	2.89e-02	0.00046		6.0866193	8.74e-04	0.01335
	TRBDF2	6.0607239	2.68e-02	0.00064		6.0866508	8.42e-04	0.02056
	BS_CN	6.0728822	1.46e-02	0.00054		6.0874802	1.31e-05	0.01779
	BS_RAN	6.0827446	4.75e-03	0.00060		6.0874470	4.63e-05	0.01673
	BS_C_RAN	6.0679704	1.95e-02	0.00083		6.0869083	5.85e-04	0.02587
	BS_TRBDF2	6.0871552	3.38e-04	0.00085		6.0874881	5.27e-06	0.02713
	RE_TRBDF2	6.0853986	2.09e-03	0.00097		6.0875271	3.37e-05	0.03049
40	CN	6.0746091	1.29e-02	0.00084	1280	6.0870732	4.20e-04	0.02637
	RAN	6.0730455	1.44e-02	0.00086		6.0870623	4.31e-04	0.02659
	TRBDF2	6.0738304	1.37e-02	0.00125		6.0870716	4.22e-04	0.04036
	BS_CN	6.0869160	5.77e-04	0.00106		6.0874891	4.26e-06	0.03425
	BS_RAN	6.0855687	1.92e-03	0.00117		6.0874786	1.47e-05	0.03315
	BS_C_RAN	6.0778191	9.67e-03	0.00177		6.0872025	2.91e-04	0.05264
	BS_TRBDF2	6.0873354	1.58e-04	0.00185		6.0874901	3.17e-06	0.05439
	RE_TRBDF2	6.0869369	5.56e-04	0.00212		6.0874923	1.01e-06	0.06063
80	CN	6.0809446	6.55e-03	0.00182	2560	6.0872819	2.11e-04	0.05278
	RAN	6.0803442	7.15e-03	0.00202		6.0872790	2.14e-04	0.05242
	TRBDF2	6.0806670	6.83e-03	0.00277		6.0872814	2.12e-04	0.08018
	BS_CN	6.0871705	3.23e-04	0.00245		6.0874902	3.08e-06	0.06633
	BS_RAN	6.0866839	8.09e-04	0.00236		6.0874876	5.75e-06	0.07576
	BS_C_RAN	6.0827291	4.76e-03	0.00376		6.0873484	1.45e-04	0.10143
	BS_TRBDF2	6.0873887	1.05e-04	0.00379		6.0874922	1.09e-06	0.11260
	RE_TRBDF2	6.0875036	1.03e-05	0.00422		6.0874913	2.02e-06	0.12679
160	CN	6.0841717	3.32e-03	0.00346	5120	6.0873885	1.05e-04	0.10427
	RAN	6.0839144	3.58e-03	0.00333		6.0873856	1.08e-04	0.10411
	TRBDF2	6.0840889	3.40e-03	0.00498		6.0873883	1.05e-04	0.15996
	BS_CN	6.0873924	1.01e-04	0.00404		6.0874926	7.06e-07	0.13479
	BS_RAN	6.0871779	3.15e-04	0.00419		6.0874909	2.44e-06	0.13545
	BS_C_RAN	6.0851193	2.37e-03	0.00617		6.0874212	7.21e-05	0.20462
	BS_TRBDF2	6.0874683	2.50e-05	0.00658		6.0874939	5.58e-07	0.22144
	RE_TRBDF2	6.0875107	1.74e-05	0.00793		6.0874952	1.87e-06	0.23932
320	CN	6.0858019	1.69e-03	0.00643	10240	6.0874410	5.23e-05	0.20819
	RAN	6.0857199	1.77e-03	0.00660		6.0874401	5.33e-05	0.20794
	TRBDF2	6.0857746	1.72e-03	0.00992		6.0874409	5.24e-05	0.31736
	BS_CN	6.0874354	5.79e-05	0.00885		6.0874931	2.13e-07	0.27313
	BS_RAN	6.0873654	1.28e-04	0.00811		6.0874922	1.12e-06	0.29584
	BS_C_RAN	6.0863136	1.18e-03	0.01345		6.0874573	3.60e-05	0.41086
	BS_TRBDF2	6.0874880	5.33e-06	0.01389		6.0874933	5.01e-08	0.44853
	RE_TRBDF2	6.0874603	3.30e-05	0.01554		6.0874936	2.62e-07	0.47768

Table 2.A.1: TR-BDF2 and Crank-Nicolson convergence for an American put, the reference value of 6.0874933186 has been obtained via [164]. CN, RAN, TRBDF2 denote respectively the Crank-Nicolson, Rannacher and TR-BDF2 schemes with the order-1 approximation for the free boundary problem. BS_CN, BS_C_RAN, BS_TRBDF2, BS_RAN are respectively the Crank-Nicolson, Rannacher (applied at each time-step), TR-BDF2 and Rannacher schemes solved by Brennan-Schwarz. RE_TRBDF2 is Richardson extrapolation in time applied to TR-BDF2 with the order-1 approximation.

Spacesteps	Timesteps	Value	Change	Ratio	Time(s)
		Rannacher with order-1 solver			
68	25	14.656895			3.31e-04
135	50	14.669132	1.22e-02		8.82e-04
269	100	14.674421	5.29e-03	2.3	2.61e-03
537	200	14.676791	2.37e-03	2.2	7.46e-03
1073	400	14.677882	1.09e-03	2.2	2.81e-02
		TR-BDF2 with order-1 solver			
68	25	14.661263			2.03e-03
135	50	14.670690	9.43e-03		6.80e-03
269	100	14.675000	4.31e-03	2.2	1.59e-02
537	200	14.677007	2.01e-03	2.1	9.90e-03
1073	400	14.677966	9.60e-04	2.1	3.66e-02
		Rannacher with Brennan-Schwartz solver			
68	25	14.665532			3.57e-04
135	50	14.674220	8.69e-03		8.60e-04
269	100	14.677160	2.94e-03	3.0	2.72e-03
537	200	14.678218	1.06e-03	2.8	8.83e-03
1073	400	14.678625	4.07e-04	2.6	3.27e-02
		TR-BDF2 with Brennan-Schwartz solver			
68	25	14.671270			4.04e-04
135	50	14.676364	5.09e-03		1.19e-03
269	100	14.678075	1.71e-03	3.0	3.90e-03
537	200	14.678598	5.23e-04	3.3	1.53e-02
1073	400	14.678779	1.81e-04	2.9	4.91e-02

Table 2.A.2: Value of an American put option, $T = .25$, $r = .10$, $K = 100$, $S = 100$. "Change" is the difference in the solution from the coarser grid. "Ratio" is the ratio of the changes on successive grids. Constant time steps. The payoff is smoothed at maturity.

2

Spacesteps	Timesteps	Max Gamma Error	Max Error	Time(s)	Ratio
		Rannacher, $\lambda = 1$			
40	40	6.01e-05	1.80e-02	7.40e-03	
80	80	1.33e-05	5.47e-03	2.70e-02	3.3
160	160	2.38e-06	1.67e-03	5.58e-02	3.3
320	320	7.41e-07	5.69e-04	9.78e-03	2.9
640	640	2.43e-07	2.01e-04	3.86e-02	2.8
1280	1280	8.36e-08	7.41e-05	1.32e-01	2.7
2560	2560	2.92e-08	2.75e-05	4.84e-01	2.7
		Rannacher, $\lambda = 4$			
40	10	1.44e-04	3.75e-02	2.48e-04	
80	20	3.77e-04	1.38e-02	4.24e-04	2.7
160	40	6.66e-04	5.29e-03	9.97e-04	2.6
320	80	5.57e-04	2.09e-03	3.05e-03	2.5
640	160	7.50e-04	8.58e-04	1.04e-02	2.4
1280	320	8.50e-04	3.56e-04	3.27e-02	2.4
2560	640	7.45e-04	1.48e-04	1.17e-01	2.4
		TR-BDF2, $\lambda = 1$			
40	40	6.27e-05	1.51e-02	3.24e-03	
80	80	1.43e-05	4.17e-03	1.12e-02	3.6
160	160	2.67e-06	1.16e-03	1.36e-02	3.6
320	320	4.77e-07	3.33e-04	1.20e-02	3.5
640	640	1.36e-07	1.00e-04	4.76e-02	3.3
1280	1280	4.07e-08	3.17e-05	1.70e-01	3.1
2560	2560	1.18e-08	9.81e-06	6.84e-01	3.2
		TR-BDF2, $\lambda = 4$			
40	10	7.11e-05	1.46e-02	1.54e-04	
80	20	1.18e-05	4.89e-03	2.88e-04	3.0
160	40	2.10e-06	1.61e-03	7.95e-04	3.0
320	80	7.25e-07	6.16e-04	2.84e-03	2.6
640	160	2.73e-07	2.48e-04	1.25e-02	2.5
1280	320	1.08e-07	1.03e-04	4.31e-02	2.4
2560	640	4.30e-08	4.32e-05	1.76e-01	2.4

Table 2.A.3: Maximum error in the price and gamma of an American put option, $T = .25$, $r = .05$, $K = 100$, $S = 100$, $\sigma = 0.4$. Ratio is the ratio of the error in price on successive grids. λ is the ratio spacesteps over time steps. The linear complementarity problem is solved by Brennan-Schwartz.

Spacesteps	Timesteps	Max Gamma Error	Max Error	Time(s)	Ratio
		Rannacher with Richardson Extrapolation, $\lambda = 1$			
40	40	1.20e-04	1.46e-02	1.29e-03	
80	80	3.17e-05	3.56e-03	4.11e-03	4.1
160	160	5.45e-06	9.71e-04	9.81e-03	3.7
320	320	9.29e-07	2.40e-04	1.18e-02	4.1
640	640	1.49e-07	5.41e-05	3.76e-02	4.4
1280	1280	6.11e-08	1.28e-05	1.45e-01	4.2
2560	2560	1.08e-07	2.43e-06	5.80e-01	5.2
		Rannacher with Richardson Extrapolation, $\lambda = 4$			
40	10	9.52e-03	3.62e-02	2.33e-04	
80	20	2.30e-02	1.90e-02	3.25e-04	1.9
160	40	5.95e-02	9.43e-03	7.92e-04	2.0
320	80	8.45e-02	3.35e-03	2.62e-03	2.8
640	160	1.18e-01	1.19e-03	9.56e-03	2.8
1280	320	1.80e-01	4.30e-04	3.73e-02	2.8
2560	640	2.44e-01	1.54e-04	1.45e-01	2.8
		TR-BDF2 with Richardson Extrapolation, $\lambda = 1$			
40	40	1.12e-04	1.53e-02	1.94e-03	
80	80	4.34e-05	4.00e-03	9.82e-03	3.8
160	160	1.71e-06	1.08e-03	8.93e-03	3.7
320	320	9.35e-07	2.82e-04	1.41e-02	3.8
640	640	1.08e-07	7.07e-05	5.04e-02	4.0
1280	1280	2.71e-08	1.79e-05	1.97e-01	4.0
2560	2560	5.11e-09	2.82e-06	7.89e-01	6.3
		TR-BDF2 with Richardson Extrapolation, $\lambda = 4$			
40	10	2.26e-03	2.20e-02	2.36e-04	
80	20	3.13e-04	5.58e-03	3.61e-04	3.9
160	40	5.89e-06	1.95e-03	9.90e-04	2.9
320	80	7.45e-07	5.25e-04	3.32e-03	3.7
640	160	2.16e-07	1.63e-04	1.31e-02	3.2
1280	320	6.06e-08	4.96e-05	4.99e-02	3.3
2560	640	1.55e-08	1.33e-05	1.97e-01	3.7

Table 2.A.4: Maximum error in the price and gamma of an American put option, $T = .25$, $r = .05$, $K = 100$, $S = 100$, $\sigma = 0.4$. Ratio is the ratio of the error in price on successive grids. λ is the ratio spacesteps over time steps. The linear complementarity problem is solved by the order-1 approximation and the payoff is smoothed by averaging at maturity. Richardson extrapolation is applied using a value computed with half of the time steps.

3

POSITIVE SECOND-ORDER FINITE DIFFERENCE METHODS FOR FOKKER-PLANCK EQUATIONS WITH DIRAC INITIAL DATA

One approach to price financial derivatives in an arbitrage free manner is to start from the probability density function. For many models, it is possible to find an expansion of the density that follows a Fokker-Planck partial differential equation. In order to keep the arbitrage-free property numerically, it is particularly important to use a positivity preserving finite difference scheme. With a discontinuous initial condition like a Dirac delta function, many schemes will produce oscillations or negative densities. This chapter analyzes the behavior of a few simple schemes related to the backward Euler scheme, namely the BDF2, Lawson-Morris and Lawson-Swayne schemes on the specific problem of a diffusion with Dirac delta initial condition. The case of the arbitrage free SABR model for interest rate derivatives is then evaluated.

Keywords: SABR · Fokker-Planck · Dirac · BDF2 · finite difference method.

3.1. INTRODUCTION

One approach to price financial derivatives in an arbitrage free manner is to start from the probability density function. For many models, it is possible to find an expansion of the density that follows a Fokker-Planck partial differential equation (PDE), for example following Andreasen and Huge [13] or Hagan et al. [84].

The first-order backward Euler scheme (BDF1) is known to be monotone and positivity preserving. Those are particularly important properties when the partial differential equation represents a density with a discontinuous initial condition like a Dirac delta function. Many higher-order finite difference schemes will produce oscillations or negative densities, including the popular A-stable Crank-Nicolson scheme.

The second-order backward difference scheme (BDF2) or even a simple Richardson extrapolation are not positivity preserving in a general setting [27, 96]. However, on the more specific problem of a Fokker-Planck partial differential equation, we will see that much less restricting conditions for positivity are possible.

This chapter analyzes the behavior of a few simple schemes related to the backward Euler, Crank-Nicolson, BDF2, Lawson-Morris schemes, as well as the *L*-stable Lawson-Swayne and TR-BDF2 schemes on the specific problem of a diffusion with Dirac delta initial condition. For the sake of analytical tractability, a constant diffusion coefficient and infinite boundaries are considered. Our analysis is similar to a von Neumann stability analysis. We are however not interested in the amplification factor relating the L2-

norm of the solution at subsequent time steps, but we focus our analysis on the discrete probability density values at the Dirac delta location, and whether they stay positive, or whether they oscillate. While this seems overly restrictive, we find that in practice, it explains well the phenomenology of more realistic Fokker-Planck PDEs, for example, the arbitrage-free SABR PDE of [84, 131], under the various time stepping schemes.

3.2. BACKWARD EULER ATTENUATION OF A DIRAC INITIAL CONDITION

We focus our analysis on a Fokker-Planck like partial differential equation (PDE):

$$\frac{\partial Q}{\partial t} = \frac{1}{2}\sigma^2 \frac{\partial^2 Q}{\partial x^2}, \tag{3.1}$$

with $\lim_{t \to 0} Q(x,t) = \delta(x-f)$ and δ is the Dirac delta function. σ corresponds to a constant volatility parameter.

Let us consider a uniform discretization defined by (x_j), $j \in \{-m,..,m\}$, $h = x_j - x_{j-1}$, and define the central second difference operator $\mathcal{D}_x^2$ as:

$$\mathcal{D}_x^2 f_{j,l} = \frac{f_{j+1,l} - 2f_{j,l} + f_{j-1,l}}{h^2}. \tag{3.2}$$

The backward Euler finite difference scheme results in

$$(I - \frac{1}{2}\sigma^2 k \mathcal{D}^2)Q^{n+1} = Q^n, \tag{3.3}$$

with initial conditions $Q_0^0 = \frac{1}{h}$, $Q_j^0 = 0$, for $j \neq 0$, and where $k = t_{n+1} - t_n$ is the time step size betwenn t_n and t_{n+1}, Q^n is the vector of discrete probability density values.

The mixed discrete/continuous Fourier transform pair reads [73, 185]

$$Q_j^n = \frac{1}{2\pi h} \int_{-\pi}^{\pi} \hat{Q}^n(u) e^{iju} \, du, \tag{3.4}$$

$$\hat{Q}^n(u) = h \sum_{j=-\infty}^{+\infty} Q_j^n e^{-iju}. \tag{3.5}$$

The Fourier transform of equation (3.3) is given by

$$\hat{Q}^{n+1}(u) = \frac{1}{1 + 2\alpha \sin^2(\frac{u}{2})} \hat{Q}^n(u), \tag{3.6}$$

with $\alpha = \frac{\sigma^2 k}{h^2}$. Let us apply the inverse transform to go back to Q at the first time step.

$$Q_j^1 = \frac{1}{2\pi h} \int_{-\pi}^{\pi} \frac{Q_j^0(u)}{1 + 2\alpha \sin^2(\frac{u}{2})} e^{iju} \, du. \tag{3.7}$$

In particular, for the first step, we have at the spike ($j = 0$)

$$Q_0^1 = \frac{1}{2\pi h} \int_{-\pi}^{\pi} \frac{1}{1 + 2\alpha \sin^2(\frac{u}{2})} \, du = \frac{1}{h\sqrt{2\alpha + 1}}. \tag{3.8}$$

And for the second step, we obtain

$$Q_0^2 = \frac{1}{2\pi h} \int_{-\pi}^{\pi} \frac{1}{\left(1 + 2\alpha \sin^2\left(\frac{u}{2}\right)\right)^2} \, du = \frac{(1+\alpha)}{h(2\alpha+1)^{\frac{3}{2}}}. \tag{3.9}$$

Of course, we notice that Q_0^1, Q_0^2 are strictly positive for any $\alpha > 0$.

3.3. SECOND-ORDER SCHEMES

3.3.1. NEGATIVE DENSITY WITH CRANK-NICOLSON SCHEME

The trapezoidal method (Crank-Nicolson scheme) can be expressed as [137].

$$(I - \frac{1}{4}\sigma^2 k \mathcal{D}^2)Q^{n+1} = (I + \frac{1}{4}\sigma^2 k \mathcal{D}^2)Q^n. \tag{3.10}$$

Applying the Fourier transform for this equation leads to

$$Q_0^1 = \frac{1}{2\pi h} \int_{-\pi}^{\pi} \frac{1 - \alpha \sin^2\left(\frac{u}{2}\right)}{1 + \alpha \sin^2\left(\frac{u}{2}\right)} \, du = \frac{1}{h}\left(\frac{2}{\sqrt{\alpha+1}} - 1\right) \tag{3.11}$$

The density at the first step Q_0^1 will be negative when $\alpha > 3$, or equivalently when

$$h^2 < \frac{1}{3}\sigma^2 k. \tag{3.12}$$

This condition is quite restrictive: in order to avoid a negative density at the spike, at the first time step, the number of time steps must increase quadratically with the number of spatial steps, very much like the explicit Euler scheme.

3.3.2. RANNACHER SMOOTHING

In order to fix the Crank-Nicolson scheme issues with discontinuous initial data, a smoothing with two half time steps of BDF1 from $t = t_0$ to $t = t_{\frac{1}{2}}$ and $t_{\frac{1}{2}}$ to t_1 before applying the Crank-Nicolson scheme is proposed in [173]. From Equations (3.9) and (3.11), we deduce the exact discrete probability density after the first Crank-Nicolson step, at $t = t_2$:

$$Q_0^2 = \frac{1}{2\pi h} \int_{-\pi}^{\pi} \frac{1 - \alpha \sin^2\left(\frac{u}{2}\right)}{\left(1 + \alpha \sin^2\left(\frac{u}{2}\right)\right)^3} \, du = \frac{1}{h} \frac{1 + \frac{1}{2}\alpha + \frac{1}{4}\alpha^2}{(1+\alpha)^{\frac{5}{2}}}, \tag{3.13}$$

and therefore Q_0^2 is positive for all $\alpha \geq 0$. By iteration, the exact discrete probability density at t_n is

$$Q_0^n = \frac{1}{2\pi h} \int_{-\pi}^{\pi} \frac{\left(1 - \alpha \sin^2\left(\frac{u}{2}\right)\right)^{n-1}}{\left(1 + \alpha \sin^2\left(\frac{u}{2}\right)\right)^{n+1}} \, du. \tag{3.14}$$

It can be shown that Q_0^n is always positive. Note that the oscillations related to the discontinuous initial conditions may still be present (see Figure 3.3.1). Giles and Carter [73] recommend four half time steps for a proper damping (see Figure 3.3.2).

(a) Absolute value

(b) Difference between consecutive steps
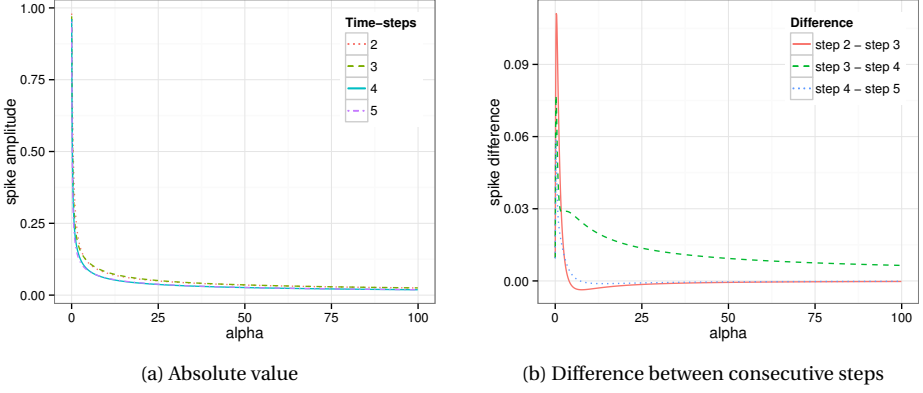
Figure 3.3.1: Density at the spike $j = 0$ for the Rannacher scheme with 2 half-steps BDF1

(a) Absolute value

(b) Difference between consecutive steps
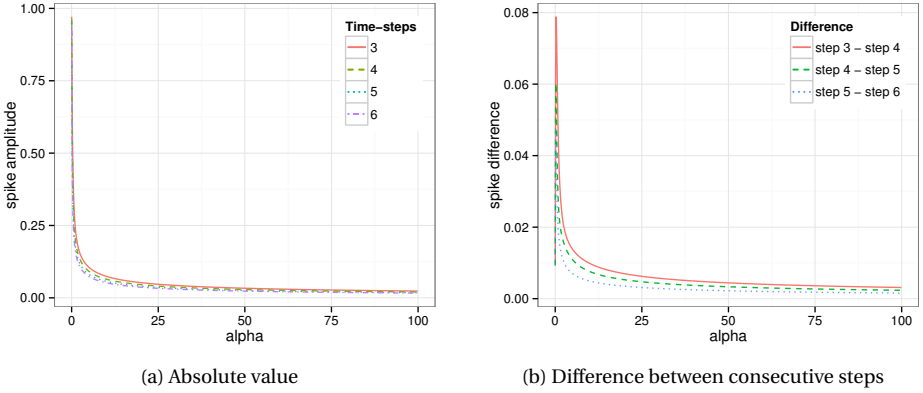
Figure 3.3.2: Density at the spike $j = 0$ for the Rannacher scheme with 4 half-steps BDF1

3.3.3. SQUARE-ROOT CRANK-NICOLSON SCHEME

Reisinger [174] proposes a $\tau = \sqrt{t}$ time transform in order to follow the natural time of the Brownian motion. Equation (3.1) becomes

$$\frac{\partial Q}{\partial \tau} = \sigma^2 \tau \frac{\partial^2 Q}{\partial x^2} \, . \tag{3.15}$$

Let $k = k_n = \tau_{n+1} - \tau_n$, the Crank-Nicolson scheme results in the following linear system

$$(I - \frac{1}{2}\sigma^2 \tau_{n+1} k \mathscr{D}^2)Q^{n+1} = (I + \frac{1}{2}\sigma^2 \tau_n k \mathscr{D}^2)Q^n \, . \tag{3.16}$$

Applying the Fourier transform to this equation leads to

$$Q_0^n = \frac{1}{2\pi h} \int_{-\pi}^{\pi} \prod_{j=0}^{n-1} \frac{1 - 2\alpha\tau_j \sin^2(\frac{u}{2})}{1 + 2\alpha\tau_{j+1} \sin^2(\frac{u}{2})} \, \mathrm{d}u$$

$$= \frac{1}{2\pi h} \int_{-\pi}^{\pi} \prod_{j=0}^{n-1} \frac{1 - 2\alpha j k \sin^2(\frac{u}{2})}{1 + 2\alpha(j+1)k \sin^2(\frac{u}{2})} \, \mathrm{d}u$$

$$= \frac{1}{2\pi h} \int_{-\pi}^{\pi} \frac{1}{1 + 2\alpha n k \sin^2(\frac{u}{2})} \prod_{j=1}^{n-1} \frac{1 - 2\alpha j k \sin^2(\frac{u}{2})}{1 + 2\alpha j k \sin^2(\frac{u}{2})} \, \mathrm{d}u. \quad (3.17)$$

And after the first time step, the exact discrete probability density is given by

$$Q_0^1 = \frac{1}{h} \left(\frac{1}{\sqrt{2\alpha\tau_1 + 1}} \right). \quad (3.18)$$

As $\tau_0 = 0$, Q_0^1 is always positive. Note that BDF1 applied to Equation (3.15) would have resulted in the exact same Q^1 as the right-hand side simply equals Q^0 at the first time step.

The probability density at the second time step reads

$$Q_0^2 = \frac{1}{h} \left(\frac{3}{\sqrt{4\alpha k + 1}} - \frac{2}{\sqrt{2\alpha k + 1}} \right). \quad (3.19)$$

As $\frac{3}{2} > \frac{2}{\sqrt{2}}$, and Q_0^2 is a decreasing function in k, Q_0^2 is always positive. At the third time step,

$$Q_0^3 = \frac{1}{h} \left(\frac{10}{\sqrt{6\alpha k + 1}} + \frac{3}{\sqrt{2\alpha k + 1}} - \frac{12}{\sqrt{4\alpha k + 1}} \right). \quad (3.20)$$

As $\frac{10}{\sqrt{6}} + \frac{3}{\sqrt{2}} - 6 > 0$, and Q_0^3 is a decreasing function in k, Q_0^3 is always positive.

It can be shown that the density is always positive at the spike, at every step, independently of the time step size: $Q_0^n > 0$.

The density however oscillates slightly at the spike when $\alpha k > 2$ (see Figure 3.3.3). Reisinger [174] suggests that choosing $\alpha k \leq \frac{1}{2}$ will result in a non-oscillating scheme, a much nicer condition than with the standard Crank-Nicolson scheme as it depends only on the ratio $\frac{k}{h}$ instead of $\frac{k}{h^2}$.

3.3.4. POSITIVE DENSITY WITH BDF2 SCHEME

The second-order backward difference scheme (BDF2) reads [137]

$$3Q^{n+2} - 4Q^{n+1} + Q^n = \sigma^2 k \mathscr{D}_x^2 Q^{n+2}, \quad (3.21)$$

or equivalently,

$$\left(I - \frac{\sigma^2 k}{3} \mathscr{D}_x^2 \right) Q^{n+2} = \frac{4}{3} Q^{n+1} - \frac{1}{3} Q^n. \quad (3.22)$$

The first step relies on backward Euler (BDF1). The second step can be seen as another backward Euler step of size $\frac{2k}{3}$ on a different initial condition. The density will be guaranteed positive if the right-hand side is positive, that is if

$$4Q_j^{n+1} - Q_j^n > 0. \quad (3.23)$$

(a) Absolute value

(b) Difference between consecutive steps
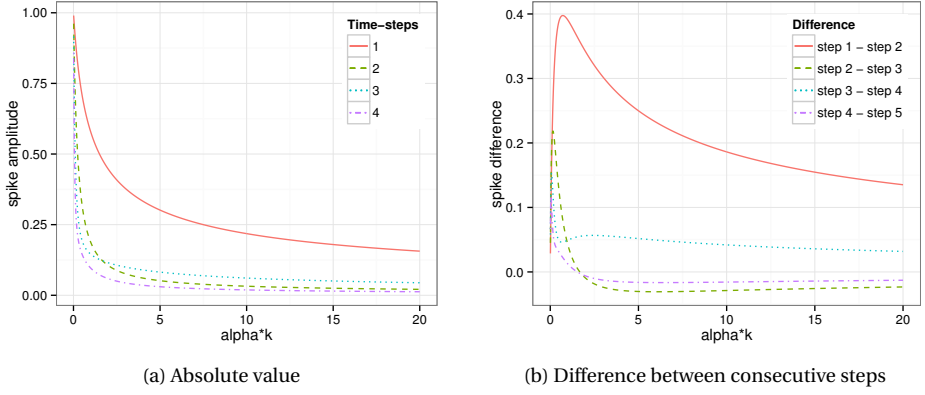
Figure 3.3.3: Density at the spike $j = 0$ for the time-changed Crank-Nicolson scheme

In the specific case of the Dirac delta initial condition, this translates to

$$Q_0^1 > \frac{1}{4h},$$ (3.24)

at the first time step. Q_j^1 corresponds to a backward Euler step and from Equation (3.8), the above inequality is equivalent to

$$h^2 < \frac{2}{15}\sigma^2 k.$$ (3.25)

This is very restrictive, similarly as for the Crank-Nicolson scheme. Instead of starting from the inequality (3.23), we may compute the exact discrete value by applying the Fourier transform to Equation (3.22). This leads to

$$\left(1 + \frac{4\alpha}{3}\sin^2\frac{u}{2}\right)\hat{Q}_0^2 = \frac{4}{3}\hat{Q}_0^1 - \frac{1}{3}\hat{Q}_0^0,$$ (3.26)

where $\hat{Q}_0^1$ is the backward Euler value obtained in Equation (3.8) and $\hat{Q}_0^0 = 1$ for a Dirac delta function. We then obtain

$$
\begin{aligned}
Q_0^2 &= \frac{1}{6\pi h}\int_{-\pi}^{\pi}\left(\frac{4}{1 + 2\alpha\sin^2\frac{u}{2}} - 1\right)\frac{1}{1 + \frac{4\alpha}{3}\sin^2\frac{u}{2}}\,\mathrm{d}u \\
&= \frac{1}{h}\left(\frac{4}{\sqrt{1 + 2\alpha}} - \frac{3}{\sqrt{1 + \frac{4}{3}\alpha}}\right).
\end{aligned}
$$ (3.27)

It can be easily shown that $Q_0^2 > 0, \forall \alpha \in \mathbb{R}^+$ (see Figure 3.3.4).
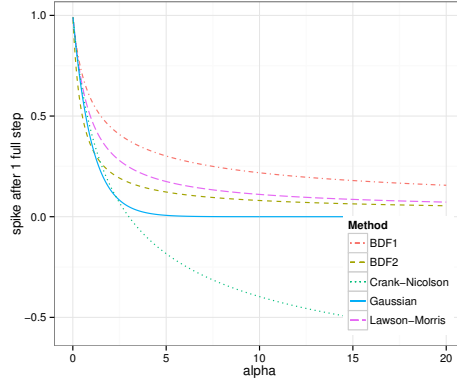
Figure 3.3.4: Density at the spike $j = 0$ after one full step

3.3.5. POSITIVE DENSITY WITH LAWSON-MORRIS SCHEME AND RICHARD-SON EXTRAPOLATION

The Lawson-Morris scheme [124] consists in applying locally, at each step, a Richardson extrapolation [177] on the BDF1 scheme. Between t_{n-1} and t_n, we compute the solution $Q^{n,k}$ implied by one time step of size k in the BDF1 scheme, and the solution $Q^{2n,\frac{k}{2}}$ implied by one time step of size $\frac{k}{2}$ to compute

$$Q^n = 2Q^{2n,\frac{k}{2}} - Q^{n,k}. \tag{3.28}$$

On the problem with the Dirac delta initial condition, we apply Equation (3.8) to obtain the exact value at the first time step

$$Q_0^1 = \frac{1}{h}\left(2\frac{1+\frac{1}{2}\alpha}{(\alpha+1)^{\frac{3}{2}}} - \frac{1}{(2\alpha+1)^{\frac{1}{2}}}\right) = \frac{1}{h}\left(\frac{2+\alpha}{(\alpha+1)^{\frac{3}{2}}} - \frac{1}{(2\alpha+1)^{\frac{1}{2}}}\right). \tag{3.29}$$

It can be easily shown that $Q_0^1 > 0, \forall \alpha \in \mathbb{R}^+$ (see Figure 3.3.4).

3.3.6. L-STABLE SCHEMES

The definition of L-stability implies that $Q_0^1 \to 0$ when $\alpha \to +\infty$ [56].

LAWSON-SWAYNE SCHEME

Let $b = 1 - \frac{\sqrt{2}}{2}$, the Lawson-Swayne scheme consists in applying two implicit Euler steps with time step of bk and an extrapolation on the values at those two steps [125]:

$$\left(I - \frac{1}{2}b\sigma^2 k\mathscr{D}^2\right)Q^{n+b} = Q^n, \tag{3.30}$$

$$\left(I - \frac{1}{2}b\sigma^2 k\mathscr{D}^2\right)Q^{n+2b} = Q^{n+b}, \tag{3.31}$$

$$Q^{n+1} = (\sqrt{2}+1)Q^{n+2b} - \sqrt{2}Q^{n+b}. \tag{3.32}$$

We apply the Fourier transform to Equations (3.30), (3.31), (3.32) and use the BDF1 Equations (3.8) and (3.9) to obtain the exact discrete probability density after the first time step

$$
\begin{aligned}
Q_0^1 &= \frac{1}{2\pi h} \int_{-\pi}^{\pi} \frac{\sqrt{2}+1}{\left(1+2b\alpha\sin^2(\frac{u}{2})\right)^2} - \frac{\sqrt{2}}{1+2b\alpha\sin^2(\frac{u}{2})} \, du \\
&= \frac{(\sqrt{2}+1)(1+b\alpha)}{h\,(2b\alpha+1)^{\frac{3}{2}}} - \frac{\sqrt{2}}{h\sqrt{2b\alpha+1}} \\
&= \frac{1-b\alpha(\sqrt{2}-1)}{h\,(2b\alpha+1)^{\frac{3}{2}}}\,.
\end{aligned}
\tag{3.33}
$$

The density is however negative when $\alpha > \frac{2}{3\sqrt{2}-4}$.

TR-BDF2 scheme

The TR-BDF2 scheme is a two-stage method where the first stage consists in applying the (weighted) trapezoidal rule (the Crank-Nicolson scheme) and the second stage consists in applying the second-order backward difference scheme (BDF2) on the first stage result and the first stage initial input [19, 137]:

$$
\left(I - \frac{1}{2}b\sigma^2 k\mathscr{D}^2\right)Q^{n+2b} = \left(I + \frac{1}{2}b\sigma^2 k\mathscr{D}^2\right)Q^n\,,
\tag{3.34}
$$

$$
\left(I - \frac{1}{2}\frac{1-2b}{2-2b}\sigma^2 k\mathscr{D}^2\right)Q^{n+1} = \frac{1}{2b(2-2b)}Q^{n+2b} - \frac{(1-2b)^2}{2b(2-2b)}Q^n\,.
\tag{3.35}
$$

The choice $b = 1 - \frac{\sqrt{2}}{2}$ gives proportional Jacobians and results in the best stability among all $b \in \mathbb{R}$ [48]. With this specific choice, the scheme reads

$$
\left(I - \frac{1}{2}b\sigma^2 k\mathscr{D}^2\right)Q^{n+2b} = \left(I + \frac{1}{2}b\sigma^2 k\mathscr{D}^2\right)Q^n\,,
\tag{3.36}
$$

$$
\left(I - \frac{1}{2}b\sigma^2 k\mathscr{D}^2\right)Q^{n+1} = \frac{1}{2}(\sqrt{2}+1)Q^{n+2b} - \frac{1}{2}(\sqrt{2}-1)Q^n\,.
\tag{3.37}
$$

Let $A = \left(I - \frac{1}{2}b\sigma^2 k\mathscr{D}^2\right)$. If we multiply the last stage of the Lawson-Swayne scheme (Equation 3.32) by A^2 and use Equations (3.30) and (3.31), we obtain

$$
A^2 Q^{n+1} = \left[(\sqrt{2}+1)I - \sqrt{2}A\right]Q^n\,.
\tag{3.38}
$$

If we multiply the last step of the TR-BDF2 scheme (Equation 3.37) by A and use Equation (3.36), we obtain

$$
\begin{aligned}
A^2 Q^{n+1} &= \frac{1}{2}(\sqrt{2}+1)\,[2I - A]\,Q^n - \frac{1}{2}(\sqrt{2}-1)AQ^n \\
&= \left[(\sqrt{2}+1)I - \sqrt{2}A\right]Q^n\,.
\end{aligned}
\tag{3.39}
$$

The density is thus exactly the same as with the Lawson-Swayne scheme with this specific choice of b. The schemes are equivalent when the volatility σ is time-independent.

POSITIVE DENSITY AFTER THE SECOND STEP

Under the Lawson-Swayne scheme, the density at the spike for the time step n is:

$$Q_0^n = \frac{1}{2\pi h} \int_{-\pi}^{\pi} \left[\frac{\sqrt{2}+1}{\left(1+2b\alpha\sin^2(\frac{u}{2})\right)^2} - \frac{\sqrt{2}}{1+2b\alpha\sin^2(\frac{u}{2})} \right]^n \mathrm{d}u. \tag{3.40}$$

At the second time step (and all even time steps), the density at the spike will be positive as the integrand is positive. It turns out that already at the third step, the density at the spike stays positive (see Figure 3.3.5a), for any positive α. Furthermore, there is no

(a) Absolute value

(b) Difference between consecutive steps
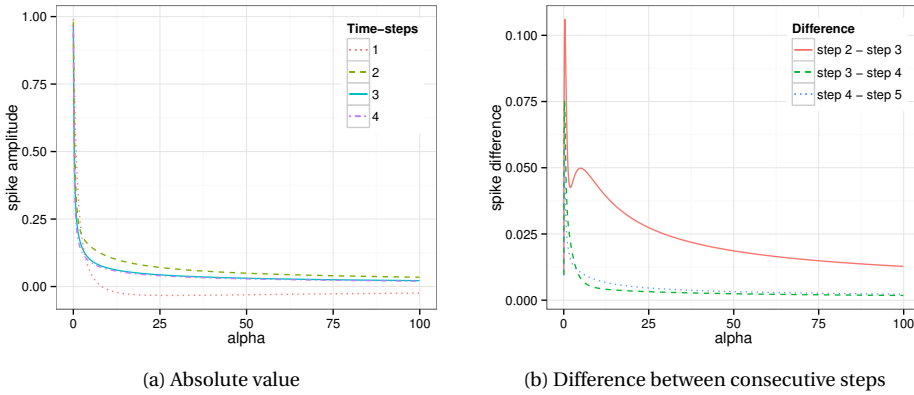
Figure 3.3.5: Density at the spike $j = 0$ for Lawson-Swayne and TR-BDF2

oscillation after the second time step (Figure 3.3.5b).

3.4. CONCLUSION

On the simple problem of a diffusion with a constant volatility and a Dirac delta initial condition, the BDF2, Lawson-Morris and BDF1 Richardson extrapolation schemes preserve the positivity of the density at the spike at every time step, for any time step size. The Lawson-Swayne and TR-BDF2 schemes preserve the positivity from the second time step onwards, for any time step size. Finally, the Rannacher smoothing also preserves positivity with an initialization of two half time steps of BDF1, but requires four half time steps of BDF1 to overcome the oscillations at the spike.

The conjecture that those results stay valid away from the spike is presented in the following appendix. Further refinements are left for future research.

3.A. BDF2 SCHEME GLOBAL POSITIVITY

We focused so far on the positivity at the spike, let's look here at the positivity everywhere, starting with the second time step. We have:

$$Q_j^2 = \frac{1}{3\pi h} \int_0^\pi \left(\frac{4}{1 + 2\alpha \sin^2 \frac{u}{2}} - 1 \right) \frac{1}{1 + \frac{4\alpha}{3} \sin^2 \frac{u}{2}} \cos(ju)\, du. \tag{3.41}$$

We know that when α is small, Q_j is positive as the scheme becomes monotone. When α is large, let us define $u_0 = 2 \arcsin \sqrt{\frac{3}{2\alpha}}$, with $0 < u_0 < \pi$. This specific value of u makes the integrand of equation (3.41) to be zero. Let us consider the case where $u_0 < \frac{\pi}{2}$, we have then

$$3\pi h Q_j^2 \geq \int_0^{u_0} \left(\frac{4}{1 + 2\alpha \sin^2 \frac{u}{2}} - 1 \right) \frac{1}{1 + \frac{4\alpha}{3} \sin^2 \frac{u}{2}} \cos(ju_0)\, du - \int_{u_0}^\pi \frac{1}{1 + \frac{4\alpha}{3} \sin^2 \frac{u}{2}}\, du$$

$$\geq \frac{14}{\sqrt{4\alpha + 1}} \arctan \frac{\sqrt{4\alpha + 1} \sin \frac{u_0}{2}}{\cos \frac{u_0}{2}} \cos(ju_0) - \frac{8}{\sqrt{2\alpha + 1}} \arctan \frac{\sqrt{2\alpha + 1} \sin \frac{u_0}{2}}{\cos \frac{u_0}{2}} \cos(ju_0)$$

$$- \frac{\pi}{\sqrt{4\alpha + 1}} + \frac{2}{\sqrt{4\alpha + 1}} \arctan \frac{\sqrt{4\alpha + 1} \sin \frac{u_0}{2}}{\cos \frac{u_0}{2}} = Q_L.$$

When $\alpha \to +\infty$, $\arctan \frac{\sqrt{4\alpha+1} \sin \frac{u_0}{2}}{\cos \frac{u_0}{2}} \to \arctan(\sqrt{6})$, $\arctan \frac{\sqrt{2\alpha+1} \sin \frac{u_0}{2}}{\cos \frac{u_0}{2}} \to \arctan(\sqrt{3})$ and the right hand side Q_L behaves like

$$Q_L \sim \left(8 \arctan(\sqrt{6}) - \frac{8}{\sqrt{2}} \arctan(\sqrt{3}) - \frac{\pi}{2} \right) \frac{1}{\sqrt{\alpha}}. \tag{3.42}$$

The right hand side is greater than $1.97096 \frac{1}{\sqrt{\alpha}}$ and therefore $Q_j^2 > 0$ for sufficiently large α for any j.

3.B. LAWSON-MORRIS SCHEME GLOBAL POSITIVITY

$$Q_j^1 = \frac{1}{\pi h} \int_0^\pi \left[\frac{2}{\left(1 + \alpha \sin^2(\frac{u}{2}) \right)^2} - \frac{1}{1 + 2\alpha \sin^2(\frac{u}{2})} \right] \cos(ju)\, du. \tag{3.43}$$

We proceed similarly as with the BDF2 scheme and consider $u_0 = 2 \arcsin \sqrt{\frac{1 + \sqrt{2}}{\alpha}}$ that makes the integrand zero, $u_0 \in (0, \pi)$. Let us consider α large enough so that $u_0 \in (0, \frac{\pi}{2})$,
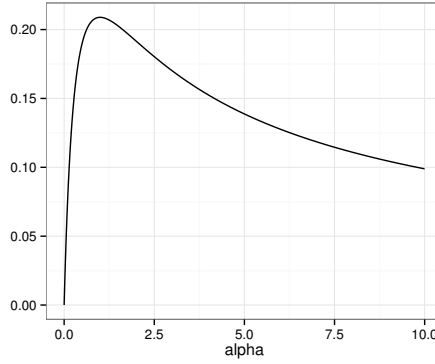
Figure 3.A.1: BDF2 scaled density hQ_j^2 with $j = 1$. Other j give a similar shape.

$$\pi h Q_j^1 \geq \int_0^{u_0} \left[\frac{2}{\left(1 + \alpha \sin^2(\frac{u}{2})\right)^2} - \frac{1}{1 + 2\alpha \sin^2(\frac{u}{2})} \right] \cos(j u_0) \, \mathrm{d}u$$

$$+ \int_{u_0}^{\pi} \frac{2}{(1+\alpha)^2} - \frac{1}{1 + 2\alpha \sin^2(\frac{u}{2})} \, \mathrm{d}u = Q_L$$

The right-hand side Q_L can be computed in closed form:

$$Q_L = +2 \frac{\sqrt{\alpha + 1}(\alpha + 2)\left(\alpha \sin^2(\frac{u_0}{2}) + 1\right) \arctan\left(\sqrt{\alpha + 1}\tan(\frac{u_0}{2})\right)}{(\alpha + 1)^2 + \alpha(\alpha + 1)^2 \sin^2(\frac{u_0}{2})} \cos(j u_0)$$

$$+ 2 \frac{\alpha \cos(\frac{u_0}{2}) \sin(\frac{u_0}{2})}{(\alpha + 1) + \alpha(\alpha + 1)\sin^2(\frac{u_0}{2})} \cos(j u_0)$$

$$- \frac{\pi}{\sqrt{2\alpha + 1}} + \frac{2(\pi - u_0)}{(1 + \alpha)^2}.$$

When $\alpha \to +\infty$,

$$Q_L \sim \frac{2(2 + \sqrt{2}) \arctan(\sqrt{1 + \sqrt{2}}) + 2\sqrt{1 + \sqrt{2}}}{(2 + \sqrt{2})\sqrt{\alpha}} - \frac{\pi}{\sqrt{2\alpha}}. \tag{3.44}$$

The right-hand side is greater than $\frac{0.6866}{\sqrt{\alpha}}$ and therefore Q_j^1 is positive for sufficiently large α.

4

FINITE DIFFERENCE TECHNIQUES FOR THE ARBITRAGE-FREE SABR MODEL

In the current low rates environment, the classic SABR formula used to compute option implied volatilities lead to arbitrage. Hagan et al. recently proposed a new arbitrage-free SABR solution, based on a finite difference discretization of an expansion of the probability density function. They rely on a Crank-Nicolson discretization, which can lead to undesirable oscillations in the option price. In this chapter, we apply a variety of second-order finite difference schemes to the SABR arbitrage-free density problem and explore alternative formulations. It is found that the TR-BDF2 and Lawson-Swayne schemes stand out on this problem in terms of stability and speed. The probability density formulation is the most stable and benefits greatly from a variable transformation. A partial differential equation is also derived for the so-called free-boundary SABR model, which allows for negative interest rates without any additional shift parameter, leading to a new arbitrage-free solution for this model. Finally, the free-boundary model behavior is analyzed.

Keywords: stochastic volatility · SABR · arbitrage · TR-BDF2 · Crank-Nicolson · finite difference method · finance.

4.1. INTRODUCTION

It is now well-known that the original SABR analytic formula from Hagan et al. [85] used to compute option implied volatility is not arbitrage-free as the probability density can become negative for low strike prices and long maturities. Given the current low rates environment, many authors have proposed various improvements to the original formula [23, 114, 162, 167]. A single step finite difference method is proposed by Andreasen and Huge in [13], which leads to an arbitrage-free 'SABR-like' model. Whilst the approach from Andreasen and Huge converges for short maturities to the original SABR analytic formula, it is (deliberately) different for longer expiries, even at the money. Through an expansion of the probability density, Doust [51] describes another arbitrage-free SABR method, but the required absorption probability involves costly numerical computations.

Hagan et al. [84] recently proposed a new arbitrage-free SABR solution, based on a finite difference discretization of the probability density. This approach provides a solu-

---

tion very close to the original, widely used, SABR analytic formula, while being arbitrage-free by construction, and thus allowing pricing with low rates. The authors use a Crank-Nicolson time stepping scheme, which is known to have oscillation issues [52, 73] as it is only A-stable but not L-stable [137]. We will show that this issue arises in the context of SABR pricing, and propose alternative schemes that are not very well known in computational finance, and yet are effective on this problem.

Speed and accuracy were key ingredients in popularising the original SABR formula. Given that for a 30 year cap on a 3M LIBOR rate, there are potentially 119 PDEs to solve, we will focus our attention on the performance of the proposed schemes, as well as to what extent the discretization grid can be reduced in size.

Negative interest rates are now a common feature of the market. As a consequence, dealers quote swaptions in terms of basis point volatilities (b.p. vols) or in terms of shifted lognormal volatility. In terms of modeling with the popular SABR model of Hagan et al. [85], one possibility is to use the so-called normal SABR model, with $\beta = 0$, that naturally allows negative forwards. Practitioners prefer however to use a shifted SABR model that allows for negative forwards up to a shift b, as in [84], while keeping β free. Both can be summarized in the following framework:

$$\begin{cases} dF & = AL(F)dW_F, \\ dA & = \nu A dW_A, \end{cases} \tag{4.1}$$

where F is the forward swap rate[1] in time for a given maturity date and swap tenor, with W_F, W_A correlated Brownian motions with correlation ρ. In the normal case, we have:

$$L(F) = 1. \tag{4.2}$$

In the shifted lognormal case, we have:

$$L(F) = (F + b)^\beta. \tag{4.3}$$

In order to handle negative interest rates without an additional shift parameter, while still keeping control over the backbone[2] through the β SABR parameter, Antonov et al. [14] propose an alternate SABR model they call free-boundary SABR model. It is defined with:

$$L(F) = |F|^\beta. \tag{4.4}$$

The authors derive a semi-analytical formula, involving double numerical integration. While the formula is shown to be reasonably accurate in practice, it is not, a priori, arbitrage-free. To illustrate the flexibility of the arbitrage-free PDE approach, we will apply it to this model as well.

4.2. Mathematical models

4.2.1. Arbitrage Free SABR model

Hagan et al. [84] use asymptotic techniques to reduce the SABR model from two dimensions to one dimension. Pricing, with SABR parameters α, β, ρ, ν and initial forward swap

---

[1]The forward swap rate is the forward rate that would apply between the maturity of the option and the tenor of the underlying swap such that the swap, at the maturity date, would have a present value of zero.

[2]The backbone is the change in at-the-money implied volatility for a change in the forward rate.

rate $F(0) = f$ for the maturity τ_{ex}, then relies on the solution of the Fokker-Planck[3] PDE on the probability density Q:

$$\frac{\partial Q}{\partial T}(T,F) = \frac{\partial^2 M(T,F)Q(T,F)}{\partial F^2} \text{ and } \begin{cases} \frac{\partial Q_L}{\partial T}(T) = \lim_{F \to F_{\min}} \frac{\partial M(T,F)Q(T,F)}{\partial F}, \\ \frac{\partial Q_R}{\partial T}(T) = \lim_{F \to F_{\max}} \frac{\partial M(T,F)Q(T,F)}{\partial F}, \end{cases} \tag{4.5}$$

with

$$M(T,F) = \frac{1}{2}D^2(F)E(T,F), \ E(T,F) = e^{\rho v \alpha \Gamma(F) T}, \ \Gamma(F) = \frac{F^\beta - f^\beta}{F - f}, \tag{4.6}$$

$$D(F) = \sqrt{\alpha^2 + 2\alpha\rho v y(F) + v^2 y(F)^2} F^\beta, \ y(F) = \frac{F^{1-\beta} - f^{1-\beta}}{1 - \beta}, \tag{4.7}$$

and initial condition

$$\lim_{T \to 0} Q(T,F) = \delta(F - f). \tag{4.8}$$

Undiscounted vanilla option prices can then be computed through the Breeden-Litzenberger formula [28]:

$$V_{\text{call}}(T,K) = \int_K^{F_{\max}} (F - K)Q(T,F)dF + (F_{\max} - K)Q_R(T), \tag{4.9}$$

$$V_{\text{put}}(T,K) = (K - F_{\min})Q_L(T) + \int_{F_{\min}}^K (K - F)Q(T,F)dF. \tag{4.10}$$

4.2.2. Forward Dupire model
The term $M(T,F)$ represents the diffusion coefficient, and so, in financial terms, $D(F)\sqrt{E(T,F)}$ can be regarded as the normal local volatility. In [13], a slightly simpler (less accurate for long maturities) expansion of the local volatility is found and directly used in the normal Dupire forward PDE on the call prices V_{call}:

$$\frac{\partial V_{\text{call}}}{\partial T}(T,F) = \frac{1}{2}\vartheta^2(T,F)\frac{\partial^2 V_{\text{call}}}{\partial F^2}(T,F), \tag{4.11}$$

with initial condition $V_{\text{call}}(0,F) = (f - F)^+$ and

$$\vartheta(T,F) = D(F). \tag{4.12}$$

Both approaches are strikingly similar if the same local volatility approximation as well as the same PDE discretization is used. One difference lies in the boundary conditions: Hagan uses an absorbing condition at $F_{\min}$ and $F_{\max}$, while Andreasen and Huge use the standard Hagan expansion formula at the boundaries. It is also possible

---

[3]At a later time, the probability density will follow a different Fokker-Planck equation, as the forward f will have moved. The true underlying process can not be represented by a one-dimensional diffusion, only its realization at a specific time can, which is precisely what we care about numerically here. This is not to be confused with the 2D Fokker-Planck equation stemming from the classical SABR model stochastic differential equations.

to use the more classic linear boundaries condition $\frac{\partial^2 V_{\text{call}}}{\partial F^2}(F_{\min}) = \frac{\partial^2 V_{\text{call}}}{\partial F^2}(F_{\max}) = 0$ in the Dupire forward PDE, which is even closer then to an absorbing condition in the probability density, since the marginal probability density Q satisfies $Q(F_{\min}) = Q(F_{\max}) = 0$, and the marginal probability density corresponds to the second derivative of the undiscounted option prices.

While our focus is mainly on the PDE in probability density, we will also have a quick look at the nearly equivalent Dupire representation in order to find out if one approach is more efficient or not.

4.2.3. Free-boundary PDE

The difference between the classic SABR PDE and the free-boundary SABR PDE formulations lies in the formulae related to $L(F)$ and in the choice of $F_{\min}$. The probability density Q is the solution of:

$$\frac{\partial Q}{\partial T}(T,F) = \frac{\partial^2 M(T,F)Q(T,F)}{\partial F^2} \text{ and } \begin{cases} \frac{\partial Q_L}{\partial T}(T) = \lim_{F \to F_{\min}} \frac{\partial M(T,F)Q(T,F)}{\partial F}, \\ \frac{\partial Q_R}{\partial T}(T) = \lim_{F \to F_{\max}} \frac{\partial M(T,F)Q(T,F)}{\partial F}, \end{cases} \tag{4.13}$$

with

$$M(T,F) = \frac{1}{2} D^2(F) E(T,F), \, E(T,F) = e^{\rho v \alpha \Gamma(F) T}, \tag{4.14}$$

$$D(F) = \sqrt{\alpha^2 + 2\alpha\rho v y(F) + v^2 y(F)^2} |F|^\beta, \tag{4.15}$$

using

$$\Gamma(F) = \frac{|F|^\beta - |f|^\beta}{F - f}, \tag{4.16}$$

$$y(F) = \int_f^F \frac{du}{L(u)} = \frac{\text{sgn}(F)|F|^{1-\beta} - \text{sgn}(f)|f|^{1-\beta}}{1 - \beta}, \tag{4.17}$$

and initial condition

$$\lim_{T \to 0} Q(T,F) = \delta(F - f). \tag{4.18}$$

In effect, only L, Γ, and y have changed compared to the classic SABR model with absorption at 0. Furthermore, instead of placing the left boundary at 0 (or at a shift $-b$), the left boundary should be located far enough on the negative side, a typical choice would be $F_{\min} = -F_{\max}$. It is important to keep the absorbing behaviour at the boundaries, even if the absorption should be in practice quite small, as it allows to preserve the zero-th and first moments (corresponding to cumulative density and forward) exactly numerically (proof in Section 4.4).

4.3. Change of variables

4.3.1. Transformation of the Fokker-Planck PDE

One practical difficulty that arises with the arbitrage-free PDE described in Equations (4.5) is the choice of $F_{\max}$. Hagan et al. [84] propose a formula to estimate the required

$F_{\max}$, that, for some parameters is not suitable. It can be very large for long term option contracts and as a consequence the discretization requires a very large number of points to obtain an acceptable accuracy. The technique becomes inefficient. However, this type of problem is not new and a common approach is to consider a change of variables as a remedy. The Lamperti transform consists in a change of variables that makes the PDE closer to a unit diffusion PDE, and thus the solution, closer to a Gaussian density function [123]. The technique has been applied in finance in [9, p. 292 Section 7.4]. On this particular problem, the following change of variables works well whilst still preserving the moments [83]:

$$z(F) = \int_f^F \frac{du}{D(u)}. \tag{4.19}$$

This leads to a PDE in $\theta(T, z) = Q(T, F(z))D(F(z)) = Q(T, F(z))C(z)$ with $C(z) = D(F(z))$:

$$\frac{\partial \theta}{\partial T}(T, z) = \frac{1}{2} \frac{\partial}{\partial z}\left\{ \frac{1}{C(z)} \frac{\partial C(z)E(T, F(z))\theta(T, z)}{\partial z} \right\} \text{ and } \begin{cases} \theta(T, z) = 0 \text{ as } z \to z^- = z(F_{\min}), \\ \theta(T, z) = 0 \text{ as } z \to z^+ = z(F_{\max}), \end{cases} \tag{4.20}$$

with initial condition

$$\lim_{T \to 0} \theta(T, z) = \delta(z - z(y(f))). \tag{4.21}$$

The probabilities of absorption P_L, P_R at $z = z^-$ and $z = z^+$ boundaries accumulate according to

$$\frac{\partial P_L}{\partial T}(T) = \lim_{z \to z^-} \frac{1}{2} \frac{1}{C(z)} \frac{\partial C(z)E(T, F(z))\theta(T, z)}{\partial z}, \tag{4.22}$$

$$\frac{\partial P_R}{\partial T}(T) = \lim_{z \to z^+} -\frac{1}{2} \frac{1}{C(z)} \frac{\partial C(z)E(T, F(z))\theta(T, z)}{\partial z}. \tag{4.23}$$

With the change of variable defined by Equation (4.19), the relation between the forward swap rate F and the new coordinate z reads

$$F(y) = \left[f^{1-\beta} + (1-\beta)y \right]^{\frac{1}{1-\beta}}, \tag{4.24}$$

with

$$y(z) = \frac{\alpha}{v}\left[\sinh(vz) + \rho(\cosh(vz) - 1) \right], \tag{4.25}$$

and where f is the initial forward swap rate .

As a result, the effect of the diffusion term D has almost been cancelled, and the probability density θ is closer to a Gaussian in z. The values z^+ and z^- are then naturally chosen to be $\pm n_{\text{sd}}\sqrt{\tau_{ex}}$, corresponding to n_{sd} standard deviations above and below the forward located at $z = 0$ (taking care of truncating at the barrier $F = 0$ if necessary). Figure 4.3.1 shows that the probability density will be computed with a high concentration of points around the forward, and a much lower number near the upper boundary.
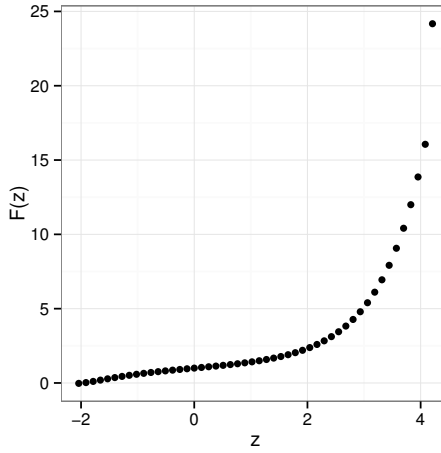
Figure 4.3.1: $F(z)$ with $\alpha = 35\%, \beta = 0.25, \rho = -10\%, \nu = 100\%, \tau_{ex} = 1$.

The call and put prices are obtained by integrating on the transformed density:

$$V_{\text{call}}(T, K) = \int_{z(K)}^{z^+} (F(z) - K)\theta(T, z)\,dz + (F_{\max} - K)P_R(T), \tag{4.26}$$

$$V_{\text{put}}(T, K) = (K - F_{\min})P_L(T) + \int_{z^-}^{z(K)} (K - F(z))\theta(T, z)\,dz. \tag{4.27}$$

For some extreme SABR parameters, the change of variables allows high accuracy with a small number of points. The uniform discretization of Q in F can require approximately 1000 times more points to reach a similar accuracy (Table 4.3.1). The number

	Uniform discretization of Q in F				Discretization of θ in z			
$F_{\max}$	Points	Steps	Price	Vol	n_{sd}	Points	Steps	Price	Vol
5	10	5	0.65010	87.205	3	10	5	0.79848	198.504
50	100	10	0.78769	155.773	3	100	10	0.79853	199.148
500	1000	20	0.79782	191.658	4	100	20	0.79847	198.338
5000	10000	160	0.79835	196.930	10	10000	160	0.79845	198.134

Table 4.3.1: Price by the Lawson-Swayne method without and with variable transformation for extreme SABR parameters: $\alpha = 100\%, \beta = 0.30, \rho = 90\%, \nu = 100\%, \tau_{ex} = 10, f = 1$.

of points used can not be too small: the forward should not be at the boundary. This restriction is much stricter for the uniform discretization of Q than for the discretization in the changed variable θ.

4.3.2. COORDINATE TRANSFORMATION FOR THE FORWARD DUPIRE PDE

The same variable transformation (4.19) can be applied to the Dupire forward PDE where $\vartheta^2(T, F) = D^2(F)E(F, T)$ resulting in:

$$\frac{\partial V_{\text{call}}}{\partial T}(T, z) = \frac{1}{2}C(z)E(T, F(z))\frac{\partial}{\partial z}\left\{\frac{1}{C(z)}\frac{\partial V_{\text{call}}(T, z)}{\partial z}\right\} \tag{4.28}$$

with initial condition $V_{\text{call}}(T = 0, z) = (f - F(z))^+$, and $C(z) = D(F(z))$, where $D(F)$, $E(F)$ are defined in Equations (4.6), (4.7) .

A slightly simpler alternative approach consists in using an equivalent non-uniform grid in F inside a finite difference discretization of the forward Dupire PDE (4.11) as described in [9]. The equivalent non-uniform grid is defined by $F(z)$, where z is a uniform discretization. Care must be taken to place the forward f in the middle of two nodes in order to decrease the numerical error [188]. Another technique to reduce the numerical error is to smooth out the hockey-stick payoff at maturity by averaging, but this would not preserve the put-call parity.

Let's define a uniform grid in the coordinate z, for $j = 0, ..., J + 1$:

$$\tilde{z}_j = z^- + jh \, , \, h = \frac{1}{J+1}(z^+ - z^-). \tag{4.29}$$

Using Equations (4.25) and (4.24), the corresponding grid in F would be:

$$\tilde{F}_j = F\left(y(\tilde{z}_j)\right) = F\left(y\left(z^- + \frac{j}{J+1}(z^+ - z^-)\right)\right). \tag{4.30}$$

To place the initial forward f in the middle of two consecutive points, we first locate the index j_0 so that $\tilde{F}_{j_0} \leq f < \tilde{F}_{j_0+1}$, that is:

$$j_0 = \left\lfloor \frac{z(y(f)) - z^-}{h} \right\rfloor. \tag{4.31}$$

Then we shift the grid by a distance d, defined by:

$$d = z(y(f)) - z\left(y\left(\frac{1}{2}(\tilde{F}_{j_0} + \tilde{F}_{j_0+1})\right)\right). \tag{4.32}$$

This leads to a new grid $(z_j)_{j=0,...,J+1}$ or equivalently $(F_j)_{j=0,...,J+1}$ with

$$F_j = F\left(y(z^- + jh + d)\right), \tag{4.33}$$

for $j = 1, ..., J$. In addition, we make sure to keep the original domain boundaries, this is especially important as z^- often corresponds to the absorbing barrier by forcing $F_0 = F(y(z^-))$ and $F_{J+1} = F(y(z^+))$.

Finally, to compute the price of an option in between two grid nodes, we interpolate the discrete prices using a natural cubic spline in order to preserve the continuity of the second derivative (and therefore the continuity of the probability density function) everywhere.

4.3.3. TRANSFORMATION OF THE FREE-BOUNDARY PDE

We rely on the same variable transform (Equation 4.19) as in the case of the standard arbitrage-free SABR PDE. This leads to a PDE in $\theta(z) = Q(T, F(z))D(F(z)) = Q(T, F(z))C(z)$ with $C(z) = D(F(z))$:

$$\frac{\partial \theta}{\partial T}(T, z) = \frac{1}{2}\frac{\partial}{\partial z}\left\{\frac{1}{C(z)}\frac{\partial C(z)E(T, z)\theta(T, z)}{\partial z}\right\} \text{ and } \begin{cases} \theta(T, z) = 0 \text{ as } z \to z^- = z(F_{\min}), \\ \theta(T, z) = 0 \text{ as } z \to z^+ = z(F_{\max}), \end{cases}$$
(4.34)

with initial condition

$$\lim_{T \to 0} \theta(T, z) = \delta(z - z(y(f))).$$
(4.35)

Note that $z(y)$ is unchanged with respect to the arbitrage-free case as, in this coordinate, it is independent of the variable $L(F)$:

$$z(y) = \int_{y(f)}^{y(F)} \frac{dy'}{\sqrt{\alpha^2 + 2\alpha\rho v y' + v^2 y'^2}}.$$
(4.36)

Therefore $y(z)$ is also given by Equation 4.25. Only $F(y)$ is modified by the free-boundary model. We just invert Equation (4.17):

$$F(y) = \text{sgn}(y - \bar{y})\left[(1 - \beta)|y - \bar{y}|\right]^{\frac{1}{1-\beta}}$$
(4.37)

with $\bar{y} = y(F = 0) = -\frac{\text{sgn}(f)|f|^{1-\beta}}{1-\beta}$.

Again, the boundary z^- should now be taken simply as $z^- = -z^+ = -n_{\text{sd}}\sqrt{\tau}$ where n_{sd} is a number of standard deviations. In practice $n_{\text{sd}} = 4$ is highly accurate.

4.4. ALTERNATIVE DISCRETIZATION SCHEMES

We will focus our analysis on the PDE in θ, but similar conclusions can be drawn for the PDE in Q. For a constant step size h, let us define for $j = 1, ..., J$:

$$z_j = z^- + jh \text{ , } \hat{F}_j = F\left(y\left(z_j - \frac{h}{2}\right)\right),$$
(4.38)

$$\hat{C}_j = D(\hat{F}_j) \text{ , } \hat{\Gamma}_j = \frac{L(\hat{F}_j) - L(f)}{\hat{F}_j - f} \text{ , } \hat{E}_j(T) = e^{\rho v \alpha \hat{\Gamma}_j T}.$$
(4.39)

For $j = 0$ and $j = J + 1$, let $F_{\min} = F(y(z_0))$, $F_{\max} = F(y(z_J))$ we define the shadow points $\hat{F}_0$ and $\hat{F}_{J+1}$ as:

$$\hat{F}_0 = 2F_{\min} - \hat{F}_1 \text{ , } \hat{F}_{J+1} = 2F_{\max} - \hat{F}_J.$$
(4.40)

We also define for $n = 0, ..., N - 1$:

$$t_n = n\delta \text{ with } \delta = \frac{\tau_{ex}}{N},$$
(4.41)

$$\theta_j(T) = \frac{1}{h} \int_{z_{j-1}}^{z_j} \theta(z, T) dz, \text{ and } \quad \theta_j^n = \theta_j(t_n). \tag{4.42}$$

Note that we would obtain the same results with the definition $\theta_j(T) = \theta(z_j - \frac{h}{2}, T)$. In order to preserve the zero-th and first moments of F, the PDE (4.20) is discretized in z as in [83]:

$$\frac{\partial \theta_j}{\partial T}(t_n) = \mathscr{L}_j^n \theta_j(t_n), \tag{4.43}$$

for $j = 1, ..., J$ with $\mathscr{L}_j^n$ the discrete operator defined by

$$
\begin{aligned}
\mathscr{L}_j^n \theta_j(t_n) = {} & \frac{1}{2h} \frac{\hat{C}_{j-1}}{\hat{F}_j - \hat{F}_{j-1}} \hat{E}_{j-1}(t_n)\theta_{j-1}(t_n) \\
& - \frac{1}{2h} \left(\frac{\hat{C}_j}{\hat{F}_{j+1} - \hat{F}_j} + \frac{\hat{C}_j}{\hat{F}_j - \hat{F}_{j-1}} \right) \hat{E}_j(t_n)\theta_j(t_n) \\
& + \frac{1}{2h} \frac{\hat{C}_{j+1}}{\hat{F}_{j+1} - \hat{F}_j} \hat{E}_{j+1}(t_n)\theta_{j+1}(t_n),
\end{aligned}
\tag{4.44}
$$

and for the boundaries at $j = 0$ and $j = J + 1$:

$$\frac{\hat{C}_0}{\hat{F}_1 - \hat{F}_0} \hat{E}_0(T)\theta_0(T) = -\frac{\hat{C}_1}{\hat{F}_1 - \hat{F}_0} \hat{E}_1(T)\theta_1(T) \tag{4.45}$$

$$\frac{\hat{C}_{J+1}}{\hat{F}_{J+1} - \hat{F}_J} \hat{E}_{J+1}(T)\theta_{J+1}(T) = -\frac{\hat{C}_J}{\hat{F}_{J+1} - \hat{F}_J} \hat{E}_J(T)\theta_J(T), \tag{4.46}$$

The boundary condition described by Equations (4.45) and (4.46) is applicable to all schemes considered in this section as it is independent of the time stepping. The definition of the shadow points $\hat{F}_0$ and $\hat{F}_{J+1}$ makes sure that $\theta(z(F_{\min}), t_n) = 0$ and $\theta(z(F_{\max}), t_n) = 0$.

The probability accumulated at the boundaries (Equation 4.22) is discretized as:

$$\frac{\partial P_L}{\partial T}(T) = \frac{\hat{C}_1}{\hat{F}_1 - \hat{F}_0} \hat{E}_1(T)\theta_1(T), \tag{4.47}$$

$$\frac{\partial P_R}{\partial T}(T) = \frac{\hat{C}_J}{\hat{F}_{J+1} - \hat{F}_J} \hat{E}_J(T)\theta_J(T). \tag{4.48}$$

Zero-th moment conservation. Let $S_j^n = \hat{C}_j \hat{E}_j(t_n)\theta_j(t_n)$, summing Equation (4.43)

over the nodes j along with the probability accumulated at the boundaries leads to:

$$\frac{\partial P_L}{\partial T}(t_n) + \int_{z_{\min}}^{z_{\max}} \frac{\partial \theta}{\partial T}(z, t_n)dz + \frac{\partial P_R}{\partial T}(t_n) = \frac{\partial P_L}{\partial T}(t_n) + \sum_{j=1}^{J} \frac{\partial \theta_j}{\partial T}(t_n)h + \frac{\partial P_R}{\partial T}(t_n)$$

$$= \frac{S_1^n}{\hat{F}_1 - \hat{F}_0} + \sum_{j=1}^{J} \mathcal{L}_j^n \theta_j(t_n)h + \frac{S_J^n}{\hat{F}_{J+1} - \hat{F}_J}$$

$$= \frac{S_1^n - S_0^n}{2(\hat{F}_1 - \hat{F}_0)} + \sum_{j=0}^{J-1} \frac{1}{2} \frac{S_j^n}{\hat{F}_{j+1} - \hat{F}_j}$$

$$- \sum_{j=1}^{J} \frac{1}{2} \left(\frac{S_j^n}{\hat{F}_{j+1} - \hat{F}_j} + \frac{S_j^n}{\hat{F}_j - \hat{F}_{j-1}} \right)$$

$$+ \sum_{j=2}^{J+1} \frac{1}{2} \frac{S_j^n}{\hat{F}_j - \hat{F}_{j-1}} + \frac{S_J^n - S_{J+1}^n}{2(\hat{F}_{J+1} - \hat{F}_J)}$$

$$= 0.$$

where we used the boundary conditions (4.45) and (4.46). Therefore, the total probability stays constant, i.e., equal to 1.

First moment conservation. Regarding the conservation of the first moment, we find,

$$F_{\min} \frac{\partial P_L}{\partial T}(t_n) + \int_{z_{\min}}^{z_{\max}} F(z) \frac{\partial \theta}{\partial T}(z, t_n)dz + F_{\max} \frac{\partial P_R}{\partial T}(t_n)$$

$$= F_{\min} \frac{S_1^n}{\hat{F}_1 - \hat{F}_0} + \sum_{j=1}^{J} \hat{F}_j \mathcal{L}_j^n \theta_j(t_n)h + F_{\max} \frac{S_J^n}{\hat{F}_{J+1} - \hat{F}_J}$$

$$= \frac{(\hat{F}_1 + \hat{F}_0)S_1^n}{2(\hat{F}_1 - \hat{F}_0)} + \sum_{j=0}^{J-1} \frac{\hat{F}_{j+1}}{2} \frac{S_j^n}{\hat{F}_{j+1} - \hat{F}_j} - \sum_{j=1}^{J} \frac{\hat{F}_j}{2} \left(\frac{S_j^n}{\hat{F}_{j+1} - \hat{F}_j} + \frac{S_j^n}{\hat{F}_j - \hat{F}_{j-1}} \right)$$

$$+ \sum_{j=2}^{J+1} \frac{\hat{F}_{j-1}}{2} \frac{S_j^n}{\hat{F}_j - \hat{F}_{j-1}} + \frac{(\hat{F}_J + \hat{F}_{J+1})S_J^n}{2(\hat{F}_{J+1} - \hat{F}_J)}$$

$$= \frac{(-\hat{F}_1 + \hat{F}_0)S_1^n}{2(\hat{F}_1 - \hat{F}_0)} + \frac{(\hat{F}_2 - \hat{F}_1)S_1^n}{2(\hat{F}_2 - \hat{F}_1)} + \sum_{j=2}^{J-1} \frac{1}{2} \left(\frac{\hat{F}_{j+1} - \hat{F}_j}{\hat{F}_{j+1} - \hat{F}_j} - \frac{\hat{F}_j - \hat{F}_{j-1}}{\hat{F}_j - \hat{F}_{j-1}} \right) S_j^n$$

$$+ \frac{(-\hat{F}_J + \hat{F}_{J+1})S_J^n}{2(\hat{F}_{J+1} - \hat{F}_J)} + \frac{(\hat{F}_{J-1} - \hat{F}_J)S_J^n}{2(\hat{F}_J - \hat{F}_{J-1})}$$

$$= 0$$

where we used the definition of $\hat{F}_0$ and $\hat{F}_{J+1}$ (Equation 4.40) as well as the boundary conditions (4.45) and (4.46). Therefore, the first moment is conserved over time and is equal to the initial forward swap rate f.

Lower boundary. It is suggested that the lower boundary $F_{\min}$ for the standard SABR model is placed at or near zero. However, the finite difference grid starts at $\hat{F}_0$, potentially requiring the evaluation of functions that are not well-defined for negative values

of $\hat{F}_0$. Fortunately, only the product $\hat{C}_0 \hat{E}_0(T) \theta_0(T)$ is used in the discretization of Equation (4.43) and it is entirely defined by $\hat{C}_1 \hat{E}_1(T) \theta_1(T)$ because of the mirror-like boundary condition imposed at the fictitious point $F_{\min}$ described by Equation (4.45). By direct application of the latter equation, $\hat{C}_0 \hat{E}_0(T) \theta_0(T)$ will take the value $-\hat{C}_1 \hat{E}_1(T) \theta_1(T)$. Another alternative would be to place the grid so that $\hat{F}_0 = F_{\min}$ and use boundary condition $\theta_0(T) = 0$ there. The probability of absorption P_L could then be evaluated with a forward finite difference first derivative estimate. The scheme would still be moment preserving. However, this comes at the cost of a slight loss of accuracy as, effectively, the derivative would be estimated using $\theta(z_1, T) = \theta(h, T)$ instead of $\theta\left(z_1 - \frac{h}{2}, T\right) = \theta\left(\frac{h}{2}, T\right)$.

The formula for Γ is also undefined for $F = f$, in which case we just use $\Gamma(f) = \frac{\partial C}{\partial F}(f)$.

Call and put prices. The undiscounted call and put prices are obtained by integrating with the mid-point method. Let $z^* = z(y(K))$. We first suppose that $z^- < z^* < z^+$. Let k be the index such that $z^- + (k-1)h < z^* \le z^- + kh$ and $F_k = F(y(z^- + kh))$. Then

$$V_{\text{call}}(K, T) = \int_{z^*}^{z_k} (F(z) - K) \theta(z) \, dz + \sum_{j=k+1}^{J-1} (\hat{F}_j - K) h \theta_j + (F_{\max} - K) P_R, \qquad (4.49)$$

$$V_{\text{put}}(K, T) = \int_{z^*}^{z_k} (K - F(z)) \theta(z) \, dz + \sum_{j=1}^{k} (K - \hat{F}_j) h \theta_j + (K - F_{\min}) P_L. \qquad (4.50)$$

For the call option case, note that the first term of Equation (4.49) is approximated as follows. We have

$$\int_{z^*}^{z_k} (F(z) - K) \theta(z) \, dz = \int_{K}^{F_k} (F - K) \frac{\theta(z(F))}{D(F)} \, dF. \qquad (4.51)$$

We then assume θ to be constant between z_{k-1} and z_k, and make the approximation $D(F) = \frac{\partial F}{\partial z} \approx 2 \frac{F_k - \hat{F}_k}{h}$ (we found that this choice preserved a smoother numerical density). This leads to

$$\int_{z^*}^{z_k} (F(z) - K) \theta(z) \, dz \approx \frac{h}{4(F_k - \hat{F}_k)} (F_k - K)^2 \theta_k. \qquad (4.52)$$

When $z^* \le z^-$, $V_{\text{call}} = f - K$ and $V_{\text{put}} = 0$. When $z^* \ge z^+$, $V_{\text{call}} = 0$ and $V_{\text{put}} = K - f$. Equations (4.49) and (4.50) preserve the put-call parity exactly:

$$V_{\text{call}}(K, T) - V_{\text{put}}(K, T) = (F_{\min} - K) P_L + \sum_{j=1}^{J-1} (\hat{F}_j - K) h \theta_j + (F_{\max} - K) P_R$$

$$= F_{\min} P_L + \sum_{j=1}^{J-1} \hat{F} h \theta_j + F_{\max} P_R - K \left[P_L + \sum_{j=1}^{J-1} h \theta_j + P_R \right]$$

$$= F - K,$$

where we used the conservation of the zero-th and first moments to obtain the last equality.

4.4.1. Moment preserving implicit Euler scheme

The backward Euler time stepping scheme applied to Equation (4.43) leads to:

$$\theta_j^{n+1} - \theta_j^n = \delta \mathcal{L}_j^{n+1} \theta_j^{n+1}, \tag{4.53a}$$

$$P_L(t_{n+1}) - P_L(t_n) = \delta \frac{\hat{C}_1}{\hat{F}_1 - \hat{F}_0} \hat{E}_1(t_{n+1})\theta_1^{n+1}, \tag{4.53b}$$

$$P_R(t_{n+1}) - P_R(t_n) = \delta \frac{\hat{C}_J}{\hat{F}_{J+1} - \hat{F}_J} \hat{E}_J(t_{n+1})\theta_J^{n+1}, \tag{4.53c}$$

for $j = 1, ..., J$ and $n = 0, ..., N-1$, where θ is the transformed probability density and P_L, P_R are the probabilities of absorption at $z = z^-$ and $z = z^+$.

4.4.2. Moment preserving Crank-Nicolson scheme

The trapezoidal time stepping applied to Equation 4.43 leads to:

$$\theta_j^{n+1} - \theta_j^n = \frac{\delta}{2} \left(\mathcal{L}_j^{n+1} \theta_j^{n+1} + \mathcal{L}_j^n \theta_j^n \right), \tag{4.54a}$$

$$P_L(t_{n+1}) - P_L(t_n) = \frac{\delta}{2} \frac{\hat{C}_1}{\hat{F}_1 - \hat{F}_0} \left(\hat{E}_1(t_{n+1})\theta_1^{n+1} + \hat{E}_1(t_n)\theta_1^n \right), \tag{4.54b}$$

$$P_R(t_{n+1}) - P_R(t_n) = \frac{\delta}{2} \frac{\hat{C}_J}{\hat{F}_{J+1} - \hat{F}_J} \left(\hat{E}_J(t_{n+1})\theta_J^{n+1} + \hat{E}_J(t_n)\theta_J^n \right), \tag{4.54c}$$

for $j = 1, ..., J$ and $n = 0, ..., N-1$.

4.4.3. Crank-Nicolson oscillations with the SABR model

(a) PDE in Q with 40 time steps and $F_{\max} = 5$ (b) PDE in θ with 80 time steps and $n_{sd} = 4$
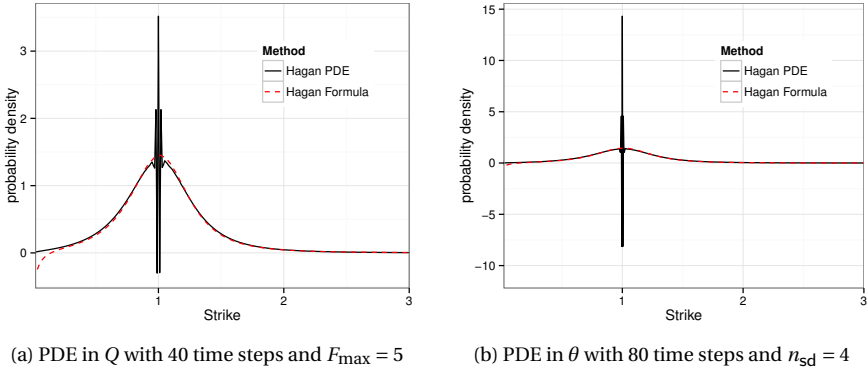
Figure 4.4.1: Probability density in Hagan PDE discretized with Crank-Nicolson with 500 points. $\alpha = 35\%, \beta = 0.25, \rho = -10\%, \nu = 100\%, \tau_{ex} = 1$

We use the same parameters as the example of negative density with the standard SABR formula in [84]: $\alpha = 35\%, \beta = 0.25, \rho = -10\%, \nu = 100\%$ and forward swap rate $f = 1$

at $\tau_{ex} = 1$, a relatively fine discretization in the rate dimension (500 points, that is $h = 0.01005$) and large time steps (40 steps, that is $\delta = 0.025$). The authors in [84] recommend between 200 and 500 points and 30 to 100 time steps.

Figure 4.4.1a shows strong oscillations around the forward. To guarantee the absence of oscillations, the *Courant number* should be small enough $\Psi \leq 1$ (Theorem 2.2 in [157]). For the uniform discretization of $Q(F)$, $\Psi_Q = M\frac{\delta}{h^2}$. This corresponds directly to the stability of the explicit Euler part of Crank-Nicolson. In practice, a higher value is acceptable because of a slight damping in the Crank-Nicolson scheme [124]. Although, as per Equation (4.6), M depends on F, we can use the at-the-money value corresponding to $F = f$, as the spike is located there; that is,

$$\Psi_Q = \frac{1}{2}\alpha^2 f^{2\beta}\frac{\delta}{h^2}, \qquad (4.55)$$

$$\Psi_\theta = f^\beta \frac{\delta}{h^2}. \qquad (4.56)$$

(a) with 40 time steps $\Psi_Q = 15.16$ (b) with 1280 time steps $\Psi_Q = 0.47$
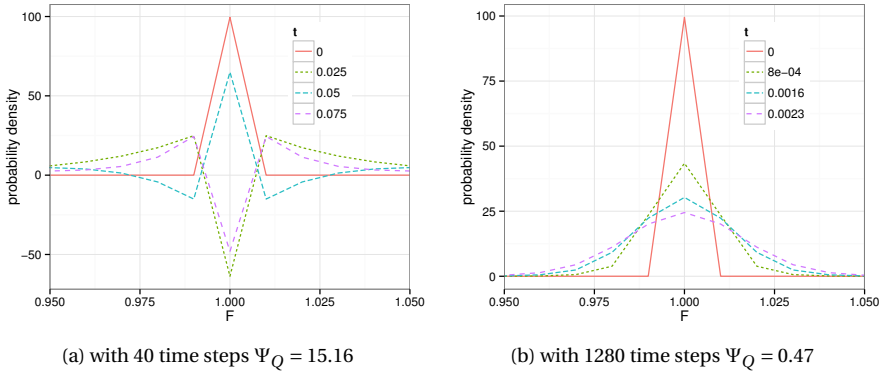
Figure 4.4.2: First 4 time steps of the probability density in Hagan PDE discretized with Crank-Nicolson

In our example, in Figures 4.4.1a and 4.4.2a $\Psi_Q \approx 15$ while Figure 4.4.2b shows that indeed when $\Psi < 1$ there are no oscillations. The Crank-Nicolson oscillations are even stronger with the PDE in θ as for $\alpha \ll 1$, we have $\Psi_\theta \gg \Psi_Q$. Using the same SABR parameters and $n_{sd} = 3$ (corresponding to $F_{max} \approx 5$), $\Psi_\theta \approx 250$. In the next sections it is shown that a much smaller number of time steps can be used with other finite difference time stepping techniques whilst still preserving good accuracy.

4.4.4. RANNACHER TIME STEPPING

A common fix for Crank-Nicolson oscillations related to non smooth initial data is the Rannacher time stepping [73, 172, 173]. It consists of introducing two half time steps of implicit Euler time stepping before applying the Crank-Nicolson scheme, because the implicit Euler scheme has much stronger damping properties. This comes at a cost in accuracy as implicit Euler is an order-1 scheme in time, especially when only a few time

steps are needed. The SABR density discretization will still be moment preserving if we discretize the Euler half steps as:

$$\theta_j^{n+\frac{1}{2}} - \theta_j^n = \frac{\delta}{2} \mathscr{L}_j^{n+\frac{1}{2}} \theta_j^{n+\frac{1}{2}}, \tag{4.57a}$$

$$P_L(t_{n+\frac{1}{2}}) - P_L(t_n) = \frac{\delta}{2} \frac{\hat{C}_1}{\hat{F}_1 - \hat{F}_0} \hat{E}_1(t_{n+\frac{1}{2}}) \theta_1^{n+\frac{1}{2}}, \tag{4.57b}$$

$$P_R(t_{n+\frac{1}{2}}) - P_R(t_n) = \frac{\delta}{2} \frac{\hat{C}_J}{\hat{F}_{J+1} - \hat{F}_J} \hat{E}_J(t_{n+\frac{1}{2}}) \theta_J^{n+\frac{1}{2}}, \tag{4.57c}$$

for $j = 1, ..., J$ and $n = 0, \frac{1}{2}, 1, \frac{3}{2}$. The next steps are Crank-Nicolson steps for $n = 2, ..., N-1$.

4.4.5. BDF2 SCHEME
The second-order backward difference scheme (BDF2) is an A-stable and L-stable multi-step implicit scheme and will therefore damp any oscillation very quickly. Multi-step schemes have however severe limitations: instabilities will occur for sudden changes in the system variables, and initialization by another method is needed for the first steps [199]. For example they can not be applied to linear complimentary problems like the pricing of American options through the discretization of the Black-Scholes PDE [127]. Those issues don't arise with the SABR density PDE. The first moments will be preserved with the following discretization:

$$3\theta_j^{n+2} - 4\theta_j^{n+1} + \theta_j^n = 2\delta \mathscr{L}_j^{n+2} \theta_j^{n+2}, \tag{4.58a}$$

$$3P_L(t_{n+2}) - 4P_L(t_{n+1}) + P_L(t_n) = 2\delta \frac{\hat{C}_1}{\hat{F}_1 - \hat{F}_0} \hat{E}_1(t_{n+2}) \theta_1^{n+2}, \tag{4.58b}$$

$$3P_R(t_{n+2}) - 4P_R(t_{n+1}) + P_R(t_n) = 2\delta \frac{\hat{C}_J}{\hat{F}_{J+1} - \hat{F}_J} \hat{E}_J(t_{n+2}) \theta_J^{n+2}, \tag{4.58c}$$

for $j = 1, ..., J$ and $n = 0, ..., N-2$. The implicit Euler scheme is used to compute θ_j^1, P_L^1, P_R^1 at $n = 0$.

4.4.6. IMPLICIT RICHARDSON EXTRAPOLATION
A simple Richardson extrapolation in time [177] on implicit Euler will also provide a nearly order-2 scheme in time, keeping strong damping properties of the implicit Euler scheme at the cost of increased computational load: the implicit Euler scheme (Equations 4.57) is evaluated with $\frac{\delta}{2}$ and δ. In practice, it is around twice as slow as the Crank-Nicolson scheme. At $T = N\delta = \tau_{ex}$, we apply:

$$\theta(z) = 2\bar{\theta}^{\frac{\delta}{2}}(z) - \bar{\theta}^\delta(z) \tag{4.59a}$$

$$P_L = 2\bar{P}_L^{\frac{\delta}{2}} - \bar{P}_L^\delta \tag{4.59b}$$

$$P_R = 2\bar{P}_R^{\frac{\delta}{2}} - \bar{P}_R^\delta \tag{4.59c}$$

where the $\bar{\theta}^\delta, \bar{P}_L^\delta, \bar{P}_R^\delta$ are the approximations of θ, P_L, P_R, computed with the implicit Euler scheme and a time step of δ.

4.4.7. LAWSON-MORRIS-GOURLAY SCHEME

A local Richardson extrapolation in time of second- and third-order is proposed in [124] and [76]. In practice, it is a faster alternative to the standard Richardson extrapolation because the tridiagonal matrix stemming from the finite difference discretization can be reused, while keeping L-stability and thus strong damping properties.

For the second-order scheme, at each time step, Equation (4.59) is applied. For the third-order scheme, at each time step we apply:

$$\theta(F) = 4.5\bar{\theta}^{\frac{\delta}{3}}(F) - 4.5\bar{\theta}^{\frac{2\delta}{3}}(F) + \bar{\theta}^{\delta}(F) \tag{4.60a}$$

$$P_L = 4.5\bar{P}_L^{\frac{\delta}{3}} - 4.5\bar{P}_L^{\frac{2\delta}{3}} + \bar{P}_L^{\delta} \tag{4.60b}$$

$$P_R = 4.5\bar{P}_R^{\frac{\delta}{3}} - 4.5\bar{P}_R^{\frac{2\delta}{3}} + \bar{P}_R^{\delta} \tag{4.60c}$$

where $\bar{\theta}^{\frac{\delta}{3}}$ is θ computed by implicit Euler with 3 time steps of size $\frac{\delta}{3}$ and $\bar{\theta}^{\frac{2\delta}{3}}$ is θ computed by implicit Euler with a time step of $\frac{2\delta}{3}$ and $\frac{\delta}{3}$. Being linear combinations of implicit Euler, those schemes are moment preserving.

4.4.8. LAWSON-SWAYNE SCHEME

A slightly faster second-order unconditionally stable scheme is presented as a remedy to Crank-Nicolson in [124, 125]. With $a = 1 - \frac{\sqrt{2}}{2}$, it consists in applying two implicit Euler steps with time step of $a\delta$ and an extrapolation on the values at those two steps.

First stage:

$$\theta_j^{n+a} - \theta_j^n = a\delta\mathscr{L}_j^{n+a}\theta_j^{n+a},$$

$$P_L(t_{n+a}) - P_L(t_n) = a\delta\frac{\hat{C}_1}{\hat{F}_1 - \hat{F}_0}\hat{E}_1(t_{n+a})\theta_1^{n+a}, \tag{4.61a}$$

$$P_R(t_{n+a}) - P_R(t_n) = a\delta\frac{\hat{C}_J}{\hat{F}_{J+1} - \hat{F}_J}\hat{E}_J(t_{n+a})\theta_J^{n+a}.$$

Second stage:

$$\theta_j^{n+2a} - \theta_j^{n+a} = a\delta\mathscr{L}_j^{n+2a}\theta_j^{n+2a},$$

$$P_L(t_{n+2a}) - P_L(t_{n+a}) = a\delta\frac{\hat{C}_1}{\hat{F}_1 - \hat{F}_0}\hat{E}_1(t_{n+2a})\theta_1^{n+2a}, \tag{4.61b}$$

$$P_R(t_{n+2a}) - P_R(t_{n+a}) = a\delta\frac{\hat{C}_J}{\hat{F}_{J+1} - \hat{F}_J}\hat{E}_J(t_{n+2a})\theta_J^{n+2a}.$$

And finally:

$$\theta_j^{n+1} = (\sqrt{2}+1)\theta_j^{n+2a} - \sqrt{2}\theta_j^{n+a},$$

$$P_L(t_{n+1}) = (\sqrt{2}+1)P_L(t_{n+2a}) - \sqrt{2}P_L(t_{n+a}), \tag{4.61c}$$

$$P_R(t_{n+1}) = (\sqrt{2}+1)P_R(t_{n+2a}) - \sqrt{2}P_R(t_{n+a}),$$

for $j = 1, ..., J$ and $n = 0, ..., N-1$.

The scheme is moment-preserving as it can also be seen as a linear combination of implicit Euler schemes.

4.4.9. TR-BDF2 scheme

TR-BDF2 is a two-stage method where the first stage consists in applying the (weighted) trapezoidal rule (Crank-Nicolson) and the second stage consists in applying the second-order backward difference scheme (BDF2) on the first stage result and the first stage initial input [19, 137]. It is second-order accurate in time and L-stable.

First stage:

$$\theta_j^{n+a} - \theta_j^n = \frac{a\delta}{2} \left(\mathscr{L}_j^{n+a} \theta_j^{n+a} + \mathscr{L}_j^n \theta_j^n \right),$$

$$P_L(t_{n+a}) = P_L(t_n) + b\delta \frac{\hat{C}_1}{\hat{F}_1 - \hat{F}_0} \left(\hat{E}_1(t_{n+a})\theta_1^{n+a} + \hat{E}_1(t_n)\theta_1^n \right), \tag{4.62a}$$

$$P_R(t_{n+a}) = P_R(t_n) + b\delta \frac{\hat{C}_J}{\hat{F}_{J+1} - \hat{F}_J} \left(\hat{E}_J(t_{n+a})\theta_J^{n+a} + \hat{E}_J(t_n)\theta_J^n \right).$$

Second stage:

$$\theta_j^{n+1} = \frac{1}{2-a} \left(\frac{1}{a}\theta_j^{n+a} - \frac{(1-a)^2}{a}\theta_j^n + \delta(1-a)\mathscr{L}_j^{n+1}\theta_j^{n+1} \right),$$

$$P_L(t_{n+1}) = \frac{1}{2-a} \left(\frac{1}{a}P_L(t_{n+a}) - \frac{(1-a)^2}{a}P_L(t_n) + \delta(1-a)\frac{\hat{C}_1}{\hat{F}_1 - \hat{F}_0}\hat{E}_1(t_{n+1})\theta_1^{n+1}) \right),$$

$$P_R(t_{n+1}) = \frac{1}{2-a} \left(\frac{1}{a}P_R(t_{n+a}) - \frac{(1-a)^2}{a}P_R(t_n) + \delta(1-a)\frac{\hat{C}_J}{\hat{F}_{J+1} - \hat{F}_J}\hat{E}_J(t_{n+1})\theta_J^{n+1}) \right).$$

$$\tag{4.62b}$$

The weight a can be chosen to match Crank-Nicolson ($a = \frac{1}{2}$) or to have proportional Jacobians ($a = 2 - \sqrt{2}$). The latter provides optimal stability [48].

This can be extended to three-stages, with two stages of the trapezoidal rule and one stage of third-order backward difference scheme (BDF3) as in [22], resulting in a method with even stronger damping properties that we will name "Bathe":

$$\theta_j^{n+\frac{1}{3}} = \theta_j^n + \frac{\delta}{6} \left(\mathscr{L}_j^n \theta_j^n + \mathscr{L}_j^{n+\frac{1}{3}}\theta_j^{n+\frac{1}{3}} \right), \tag{4.63a}$$

$$\theta_j^{n+\frac{2}{3}} = \theta_j^n + \frac{\delta}{6} \left(\mathscr{L}_j^{n+\frac{1}{3}}\theta_j^{n+\frac{1}{3}} + \mathscr{L}_j^{n+\frac{2}{3}}\theta_j^{n+\frac{2}{3}} \right), \tag{4.63b}$$

$$\theta_j^{n+1} = \frac{1}{11} \left(18\theta_j^{n+\frac{2}{3}} - 9\theta_j^{n+\frac{1}{3}} + 2\theta_j^n + 2\delta\mathscr{L}_j^{n+1}\theta_j^{n+1} \right). \tag{4.63c}$$

4.4.10. Optimizing for Performance

The function $E(T, F)$, defined in Equation (4.6), needs to be computed for every grid point (F_j, t_n). The performance of the overall algorithm can be greatly improved by minimising the number of evaluations of the pow and exp functions as those are expensive.

The quantities $D(F)$ and $\Gamma(F)$ are constant in time and can thus be cached between time steps. A further improvement is to decompose t_{n+1} as $t_n + \delta$, then

$$e^{\rho v \alpha \Gamma t_{n+1}} = e^{\rho v \alpha \Gamma t_n} e^{\rho v \alpha \Gamma \delta} \qquad (4.64)$$

We can therefore just compute $e_j = e^{\rho v \alpha \Gamma(F_j)\delta}$ for $j = 0, ..., J+1$ once, and at each step simply update E as:

$$E_j^{n+1} = e_j E_j^n \qquad (4.65)$$

with initial value $E_j^0 = 1$. This can be easily extended to multiple time step sizes used in multi-stage schemes. We used the above optimization for the tests presented in the next section.

For multi-stage schemes, another approach is to consider E as piecewise constant between full time steps and thus to avoid its computation for fractions of time steps. In our tests, the latter technique led to a slightly decreased accuracy and little performance gain. In particular, the increase in error was particularly visible for long term options and large time steps, and we thus did not use it in our tests.

4.5. NUMERICAL RESULTS

4.5.1. OSCILLATIONS
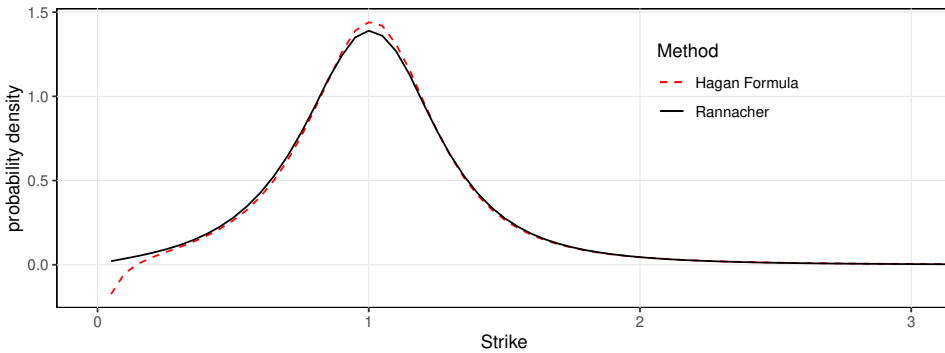
Figure 4.5.1: Probability density in Hagan PDE using a total of 5 time steps, compared to the probability density implied by the Hagan formula at $t_N = \tau_{ex}$.

With the same parameters as in Section 4.4.3, Figure 4.5.1 shows a smooth positive probability density using only a total of 5 time steps when the Rannacher smoothing is applied to the Crank-Nicolson scheme. The density computed using the second- or third-order Lawson-Morris-Gourlay (LMG2, LMG3), BDF2, Lawson-Swayne (LS), TR-BDF2 schemes or Richardson extrapolation on the implicit Euler scheme (RE) would look very similar. Figure 4.5.2b shows no apparent oscillations in the first steps for the Rannacher scheme. BDF2 and LMG2 would look the same. The Lawson-Swayne scheme shows a nearly imperceptible oscillation at the first step, and no more afterwards (Figure 4.5.2c). The TR-BDF2 and Bathe schemes behave similarly. In contrast, the Crank-Nicolson scheme had strong oscillations visible at $T = \tau_{ex}$ with 40 time steps for the PDE in Q and even stronger oscillations with 80 time steps for the PDE in θ.

(a) Crank-Nicolson   (b) Rannacher   (c) Lawson-Swayne
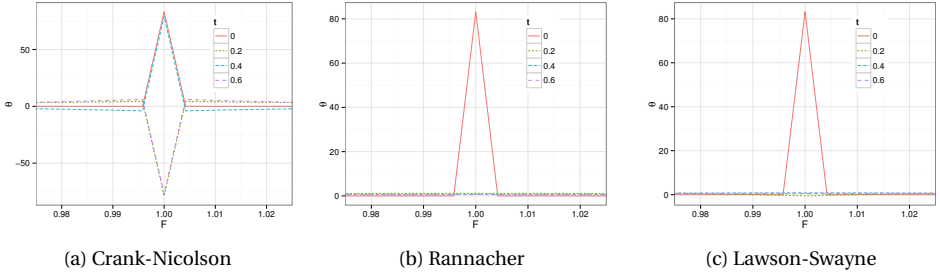
Figure 4.5.2: Transformed density for the first 4 time step in Hagan PDE discretized with various finite difference scheme using a total of 5 time steps.

4.5.2. PERFORMANCE

Hagan example.   With the same parameters as in Section 4.4.3, Figure 4.5.3 displays the maximum error in the probability density with a varying number of time steps and 500 points for the rate dimension. The reference is the probability obtained by the Crank-

(a) Accuracy vs. number of time steps   (b) Accuracy vs. time
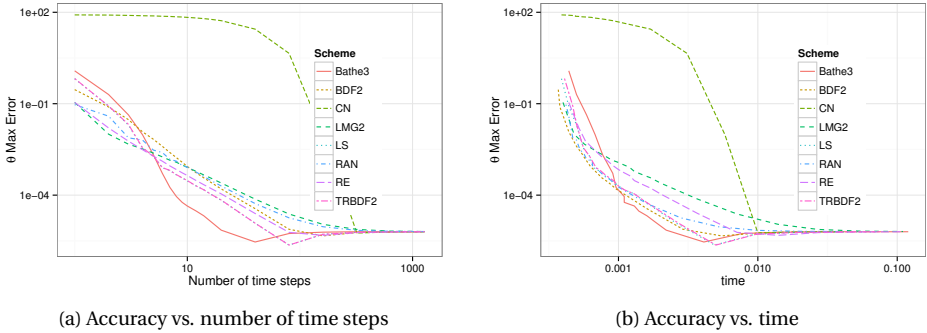
Figure 4.5.3: Performance on Hagan example

Nicolson scheme with 5120 points for the rate dimension and enough time steps to ensure that $\Phi_\theta < 1$. All schemes, except Crank-Nicolson and Bathe exhibit a second order convergence. The Crank-Nicolson scheme shows a very low convergence below 100 time steps while the Bathe scheme shows higher than order-2 convergence. Because we use a fixed number of points in the rate dimension, around ten times smaller than for the reference values, the maximum error in θ is floored for a large number of time-steps. The performance of each scheme is better assessed on the plot of the error against the computational time. On this example, The BDF2, TR-BDF2 and Lawson-Swayne schemes exhibit the best performance vs accuracy.

Other tests we performed using the implied volatility maximum error or even the at-the-money implied volatility error lead to similar conclusions. Furthermore, a Black implied volatility with an absolute error below 0.1% was achieved with only 3 time steps

for Bathe, 6 for Lawson-Swayne and TR-BDF2, 10 for LMG2, and 12 for BDF2 and RAN. Lawson-Swayne is the most efficient scheme on this problem, closely followed by TR-BDF2, Rannacher and BDF2.

Higher-order schemes like BDF3, LMG3 or a third-order Richardson extrapolation were found to be no better performing than their second-order variation on this problem.

Andreasen-Huge example. We consider the SABR parameters used in [13]: $\alpha = 0.0873, \beta = 0.7, \rho = -0.48, \nu = 0.47$ with a forward of $f = 0.025$ and a maturity $\tau_{ex} = 10.0$ and look at the maximum error in implied volatility between $0.2f$ and $2f$ using 500 points for the rate dimension, and varying the number of time steps.

(a) Accuracy vs. number of time steps   (b) Accuracy vs. time
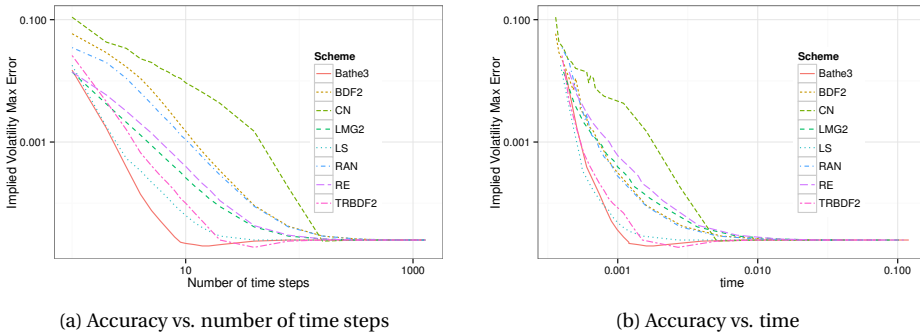
Figure 4.5.4: Performance on Andreasen-Huge example

Only 3 time steps are enough to achieve a Black implied volatility accuracy better than 0.1% with Lawson-Swayne and Bathe schemes, 4 time steps for TR-BDF2, 5 for LMG2, 12 for RAN and BDF2 (Figure 4.5.4a).

4.5.3. DUPIRE FORWARD PDE

The two different approaches result in the same smile, even with a relatively small number of time steps. With the Lawson Swayne finite difference method, the difference in implied volatility between the two approaches with 5 time steps and $J = 50, n_{sd} = 4$ is always below 0.04%. Figure 4.5.5a displays the probability density computed by numerical differentiation of the prices, using the SABR parameters of Andreasen-Huge.

If one pushes the number of time steps smaller yet, then a difference appears in favour the the probability density approach (Figure 4.5.5b with 2 steps).

The probability density approach is more accurate with fewer time steps, and more stable. With only two time steps, the Dupire approach leads to a large oscillation in probability density. As Lawson-Swayne is strongly L-stable, it disappears very quickly: with three time steps or more.

(a) with 5 time steps   (b) with 2 time steps
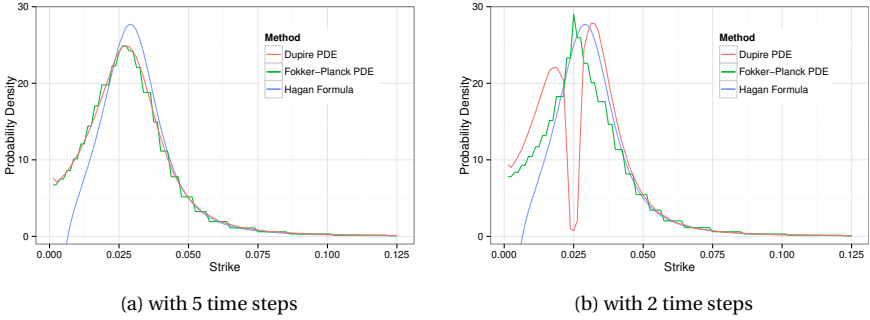
Figure 4.5.5: Numerical Probability Density on Andreasen-Huge example

(a) with 5 time steps   (b) with 2 time steps
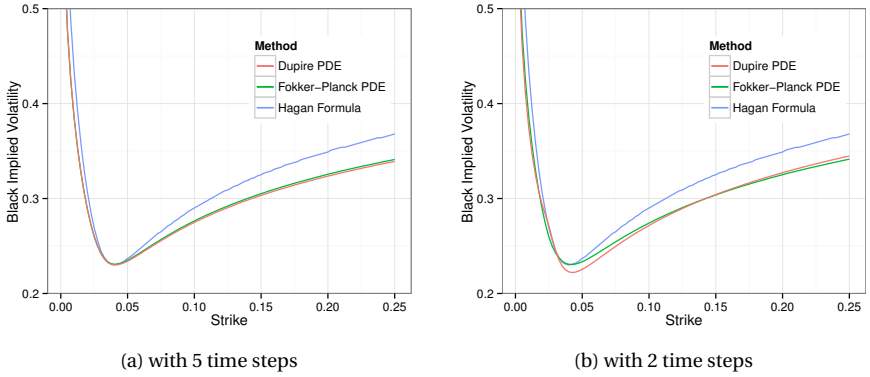
Figure 4.5.6: Black implied volatility on Andreasen-Huge example

4.6. FREE-BOUNDARY SABR MODEL BEHAVIOR

4.6.1. IMPLIED VOLATILITY SMILE

We first consider the same parameters as in [14] to validate the PDE approach presented in Section 4.2.3. The arbitrage-free PDE (4.13) reproduces the same probability density (Figure 4.6.1a). We observe a bigger and narrower spike around zero than Antonov et al. [14]. We would obtain a smaller spike had we employed larger steps to compute the density. Note that this spike is not the result of a numerical error propagated in the finite difference scheme, but is inherent to the free-boundary SABR model. The finite difference scheme actually behaves very well presenting no oscillation around the spike. Furthermore, the option delta stays smooth around the spike, near $f = 0$ or $K = 0$.

The presence of such a spike might look unnatural at first. This spike is a feature of the free-boundary and ensures that rates are 'sticky' around zero in the model. This is viewed a strength of the free-boundary approach, as stickiness in rates near 0 has been observed in historical rates [142, 181], the spike in the probability density corresponds

(a) probability density function

(b) b.p. vols
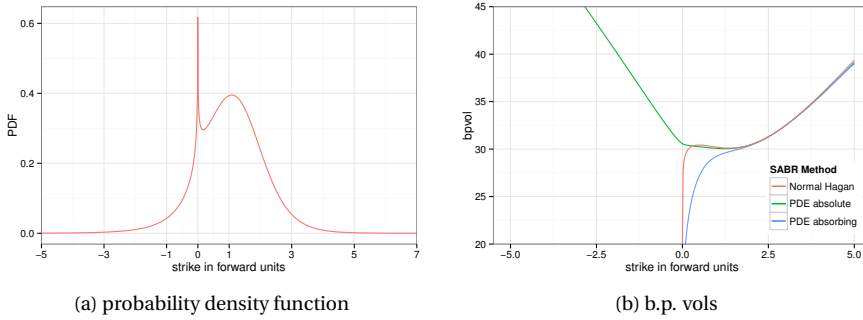
Figure 4.6.1: Lawson-Swayne on the free-boundary SABR PDE with $f = 50$ b.p., $\beta = 0.1, \alpha = 0.5 f^{1-\beta}, \rho = -30\%, v = 30\%, \tau_{ex} = 3$

to this stickiness. Stickiness at a positive rate $-b$ could be represented by a shifted free-boundary model where $L(F) = |F + b|^{\beta}$ with the shift b being negative. The β parameter controls the stickiness intensity.

Table 4.6.1 shows that the normal volatilities are quite close to the reference values of Antonov et al. [14]. The maximum error from their analytic approximation on the same

K	Lawson-Swayne	Reference	Difference
-0.95	30.72	30.93	-0.21
-0.80	29.70	29.95	-0.25
-0.65	28.69	28.97	-0.28
-0.5	27.70	27.99	-0.29
-0.35	26.74	27.04	-0.30
-0.2	25.87	26.15	-0.28
-0.05	25.21	25.46	-0.25
0.1	25.71	25.85	-0.14
0.25	26.65	26.69	-0.04
0.4	27.43	27.39	0.04
0.55	28.06	27.97	0.09
0.7	28.58	28.45	0.13
0.85	29.03	28.87	0.16
1.0	29.42	29.25	0.17
1.15	29.79	29.60	0.19
1.3	30.14	29.94	0.20
1.45	30.48	30.29	0.19
1.6	30.84	30.63	0.21
1.75	31.20	30.99	0.21
1.9	31.58	31.37	0.21

Table 4.6.1: PDE accuracy with $f = 50$ b.p., $\beta = 0.25, \alpha = 0.5 f^{1-\beta}, \rho = -30\%, v = 30\%, \tau_{ex} = 3$. The reference values are obtained by Monte-Carlo simulation in [14].

data is 0.20 b.p. while the PDE leads to a maximum error of 0.30 b.p. when compared to

their Monte-Carlo reference values. When compared to the classic normal SABR formula from Hagan et al. [85], the error is slightly lower for positive strikes: the PDE, stemming from an expansion of the same order as the one used in Hagan normal formula, stays closer to it rather than to Monte-Carlo prices, which realises the theoretical SABR model. This is particularly true in the right wing $K \geq f$ where the error in b.p. vol compared to the normal Hagan formula is between 0.20 and 0.03, while the error against Monte-Carlo is between 0.17 and 0.21.

Figure 4.6.1b shows that the smile presents an inflection point at $F = 0$. This is a typical behavior of the free-boundary SABR model under low rates. In contrast, the shifted SABR model assumes that this point is not special as absorption occurs at a different point, the shift $F = -b$ that no forward rate is supposed to be able to reach.

4.6.2. THE ABSENCE OF KNEE

Different recent studies show that the at-the-money normal volatilities observed in the market have a knee like shape [44, 93]: they are linear under very low-rate and are reasonably constant from low to high forward rates.

Hagan explains that this has led people to believe that the market switches from normal to lognormal when the rates become very low, but that in reality, absorption at zero creates this behavior even in the normal model [84]. We reproduce the example in the normal SABR case $\beta = 0$, with absorption at $F = 0$ and see that the free-boundary SABR model behaves just like the standard normal SABR model without absorption in this case (Figure 4.6.2a).

(a) $\beta = 0$ (b) $\beta = 0.1$
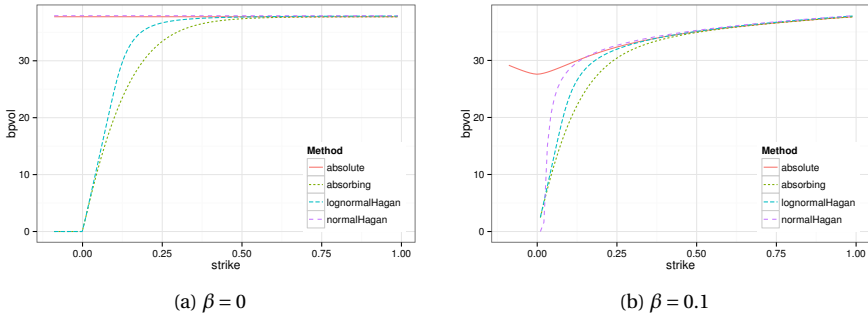
Figure 4.6.2: At-the-money b.p. volatilities with $f = 1, \alpha = 0.35, \rho = 0\%, \nu = 100\%, \tau_{ex} = 1$

An increase of β results in only a very mild knee (Figure 4.6.2b).

4.7. CONCLUSION

It is possible to accurately compute option prices under the arbitrage-free SABR approach with very few time steps, even for long maturities. The Rannacher smoothing is a particularly simple way to improve accuracy significantly compared to Crank-Nicolson on this problem. However, as the number of time steps decreases, the lower convergence of the Euler smoothing steps becomes more apparent. The simpler BDF2 scheme

is more efficient on this problem. Other less well known schemes such as TR-BDF2 or Lawson-Swayne further increase the efficiency. In our experiments, the TR-BDF2 and Lawson-Swayne schemes were robust and had similar stability and convergence properties.

Thus, with a careful choice of finite difference scheme, the arbitrage-free PDE of Hagan et al. [84] is particularly competitive to the one step finite difference approach of Andreasen and Huge [13]. It can also lead to arbitrage-free pricing of alternative SABR models such as the free-boundary SABR model.

4

4.A. POSITIVE DENSITY ON THE ARBITRAGE-FREE SABR OF HA-GAN

We have seen in the previous chapter, that on the pure diffusion equation with Dirac initial condition, the BDF2 scheme always leads to a positive density at the Dirac location, regardless of the ratio of time steps over space-steps. Similarly, we have seen that the Lawson-Swayne leads to a positive discrete density after the second time step. Let us look now, in practice, on the arbitrage-free SABR PDE, when does the density stay positive.

As an example, we choose the parameters of Hagan et al. [84], namely $\alpha = 35\%, \beta = 25\%, \rho = -10\%, \nu = 100\%, f = 1$ with a dense grid in the transformed coordinate z (number of space-steps $N = 50000$), varying the time to expiry T with only 2 time steps in order to assess the at-the-money positivity of the density Q when the ratio of space-steps over time steps, that is, when $\frac{k}{h^2}$ is very large.

Our implementation of BDF2 leads to a positive density for $T \leq 91$ and to a negative density for $T \geq 92$. Interestingly, it will lead to negative density as soon as $N \geq 81$, which suggests an IEEE 754 double accuracy representation issue of our implementation instead of an inherent instability of the scheme related to the ratio $\frac{k}{h^2}$ (see Table 4.A.1). In any case, a time to expiry of more than 90 years is very extreme, and under more realistic parameters, there is no negative density.

T	$\frac{k}{h^2}$	Positive
91	$6.62 \cdot 10^2$	Yes
91	$2.84 \cdot 10^8$	Yes
92	$2.87 \cdot 10^8$	No
92	$6.62 \cdot 10^2$	No

Table 4.A.1: Probability density positivity with SABR parameters: $\alpha = 35\%, \beta = 25\%, \rho = -10\%, \nu = 100\%, f = 1$

In contrast, the Crank-Nicolson scheme will always lead to a negative density as the space-step size h is itself dependent on the time-to-maturity T and $\frac{k}{h^2}$ can not be made small enough without increasing the number of time steps (we don't have $\frac{k}{h^2} \to 0$ when $T \to 0$).

STOCHASTIC COLLOCATION FOR AN ARBITRAGE-FREE IMPLIED VOLATILITY, PART I

This chapter explains how to calibrate a stochastic collocation polynomial against market option prices directly. The method is first applied to the interpolation of short maturity equity option prices in a fully arbitrage-free manner and then to the joint calibration of the constant maturity swap convexity adjustments with the interest rate swaptions smile. To conclude, we explore some limitations of the stochastic collocation technique.

5.1. INTRODUCTION

The financial markets provide option prices for a discrete set of strike prices and maturity dates. In order to price over-the-counter vanilla options with different strikes, or to hedge complex derivatives with vanilla options, it is useful to have a continuous arbitrage-free representation of the option prices, or equivalently of their implied volatilities. For example, the variance swap replication of Carr and Madan consists in integrating a specific function over a continuum of vanilla put and call option prices [31, 33]. More generally, Breeden and Litzenberger [28] have shown that any path-independent claim can be valued by integrating over the probability density implied by market option prices. An arbitrage-free representation is also particularly important for the Dupire local volatility model [55], where arbitrage will translate to a negative local variance. In this chapter, we describe a new technique to interpolate the market option prices in an arbitrage-free manner.

A rudimentary, but popular representation is to interpolate market implied volatilities with a cubic spline across option strikes. Unfortunately this may not be arbitrage-free as it does not preserve the convexity of option prices in general. A typical convex interpolation of the call option prices by quadratic splines or rational splines is also not satisfactory in general since it may generate unrealistic oscillations in the corresponding implied volatilities, as evidenced in [109]. Kahale [116] designs an arbitrage-free interpolation of the call prices, which however requires convex input quotes, employs two embedded non-linear minimizations, and it is not proven that the algorithm for the interpolation function of class C^2 converges. In reality, it is often not desirable to strictly interpolate option prices as those fluctuate within a bid-ask spread. Interpolation will

lead to a noisy estimate of the probability density (which corresponds to the second derivative of the undiscounted call option price).

More recently, Andreasen and Huge [12] have proposed to calibrate the discrete piecewise-constant local volatility corresponding to a single-step finite difference discretization of the forward Dupire equation. In their representation of the local volatility, the authors use as many constants as the number of market option strikes for an optimal fit. It is thus sometimes considered to be "non-parametric". Their technique works well but often yields a noisy probability density estimate, as the prices are typically over-fitted. Furthermore the output of their technique is a discrete set of option prices, which, while relatively dense, must still be interpolated carefully to obtain the price of options whose strike falls in between nodes.

An alternative is to rely on a richer underlying stochastic model, which allows for some flexibility in the implied volatility smile, such as the Heston or SABR stochastic volatility models. While semi-analytic representations of the call option price exist for the Heston model [91], the model itself does not allow to represent short maturity smiles accurately. The SABR model is better suited for this, but has only closed-form approximations for the call option price, which can lead to arbitrage [84, 85].

Grzelak and Oosterlee [78] use stochastic collocation to fix the Hagan SABR approximation formula defects and produce arbitrage-free option prices starting from the Hagan SABR formula. Here, we will explore how to calibrate the stochastic collocation polynomial directly to market prices, without going through an intermediate model.

This is of particular interest to the richer collocating local volatility (CLV) model, which allows to price exotic options through Monte-Carlo or finite difference methods [77]. A collocation polynomial calibrated to the vanilla options market is key for the application of this model in practice.

Another application of our model-free stochastic collocation is to price constant maturity swaps (CMS) consistently with the swaption implied volatility smile. In the standard approximation of Hagan [82], the CMS convexity adjustment consists in evaluating the second moment of the distribution of the forward swap rate. It can be computed in closed-form with the stochastic collocation. This allows for an efficient method to calibrate the collocation method jointly to the swaptions market implied volatilities and to the CMS spread prices.

The outline of the chapter is as follows. Section 5.2 presents the stochastic collocation technique in detail. Section 5.3 explains how to calibrate the stochastic collocation directly to market prices, and how to ensure the arbitrage-free calibration transparently, through a specific parameterization of the collocation polynomial. We also describe a general technique to create an arbitrage-free discrete set of option prices from an initial set of quotes, which may contain arbitrage. Section 5.4 reviews some popular option implied volatility interpolation methods, and illustrates the various issues that may arise with those on a practical example. Section 5.5 applies the direct collocation technique on two different examples of equity index option prices. Section 5.6 introduces the joint calibration of CMS convexity adjustments and swaption prices in general. Section 5.7 applies the model-free stochastic collocation on the joint calibration of CMS and swaption prices. Finally, Section 5.8 explores some limitations of the stochastic collocation technique along with possible remedies.

5.2. Overview of the stochastic collocation method

Collocation methods are commonly used to solve ordinary or partial differential equations [138]. The underlying principle is to solve the equations in a specific finite dimensional space of solutions, such as polynomials up to a certain degree. In contrast, the stochastic collocation method [151] consists in mapping a physical random variable Y to a point X in an artificial stochastic space. Collocation points x_i are used to approximate the function mapping X to Y, $\Phi_X^{-1} \circ \Phi_Y$, typically by a polynomial, where Φ_X, Φ_Y are respectively the cumulative distribution functions (CDF) of X and Y. Thus only a small number of inversions of Y (and evaluations of Φ_Y) are used. This allows the problem to be solved in the "cheaper" artificial space.

In the context of option price interpolation, the stochastic collocation allows us to interpolate the market CDF in a better set of coordinates. In particular, we follow Grzelak and Oosterlee [78] and use a Gaussian distribution for X.

In [78], the stochastic collocation is applied to the survival distribution function $\bar{\Phi}_Y$, where $\bar{\Phi}_Y(y) = 1 - \Phi_Y(y)$ with Φ_Y being the cumulative density function of the asset price process. When the survival density function is known for a range of strike prices, their method can be summarized by the following steps:

1. Given a set of collocation strikes y_i, $i = 0, ..., N$, compute the survival density p_i at those points: $p_i = \bar{\Phi}_Y(y_i)$.

2. Project on the Gaussian distribution by transforming the p_i using the inverse cumulative normal distribution Φ^{-1} resulting in $x_i = \Phi^{-1}(1 - p_i)$.

3. Interpolate (x_i, y_i) with a monotonic and derivable function g on $\mathbb{R}$. Grzelak and Oosterlee [78] use a Lagrange polynomial for g but the technique can be applied to any derivable and monotonic function. Further on, we will consider a monotonic spline.

4. Price by integrating the density with the integration variable $x = \Phi^{-1}(1 - \bar{\Phi}_Y(y))$, using the approximation g to map the coordinates x to the strikes y.

In order to illustrate the mapping involved in the stochastic collocation technique, we consider four options with strikes $y_0 = 40$, $y_1 = 70$, $y_2 = 120$, $y_3 = 215$ and maturity time $T = 2$ in the Black-Scholes model with constant volatility $\sigma = 20\%$ and forward price to maturity $F = 100$. Figure 5.2.1a details the mapping from the four market strikes y_i to the cumulative probability density p_i (step 1) and Figure 5.2.1b shows the mapping from the coordinate x_i to y_i (step 2). The initial goal of step 3 is to find a smooth function that approximates well the theoretical mapping in the coordinates from x to y. The mapping function only needs to be monotonic, and to conserve the first moment, in order for the collocation method to be arbitrage-free.

The figures show the mapping with the Black-Scholes model, which constitutes the reference, and with the polynomial collocation presented in this chapter, based on the four options. The cumulative density for the B-spline collocation is obtained after computing the optimal collocation cubic polynomial in the x, y coordinates, based on the four points $(x_i, y_i)_{i=0,...,3}$.

(a) Cumulative probability density from strike prices y_i.

(b) x_i from y_i.
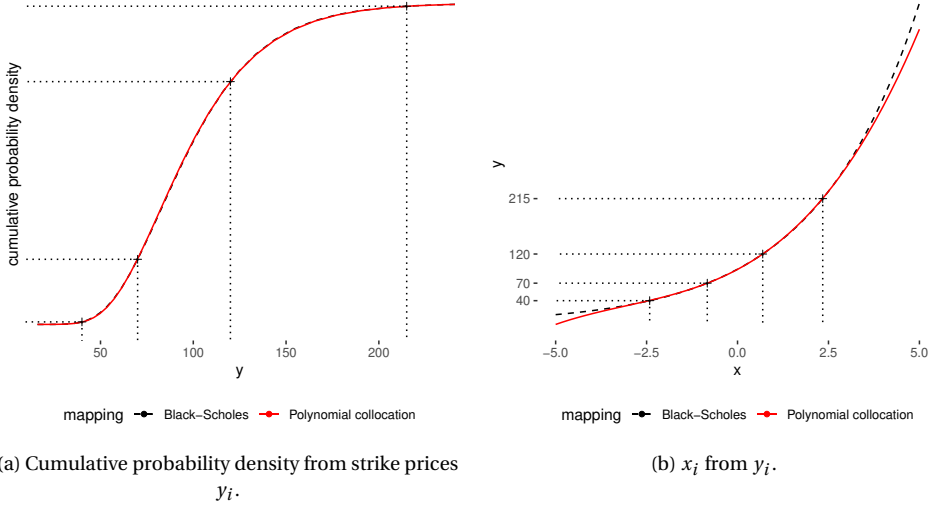
Figure 5.2.1: Mapping in the stochastic collocation technique for the Black-Scholes model with volatility $\sigma = 20\%$.

In reality, we are really interested in minimizing the error in terms of option prices (or equivalently implied volatilities). The discrete set of reference option prices either comes directly from the financial markets, or from a prior model. And this is where step 4 becomes also critical.

Let us now detail step 4. The undiscounted price of an option with strike price K is obtained by integrating over the probability density [28]:

$$V_{\text{call}}(K) = \int_0^{+\infty} \max(y - K, 0) \phi_Y(y) dy,$$

where ϕ_Y the probability density implied by the options prices. We then perform the change of variable $x = \Phi^{-1}(1 - \bar{\Phi}_Y(y))$ to obtain

$$V_{\text{call}}(K) = \int_{\Phi^{-1}(0)}^{\Phi^{-1}(1)} \max(\bar{\Phi}_Y^{-1}(1 - \Phi(x)) - K, 0) \phi(x) dx.$$

As $g(x) \approx \bar{\Phi}_Y^{-1}(1 - \Phi(x))$, we have

$$V_{\text{call}}(K) \approx \int_{-\infty}^{\infty} \max(g(x) - K, 0) \phi(x) dx$$
$$= \int_{x_K}^{\infty} (g(x) - K) \phi(x) dx, \tag{5.1}$$

where $\phi(x)$ is the Gaussian density function and

$$x_K = g^{-1}(K).$$

The change of variables is valid when the survival density is continuous and its derivative is integrable. In particular, it is not necessary for the derivative to be continuous.

In this chapter, we will focus on the collocation towards a polynomial g_N of degree N and will use the notation $g(x) = g_N(x)$. As shown in [98], a polynomial multiplied by a Gaussian can be integrated analytically as integration by parts leads to a recurrence relationship on the partial moments $m_i(b) = \int_b^\infty x^i \phi(x) dx$. This idea is also the basis of the Sali tree method [92]. The recurrence is given by

$$m_{i+2}(b) = (i+1) m_i(b) + b^{i+1} \phi(b), \tag{5.2}$$

with $m_0(b) = \Phi(-b), m_1(b) = \phi(b)$. We have then:

$$V_{\text{call}}(K) = \sum_{i=0}^{N} a_i m_i(x_K) - \Phi(-x_K) K, \tag{5.3}$$

where a_i are the coefficients of the polynomial in increasing powers.

According to Equation 5.2, the term $m_i(x_K)$ can be computed with $O(i)$ multiplications and additions, as well as the knowledge of $\phi(x_K)$ and $\Phi(-x_K)$. The overall computational cost for pricing one vanilla option can be approximated by the cost of finding x_K and the cost of one normal density function evaluation plus one cumulative normal density function evaluation. For cubic polynomials, x_K can be found analytically through Cardano's formula [161] and the cost is similar to the Black-Scholes formula. In the general case of a polynomial g_N of degree N, the roots can be computed in $O(N^3)$ operations as the eigenvalues of the associated Frobenius companion matrix M, defined by,

$$M(g_N) = \begin{pmatrix} 0 & 0 & \cdots & 0 & -\frac{a_0}{a_N} \\ 1 & 0 & \cdots & 0 & -\frac{a_1}{a_N} \\ 0 & 1 & & 0 & -\frac{a_2}{a_N} \\ \vdots & \vdots & \ddots & \vdots & \vdots \\ 0 & 0 & \cdots & 1 & -\frac{a_{N-1}}{a_N} \end{pmatrix}.$$

We have indeed $\det(\lambda I - M) = g_N(\lambda)$. This is, for example, how the Octave or Matlab `roots` function works [155]. Note that for a high degree N, the system can be very ill-conditioned. A remedy is to use a more robust polynomial basis such as the Chebyshev polynomials and compute the eigenvalues of the colleague matrix [75, 190]. Jenkins and Traub solve directly the problem of finding the roots of a real polynomial in [112].

A simple alternative, particularly relevant in our case as the polynomial needs to be invertible and thus monotonic, is to use the third-order Halley's method [68] with a simple initial guess $x_K = -1$n, if $K < F(0, T)$, or $x_K = 1$, if $K \geq F(0, T)$, with $F(0, T)$ the forward price of the asset to maturity T. In practice not more than three iterations are necessary to achieve an accuracy around machine epsilon.

The put option price is calculated through the put-call parity relationship, namely

$$V_{\text{call}}(K) - V_{\text{put}}(K) = F(0, T) - K,$$

where $V_{\text{put}}(K)$ is the undiscounted price today of a put option of maturity T.

5.3. CALIBRATION OF THE STOCHASTIC COLLOCATION TO MARKET OPTION PRICES

A Lagrange polynomial g_N can not always be used to interpolate directly on the collocation points implied by the market option strikes $(y_i)_{i=0,...,N}$, because on one side N might be too large for the method to be practical (there are typically more than hundred market option prices on the SPX500 equity index for a given maturity), and on the other hand, there is no guarantee that the Lagrange polynomial will be monotonic, not even for a small number of strikes. Grzelak and Oosterlee [78] propose to rely on a set of collocation points $(x_i)_{i=0,...,N}$ determined in an optimal manner from the zeros of an orthogonal polynomial. It corresponds to the set of the Hermite quadrature points in the case of the Gaussian distribution. This presupposes that we know the survival distribution function values at strikes which do not correspond to any quoted market strike. In [78], those values are given by the SABR model. Even with known survival distribution function values at the Hermite collocation points, the resulting polynomial is not guaranteed to be monotonic. For example, we consider options expiring in 20 years on an asset with spot price $S = 100$ that follows the Black-Scholes model with a constant volatility $\sigma = 25\%$. The Lagrange collocation polynomial of degree $N = 3$ or $N = 5$ implied by the Gauss-Hermite nodes is not monotonically increasing, we have $g_5'(-2.34) = -15.2$ (see Table 5.3.1 for the polynomial details). Another simple example we encountered comes from fitting SPX500 options of maturity 10 years, with the Gatheral SVI parametrization [72]. In the SVI parameterization, the implied variance σ^2 for a given option maturity is represented by

$$\sigma^2(k) = a + b\left[\rho(k-m) + \sqrt{(k-m)^2 + s^2}\right],$$

where $k = \ln\frac{K}{F(0,T)}$ is the log-moneyness for the strike price K. Our example corresponds to the following SVI parameters $a = 0.004$, $b = 0.027$, $s = 0.72$, $\rho = -0.99$ $m = 1.0$. The Lagrange quintic polynomial obtained at the Gauss-Hermite nodes implied by those SVI parameters decreases around $x = -2.36$ as we have $g_5'(-2.36) = -16.5$.

Table 5.3.1: Collocation polynomials at the Gauss-Hermite nodes for the Black-Scholes model with volatility 25%, and for the SVI parameters corresponding to a least squares fit of SPX500 options of maturity 10y. The polynomial is expressed by the coefficients c_i as $g_N(x) = \sum_{i=0}^{5} c_i x^i$.

x_i	p_i	Black-Scholes 20y		SVI 10y	
		y_i	c_i	y_i	c_i
-3.324257433552119	0.999556728408099	1.302	56.569	0.000608	88.616
-1.889175877753710	0.970565867070729	6.475	60.296	1.196	90.181
-0.616706590192594	0.731285863197276	26.861	24.385	39.392	12.040
0.616706590192594	0.268714136802723	106.662	11.119	146.921	-8.065
1.889175877753710	0.029434132929270	442.452	6.348	255.167	-0.267
3.324257433552119	0.000443271591900	2201.299	1.210	378.042	0.457

Here, we don't want to assume a prior model. Instead of using a Lagrange polynomial g_N to interpolate on well-chosen $(x_i)_{i=0,..,N}$ as in step 3 of the collocation method

described in Section 5.2, we will directly calibrate a *monotonic polynomial* g_N to the market option prices at strikes $(y_i)_{i=0,...,m}$, with m typically much larger than N. The monotonicity will be guaranteed through a specific isotonic parametrization. The proposed parametrization will also conserve the first moment of the distribution exactly.

In order to apply the stochastic collocation directly to market option prices, we thus need to:

- find an estimate of the survival density from the market option prices (corresponding to the step 1 of the collocation method described in Section 5.2),

- find a good initial guess for the monotonic polynomial g_N,

- optimize the polynomial coefficients so that the collocation prices are closest to the market option prices.

We will detail each step.

5.3.1. A rough estimate of the market survival density

Kahale [116] proposes a straightforward estimate. Let $(y_i)_{i=0,...,m}$ be the market strikes and $(c_i)_{i=0,...,m}$ the market call option prices corresponding to each strike, with $y_0 < y_1 < ... < y_n$., the call price derivative c_i' towards the strike K_i can be estimated by

$$c_i' \approx \frac{l_i + l_{i+1}}{2} \text{ where } l_i = \frac{c_i - c_{i-1}}{y_i - y_{i-1}} \tag{5.4}$$

for $i = 1, ..., m-1$, and with $c_0' = l_1$, $c_m' = l_m$.

Lemma 1 of Kahale [116] states that there is no arbitrage in those prices if and only if

$$-1 < \frac{c_i - c_{i-1}}{y_i - y_{i-1}} < \frac{c_{i+1} - c_i}{y_{i+1} - y_i} < 0, \text{ for } i = 1, ..., m-1. \tag{5.5}$$

To be more precise, we should also have $\max(F - y_i, 0) < c_i < F$, where F is the underlying forward price to the option maturity.

When Equation (5.5) holds, it is guaranteed that $-1 < c_i' < 0$ and the c_i' are increasing. A more precise estimate consists in using the parabola that passes through the three points c_{i-1}, c_i, c_{i+1} to estimate the slopes:

$$c_i' \approx \frac{l_i(y_{i+1} - y_i) + l_{i+1}(y_i - y_{i-1})}{y_{i+1} - y_{i-1}} \text{ where } l_i = \frac{c_i - c_{i-1}}{y_i - y_{i-1}} \tag{5.6}$$

for $i = 1, ..., m-1$, and with $c_0' = l_1$, $c_m' = l_m$. It will still lead to $-1 < c_i' < 0$ and increasing c_i'.

We can build a continuous representation of the survival density by interpolating the call prices $(y_i, c_i)_{i=0,...,m}$ with the C^1 quadratic spline interpolation of Schumaker [179], where additional knots are inserted to preserve monotonocity and convexity[1]. By construction, at each market strike price, the derivative will be equal to each c_i'.

---

[1]A C^1 polynomial spline on a fixed set of knots can not preserve monotonicity and convexity in the general case [166].

The survival density corresponds to

$$\bar{\Phi}_Y(y) = -\frac{\partial V_{\text{call}}}{\partial y}(y), \tag{5.7}$$

or equivalently through the undiscounted put option prices V_{put}:

$$\bar{\Phi}_Y(y) = 1 - \frac{\partial V_{\text{put}}}{\partial y}(y). \tag{5.8}$$

In practice one will use out-of-the-money options to compute the survival density using alternatively the Equations (5.7) and (5.8). While in the case of the SABR model, it is important to integrate the probability density (or the second derivative of the call price) from y to ∞ [78], here we are only interested in a rough guess[2].

From the survival density at the strikes y_i, it is then trivial to compute the normal coordinates x_i.

5.3.2. MAKING MARKET CALL PRICES ARBITRAGE-FREE

For each strike and maturity, at a given time, the market quotes two prices for an option contract: the bid price and the ask price. In order to calibrate directly the collocation function (a polynomial or a spline) to the market quotes, we need a single estimate of the implied cumulative probability density. It is common practice to use the average of the bid and ask prices, the mid price for this purpose. Alternatively, we could also build two distinct representations: one for the bid prices and one or the ask prices.

When considered separately, the bid, ask or mid prices are not guaranteed to be arbitrage-free in theory: there can be some theoretical arbitrage within the bid-ask spread that can not be taken advantage of in practice. Like most financial models, the collocation method is really only well defined in the absence of arbitrage: the implied cumulative probability density needs to be monotonic. We will explore in this section different ways to smooth the quotes and make them arbitrage-free. While the polynomial calibration method we propose will still work well on a non-convex set of call prices, starting the optimization from a convex set has two more general advantages: a better initial estimate of the survival density and thus a better initial guess, and the ability to use a monotonic interpolation of the survival density.

When the undiscounted call option prices c_i contain some arbitrage, we need to solve the following quadratic programming problem:

$$\tilde{c} = \underset{z \in \mathbb{R}^{n+1}}{\operatorname{argmin}} \| W \cdot (z - c) \|_2^2 \tag{5.9}$$

subject to

$$-1 < \frac{z_i - z_{i-1}}{y_i - y_{i-1}} < \frac{z_{i+1} - z_i}{y_{i+1} - y_i} < 0, \text{ for } i = 1, ..., m-1, \tag{5.10}$$

where W is a diagonal matrix of weights. For equal weights W is the identity matrix I_{n+1}. We can include information on the bid-ask spread, for example by taking w_i to be the inverse of the bid-ask spread at strike y_i.

---

[2]Integration is still possible with the quadratic spline interpolation approach.

We have

$$\|W \cdot (z - c)\|_2^2 = z^T W^T W z - 2(W^T W c)^T z + (W c)^T W c.$$

The minimization problem can thus be formulated as a quadratic programming problem:

$$\tilde{c} = \underset{z \in \mathbb{R}^{n+1}, Gz \le h}{\text{argmin}} \ \frac{1}{2} z^T Q z + q^T z \qquad (5.11)$$

with

$$Q = W^T W,$$
$$q = -W^T W c,$$

and the elements $G_{i,j}$ of the matrix G, that specifies the linear constraints in (5.11), are

$$G_{i,i-1} = -\frac{1}{y_i - y_{i-1}}, \quad G_{i,i} = \frac{1}{y_i - y_{i-1}} + \frac{1}{y_{i+1} - y_i}, \quad G_{i,i+1} = -\frac{1}{y_{i+1} - y_i},$$

for $i = 1, ..., n-1$, and

$$G_{0,0} = \frac{1}{y_1 - y_0}, \quad G_{0,1} = -\frac{1}{y_1 - y_0},$$
$$G_{n,n} = \frac{1}{y_n - y_{n-1}}, \quad G_{n,n-1} = -\frac{1}{y_n - y_{n-1}}.$$

and the vector h by $h_0 = 1.0 - \epsilon$, $h_i = -\epsilon$ for $i > 0$. The constant ϵ defines a maximum acceptable slope and ensures that the call prices are strictly convex.

In order to tune the smoothing of option prices, we could add a Tikhonov regularization, using the matrix of second-order differences as Tikhonov matrix. This is however not necessary for the B-spline collocation, as we already add a regularization when computing the B-spline representation based on the initial guess.

Once the quadratic programming problem has been solved[3], we can estimate the call price slope c_i' at each strike y_i using the parabola that passes through the three points $\tilde{c}_{i-1}, \tilde{c}_i, \tilde{c}_{i+1}$ (Equation 5.6) for $i = 1, ..., m-1$, and with $c_0' = l_1$, $c_m' = l_m$. It will lead to $-1 < c_i' < 0$ and increasing c_i', as the call prices $\tilde{c}_i$ obeys the conditions of lemma 1 of Kahale [116]. This gives a direct estimate of the survival density $p_i = -c_i'$ and thus of the abscissa x_i.

Another approach to find an initial guess, is to rely on a very rough estimate, which may be a good starting point for the optimization. A straightforward initial guess for the implied cumulative probability density is to consider the density implied by a flat Bachelier volatility. The at-the-money market implied volatility is a natural choice. For a given option price, the Bachelier implied volatility σ_N possesses a simple expression in

---

[3]We used quadprog [192] in our numerical examples.

terms of rational functions, with machine epsilon accuracy [129]. The collocation points can then be obtained directly:

$$x_i = -\frac{F - y_i}{\sigma_N \sqrt{T}}.$$

(5.12)

With a constant Bachelier volatility, x is an affine function of y.

5.3.3. FILTERING OUT THE MARKET CALL PRICES QUOTES

In the previous subsection, we proposed a quadratic programming approach to build a convex set that closely approximates the initial set of market prices. It may however be relatively slow when the number of market quotes is very large. Using the `quadprog` solver, the algorithm takes 9 milliseconds on a Core i7 7700U, for the 174 SPX500 option prices as of January 23, 2018 from our example in Section 5.5.

When the goal is to calibrate a polynomial (as opposed to a spline), a much simpler approach is to merely filter out problematic quotes, i.e. the quotes that will lead to a call price derivative estimate lower than -1 or positive. We assume that the strikes $(y_i)_{0 \le i \le m}$ are sorted in ascending order. The algorithm starts from a specific index $k \in \{0, ..., m\}$. We will use $k = 0$ but we let the algorithm to be more generic. The forward sweep to filter out problematic quotes consists then in:

1. Start from strike y_k. Let the filtered set be $\mathscr{S} = \{(y_k, x_k)\}$. Let $j^\star = k$,

2. Search for the next lowest index j, such that $-1 + \epsilon < \frac{c_j - c_{j^\star}}{y_j - y_{j^\star}} < -\epsilon$ and $j^\star < j \le m$. Replace $j^\star$ by j,

3. Add $(y_{j^\star}, c_{j^\star})$ to the filtered set $\mathscr{S}$. Repeat steps (ii) and (iii).

In our examples, we set the tolerance $\epsilon = 10^{-7}$ to avoid machine epsilon accuracy issues close to -1. A small error in the derivative estimate near -1 or near 0 will lead to a disproportionally large difference in the coordinate x.

While the above algorithm will not produce a convex set, we will see that it can be surprisingly effective to compute a good initial guess for the collocation polynomial.

We could also derive a similar backward sweep algorithm, and combine the two algorithms to start at the strike y_k close to the forward price $F(0, T)$. For our examples, this was not necessary.

5.3.4. AN INITIAL GUESS FOR THE COLLOCATION POLYNOMIAL

In order to obtain an arbitrage-free price, it is not only important that the density (zero-th moment) sums up to 1, which the collocation method will obey by default, but it is also key to preserve the martingale property (the first moment), that is

$$\int_{-\infty}^{\infty} g_N(x)\phi(x) = F(t, T).$$

(5.13)

Using the recurrence relation (Equation (5.2)), this translates to

$$a_0 + \sum_{i=1}^{\frac{N-1}{2}} a_{2i}(2i - 1)!! = F(t, T).$$

(5.14)

Instead of trying to find directly good collocation points, a simple idea for an initial guess is to consider the polynomial $h_N(x) = \sum_{k=0}^{N} b_k x^k$ corresponding to the least-squares fit of x_i, y_i:

$$b_0, ..., b_N = \min_{(a_0,...,a_N) \in \mathbb{R}^{N+1}} \left\{ \sum_{i=0}^{m} \left[\left(\sum_{k=0}^{N} a_k x_i^k \right) - y_i \right]^2 \right\}, \tag{5.15}$$

with the additional martingality constraint. This is a linear problem and is very fast to solve, for example by QR decomposition. Unfortunately, the resulting polynomial might not be monotonic.

As we want to impose the monotonicity constraint by a clever parameterization of the problem, we will only consider the least-squares (with additional martingality constraint) cubic polynomial as the starting guess. The following lemma helps us determine if it is monotonic.

Lemma 5.3.1. *A cubic polynomial $a_0 + a_1 x + a_2 x^2 + a_3 x^3$ is strictly monotonic and increasing on $\mathbb{R}$ if and only if $a_2^2 - 3 a_1 a_3 < 0$.*

Proof. The derivative has no roots if and only if the discriminant $a_2^2 - 3 a_1 a_3 < 0$. $\qquad \square$

If our first attempt for a cubic initial guess is not monotonic, we follow the idea of Murray [158] and fit a cubic polynomial of the form $A + Bx + Cx^3$. For this specific case, the linear system to solve is then given by

$$\begin{pmatrix} 1 & 0 & 0 \\ 0 & \sum_{i=0}^{m} x_i^2 & \sum_{i=0}^{m} x_i^4 \\ 0 & \sum_{i=0}^{m} x_i^4 & \sum_{i=0}^{m} x_i^6 \end{pmatrix} \begin{pmatrix} A \\ B \\ C \end{pmatrix} = \begin{pmatrix} F(t,T) \\ \sum_{i=0}^{m} x_i y_i \\ \sum_{i=0}^{m} x_i^3 y_i \end{pmatrix}. \tag{5.16}$$

In our case, Lemma 1 reduces to $B > 0$ and $C > 0$. As the initial guess, we thus use the cubic polynomial with coefficients $a_0 = A = F(t,T)$, $a_1 = |B|$, $a_2 = 0$, $a_3 = |C|$.

5.3.5. The measure

The goal is to minimize the error between specific model implied volatilities and the market implied volatilities, taking into account the bid-ask spread. The implied volatility error measure corresponds then to the weighted root mean square error of implied volatilities:

$$M_\sigma = \frac{\sqrt{\sum_{i=0}^{m} w_{\sigma_i}^2 (\sigma(\xi, K_i) - \sigma_i)^2}}{\sqrt{\sum_{i=0}^{m} w_{\sigma_i}^2}}, \tag{5.17}$$

where $\sigma(\xi, K_i)$ is the Black implied volatility[4] obtained from the specific model considered, with parameters ξ, σ_i is the market implied volatility and w_{σ_i} is the weight associated to the implied volatility σ_i. In our numerical examples, we will choose $w_{\sigma_i} = 1$. In practice, it is typically set as the inverse of the bid-ask spread.

---

[4]Fast and robust algorithms to obtain the implied volatility from an option price are given in [110, 140]. When no implied volatility corresponds to the model option price, which can happen because of numerical error, we just fix the implied volatility to zero.

An alternative is to use the root mean square error of prices:

$$M_V = \frac{\sqrt{\sum_{i=0}^{m} w_{c_i}^2 \left(V_{\text{call}}(\xi, K_i) - c_i \right)^2}}{\sqrt{\sum_{i=0}^{m} w_{c_i}^2}}, \tag{5.18}$$

where $V_{\text{call}}(\xi, K_i)$ is the model[5] option price and c_i is the market option price at strike K_i. Although this is not necessary in the context of the stochastic collocation method, it may be preferable in general to use only out-of-the-money options in the above measure, i.e. to use V_{put} instead of V_{call} and market put prices instead of c_i for $K_i < F(0, T)$, in order to reduce the numerical errors related to the limited machine precision.

We can find a weight w_{c_i} that makes the solution similar to the one under the measure M_σ by matching the gradients of each problem. We compare

$$\sum_{i=0}^{m} 2 w_{c_i}^2 \frac{\partial V_{\text{call}}}{\partial \xi}(\xi, K_i) \left(c_i - V_{\text{call}}(\xi, K_i) \right),$$

with

$$\sum_{i=0}^{m} 2 w_{\sigma_i}^2 \frac{\partial \sigma}{\partial \xi}(\xi, K_i) \left(\sigma_i - \sigma(\xi, K_i) \right).$$

As we know that $\frac{\partial V_{\text{call}}}{\partial \xi} = \frac{\partial \sigma}{\partial \xi} \frac{\partial V_{\text{call}}}{\partial \sigma}$, we approximate $\frac{\partial V_{\text{call}}}{\partial \sigma}$ by the market Black-Scholes Vega, the term $(c_i - V_{\text{call}}(\xi, K_i))$ by $\frac{\partial V_{\text{call}}}{\partial \xi}(\xi_{opt} - \xi)$, and $(\sigma_i - \sigma(\xi, K_i))$ by $\frac{\partial \sigma}{\partial \xi}(\xi_{opt} - \xi)$ to obtain

$$w_{ci} \approx \frac{1}{\frac{\partial c_i}{\partial \sigma_i}} w_{\sigma_i}. \tag{5.19}$$

In practice the inverse vega needs to be capped to avoid taking into account too far out-of-the money prices, which won't be all that reliable numerically and we take

$$w_{c_i} = \min \left(\frac{1}{\nu_i}, \frac{1}{\nu_{\min}} \right) w_{\sigma_i}, \tag{5.20}$$

where $\nu_i = \frac{\partial c_i}{\partial \sigma}$ is the Black-Scholes vega corresponding the market option price c_i and $\nu_{\min}$ is a vega floor. We will take $\nu_{\min} = 10^{-6} F(0, T)$ for the collocation method.

5.3.6. OPTIMIZATION UNDER MONOTONICITY CONSTRAINTS
We wish to minimize the error measure M_V while taking into account the martingality and the monotonicity constraints (Lemma 1) at the same time. The polynomial g_N is strictly monotonically increasing if its derivative polynomial is strictly positive. We follow the central idea of Murray [158] and express g_N in an isotonic parameterization:

$$g_N(x) = a_0 + \int_0^x p(x) dx, \tag{5.21}$$

---

[5] In the case of the stochastic collocation, ξ corresponds to the coefficients of the collocation polynomial.

where $p(x)$ is a strictly positive polynomial of degree $N-1 = 2Q$. It can thus be expressed as a sum of two squared polynomials of respective degrees at most Q and at most $Q-1$ [176]:

$$p(x) = p_1(x)^2 + p_2(x)^2. \tag{5.22}$$

As in the case of the cubic polynomial, we can refine the initial guess by first finding the optimal positive least-squares polynomial with the sum of squares parameterization. Let $(\beta_{1,0}, ..., \beta_{1,q}) \in \mathbb{R}^{q+1}$ be the coefficients of the polynomial p_1 and $(\beta_{2,0}, ..., \beta_{2,q-1}) \in \mathbb{R}^q$ be the coefficients of the polynomial p_2. The coefficients $(\gamma_k)_{k=0,...,N-1}$ of p can be computed by adding the convolution of β_1 with itself to the convolution of β_2 with itself, that is

$$\gamma_k = \sum_{l=0}^{k} \beta_{1,l}\beta_{1,k-l} + \sum_{l=0}^{k} \beta_{2,l}\beta_{2,k-l}, \tag{5.23}$$

with $\beta_{1,l} = 0$ for $l > q$ and $\beta_{2,l} = 0$ for $l > q-1$. The martingality condition leads to

$$g_N(x) = F(t,T) - \sum_{k=1}^{\frac{N-1}{2}} \frac{\gamma_{2k-1}}{2k}(2k-1)!! + \sum_{k=1}^{N} \frac{\gamma_{k-1}}{k}x^k. \tag{5.24}$$

Lemma 5.3.2. *The gradient of g_N towards $(\beta_{1,0}, ..., \beta_{1,q}, \beta_{2,0}, ..., \beta_{2,q-1})$ can be computed analytically and we have*

$$\frac{\partial g_N}{\partial \beta_{l,j}}(x_i) = 2 \sum_{k=0}^{q} \frac{\beta_{l,k}x_i^{j+k+1}}{k+j+1} - \sum_{k=1}^{q} \frac{(2k-1)!!}{k}\beta_{l,2k-j-1}, \tag{5.25}$$

with $\beta_{l,k} = 0$ for $k < 0$ and $\beta_{1,k} = 0$ for $k > q$ and $\beta_{2,k} = 0$ for $k > q-1$.

Proof.

$$g_N(x) = a_0 + \int_0^x \sum_{k=0}^{2q}\sum_{l=0}^{k}\beta_{1,l}\beta_{1,k-l}x^k + \sum_{k=0}^{2q-2}\sum_{l=0}^{k}\beta_{2,l}\beta_{2,k-l}x^k dx$$

$$= a_0 + \sum_{k=0}^{2q}\frac{1}{k+1}\sum_{l=0}^{k}\beta_{1,l}\beta_{1,k-l}x^{k+1} + \sum_{k=0}^{2q-2}\frac{1}{k+1}\sum_{l=0}^{k}\beta_{2,l}\beta_{2,k-l}x^{k+1}.$$

We thus have

$$a_{k+1} = \begin{cases} \frac{1}{k+1}\left(\sum_{l=0}^{k}\beta_{1,l}\beta_{1,k-l} + \sum_{l=0}^{k}\beta_{2,l}\beta_{2,k-l}\right) & \text{for } 0 \le k \le 2q-2, \\ \frac{1}{k+1}\sum_{l=0}^{k}\beta_{1,l}\beta_{1,k-l} & \text{for } k = 2q-1, 2q. \end{cases}$$

We recall that the martingality condition implies

$$a_0 = F(t,T) - \sum_{k=1}^{q} a_{2k}(2k-1)!!.$$

We have

$$\frac{\partial a_0}{\partial \beta_{l,j}} = -\sum_{k=1}^{q}(2k-1)!!\frac{\partial a_{2k}}{\partial \beta_{l,j}},$$

and

$$\frac{\partial a_{k+1}}{\partial \beta_{1,j}} = \frac{1}{k+1} 2\beta_{1,k-j} \text{ for } j \le k \le 2q,$$

$$\frac{\partial a_{k+1}}{\partial \beta_{2,j}} = \frac{1}{k+1} 2\beta_{2,k-j} \text{ for } j \le k \le 2q-2,$$

$$\frac{\partial a_{k+1}}{\partial \beta_{l,j}} = 0 \text{ for } k < j \text{ and } l = 1,2.$$

Thus

$$\frac{\partial a_0}{\partial \beta_{l,j}} = -\sum_{k=1}^{q} \frac{(2k-1)!!}{k} \beta_{l,2k-j-1},$$

with $\beta_{l,k} = 0$ for $k < 0$ and $\beta_{1,k} = 0$ for $k > q$ and $\beta_{2,k} = 0$ for $k > q-1$.   □

In particular, for a cubic polynomial, we have

$$\frac{\partial g_3}{\partial \beta_{1,0}}(x_i) = 2\beta_{1,0}x_i + \beta_{1,1}x_i^2 - \beta_{1,1}, \quad \frac{\partial g_3}{\partial \beta_{2,0}}(x_i) = 2\beta_{2,0}x_i,$$

$$\frac{\partial g_3}{\partial \beta_{1,1}}(x_i) = \beta_{1,0}x_i^2 + \frac{2\beta_{1,1}}{3}x_i^3 - \beta_{1,0},$$

and for a quintic polynomial,

$$\frac{\partial g_5}{\partial \beta_{1,0}}(x_i) = 2\beta_{1,0}x_i + \beta_{1,1}x_i^2 + \frac{2\beta_{1,2}}{3}x_i^3 - \beta_{1,1},$$

$$\frac{\partial g_5}{\partial \beta_{2,0}}(x_i) = 2\beta_{2,0}x_i + \beta_{2,1}x_i^2 - \beta_{2,1},$$

$$\frac{\partial g_5}{\partial \beta_{1,1}}(x_i) = \beta_{1,0}x_i^2 + \frac{2\beta_{1,1}}{3}x_i^3 + \frac{\beta_{1,2}}{2}x_i^4 - \beta_{1,0} - \frac{3}{2}\beta_{1,2},$$

$$\frac{\partial g_5}{\partial \beta_{2,1}}(x_i) = \beta_{2,0}x_i^2 + \frac{2\beta_{2,1}}{3}x_i^3 - \beta_{2,0},$$

$$\frac{\partial g_5}{\partial \beta_{1,2}}(x_i) = \frac{2\beta_{1,0}}{3}x_i^3 + \frac{\beta_{1,1}}{2}x_i^4 + \frac{2\beta_{1,2}}{5}x_i^5 - \frac{3}{2}\beta_{1,1}.$$

The cubic polynomial initial guess can be rewritten in the isotonic form as follows,

$$a_0 + a_1 x + a_2 x^2 + a_3 x^3 = a_0 + \int_0^x \left(a_1 + 2a_2 t + 3a_3 t^2\right) dt$$

$$= a_0 + \int_0^x \left(\sqrt{3a_3}\, t + \frac{a_2}{\sqrt{3a_3}}\right)^2 + \left(\sqrt{a_1 - \frac{a_2^2}{3a_3}}\right)^2 dt. \quad (5.26)$$

Based on the initial guess (refined or cubic), we can use a standard unconstrained Levenberg-Marquardt algorithm to minimize the measure M_V, based on the isotonic parameterization. This results in the optimal coefficients $(\beta_{1,0}, ..., \beta_{1,q})$ and

$(\beta_{2,0}, ..., \beta_{2,q-1})$, which we then convert back to a standard polynomial representation, as described above.

The gradient of the call prices towards the isotonic parameters can also be computed analytically from Equation (5.1), as we have

$$\frac{\partial V_{\text{call}}}{\partial \beta_{l,j}}(K) = \frac{\partial x_K}{\partial \beta_{l,j}}(K) V_{\text{call}}(K) + \int_{x_K}^{\infty} \frac{\partial g_N}{\partial \beta_{l,j}}(x) \phi(x) dx,$$

where x_K is the integration cut-off point defined by Equation (5.2). As $\frac{\partial g_N}{\partial x}(\beta, x_K) > 0$, we can use the implicit function theorem to compute the partial derivatives $\frac{\partial x_K}{\partial \beta_{l,j}}(K)$:

$$\nabla x_K(\beta) = -\frac{1}{\frac{\partial g_N}{\partial x}(\beta, x_K)} \nabla g_N(\beta, x_K),$$

where $\nabla x_K = \left(\frac{\partial x_K}{\partial \beta_{1,0}}, ..., \frac{\partial x_K}{\partial \beta_{2,q-1}} \right)$ and $\nabla g_N = \left(\frac{\partial g_N}{\partial \beta_{1,0}}, ..., \frac{\partial g_N}{\partial \beta_{2,q-1}} \right)$.

5.4. EXAMPLES OF EQUITY INDEX SMILES

We consider a set of vanilla option prices on the same underlying asset, with the same maturity date. As an illustrating example, we will use SPX500 option quotes expiring on March 7, 2018, as of February, 5, 2018 from appendix 5.C. The options' maturity is thus nearly one month. The day before this specific valuation date, a big jump in volatility across the whole stock market occurred. One consequence is a slightly more extreme (but not exceptional) volatility smile.

5.4.1. A SHORT REVIEW OF IMPLIED VOLATILITY INTERPOLATIONS

Let us recall shortly some of the different approaches to build an arbitrage-free implied volatility interpolation, or equivalently, to extract the risk neutral probability density.

We can choose to represent the asset dynamics by a stochastic volatility model such as Heston [91], Bates [20], Double-Heston [36]. This implies a relatively high computational cost to obtain vanilla option prices and thus to calibrate the model, especially when time-dependent parameters are allowed. Furthermore, those models are known to not fit adequately the market of vanilla options with short maturities. Their implied volatility smile is typically too flat.

Many practitioners revert to a parameterization based on, or inspired from a stochastic volatility model, such as the Hagan SABR expansion [85], or the Gatheral SVI model [63, 72]. These are much faster to calibrate. SVI is one of the most popular parameterizations to represent the equity option volatility smile, because of its simplicity, its relation to stochastic volatility models asymptotically, and its almost arbitrage-free property. However, as we shall see, the fit for options on equities can still be poor (Figure 5.4.1a). SVI manages to fit only a part of the left wing and fails to represent well the market quotes in the region of high implied volatility curvature. SVI and SABR are usually much better at fitting longer option maturities.

Another approach is to not assume any underlying model, and use an exact interpolation. A cubic spline interpolation of the implied volatilities is not arbitrage-free,

(a) Implied volatility.

(b) Probability density.
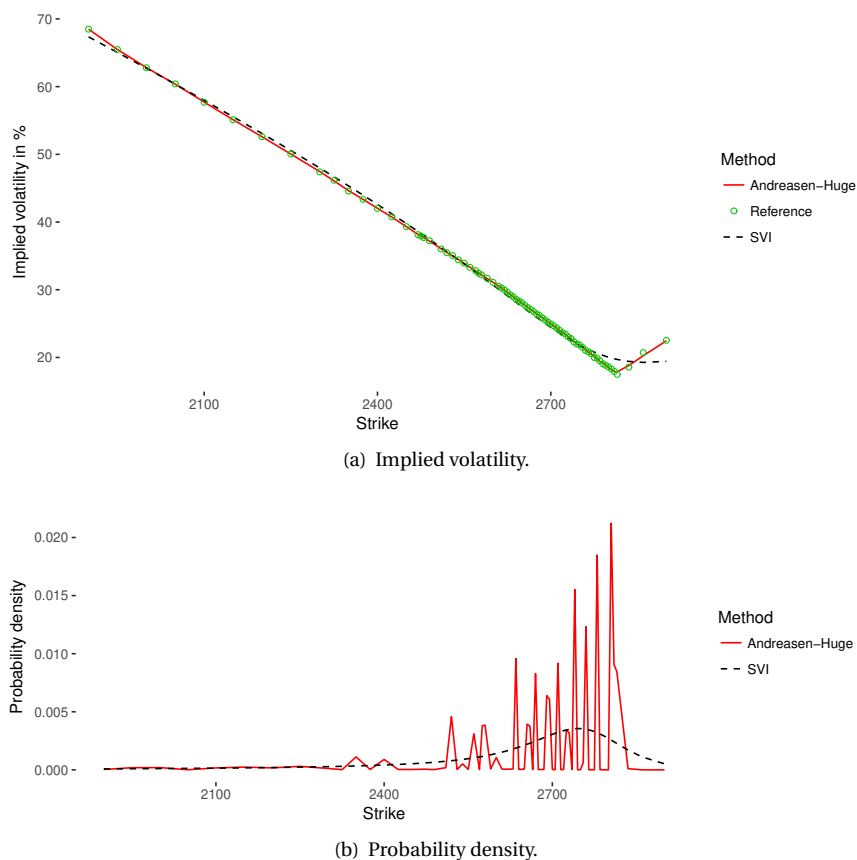
Figure 5.4.1: SVI and Andreasen-Huge calibrations on 1m SPX500 options as of February, 05, 2018.

although it is advocated[6] by Malz [150]. Kahale [116] proposes an arbitrage-free spline interpolation of the option prices. Unfortunately, it is not guaranteed that his algorithm for C^2 interpolation, necessary for a continuous probability density, converges. Furthermore, it assumes that the input call option quotes are convex and decreasing by strike. However, the market quotes are not convex in general, mainly because of the bid-ask spread. While we propose in Section 5.3.2 a quadratic programming based algorithm to build a convex set that closely approximates the market prices, it may be relatively slow when the number of option quotes is large. Finally, the resulting implied probability density will be noisy, as evidenced by Syrdal [186].

A smoothing spline or a least-squares cubic spline will allow to avoid overfitting the market quotes. For example, Syrdal [186], Bliss and Panirgitzoglou [25] use a smoothing spline on the implied volatilities as a function of the option deltas[7], with flat extrapola-

---

[6]Malz precises that the challenge of his approach is to find a good filter for the quotes, which he does not describe.

[7]Especially for options on a foreign exchange rate, the implied volatility may be parameterized as a function

tion. Smoothing is ensured by adding a penalty multiplied by the integral of the second derivative of the spline function to the objective function. The smoothing parameter is challenging to pick. In fact, Syrdal reverts to a manual ad-hoc choice of this parameter. Furthermore, the interpolation is a priori not arbitrage-free. In order to make it arbitrage-free, an additional non-linear penalty term against butterfly spread arbitrage needs to be added to the objective function. Instead of a smoothing parameter, the least-squares spline requires to choose the number of knots and their locations, which can also seem arbitrary. A slightly different approach is taken by Wystup in [202, p. 47] for the foreign exchange options market, where a Gaussian kernel smoother is applied to the market volatilities as a function of the option delta. The kernel bandwidth is fixed and the number of kernel points (specific deltas) is typically lower than the number of market option strike prices. Wystup recommends to use up to 7 kernel points. While a larger number of points leads to a better fit on our example, it may also lead to a negative density. With the Gaussian kernel smoothing, the shape of the implied volatility looks unnatural[8] around the point of high curvature (Figure 5.4.2a), and the density can become negative (Figure 5.4.2b). It is thus not always arbitrage-free.

In order to guarantee the arbitrage-free property by construction and still stay model-free, Andreasen and Huge [12] use a specific one-step implicit finite difference where a discrete piecewise-constant local volatility function is calibrated against market prices. While it is simple and fast, it leads to a noisy implied density, even if we replace the piecewise constant parameters by a cubic spline (Figure 5.4.1b). This is because, by design, similarly to a spline interpolation, the method overfits the quotes as the number of parameters is the same as the number of market option quotes.

Finally, we can model directly the risk-neutral probability density (RND). Many papers use the double lognormal mixture of Bahra [15, 18] to represent the RND. The double lognormal mixture is not flexible enough to capture our example of short maturity smile (Figure 5.4.3a). This is extended in [35] to a mixture of multiple lognormal distributions. With a mixture of 6 lognormal distributions, the root mean square error of the model volatilities against market volatilities is nearly as low as with Andreasen-Huge (table 5.4.1), and the RND is very smooth. Furthermore, the model is also fully arbitrage-free by construction. But, in a similar fashion as the Gaussian kernel smoother [202], the mixture of lognormal distributions tends to create artificial peaks in the RND (Figures 5.4.2b and 5.4.3b), just to fit the input quotes better on our example.

Compared to the Gaussian kernel smoothing, the mixture of lognormal distributions results in fewer peaks as the volatility of each distribution is optimized, but there are still clearly multiple modes in the density. In reality, as we will see with the collocation method, there is no particular reason to have multiple modes. Mixtures of normal or lognormal distributions will, by their nature, tend to create multi-modal densities.

Let us give more details about the setup of each technique on our example. For the SVI parameterization, we use the quasi-explicit calibration method described in [203], which leads to the parameters of table 5.4.2. For the Andreasen-Huge method, we use

---

of the option delta, instead of the option strike. Note that the delta is itself a function of the implied volatility, see appendix 5.A.

[8]This could be remedied by a kernel smoothing on the strikes instead of the deltas, but then the probability density goes negative in more places. We thus preferred to stay close to Wystup's original idea.

(a) Implied volatility.

(b) Probability density.
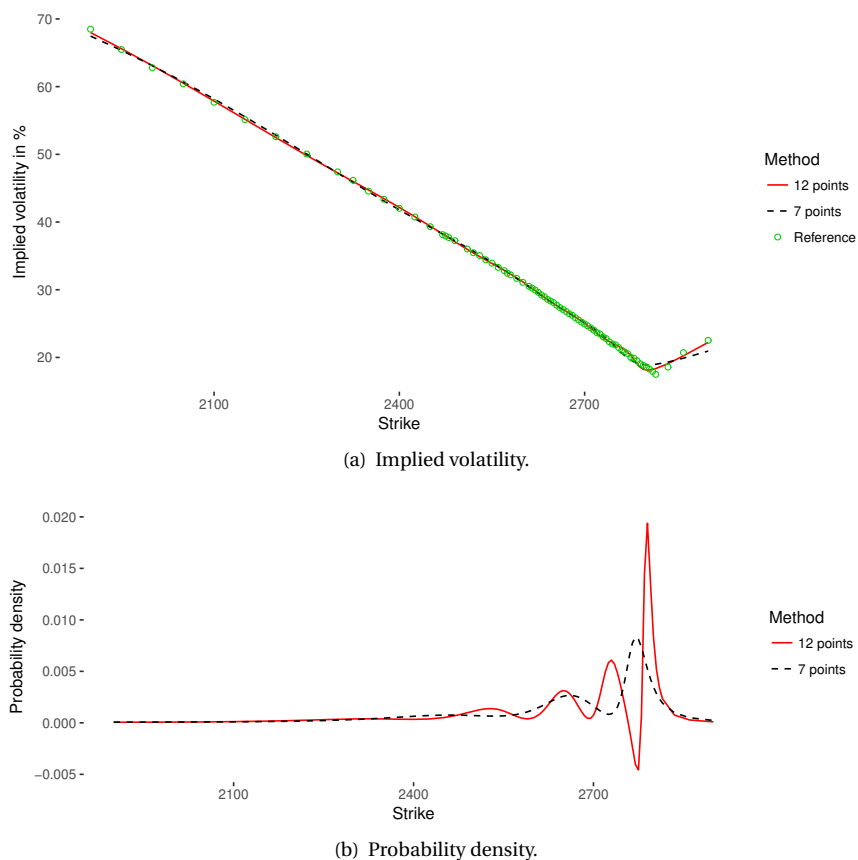
Figure 5.4.2: Gaussian kernel smoothing calibrations on 1m SPX500 options as of February, 05, 2018.

Table 5.4.1: Root mean square error (RMSE) of the calibrated model volatilities against the market volatilities.

Model	Free parameters	RMSE
SVI	5	0.00757
Andreasen-Huge	75	0.00088
Gaussian smoothing kernel	7	0.00400
Gaussian smoothing kernel	12	0.00175
Mixture of 2 lognormals	4	0.01807
Mixture of 4 lognormals	10	0.00252
Mixture of 6 lognormals	16	0.00094

a dense log-uniform grid composed of 800 points, solve the probability density (the Fokker-Planck equation) instead of the call prices. We then interpolate in between grid points by integrating the density to obtain the call option prices to preserve the arbitrage-

(a) Implied volatility.

(b) Probability density.
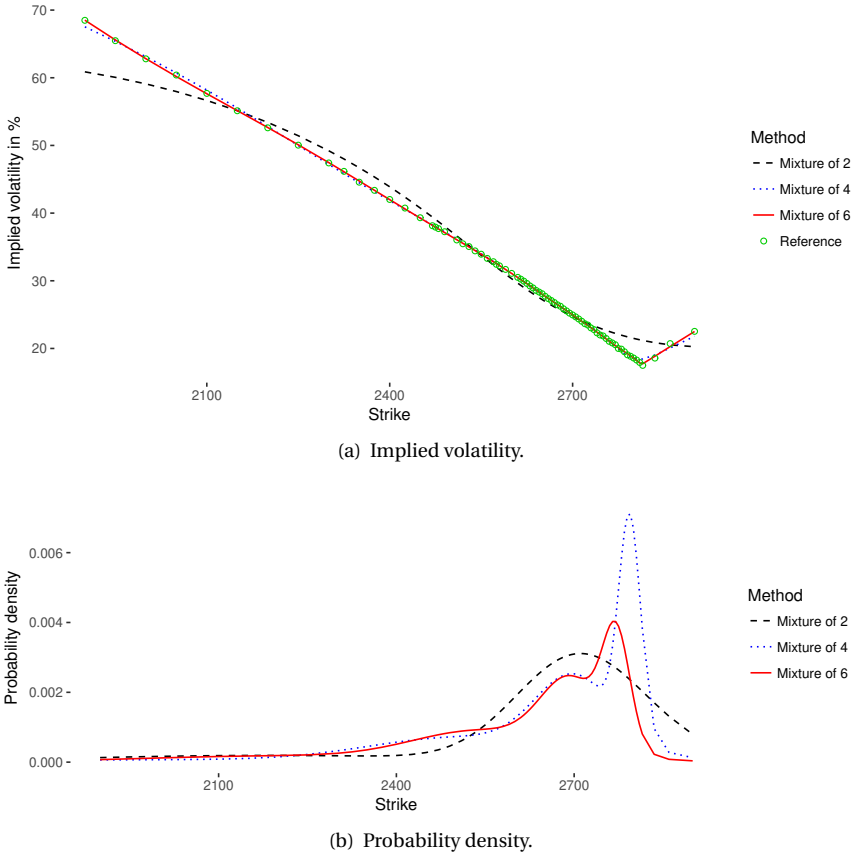
Figure 5.4.3: Mixture of lognormal distributions calibration on 1m SPX500 options as of February, 05, 2018.

free property everywhere in a similar spirit as [84, 131]. We minimize the error measure M_V with the Levenberg-Marquardt algorithm. The Gaussian kernel smoother calibration is described in appendix 5.A. We use respectively 7 and 12 kernel points, with a bandwidth of 0.5 and 0.3. When the bandwidth is too large for the number of kernel points considered, the problem becomes ill-conditioned numerically as the optimal kernel weights α become very large numbers (table 5.4.3), while the result of the kernel is a volatility of the order of 10%. Our multiple lognormal mixture optimization is described in appendix 5.B and the calibrated parameters in table 5.B.1. Note that the optimization problem becomes very challenging numerically for a mixture of more than 7 lognormal distributions, because, on one side, the number of free parameters is relatively high ($3n-2$ free parameters for n lognormal distributions) and on the other side, the highly non-linear structure of the problem creates multiple local minima.

Table 5.4.2: SVI parameters resulting of the calibration against 1m SPX500 options as of February, 05, 2018.

a	b	ρ	s	m
0.000	0.794	-0.492	0.0537	0.0554

Table 5.4.3: Optimal kernel observations α_i resulting of the Gaussian kernel smoothing against 1m SPX500 options as of February, 05, 2018, for different bandwidths λ.

Number of points	λ	$\min|\alpha_i|$	$\max|\alpha_i|$
7	0.5	4.8E03	1.1E05
12	0.292	2.5E05	1.3E08
12	0.5	1.6E10	1.2E13

5.5. Polynomial collocation of SPX500 options

Previous litterature has explored the calibration of stochastic collocation against market quotes for interest rates swaptions, in the case of the SABR model in [78] as well as for FX options. In both cases, the set of quotes is relatively small (usually less than 10) and the risk of arbitrage in the quotes, related to the bid-ask spread size is very low. In the world of equity options, the quotes are denser (it is not unusual to have 50 quotes for liquid equity indices), or less liquid, and thus have a higher probability of containing small theoretical arbitrages.

Here, we consider the quotes of vanilla options on the index SPX500, expiring on February 23, 2018 as of January 23, 2018 for 174 distinct strikes.We first take a look at the cubic polynomial guess, least-squares quintic polynomial guess, and optimal quintic polynomial that are calibrated to the market quotes. Figure 5.5.1 shows that without any preprocessing, the cubic and quintic polynomial guesses are of relatively poor quality, because of a few outliers. Filtering out the problematic quotes by imposing hard boundaries on the resulting slope estimates is enough to fix this (see Figure 5.5.2b). The preprocessing to produce a convex set of quotes through quadratic programming results in a better quintic polynomial guess but a worse cubic polynomial initial guess (Figures 5.5.2a and 5.5.2b). This is because the cubic polynomial guess has not been refined: it has not been optimized with the monotonicity constraint. Otherwise, it would fit better than the cubic polynomial optimized against our simple filtered quotes. The difference in the polynomial guesses between the two methods is however not large. Table 5.5.1 shows that the first three moments[9] of the quintic refined guess with the forward sweep filter or with the convexity filter are close to the moments corresponding to the optimal quintic polynomial collocation. On this example, the convexity filter improves the estimate of the kurtosis significantly.

Let us take a look at the quality of the fit in terms of implied volatilities. In Figures 5.5.3 and 5.5.4, the reference implied volatilities include all market options, i.e., they are unfiltered, even when afterwards, we process those in order to apply the collocation

---

[9]Here, we calculate the statistics of the underlying asset price distribution, as implied from the option prices. We are not interested in the statistics of the market options prices themselves.
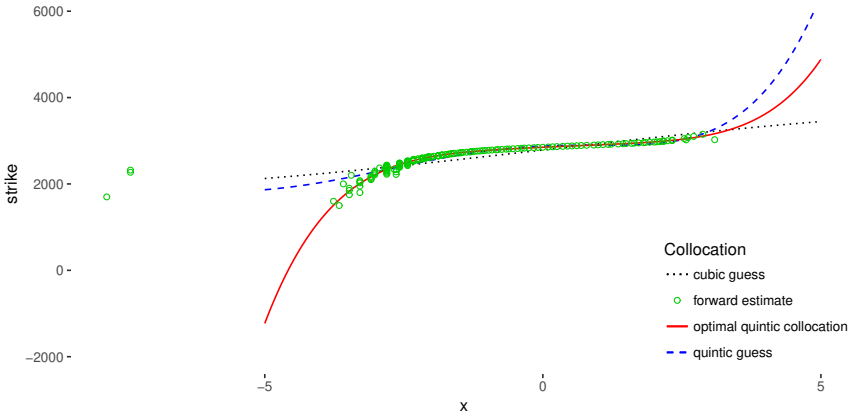
Figure 5.5.1: Strike as a function of $x = \Phi^{-1}(p)$ where p is the cumulative density for SPX500 options expiring on February 23, 2018, without applying any convexity filter.

(a) Quadratic programming convexity filter.

(b) Forward sweep filtering from $k = 0$.
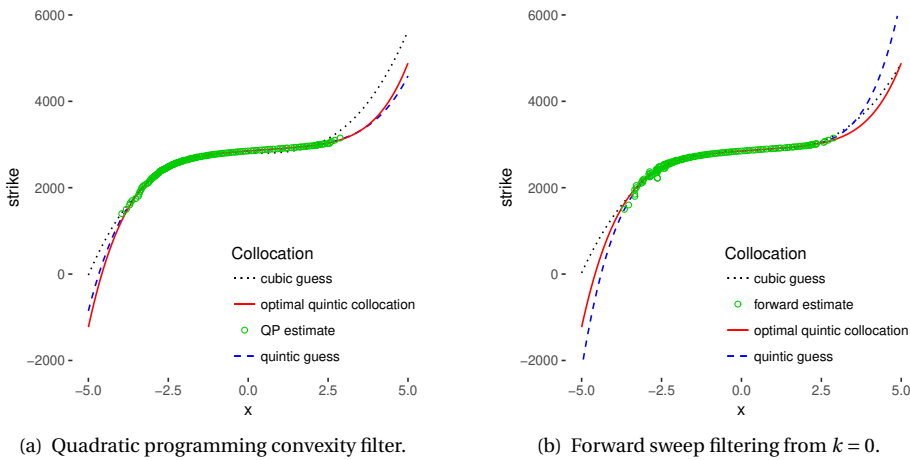
Figure 5.5.2: Strike as a function of $x = \Phi^{-1}(p)$ where p is the cumulative density for SPX500 options expiring on February 23, 2018, using a filter on the quotes.

method. On the SPX500 option quotes from January 23, 2018, Figure 5.5.3 shows that Gatheral SVI parameterization does not fit very well. While SVI is generally quite good at fitting medium and long maturities, it is often not very well suited for short maturities such as the one-month maturity we consider here. The cubic collocation, which has fewer parameters fits better than SVI, and the quintic collocation provides a nearly perfect fit on this example, which is impressive since it has the same number of free parameters as SVI.

We now consider the same SPX500 option quotes expirying on March 7, 2018, as of

Table 5.5.1: Mean, variance, skew and kurtosis corresponding to quintic polynomial collocation of SPX500 1m options as of February 5, 2018, for different filtering of market quotes.

Collocation polynomial	Mean	Variance	Skew	Kurtosis
refined quintic guess on raw quotes	2839.00	102.59	-1.59	14.72
refined quintic guess with forward sweep	2839.00	93.36	-2.74	58.97
refined quintic guess on convex quotes	2839.00	88.06	-2.63	38.87
optimal quintic polynomial collocation	2839.00	88.92	-2.71	38.52
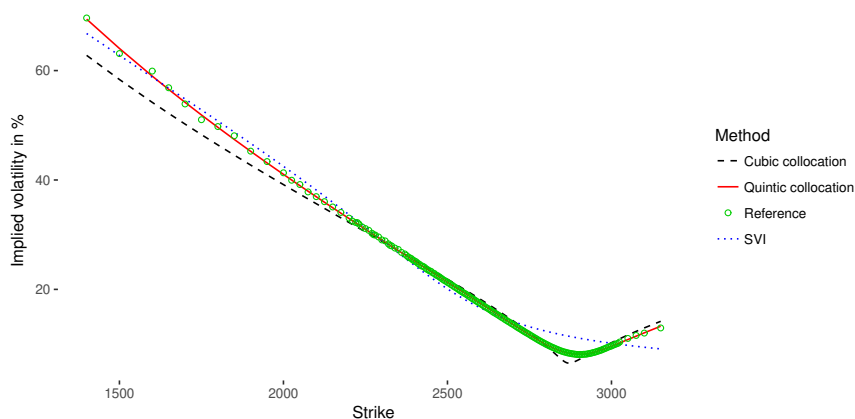
Figure 5.5.3: SPX500 smile.

February, 5, 2018 as in Section 5.4.1, and listed in appendix 5.C. The option maturities are still one month, but the valuation day corresponds to one day after a big jump in volatility across the whole stock market. The smile is more complex. Figure 5.5.4 shows that the curvature is much higher at the lowest point, and that the left wing is slightly concave. SVI manages to fit only a part of the left wing and fails to represent well the market quotes in the region of high curvature. The quintic polynomial achieves a reasonably good fit. In order to illustrate that our calibration technique still works well with a higher degree polynomial, we also calibrate a nonic polynomial. It results in a nearly perfect fit, despite the very strong curvature.

We show the corresponding probability density in Figure 5.5.5, and observe a high and narrow spike in the region where the implied volatility has a strong curvature. Contrary to the stochastic collation method, SVI does not allow to capture this spike properly. The density is also markedly different from the one obtained by the mixture of lognormal distributions in Figure 5.4.3b. In particular, it does not exhibit multiple peaks. This stays true for collocations on a polynomial of higher degree. The root mean square error (RMSE) of implied volatilities with a cubic polynomial collocation is smaller than with SVI which has two more free parameters (table 5.5.2 against table 5.4.1). The nonic polynomial collocation has a RMSE similar to the results from the Andreasen-Huge method and the mixture of 6 lognormal distributions model, while the collocation has again sig-
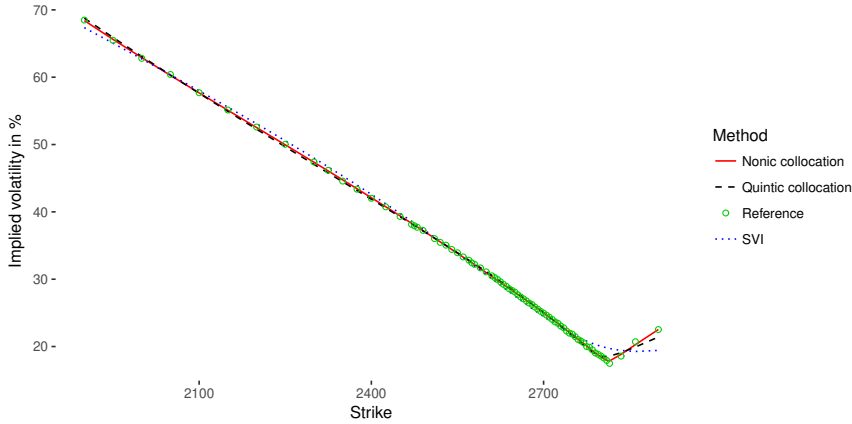
Figure 5.5.4: implied volatility smile of SPX500 1m options as of February 5, 2018.
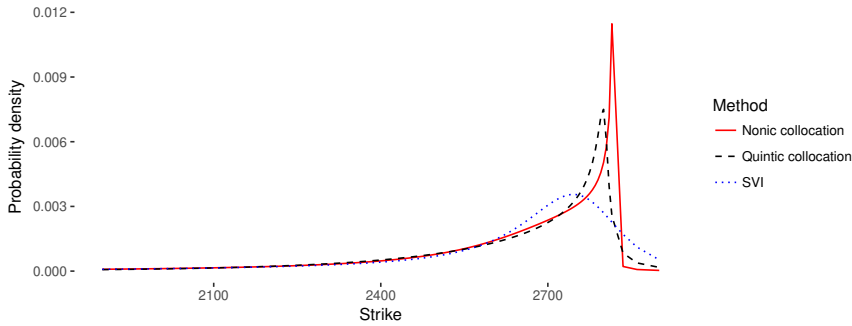
Figure 5.5.5: Implied probability density of SPX500 1m options as of February 5, 2018.

nificantly fewer free-parameters.

Table 5.5.2: Root mean square error (RMSE) of the collocation method implied volatilities against the market implied volatilities of the SPX500 1m options as of February 5, 2018.

Model	Free parameters	RMSE
Cubic collocation	3	0.00538
Quintic collocation	5	0.00280
Nonic collocation	9	0.00110
11-th degree collocation	11	0.00099

So far, we have considered individual smiles corresponding to a specific option maturity. In order to build a full volatility surface, a linear interpolation of the collocating polynomial in between maturities will preserve the arbitrage-free property across strikes as the intermediate polynomial will still be monotonic. Such an interpolation

could however introduce arbitrage in time, as it does not guarantee, a priori, that the call prices will increase with the maturity for a fixed log-moneyness. The alternative is to fit each expiry independently, and interpolate linearly in total variance across a fixed log-moneyness.

5.6. CALIBRATION OF CMS CONVEXITY ADJUSTMENTS

A constant maturity swap (CMS) is a swap where one leg refers to a reference swap rate which fixes in the future (for example, the 10 year swap rate), rather than to an interest rate index such as the LIBOR. The other leg is a standard fixed or floating interest rate leg.

By quoting the spread of the CMS rate against the equivalent standard swap rate, as well as prices of swaptions for a finite set of strike prices and maturities, the market provides information on the implied volatilities of the standard swap rates. However, even when assuming some prior interpolation of the swaption implied volatility cube, not every swaption has quotes away from at-the-money strikes, and when present, those are typically too few to allow for a robust, consistent bootstrap of the whole cube. Similarly, CMS swap spreads are only available for a few swap maturities and CMS tenors. Furthermore, the implied volatilities far from the at-the-money swaption directly influence the CMS convexity adjustments, which define the CMS spreads. It is thus important to be able to represent implied volatilities for strikes outside the quoted ones, and to be able to value CMS convexity adjustments consistently with the swaption smile.

Here, we will evaluate the quality of the stochastic collocation method on the problem of calibrating the constant maturity swaps jointly with the interest rate swaptions to the market quotes.

For a maturity T_a, the fixed rate $S_{a,b}$ for an interest rate (forward) swap exchanging interest payments at the future dates $T_{a+1}, ..., T_b$ as of date t reads [10]

$$S_{a,b}(t) = \frac{P(t, T_a) - P(t, T_b)}{\tau \sum_{j=a+1}^{b} P(t, T_j)}, \tag{5.27}$$

where τ is the year fraction for a period ($\tau = 1$ in the 30/360 daycount convention in our examples) and $P(t, T)$ is the discount factor from t to T.

In the $T_a + \delta$ forward measure, the convexity adjustment for the swap rate $S_{a,b}$ is given by

$$\text{CA}(S_{a,b}, \delta) = \mathbb{E}^{T_a + \delta} \left[S_{a,b}(T_a) \right] - S_{a,b}(0), \tag{5.28}$$

where δ is the accrual period of the swap rate. It depends on the entire evolution of the yield curve. Following Hagan's standard model [82], Mercurio and Pallavicini [152, 153] approximate the convexity adjustment by using a linear function of the underlying swap rate for the Radon-Nikodym derivative in order to express the value in the forward swap measure associated to $S_{a,b}$. This leads to

$$\text{CA}(S_{a,b}, \delta) \approx S_{a,b}(0) \theta(\delta) \left(\frac{\mathbb{E}^{a,b} \left[S_{a,b}^2(T_a) \right]}{S_{a,b}^2(0)} - 1 \right), \tag{5.29}$$

where

$$\theta(\delta) = 1 - \frac{\tau S_{a,b}(0)}{1 + \tau S_{a,b}(0)} \left(\frac{\delta}{\tau} + \frac{b - a}{\left(1 + \tau S_{a,b}(0)\right)^{b-a} - 1} \right). \tag{5.30}$$

Now $\mathbb{E}^{a,b}\left[S_{a,b}^2(T_a)\right]$ can be derived from the market swaption prices. In [82, 152, 153], the replication method is used. We will see in Section 5.7, that this expectation has a very simple closed-form expression with the collocation method. This will simplify and speed up the calibration.

As explained in [153], the market quotes the spreads $X_{m,c}$ which sets to zero the no-arbitrage value of CMS swaps starting today and paying the c-year swap rate $S'_{i,c}$ from t_{i-1} to $t_{i-1} + c$ with $t_0 = 0$. We have

$$X_{m,c} = \frac{\sum_{i=1}^{m} \left(S'_{i,c}(0) + \mathrm{CA}(S'_{i,c}, \delta)\right) P(0, t_i)}{\sum_{i=1}^{m} P(0, t_i)} - \frac{1 - P(0, t_m)}{\delta \sum_{i=1}^{m} P(0, t_i)}. \tag{5.31}$$

We will consider the example market data from Mercurio and Pallavicini [153] as of February 3, 2006, where δ corresponds to a quarter year and the CMS leg is expressed in Actual/360 while the floating leg and the spread are in 30/360 daycount convention.

In order to compute the CMS spread $X_{m,c}$, the convexity adjustments are needed for many dates not belonging to the market swaption expiries. We follow Mercurio and Pallavicini [153] and interpolate the convexity adjustments at the swaption expiries by a cubic spline (with an adjustment of zero at $t = 0$).

The market swaptions are expressed in Black volatility, and can be priced through the standard Black formula on the forward swap rate.

Mercurio and Pallavicini [152, 153] describe a global calibration, where the swaption volatility errors for each market swaption expiry and strike, plus a penalty factor multiplied by the CMS spread error for each quoted market CMS spread are minimized in a least-squares fashion. This is a single high-dimensional minimization. We will see how to apply the collocation method to this methodology, as well as a new alternative calibration.

5.7. JOINT CALIBRATION OF SWAPTIONS AND CMS CONVEXITY ADJUSTMENTS WITH THE STOCHASTIC COLLOCATION

In Section 5.6, we have described the calibration of swaptions and CMS convexity adjustments from Mercurio and Pallavicini [153]. A key estimate for their method is an approximation of the expectation $\mathbb{E}^{a,b}\left[S_{a,b}^2(T_a)\right]$ from Equation (5.29). Instead of using the replication method, when a collocation polynomial is calibrated to the market swaption prices, this expectation can be computed by a direct integration:

$$\mathbb{E}^{a,b}\left[S_{a,b}^2(T_a)\right] = \int_{-\infty}^{\infty} g_N^2(x)\phi(x)\,dx. \tag{5.32}$$

The coefficients $(b_0, .., b_{2N})$ of g_N^2 correspond to the self-convolution of the coefficients $(a_0, ..., a_N)$ of g_N. Similarly to the calculation of the first moment, the recurrence relation

(Equation (5.2)) leads to the closed-form expression

$$\mathbb{E}^{a,b}\left[S_{a,b}^2(T_a)\right] = b_0 + \sum_{i=1}^{N}(2i-1)!!\,b_{2i}\,. \tag{5.33}$$

There are two ways to include the CMS spread in the calibration of the smile to the swaption quotes, which we will label as the global and the decoupled approach. The collocation method can be used in the global approach from Mercurio and Pallavicini [153], by first computing an initial guess in the form of a list of isotonic representations, out of the market swaption quotes for each expiry according to Section 5.3. Then the least-squares minimization updates the isotonic representations iteratively.

Tables 5.7.1 and 5.7.2 show that the error with a quintic collocation polynomial is as low as with the SABR interpolation[10]. Compared to the SABR interpolation however, the advantages of stochastic collocation are: it is arbitrage-free by construction, while the SABR approximation formula has known issues with low or negative rates [84]; the accuracy of the fit can be improved by simply increasing the collocating polynomial degree; and the calculation of the CMS convexity adjustment is much faster as it does not involve an explicit replication.

Table 5.7.1: Absolute differences (in bp) between market and model swaptions implied volatilities. Strikes are expressed as absolute differences in basis points w.r.t the at-the-money values.

Strike	-200	-100	-50	-25	0	25	50	100	200
					SABR				
5x10	1.1	0.2	0.3	0.5	0.2	0.2	0.8	0.2	0.4
10x10	0.2	0.1	0.4	0.3	0.1	0.2	0.4	0.5	0.3
20x10	0.8	0.6	0.4	0.4	0	0.3	0.3	0.5	0.5
					Quintic Global				
5x10	0.1	-0.4	0.3	0.4	0.2	-0.5	-0.3	0.3	0.0
10x10	0.4	-1.8	0.4	1.0	1.3	0.2	-0.5	-1.7	1.0
20x10	0.7	-1.7	0.8	1.2	1.1	0.5	-0.7	-1.8	1.3
					Quintic Decoupled				
5x10	0.0	-0.3	0.2	0.3	0.2	-0.5	-0.3	0.4	-0.1
10x10	0.1	-0.6	0.2	0.3	0.6	-0.2	-0.3	-0.4	0.3
20x10	0.4	-2.0	0.6	1.0	1.0	0.5	-0.6	-1.6	0.9

The decoupled calibration procedure consists of the following two steps:

1. Find the optimal convexity adjustment for each market swaption expiry

   - Compute the initial guess for each convexity adjustment by fitting the swaption smile at each expiry as described in Section 5.3, without taking into account any CMS spread price.

---

[10]The SABR numbers come from Mercurio and Pallavicini [153]. For the Black model, our numbers differ slightly from Mercurio and Pallavicini, likely because of the handling of holidays.

Table 5.7.2: Absolute differences (in bp) between market CMS swap spreads and those induced by the SABR
functional form, the Black model and the collocation of a quintic polynomial for the 10y tenor.

Maturity	SABR	Black	Quintic Global	Quintic Decoupled
5y	0.8	0.0	0.3	0.3
10y	1.7	2.3	1.2	1.4
15y	1.8	3.2	1.3	1.7
20y	1.3	4.0	1.3	1.8
30y	2.1	6.3	2.3	1.9

- Compute the cubic spline which interpolates the convexity adjustments across
  the expiries. Minimize the square root of CMS spread errors, by adjusting the
  convexity adjustments and recomputing the cubic spline, for example, with
  the Levenberg-Marquardt algorithm.

2. Minimize the square of the swaption volatility error plus a penalty factor multi-
   plied by the convexity adjustment error, against the optimal convexity adjustment
   for each expiry independently.

The penalty factor allows to balance the swaption volatilities fit with the CMS spread fit.
The decoupled calibration involves $n + 1$ independent low-dimensional minimizations,
with n being the number of swaptions expiries.

Table 5.7.3 presents the optimal convexity adjustments for CMS swaps of tenor 10y
using the market data of Mercurio and Pallavicini resulting from the first step of the de-
coupled calibration method. With a cubic spline interpolation on these adjustments, the
error in market CMS spreads is then essentially zero. The adjustments resulting from the
second step are also displayed for indication.

Table 5.7.3: CMS convexity adjustments (in bp) for different expiries for the 10y tenor.

Expiry	1y	5y	10y	20y	30y
Optimal CA (step A)	1.75	10.62	20.24	35.02	49.41
Decoupled CA (step B)	1.75	10.63	20.52	37.14	60.41

As evidenced in the tables 5.7.1 and 5.7.2, the error in the swaptions volatilities and
in the CMS spreads is as small as, or smaller than the decoupled calibration when com-
pared to the global calibration. In Figure 5.7.1, we look at the smile generated by the
quintic collocation calibrated with a penalty of 1 (which corresponds to a balanced fit of
market CMS spreads versus swaption volatilities as in table 5.7.2) and a penalty of 10000
(which corresponds to a nearly exact fit to the CMS spreads).

Instead of using a monotonic quintic polynomial, we could have used a monotonic
cubic polynomial with quadratic left and right C^1-extrapolation. Two parameters of each
extrapolation would be set by the value and slope continuity conditions, and the remain-
ing extra parameter could be used to calibrate the tail against the CMS prices. Overall,
it would involve the same number of parameters to calibrate and would likely be more
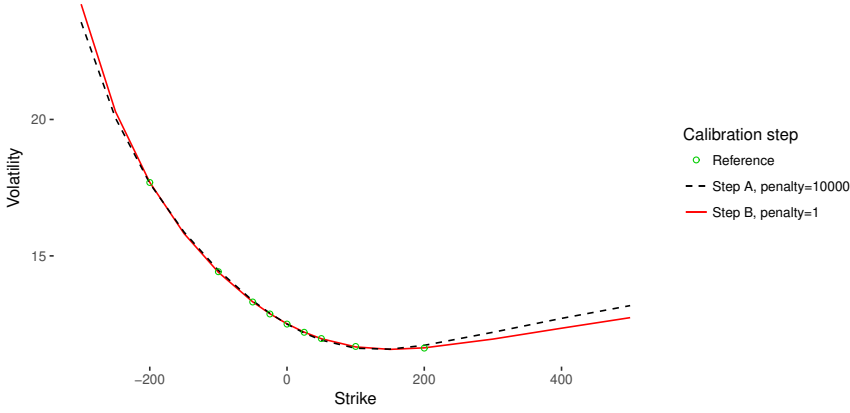
Figure 5.7.1: 20x10 swaption smile, calibrated with a penalty factor of 10000 (exact CMS spread prices) and a penalty factor of 1 (balanced fit corresponding to table 5.7.2).

5

flexible. The calibration technique would however remain the same: all the parameters would need to be recalibrated as changes in the extrapolation result in changes in the first two moments of the distribution as well.

5.8. LIMITATIONS OF THE STOCHASTIC COLLOCATION

A question which remains is whether the stochastic collocation method can also fit multi-modal distributions well?

Theorem 5.8.1. *For any continuous survival distribution function $\bar{\Phi}_Y$, there exists a stochastic collocation polynomial g_N which can approximate the survival distribution to any given accuracy $\epsilon > 0$ across an interval $[a, b]$ of $\mathbb{R}$.*

Proof. The function $g(x) = \bar{\Phi}_Y^{-1}(1 - \Phi(x))$ is continuous and monotone on $\mathbb{R}$. Wolibner [201] and Lorentz [146] have shown that for any $\eta > 0$, there exists a monotone polynomial $g_{N,\eta}$ such that

$$\sup_{x \in [a,b]} \left\| g(x) - g_{N,\eta}(x) \right\| \leq \eta$$

on any interval $[a, b]$ of $\mathbb{R}$. From Equation (5.1), the approximate survival distribution corresponding to the collocation polynomial $g_{N,\eta}$ is $G_{N,\eta} = 1 - \Phi \circ g_{N,\eta}^{-1}$ where the symbol $\circ$ denotes the function composition.

Let $I = [g_{N,\eta}(a), g_{N,\eta}(b)]$, $\Phi \circ g_{N,\eta}^{-1}$ and thus $G_{N,\eta}$ are also monotone and continuous on I. Let $J = [1 - \Phi(b), 1 - \Phi(a)]$, and $h_{N,\eta} = g_{N,\eta} \circ \Phi^{-1} \circ (1 - id)$ where id is the identity function. We have $\bar{\Phi}_Y^{-1} = g \circ \Phi^{-1} \circ (1 - id)$. As $\Phi^{-1} \circ (1 - id)$ is continuous and monotone, we have

$$\sup_{y \in J} \left\| \bar{\Phi}_Y^{-1}(y) - h_{N,\eta}(y) \right\| \leq \eta.$$

As h_N^{-1} is continuous and monotone on I, we also have

$$\sup_{x \in I} \left\| \bar{\Phi}_Y^{-1} \circ h_{N,\eta}^{-1}(x) - x \right\| \leq \eta. \tag{5.34}$$

The uniform continuity of $\bar{\Phi}_Y$ implies that for each $\epsilon > 0$, we can find an $\eta > 0$ such that, if Equation (5.34) holds, then

$$\sup_{x \in I} \left\| h_{N,\eta}^{-1}(x) - \bar{\Phi}_Y(x) \right\| \leq \epsilon.$$

$\square$

Simple multi-modal distributions can be challenging to approximate in practice, as they might require a very high degree of the collocation polynomial for an accurate representation. In order to illustrate this, we consider an equally weighted mixture of two Gaussian distributions of standard deviation 0.1 centered respectively at $f_1 = 0.8$ and $f_2 = 1.2$. We can price vanilla options based on this density, simply by summing the prices of two options using a forward at respectively f_1 and f_2 under the Bachelier model. We set the forward $F(0, T) = 1$ and consider 20 options of maturity $T = 1$ and equidistant strikes between 0.5 and 1.5.

The Black volatility smile implied by this model is absolutely not realistic (Figure 5.8.2), but it is perfectly valid and arbitrage-free theoretically, and we can still calibrate our models to it.

Figure 5.8.1a shows that the cubic and quintic polynomial collocations do not allow to capture the bimodality at all. The nonic polynomial does better in this respect, but the implied distribution is still quite poor.

(a) Polynomial collocation.   (b) Spline collocation.
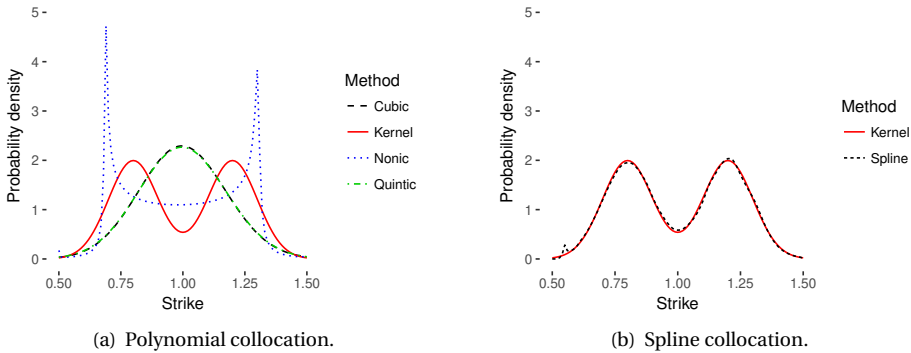
Figure 5.8.1: Probability density obtained by the stochastic collocation of a reference bimodal distribution.

One solution, here, is to collocate on a monotonic cubic spline (Figure 5.8.1b). The simple algorithms [50, 99] to produce monotone cubic splines are only guaranteed to be of class C^1. While the stochastic collocation can be applied to C^1 functions, the probability density will then only be of class C^0. The more difficult issue is the proper choice of the knots of the spline. How many knots should be used? If we place a knot at each
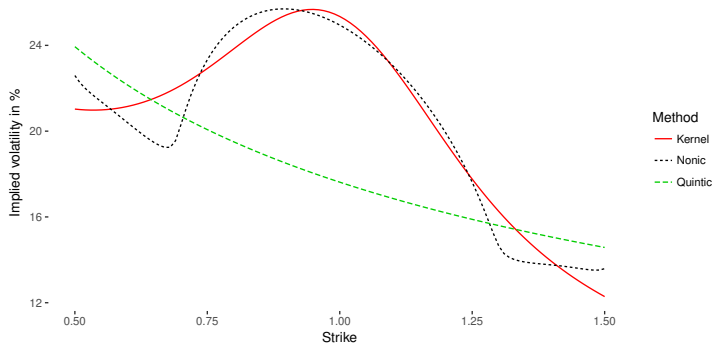
Figure 5.8.2: Implied volatility smile for a bimodal distribution and the calibrated stochastic collocation smiles with a quintic and a nonic polynomial.

market strike, we will overfit and end up with many wiggles in the probability density, like with the Andreasen-Huge method (Figure 5.4.1b).

Furthermore, the problem of optimizing the spline is numerically more challenging given that the parameterization does not enforce automatically monotonicity or moment-preservation. Regarding monotonicity, in the case of the algorithm from Hyman [100] or Dougherty et al. [50], a non-linear filter is applied, which could make the optimizer get stuck in a local minimum. Finally, there is the issue of which boundary conditions and which extrapolation to choose. A linear extrapolation, combined with the so-called natural boundary conditions would result in a smooth density[11], but the linear extrapolation still has to be of positive slope in order to guarantee the monotonicity over $\mathbb{R}$. A priori, this is not guaranteed. An alternative is to rely on the forward difference estimate as the slope, along with clamped boundary conditions, at the cost of loosing the continuity of the probability density at the boundaries.

5.9. CONCLUSION

We have shown how to apply the stochastic collocation method directly to market options quotes in order to produce a smooth and accurate interpolation and extrapolation of the option prices, even on challenging equity options examples. A specific parameterization was described, which ensures the monotonicity of the collocation polynomial as well as the conservation of the zero-th and first moments transparently during the optimization, thus guaranteeing the absence of arbitrage.

The polynomial stochastic collocation leads to a smooth implied probability density, without any artificial peak, even with high degrees of the collocation polynomial. We also applied the technique to interest rate derivatives. This results in a closed-form formula for CMS convexity adjustments, which can thus be easily calibrated jointly with interest rate swaptions.

Finally, we illustrated, on a theoretical example, how the polynomial stochastic collocation had difficulties in capturing multi-modal distributions.

---

[11]Although this makes the model relatively rigid towards the wings representation

5.A. GAUSSIAN KERNEL SMOOTHING

Let $(x_i, y_i)_{i=0,...,m}$ be $m+1$ given points. Using the points $(\hat{x}_k)_{k=0,...,n}$, which are typically within the interval (x_0, x_m), a smooth interpolation is given by the function g defined by

$$g(x) = \frac{1}{\sum_{k=0}^{n} \psi_\lambda(x - \hat{x}_k)} \sum_{k=0}^{n} \alpha_k \psi_\lambda(x - \hat{x}_k), \tag{5.35}$$

for $x \in \mathbb{R}$, $n \le m$ and where ψ_λ is the kernel. The Gaussian kernel is defined by

$$\psi_\lambda(u) = \frac{1}{\lambda\sqrt{2\pi}} e^{-\frac{u^2}{2\lambda^2}}. \tag{5.36}$$

The calibration consists in finding the α_i that minimizes the given error measure on the input $(x_i, y_i)_{i=0,...,m}$. The solution can be found by QR decomposition of the linear problem

$$\begin{pmatrix} \psi_\lambda(x_0 - \hat{x}_0) & \psi_\lambda(x_0 - \hat{x}_1) & \dots & \psi_\lambda(x_0 - \hat{x}_n) \\ \vdots & \vdots & \dots & \vdots \\ \psi_\lambda(x_m - \hat{x}_0) & \psi_\lambda(x_m - \hat{x}_1) & \dots & \psi_\lambda(x_m - \hat{x}_n) \end{pmatrix} \begin{pmatrix} \alpha_0 \\ \vdots \\ \alpha_n \end{pmatrix} = \begin{pmatrix} y_0 \sum_{k=0}^{n} \psi_\lambda(x_0 - \hat{x}_k) \\ \vdots \\ y_m \sum_{k=0}^{n} \psi_\lambda(x_m - \hat{x}_k) \end{pmatrix}. \tag{5.37}$$

The x_i are typically option strikes, log-moneynesses or deltas. The y_i are the corresponding option implied volatilities. Wystup [202] applies the method in terms of option deltas. There are multiple delta definitions in the context of volatility interpolation, we use the undiscounted call option forward delta:

$$\Delta = \Phi\left(\frac{1}{\sigma\sqrt{T}} \ln \frac{F(0,T)}{K} + \frac{1}{2}\sigma\sqrt{T}\right), \tag{5.38}$$

where Φ is the cumulative normal distribution function, $F(0,T)$ is the forward to maturity T, K is the option strike and σ is the corresponding option volatility.

When the points are defined in delta, we need to find the delta for a given option strike in order to compute the option implied volatility or the option price for a given strike. But the delta is also a function of the implied volatility. This is a non-linear problem. Equation (5.38), with $\sigma = g(\Delta)$, is solved by a numerical solver such as Toms348 [1] or a simple bisection, starting at $\Delta = 0.5$, in the interval $[0, 1]$.

Wystup recommends a bandwidth of 0.25, we find that a bandwidth of 0.5 minimizes the root mean square error of implied volatilities on our example.

5.B. MIXTURE OF LOGNORMAL DISTRIBUTIONS

Let $(x_i, y_i)_{i=0,...,m}$ be $m+1$ given points. Using the points $(\hat{x}_k)_{k=0,...,n}$, which are typically within the interval (x_0, x_m), a kernel estimate of the density on the points $\hat{x}_k$ is given by

$$g(x) = \sum_{k=0}^{n} \alpha_k \psi_{\lambda_k}(x, \hat{x}_k), \tag{5.39}$$

where ψ_{λ_k} is a kernel of bandwidth λ_k, along with the condition $\sum_{k=0}^n \alpha_k = 1$ and $\alpha_k \geq 0$ for $k = 0, \dots, n$.

In our case, $(y_i)_{i=0,\dots,m}$ are option prices, and we want to estimate the underlying distribution. We then consider that $\psi_{\lambda_k}(x)$ is a Gaussian and x is a logarithmic function of the option strike K, $x = \ln(K)$. In order to map the kernel exactly to the Black-Scholes probability density, we use

$$\psi_{\lambda_k}(x, \hat{x}_k) = \frac{1}{\lambda_k \sqrt{2\pi}} e^{-\frac{\left(x - \hat{x}_k + \frac{1}{2}\lambda_k^2\right)^2}{2\lambda_k^2} - \hat{x}_k}. \tag{5.40}$$

The option price V of strike $K = e^x$ is then given by

$$V(x) = \sum_{k=0}^n \alpha_k V_{\text{Black}}(e^x, e^{\hat{x}_k}, \lambda_k, 1), \tag{5.41}$$

where $V_{\text{Black}}(K, f, \lambda, T)$ is the price of a vanilla option of maturity T and strike K given by the Black-76 formula for an asset of forward f and volatility λ.

The calibration consist then in finding the parameters $\alpha_k, \hat{x}_k, \lambda_k$ that minimize the measure M_V. In the calibration, we will also add the martingality constraint, which will ensure that the put-call parity holds exactly in the mixture model. This translates to the additional constraint

$$\sum_{k=0}^n \alpha_k e^{\hat{x}_k} = F(0, T), \tag{5.42}$$

where $F(0, T)$ is the underlying asset forward to maturity.

We can enforce the constraints by a variable transformation. The $\sqrt{\alpha_k}$ are located on the hypersphere of radius $R = 1$ in $\mathbb{R}^{n+1}$. Let $\theta \in \mathbb{R}^n$, a point $\mathbf{u} \in \mathbb{R}^{n+1}$ is on the hypersphere if and only if

$$u_k = R \cos(\theta_k) \prod_{j=0}^{k-1} \sin(\theta_j), \tag{5.43}$$

for $k = 0, \dots, n-1$ and $u_n = \prod_{j=0}^n \sin(\theta_j)$. We thus use the transform $\alpha_k = u_k^2$. It is invertible and the inverse is

$$\theta_k = \frac{\pi}{2} - \arctan\left(\frac{u_k}{\sqrt{\sum_{j=k+1}^n u_j^2}}\right), \tag{5.44}$$

or directly in terms of α_k:

$$\theta_k = \frac{\pi}{2} - \arctan\left(\sqrt{\frac{\alpha_k}{\sum_{j=k+1}^n \alpha_j}}\right). \tag{5.45}$$

The martingality condition can be enforced the same way, using the intermediate variable $z_k = \alpha_k e^{\hat{x}_k}$. Indeed, Equation (5.42) means that z_k is located on the hypersphere of radius $R = \sqrt{F(0, T)}$ in $\mathbb{R}^{n+1}$.

This allows the use of an unconstrained algorithm such as Levenberg-Marquardt to minimize the error measure M_V on $\mathbb{R}^{3n+1}$. As initial guess, we use $\alpha_k = \frac{1}{n+1}$, $\hat{x}_k = F(0, T)$,

$\lambda_k = \sigma_{\text{ATM}} \sqrt{T}$, where σ_{ATM} is the implied volatility of the option whose strike is closest to the forward price.

If negative strikes are allowed, we can replace lognormal distributions by normal distributions, and the Black-Scholes formula by the Bachelier one. Note that if the bandwidth (λ_k) and the mean ($\hat{x}_k$) are fixed in advance, the problem becomes a quadratic programming problem.

Table 5.B.1: Calibrated mixture of lognormal distributions against 1m SPX500 options as of February, 05, 2018, for different number of distributions .

Mixture of 2 lognormals						
α	0.1664	0.8336				
$e^{\hat{x}}$	2208.46	2713.91				
λ	0.1561	0.04033				
Mixture of 4 lognormals						
α	0.09789	0.2739	0.3489	0.2793		
$e^{\hat{x}}$	2203.35	2523.00	2701.93	2793.91		
λ	0.2467	0.06519	0.02442	0.006543		
Mixture of 6 lognormals						
α	0.02164	0.1121	0.2480	0.2593	0.1794	0.1795
$e^{\hat{x}}$	2045.69	2242.37	2551.67	2696.07	2812.76	2771.53
λ	0.5711	0.1129	0.04712	0.01909	1.576e-05	0.008333

5.C. Implied volatility quotes for vanilla options on SPX500 expiring on March 7, 2018, as of February, 5, 2018

The implied volatilities were obtained by using the mid-price of call and put options. The forward price is implied from the put-call parity relationship.

Table 5.C.1: Implied volatility quotes for SPX500 options expiring on March 7, 2018, as of February, 5, 2018. In ACT/365, the option maturity is $T = 0.082192$. The implied forward price is $F(0, T) = 2629.80$. The interest rate is $r = 0.97\%$.

Strike	Logmoneyness	Implied vol.	Strike	Logmoneyness	Implied vol.
1900	-0.325055	0.684883	2650	0.007651	0.280853
1950	-0.299079	0.6548	2655	0.009536	0.277035
2000	-0.273762	0.627972	2660	0.011417	0.273715
2050	-0.249069	0.604067	2665	0.013295	0.270891
2100	-0.224971	0.576923	2670	0.01517	0.267889
2150	-0.201441	0.551253	2675	0.017041	0.264533
2200	-0.178451	0.526025	2680	0.018908	0.262344
2250	-0.155979	0.500435	2685	0.020772	0.258598
2300	-0.134	0.474137	2690	0.022632	0.2555
2325	-0.123189	0.461716	2695	0.024489	0.25219
2350	-0.112493	0.445709	2700	0.026343	0.249534
2375	-0.101911	0.433661	2705	0.028193	0.246659
2400	-0.09144	0.42016	2710	0.03004	0.243553
2425	-0.081077	0.407463	2715	0.031883	0.240202
2450	-0.070821	0.393168	2720	0.033723	0.236588
2470	-0.062691	0.381405	2725	0.03556	0.234574
2475	-0.060668	0.3793	2730	0.037393	0.230407
2480	-0.05865	0.377109	2735	0.039223	0.227866
2490	-0.054626	0.372471	2740	0.041049	0.223049
2510	-0.046626	0.360294	2745	0.042872	0.219888
2520	-0.04265	0.354671	2750	0.044692	0.218498
2530	-0.03869	0.350533	2755	0.046509	0.214702
2540	-0.034745	0.34419	2760	0.048322	0.210506
2550	-0.030815	0.339273	2765	0.050132	0.208175
2560	-0.026902	0.333069	2770	0.051939	0.205508
2570	-0.023003	0.328206	2775	0.053742	0.199967
2575	-0.021059	0.324314	2780	0.055542	0.199007
2580	-0.019119	0.322041	2785	0.057339	0.195062
2590	-0.015251	0.3168	2790	0.059133	0.190547
2600	-0.011397	0.310914	2795	0.060923	0.188427
2610	-0.007559	0.305042	2800	0.062711	0.185893
2615	-0.005645	0.302416	2805	0.064495	0.182878
2620	-0.003734	0.299488	2810	0.066276	0.179292
2625	-0.001828	0.29609	2815	0.068053	0.175001
2630	7.5E-05	0.292378	2835	0.075133	0.185751
2635	0.001974	0.289516	2860	0.083913	0.207173
2640	0.00387	0.28584	2900	0.097802	0.225248
2645	0.005762	0.283342			

6

STOCHASTIC COLLOCATION FOR AN ARBITRAGE-FREE IMPLIED VOLATILITY, PART II

This chapter explores the stochastic collocation technique, applied on a monotonic spline, as an arbitrage-free and model-free interpolation of implied volatilities. We explore various spline formulations, including B-spline representations. We explain how to calibrate the different representations against market option prices, detail how to smooth out the market quotes and choose a proper initial guess. The technique is then applied to concrete market options and the stability of the different approaches is analyzed. Finally we consider a challenging example where convex spline interpolations lead to oscillations in the implied volatility and compare the spline collocation results with those obtained through the technique of Andreasen and Huge.

6.1. INTRODUCTION

In the previous chapter, we showed how to apply the stochastic collocation technique, using a specific isotonic and moment-preserving polynomial representation, to produce an arbitrage-free interpolation and extrapolation of market option prices, without relying on a prior model. We however noticed that a polynomial, while often satisfactory, may not be able to always reproduce the market implied volatilities with enough accuracy. This may be especially critical in the context of the collocating local volatility (CLV) model of Grzelak [77].

In this chapter, instead of collocating on a polynomial, we explore various monotonic spline representations, including B-spline parametrizations. This allows for a richer representation, with as many parameters as there are market option strikes. A direct consequence is the ability to capture more complex implied probability distributions such as multi-modal distributions. We pay attention to avoid over-fitting by adding some appropriate regularization. This is reminiscent of the penalized B-spline technique for volatility modelling of Corlay [38], where a B-spline parameterization of the Radon-Nikodym derivative of the underlying's risk-neutral probability density with respect to a roughly calibrated base model is used. Concretely, Corlay's method translates to an explicit probability density representation where the probability density is a spline multiplied by a base probability density function, such as the lognormal or normal probability density

---

This chapter is based on the article 'Model-free stochastic collocation for an arbitrage-free implied volatility, Part II', published in *Risks*, 2019 [134].

function. Corlay's technique however limits the implied volatility shapes allowed, and often requires the use of a more elaborate base probability density function, such as the one stemming from the SVI parameterization of Gatheral [72], to properly fit the market in practice. We will see that the stochastic collocation on a spline is more flexible and can fit the market very well when collocating to a simple Gaussian variable.

The outline of this chapter is as follows. Section 6.2 presents how to apply the stochastic collocation on a monotonic cubic spline, while still preserving the first moment exactly. The collocation on an exponential spline is explored in Section 6.3, which results in analytical formulas not only for the price of vanilla options but also for the price of variance swaps. Section 6.4 considers B-spline representations which take into account the monotonicity and the martingale constraints explicitly. Section 6.5 details the calibration towards market option prices of each kind of representation. Finally, Section 6.6 explores the stability of the calibration on concrete market data, for the different parametrizations considered. We compare the quality of fit and the implied probability density with the Andreasen-Huge technique, regularized. In Section 6.7, we look at a challenging example of Jäckel [109], where interpolation splines applied to call prices lead to oscillations in the interpolation.

6.2. SPLINE COLLOCATION

When g is a piecewise cubic polynomial defined on the knots $(x_i, y_i)_{i=0,...,N}$, the call option price can be obtained analytically. Let $g(x) = g_i(x) = a_i + b_i(x - x_i) + c_i(x - x_i)^2 + d_i(x - x_i)^3$ for $x \in [x_i, x_{i+1}]$, and k the index such that $y_k \leq K < y_{k+1}$, assuming that $0 \leq i < N$ exists, Equation (5.1) becomes

$$
\begin{aligned}
V_{\text{call}}(K) = {}& I(\tilde{x}_{-1}, x_0) + I(\tilde{x}_N, \infty) - K\Phi(-\tilde{x}_k) \\
& + \sum_{i=k}^{N-1} \left[a_i - (b_i + d_i(\tilde{x}_i^2 + 3))x_i + c_i(x_i^2 + 1) \right] (\Phi(-\tilde{x}_i) - \Phi(-\tilde{x}_{i+1})) \\
& + \sum_{i=k}^{N-1} \left[b_i + c_i(\tilde{x}_i - 2x_i) + d_i(3x_i^2 - 3\tilde{x}_i x_i + \tilde{x}_i^2 + 2) \right] \phi(\tilde{x}_i) \\
& - \sum_{i=k}^{N-1} \left[b_i + c_i(\tilde{x}_{i+1} - 2x_i) + d_i(3x_i^2 - 3x_i\tilde{x}_{i+1} + \tilde{x}_{i+1}^2 + 2) \right] \phi(\tilde{x}_{i+1}),
\end{aligned}
\tag{6.1}
$$

with $\tilde{x}_k = g^{-1}(K)$, $\tilde{x}_{-1} = x_0$ and $\tilde{x}_i = x_i$ for $i > k$. The integral I corresponding to the left and right extrapolations is defined by

$$
I(a, b) = \int_a^b g(x)\phi(x)\,dx.
$$

In the case of a linear extrapolation with slope s and starting at the point (x, y), we have

$$
I_L(a, b) = (y - sx)(\Phi(b) - \Phi(a)) - s(\phi(b) - \phi(a)).
$$

with abuse of notation $\Phi(\infty) = 1, \Phi(-\infty) = 0$ and $\phi(\infty) = \phi(-\infty) = 0$. We use $s = s_L$, and $x = x_0, y = y_0$ for the left wing extrapolation, and $s = s_R$, and $x = x_N, y = y_N$ for the right wing extrapolatioin.

When $K < y_0$ and in the case of a linear extrapolation, Equation (6.1) is still valid, but with $\tilde{x}_{-1} = \frac{K-y_0}{s_L} + x_0$. When $K > y_N$, $C_K = I_R(\tilde{x}_N, \infty)$ with $\tilde{x}_N = \frac{K-y_N}{s_R} + x_N$.

The cut-off point $\tilde{x}_k = g_k^{-1}(K)$ can be found analytically through Cardano's formula [161].

The first moment is given by

$$
\begin{aligned}
M_1(g) = {} & I(-\infty, x_0) + I(x_N, \infty) \\
& + \sum_{i=0}^{N-1} \left[a_i - (b_i + d_i(x_i^2 + 3))x_i + c_i(x_i^2 + 1) \right] (\Phi(x_{i+1}) - \Phi(x_i)) \\
& + \sum_{i=0}^{N-1} \left[b_i - c_i x_i + d_i(x_i^2 + 2) \right] \phi(x_i) \\
& - \sum_{i=0}^{N-1} \left[b_i + c_i(x_{i+1} - 2x_i) + d_i(3x_i^2 - 3x_i x_{i+1} + x_{i+1}^2 + 2) \right] \phi(x_{i+1}).
\end{aligned} \tag{6.2}
$$

In practice, the preservation of the martingale property (and the put-call parity relation) imposes $M_1 = F$ where F is the market forward price to maturity T.

The put option price is calculated through the put-call parity relation, namely

$$
V_{\text{call}}(K) - V_{\text{put}}(K) = F - K, \tag{6.3}
$$

where $V_{\text{put}}(K)$ is the undiscounted price today of a put option of maturity T, and F is the forward price to maturity.

When put option prices are very small, and assuming that the first moment equals exactly the forward price, it is preferable to use a more direct approach. Equation (6.3) does not allow to compute prices below machine epsilon. Using the same change of variables as for the call option (Equation 5.1), we have for a put option with strike K:

$$
\begin{aligned}
V_{\text{put}}(K) &= \int_0^{+\infty} \max\left(K - y, 0\right) f(y) \, dy \\
&= \int_{-\infty}^{x_K} (g(x) - K) \phi(x) \, dx.
\end{aligned}
$$

This leads to

$$
\begin{aligned}
V_{\text{put}}(K) = {} & K\Phi(\tilde{x}_k) - I(-\infty, \tilde{x}_{-1}) - I(\tilde{x}_N, x_N) \\
& + \sum_{i=0}^{k-1} \left[a_i - (b_i + d_i(x_i^2 + 3))x_i + c_i(x_i^2 + 1) \right] (\Phi(\tilde{x}_{i+1}) - \Phi(\tilde{x}_i)) \\
& + \sum_{i=0}^{k-1} \left[b_i + c_i(\tilde{x}_i - 2x_i) + d_i(3x_i^2 - 3x_i \tilde{x}_i + \tilde{x}_i^2 + 2) \right] \phi(\tilde{x}_i) \\
& - \sum_{i=0}^{k-1} \left[b_i + c_i(\tilde{x}_{i+1} - 2x_i) + d_i(3x_i^2 - 3x_i \tilde{x}_{i+1} + \tilde{x}_{i+1}^2 + 2) \right] \phi(\tilde{x}_{i+1}),
\end{aligned} \tag{6.4}
$$

with $\tilde{x}_k = g^{-1}(K)$, $\tilde{x}_{-1} = x_0$ and $\tilde{x}_i = x_i$ for $0 \le i < k$.

6.3. EXPONENTIAL SPLINE COLLOCATION

6.3.1. VANILLA OPTIONS

Instead of interpolating on the strikes (the points $(x_i, y_i)_{i=0,...,N}$), we will interpolate the log strikes (the points $(x_i, \ln y_i)_{i=0,...,N}$) with a piecewise polynomial. This presupposes that the strikes are strictly positive and that the probability of the asset being negative equals zero. The undiscounted call price of an option with strike K is then

$$V_{\text{call}}(K) = \int_{-\infty}^{\infty} \max(e^{g(x)} - K, 0)\phi(x)\,dx, \tag{6.5}$$

where g is a monotonic piecewise polynomial function interpolating $(x_i, \ln y_i)_{i=0,...,N}$. We can not obtain a closed-form formula for a general g function, if we assume that g is a quadratic spline. Let $(\bar{x}_j)_{j=0,...,M}$ be the spline knots, and $g(x) = a_j + b_j(x - \bar{x}_j) + c_j(x - \bar{x}_j)^2$ on $[\bar{x}_j, \bar{x}_{j+1}]$, with k the index such that $\bar{y}_k \le K < \bar{y}_{k+1}$, we have then

$$V_{\text{call}}(K) = I(\tilde{x}_{-1}, \bar{x}_0) + I(\tilde{x}_M, \infty) + K\Phi(-\tilde{x}_k)$$
$$+ \sum_{j=k}^{M-1} e^{a_j - b_j \bar{x}_j + c_j \bar{x}_j^2 + \frac{1}{2} m_j^2} \frac{\Phi\left(\bar{x}_{j+1}\sqrt{1 - 2c_j} - m_j\right) - \Phi\left(\bar{x}_j\sqrt{1 - 2c_j} - m_j\right)}{\sqrt{1 - 2c_j}},$$

with $m_j = \frac{b_j - 2c_j \bar{x}_j}{\sqrt{1 - 2c_j}}$ and defining $\tilde{x}_k = g^{-1}(\ln K)$, $\tilde{x}_i = \bar{x}_i$ for $i > k$. When $1 - 2c_j < 0$, we can use the imaginary error function erfi as we have for $a, b \in \mathbb{R}$,

$$-i\frac{\Phi(ib\sqrt{2c_j - 1}) - \Phi(ia\sqrt{2c_j - 1})}{\sqrt{2c_j - 1}} = \frac{\text{erfi}\left(b\sqrt{\frac{2c_j - 1}{2}}\right) - \text{erfi}\left(a\sqrt{\frac{2c_j - 1}{2}}\right)}{2\sqrt{2c_j - 1}}.$$

For a linear extrapolation with slope s and passing by the point (x, y), corresponding to $g(u) = s(u - x) + y$, we find

$$I(a, b) = \int_a^b e^{s(u-x)+y}\phi(u)\,du$$
$$= e^{y - sx + \frac{1}{2}s^2}\left(\Phi(b - s) - \Phi(a - s)\right), \tag{6.6}$$

with some abuse of notation $\Phi(-\infty) = 0$, $\Phi(\infty) = 1$. The left wing extrapolation corresponds to $x = \bar{x}_0$ and $y = \bar{y}_0$, with $s = s_L$ a free parameter and the right wing extrapolation corresponds to $x = \bar{x}_M$, $y = \bar{y}_M$ with $s = s_R$. In order to keep the continuity of the derivative at the boundaries, we choose $s_R = g'(x_N)$ and $s_L = g'(x_0)$.

The first moment is given by

$$
\begin{aligned}
M_1 &= \int_{-\infty}^{\infty} e^{g(x)} \phi(x)\, dx \\
&= I(-\infty, \bar{x}_0) + I(\bar{x}_M, \infty) \\
&\quad + \sum_{j=0}^{M-1} e^{a_j - b_j \bar{x}_j + c_j \bar{x}_j^2 + \frac{1}{2} m_j^2} \frac{\Phi\left(\bar{x}_{j+1}\sqrt{1-2c_j} - m_j\right) - \Phi\left(\bar{x}_j\sqrt{1-2c_j} - m_j\right)}{\sqrt{1-2c_j}} \\
&= I(-\infty, \bar{x}_0) + I(\bar{x}_M, \infty) \\
&\quad + \sum_{j=0}^{M-1} e^{a_j + \frac{b_j^2 - 2b_j\bar{x}_j + 2c_j\bar{x}_j^2}{2(1-2c_j)}} \frac{\Phi\left(\bar{x}_{j+1}\sqrt{1-2c_j} - m_j\right) - \Phi\left(\bar{x}_j\sqrt{1-2c_j} - m_j\right)}{\sqrt{1-2c_j}}.
\end{aligned}
\tag{6.7}
$$

6.3.2. VARIANCE SWAP

Variance swaps contracts allow a buyer to receive the future realized variance of the price changes until a specific maturity date against a fixed strike price, paid at maturity. Conventionally, these price changes are daily log returns of a specific stock, equity index, or exchange rate based upon the most commonly used closing price (or exchange rate reset price). Variance swaps became particularly popular after Demeterfi et al. showed that a single contract could be statically replicated by a portfolio of vanilla options [45]. In the absence of jumps[1] and assuming the observations to be continuous, the problem of pricing a variance swap can be reduced to the pricing of a log-contract. The price V of a variance swap, by continuous replication, has a particularly simple closed-form expression with the exponential spline parametrization. For a newly issued variance swap with zero strike, and a transition probability density f from $t = 0$ to $t = T$, following Carr and Lee [31], we have

$$
\begin{aligned}
V(0, T) &= -\frac{2}{T} \int_0^{\infty} \ln\left[\frac{y}{F(0, T)}\right] f(y)\, dy \\
&= -\frac{2}{T} \int_{-\infty}^{\infty} \left(g(x) - \ln F(0, T)\right) \phi(x)\, dx.
\end{aligned}
\tag{6.8}
$$

In Equation (6.8), $\tilde{g} = g - F(0, T)$ is a piecewise quadratic spline. The value of the integral corresponds to the first moment of the collocation variable with the spline $\tilde{g}$, which is given explicitly by Equation (6.2). The standard replication formula from Carr and Madan [33] implies to choose an integration cut-off and the use of a numerical quadrature, typically an adaptive Gauss-Lobatto quadrature. This is not necessary with the exponential spline collocation approach. The price of the variance swap can be adjusted by changing the slope of the linear extrapolation. This allows for a fast joint calibration of the collocating B-spline to market option prices and variance swaps. The market variance swap prices give some additional information on the tail of the distribution, not covered by vanilla options.

---

[1] Although such a hypothesis may seem very strong, most practitioners value the variance swaps by replication.

6.4. B-SPLINE COLLOCATION

We recall that the goal of the stochastic collocation is to find a smooth monotonic function to represent the function g mapping the abscissas $(x_i)_{i=0,...,N}$ to the ordinates (the strikes) $(y_i)_{i=0,...,N}$ (see Figure 5.2.1b), by minimizing the error in option prices in a least-squares sense. From the previous sections, we now know how to price vanilla options by collocating on a spline, which passes through the specific points $(x_i, y_i)_{i=0,...N}$. We can then choose to optimize either the abscissas or the ordinates of those points in order to minimize the least squares error in option prices, at the condition that we use a monotonicity preserving spline and make sure to conserve the first moment in the optimization.

Instead of using an exact interpolation function on a set of points, and optimizing this interpolation through the choice of points, we can rely on a B-spline representation and optimize directly the B-spline coefficients. The method will work both on the direct strikes, or on the log strikes. We consider a quadratic B-spline representation, that is, B-splines of order $k = 3$. The B-spline representation of g on $N + 1 + k$ knots reads [43]

$$g(x) = \sum_{i=0}^{N} \alpha_i B_{i,3}(x).$$ (6.9)

We choose the nearly optimal knots $t_{i+3} = \frac{x_{i+1}+x_{i+2}}{2}$ for $i = 0, ..., N-3$ according to [43, p. 193] with the boundary knots $t_0 = t_1 = t_2 = x_0$ and $t_{N+1} = t_{N+2} = t_{N+3} = x_N$. This choice of knots ensures that g is C^1 on $[x_0, x_N]$.

Because the derivative of the equivalent piecewise polynomial representation is linear between two distinct knots, g will be monotonically increasing on an interval $[t_{i-1}, t_i]$ if and only if the derivative at the endpoints is positive. And thus, g will be monotonically increasing on the interval $[x_0, x_N]$ if and only if $\alpha_i - \alpha_{i-1} > 0$ for $i = 1, ..., N$ in Equation (6.9).

It is then particularly simple to impose the monotonicity constraints when we optimize the coefficients α_i during the calibration to market quotes. Furthermore, a least-squares fit of g directly to some input $(x_i, y_i)_{i=0,...,N}$ reduces to a simple quadratic programming problem:

$$\tilde{\alpha} = \underset{\alpha \in \mathbb{R}^{N+1}}{\operatorname{argmin}} \frac{1}{2} \alpha^T Q \alpha + q^T \alpha,$$ (6.10)

subject to $\alpha_i - \alpha_{i-1} > 0$ for $i = 1, ..., N$, with $Q = P^T P$, $q = -P^T y$ and P the matrix defined by $P_{i,j} = B_{i,3}(y_j)$. In particular P is a banded matrix [43].

The quadratic programming problem is fast to solve using a standard optimization library such as CVXOPT [11], OSQP [183] or quadprog [192], when compared to the total time taken to calibrate the spline. This will allow to start the optimization from a reasonable initial guess.

In order to price an option or to evaluate the first moment, we simply transform the B-spline representation to a piecewise quadratic polynomial [43, p. 117-119] and rely on sections 6.2 and 6.3 of this thesis, for respectively a direct B-spline collocation, and an exponential B-spline collocation.

In the case of the direct B-spline collocation, the first moment is a linear combination of the B-spline coefficients. Indeed, the first moment is a linear combination of the

piecewise polynomial coefficients in Equation (6.2) and the piecewise polynomial coefficients themselves are a linear combination of the B-spline coefficients:

$$a_j = \frac{t_{j+2} - t_{j+1}}{t_{j+3} - t_{j+1}} \left(\alpha_{j+1} - \alpha_j \right) + \alpha_j, \tag{6.11}$$

$$b_j = 2 \frac{\alpha_{j+1} - \alpha_j}{t_{j+3} - t_{j+1}}, \tag{6.12}$$

$$c_j = \frac{1}{t_{j+3} - t_{j+2}} \left(\frac{\alpha_{j+2} - \alpha_{j+1}}{t_{j+4} - t_{j+2}} + \frac{\alpha_j - \alpha_{j+1}}{t_{j+3} - t_{j+1}} \right). \tag{6.13}$$

We can thus add the martingale constraint directly to the quadratic programming problem as an additional equality constraint.

6.5. CALIBRATION OF THE SPLINE COLLOCATION TO MARKET QUOTES

We wish to minimize the weighted ℓ_2 error norm between the volatilities implied from the prices obtained by spline collocation and the market implied volatilities. For this, we can optimize the location of either the spline knots abscissas x_i or the spline knots ordinates y_i, or in the case of the B-spline representation, the coefficients α_i.

6.5.1. COORDINATE TRANSFORMATION

In order to preserve the order of the knots, we rely on the following mapping:

$$\begin{cases} z_i = x_i - x_{i-1}, \text{ for } i > 0, \\ z_0 = x_0, \end{cases}$$

and enforce $z_i \geq 0$ as box constraints in the least-squares minimization. Box constraints can be added in a relatively straightforward manner to any Levenberg-Marquardt algorithm, such as the one of Klare and Miller [120], through the projection technique described in [118].

  We use the same mapping if the ordinates or the B-spline coefficients are optimized, using y_i, respectively α_i, instead of x_i in the above equations.

6.5.2. MOMENT CONSERVATION

We also wish to preserve the first moment exactly in order for the spline representation to be fully arbitrage-free. Let $M_1(g)$ be the first moment computed by Equation (6.2) and F be the market forward price to the option maturity time T. In order to make M_1 match F, we shift the coefficient a_i of each piecewise polynomial $(g_i)_{i=0,\dots,N-1}$ and use

$$\hat{a}_i = a_i + F - M_1, \text{ for } 0 \leq i \leq N. \tag{6.14}$$

For the exponential spline representation on $M + 1$ unique knots, the adjustment is almost the same, but based on the log values; we use

$$\hat{a}_i = a_i + \ln F - \ln M_1, \text{ for } 0 \leq i \leq M. \tag{6.15}$$

The new spline $\hat{g}$ with updated coefficients $\hat{a}_i$ will satisfy exactly $M_1 = F$.

With this adjustment, there is a fundamental difference between the optimization of the abscissas x_i and the ordinates y_i: when the abscissas are optimized, the adjustment will also implicitly adjust the y_i as we have $y_i = \hat{a}_i$. Furthermore, when optimizing the ordinates y_i or the B-spline coefficients α_i, the first coordinate y_0 (respectively α_0) can be directly deduced from the martingale adjustment. Indeed, the adjustment only impacts the value of z_0 and has no effect on $z_i = u^{-1}(y_i - y_{i-1})$ for $i > 0$. This allows to reduce the number of dimensions of the optimization problem by one.

6.5.3. CHOICE OF COORDINATES

In our experiments, the optimization of the abscissas $(x_i)_{i=0,...,N}$ appeared to be the least stable. In particular, the outcome was highly dependent on the initial guess. Only with a proper regularization and a good smooth initial guess (for example, the constant Bachelier guess) was the outcome satisfactory.

In comparison, the optimization of the ordinates $(y_i)_{i=0,...,N}$ was found to be more stable, and the optimization of the B-spline coefficients was the most stable of all choices. One reason for this stability, is the initial guess for the B-spline coefficients respects the martingale constraint. Another is that the B-spline formulation is simply more stable than the piecewise-polynomial version [43]. Values from the B-spline representation are obtained from a linear combination of the coefficients, while values obtained from the monotonic cubic spline representation are neither a linear combination of the abscissas nor of the ordinates, because of the monotonicity constraint.

The flexibility of choosing a different variety of monotonic splines such as the cubic spline of Hyman [100] or Huynh [99] when optimizing the knots abscissas or ordinates does not translate to a better fit of the reference option prices. In some specific cases, such as the one we explore in Section 6.7, the optimization of the abscissas led to a better fit, but this consists in fitting towards the prices of a pre-existing model at hypothetical strikes, and not directly towards the market prices.

From now on, for clarity, we will thus focus only on the B-spline or exponential B-spline collocations where the B-spline coefficients are optimized.

6.5.4. REGULARIZATION

We will see by means of real examples that it can be useful to add regularization to the minimization as well, in order to avoid an implied probability density with many spikes. An interesting candidate for the regularization is to minimize the strain energy of a beam that is forced to pass through the given data points [74]:

$$E = \sum_{i=0}^{m} \mu_i^2 \left(\sigma(\xi, K_i) - \sigma_i\right)^2 + \lambda^2 \sum_{i=0}^{m-1} \frac{\mu_i^2 g''(x_i)^2}{\left[1 + g'(x_i)^2\right]^{\frac{5}{2}}} (x_{i+1} - x_i), \tag{6.16}$$

where $\sigma(\xi, K)$ is the implied volatility corresponding to the option prices obtained with the spline collocation and σ_i is the market implied volatility at strike K_i. For the maturity T considered, $m+1$ is the number of market strikes. We allow the number of strikes to be greater than or equal to the number of spline interpolation nodes $N + 1$. The parameter ξ represents a specific spline configuration on $N + 1$ nodes. For a B-spline, we have $\xi = (\alpha_j)_{j=0,...,N}$, where $(\alpha_j)_{j=0,...,N}$ are the coefficients of the B-spline representation.

The first term of the objective E corresponds to the square of the RMSE, while the second term is the regularization. The regularization parameter λ controls the smoothness of the spline interpolation.

In the case of the B-spline representation, Eilers and Marx [57] propose a simpler regularization. Their penalized spline (P-spline) minimizes the total variation of the second derivative. This regularization, expressed in terms of the B-spline coefficients, reads

$$E = \sum_{i=0}^{m} \mu_i^2 \left(\sigma(\xi, K_i) - \sigma_i\right)^2 + \lambda^2 \sum_{j=1}^{N-1} \frac{4\mu_i^2}{(t_{j+2} - t_{j+1})^2} \left(\frac{\alpha_{j+1} - \alpha_j}{t_{j+3} - t_{j+1}} + \frac{\alpha_{j-1} - \alpha_j}{t_{j+2} - t_j}\right)^2, \qquad (6.17)$$

where $(t_j)_{j=0,\dots,N+3}$ are the spline knots. In particular, the latter regularization is linear in the coefficients $(\alpha_j)_{j=0,\dots,N}$ and can thus be directly included in the quadratic programming problem described in Section 6.4.

6.6. EXAMPLE OF CALIBRATION ON TSLA OPTIONS

We consider options on the stock with ticker TSLA expiring on January 17, 2020 as of June 15, 2018. We first imply the forward price from the put-call parity relation at-the-money and then imply the Black-Scholes volatility from the mid price for each option strike (Table 6.A.1). In this example, the options mid prices are not arbitrage free.

We will measure the RMSE between the volatilities implied by the calibrated stochastic collocation and the market implied volatilities, with and without regularization. We use equal weights in this example. Although it is not particularly realistic, it has the advantage of making the plots of the implied volatility more explicit.

The calibration consists firstly in computing an arbitrage-free (convex) set of call option prices from the market mid quotes according to Section 5.3.2, secondly in computing the B-spline initial guess following Section 6.4, and thirdly in minimizing the error measure represented by Equation (6.16) with a Levenberg-Marquardt minimizer.

6.6.1. B-SPLINE

With a small (or zero) regularization parameter λ, the resulting implied probability density possesses many spurious spikes (Figure 6.6.1a). The use of a larger regularization parameter λ, during the non-linear minimization of the objective E described in Equation (6.16), helps smoothing the spikes, but it increases the RMSE slightly (see table 6.6.1).

Table 6.6.1: Root mean square error (RMSE) of the collocation method implied volatilities against the market implied volatilities of the TSLA 1m options as of June 18, 2018.

Method	Regularization	RMSE	Time(ms)
Exponential B-spline collocation	$\lambda = 1 \cdot 10^{-3}$	0.00437	43
B-spline collocation	$\lambda = 6 \cdot 10^{-6}$	0.00397	71
Andreasen-Huge	none	0.00356	890
Exponential B-spline collocation	$\lambda = 1 \cdot 10^{-7}$	0.00345	150
B-spline collocation	$\lambda = 1 \cdot 10^{-10}$	0.00326	37
Schumaker quadratic spline	none	0.00313	0.5
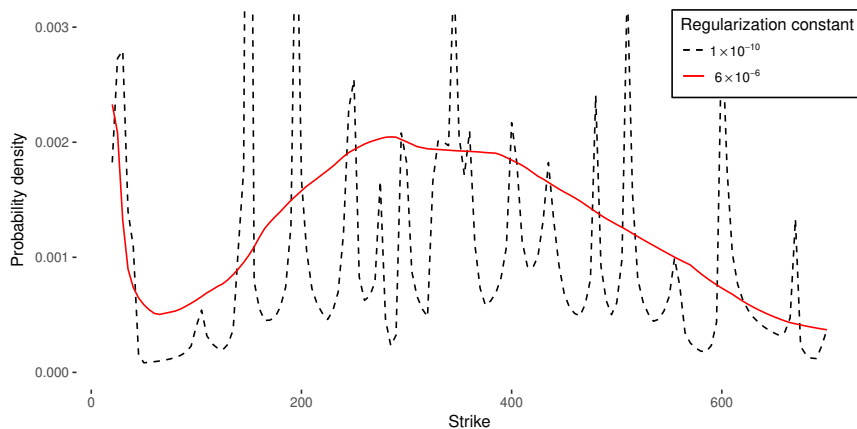
(a) Probability density implied by the prices obtained with a calibrated B-spline collocation.
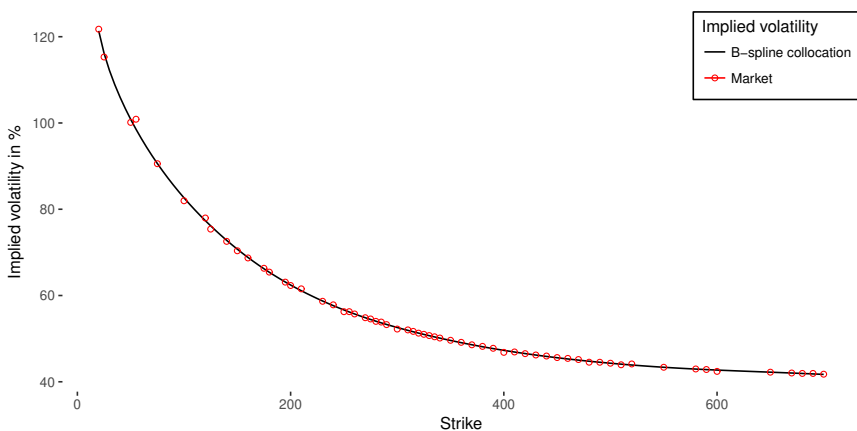
(b) Volatility smile implied by the prices obtained with B-spline collocation with regularization $\lambda = 6 \cdot 10^{-6}$.

Figure 6.6.1: Implied probability density and implied volatility for the B-spline collocation, calibrated to 1m TSLA options.

In Table 6.6.1, we also compute the RMSE with a simple convexity preserving quadratic spline [179] on the filtered market option prices (Equation 5.11). This interpolation leads to a positive and piecewise-constant probability density. On convex prices, the interpolation is exact. The RMSE is thus purely due to the filtering of the market quotes by quadratic programming.

Andreasen and Huge [12] propose a different non-parametric arbitrage-free volatility interpolation, where a discrete local volatility is calibrated to market option prices in a one-step finite-difference discretization of the forward Dupire partial differential equation. The number of free parameters corresponds effectively to the number of quotes, as in the spline collocation, and their technique will also tend to overfit. It is known to lead

to a nearly exact interpolation on arbitrage-free option prices. It does however not lead to a more accurate representation of the market implied volatilities than the B-spline collocation with a small regularization constant. The corresponding implied probability density also possesses spikes.

The B-spline collocation is not only at least as accurate as the technique of Andreasen and Huge [12] on this example, it is also significantly faster. In the latter, the involved finite difference grid must be relatively large (we used 800 points) and the corresponding tridiagonal system must be solved for each set of piecewise constant volatilities considered by the minimizer. Furthermore, the B-spline collocation offers a continuous interpolation of the option prices. In the technique of Andreasen and Huge [12], options prices are given only at the finite difference grid points. Another careful[2] arbitrage-free interpolation must be used to compute the price in between grid points. Finally, the B-spline collocation offers the ability to tune the probability density smoothness against the RMSE.

The optimal regularization parameter can be found using the L-curve method [88]. On Figure 6.6.2b we plot the L-curve for the calibrated B-spline collocation, that is the regularization norm against residual norm, in logarithmic scale, or equivalently, the second sum against the first sum of Equation (6.17), varying the regularization parameter λ. For most regularization techniques, such a curve is L-shaped, because, on linear problems, the regularization norm is a strictly decreasing function of the regularization parameter λ, and the residual norm is a strictly increasing function of λ. A good regularization parameter will achieve a good compromise between the two errors, and will correspond to a regularized solution near the "corner" of the L-curve. On non-linear least-squares problems in general, the regularization and residual norms will not be strictly monotonic, they will however be nearly monotonic and the L-curve method may still be applied [16, p. 241].

Our choice $\lambda = 6 \cdot 10^{-6}$ is the point located in the corner of the L-curve (see Figure 6.6.2b). Performing multiple calibrations to find the optimal regularization parameter, following one of the algorithms of Hansen [89], may be time-consuming. An alternative is to apply the L-curve method to the B-spline initial guess based on the convex option prices[3] (Figure 6.6.2a).

6.6.2. EXPONENTIAL B-SPLINE

The exponential B-spline initial guess does not preserve the first moment. As a consequence, its calibration tends to be less stable than the calibration of the regular B-spline. The choice of initial guess plays then an important role, and the inclusion of the regularization in the calculation of the exponential B-spline initial guess is particularly important. The RMSE in the implied volatilities is comparable to the one obtained by the Andreasen and Huge technique, and is larger than the RMSE of the regular B-spline collocation (Table 6.6.1). In spite of the larger error, the implied probability density is not as smooth as the one implied from the regular B-spline collocation (Figure 6.6.3). A

---

[2]In practice, we solve the Fokker-Planck forward PDE instead of the Dupire forward PDE, and then integrate the option payoff on the known probability density as in [84, 131] in order to obtain arbitrage-free prices everywhere.

[3]We use inverse Vega weights to fit the B-spline guess to the option prices.

(a) Initial guess on convex prices. (b) Calibrated collocation.
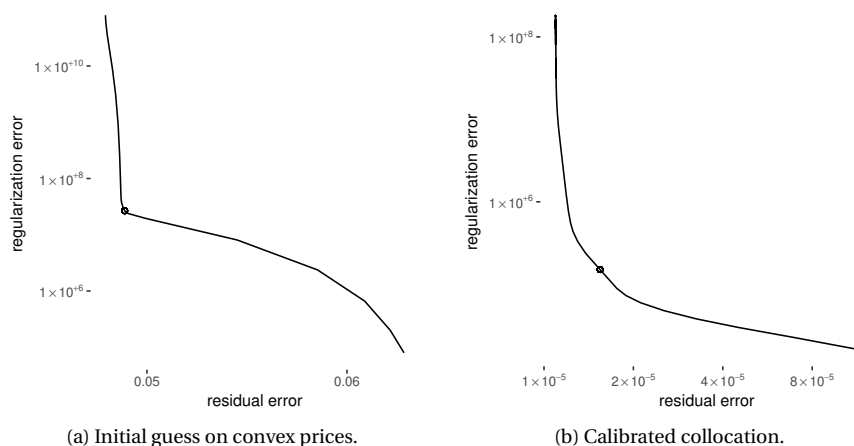
Figure 6.6.2: L-curves of the B-spline corresponding to the initial guess, and the calibration result on TSLA options.

smoother initial guess, such as the constant Bachelier volatility is then preferable.
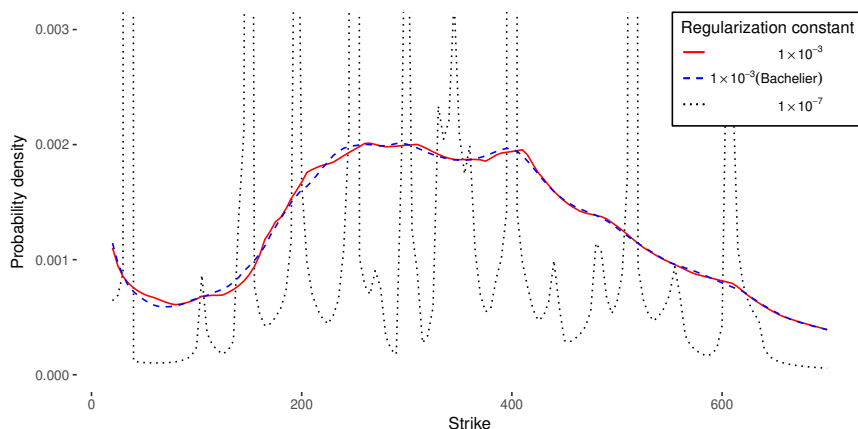
Figure 6.6.3: Implied probability density for the exponential B-spline collocation, calibrated to 1m TSLA options, with different regularization constants.

6.6.3. STARTING FROM ARBITRAGE-FREE PRICES

It is also interesting to take the filtered convex option prices (from Equation 5.11) as a basis to compare the different techniques. We expect the RMSE to be lower, eventually zero if the interpolation is exact at the market strikes. For example, the convexity preserving Schumaker quadratic spline results in an RMSE of exactly zero (but the associated implied probability density is a staircase). The B-spline collocation results in an RMSE of

around 0.0005 without regularization constant. This is lower than the RMSE produced by the Andreasen-Huge technique. In theory, their technique should be able to attain a lower RMSE, but the number of strikes, and thus the number of constants to optimize is relatively large on our problem and this creates difficulties for the numerical optimization. The collocation on an exponential B-spline leads to an RMSE similar to the one obtained with the Andreasen-Huge technique (Table 6.6.2). Of course, with a small regularization constant, the corresponding probability density possesses many spikes and is not very practical.

Table 6.6.2: Root mean square error (RMSE) of the collocation method implied volatilities against the implied volatilities of the TSLA 1m options as of June 18, 2018, based on convexity adjusted prices.

Method	Regularization	RMSE	Time (ms)
Exponential B-spline collocation	$\lambda = 10^{-3}$	0.00287	35
B-spline collocation	$\lambda = 6 \cdot 10^{-6}$	0.00239	39
Exponential B-spline collocation	$\lambda = 10^{-7}$	0.00118	160
Andreasen-Huge	none	0.00112	890
B-spline collocation	$\lambda = 10^{-10}$	0.00042	78
Schumaker quadratic spline	none	0	0.02

On other market data, for example, options on NFLX from July 2018, the same conclusions can be drawn.

6.7. A MORE EXTREME EXAMPLE - WIGGLES IN THE IMPLIED VOLATILITY

Jäckel [109] shows that undesired oscillations can appear in the graph of the implied volatility against the option strikes when the option prices are interpolated by a monotonic and convex spline. Table 6.A.2 in appendix 6.A presents a concrete example[4]. Here, the option quotes are not direct market quotes, but the solution of a sparse finite difference discretization of a local stochastic volatility model: the market never quotes so far out-of-the-money option prices. His data has a few interesting properties:

- some of the option prices are extremely small: the interpolation must be very accurate numerically.

- the option prices are free of arbitrage. In theory, an arbitrage-free interpolation can be exact.

- a cubic spline interpolation on the volatilities or the variances, often used by practitioners, is not arbitrage-free.

- a convexity preserving C^1-quadratic, or C^2-rational spline results in strong oscillations in the implied volatility.

---

[4]We are grateful to Peter Jäckel for kindly providing this data.

The interpolation proposed in [109] possesses unnatural spikes at the points of clamping, in particular, the implied density is not continuous.

For this example, the B-spline collocation leads to a relatively large RMSE when compared to Andreasen-Huge method. As a consequence, we can see an oscillation of small amplitude in the corresponding implied volatility for large strikes (Figure 6.7.1b). This is very mild compared to the spline interpolations presented in [109]. The higher error is mostly located in the left wing. The exponential B-spline collocation results in a much lower RMSE, albeit still larger than the Andreasen and Huge technique (Table 6.7.1). The volatility implied by the exponential B-spline collocation does not oscillate.
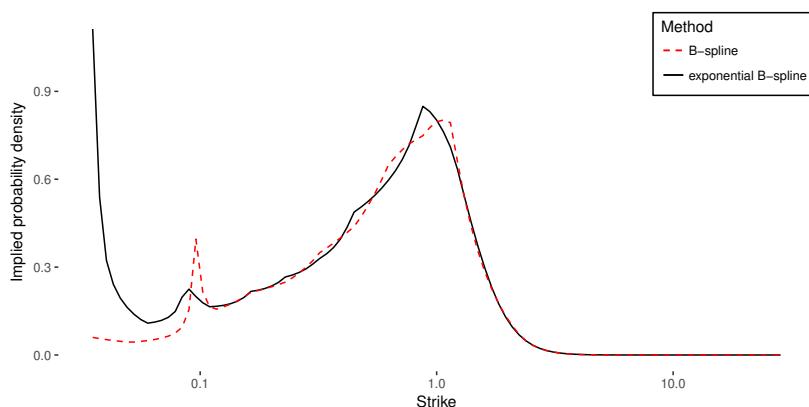
(a) Probability density.
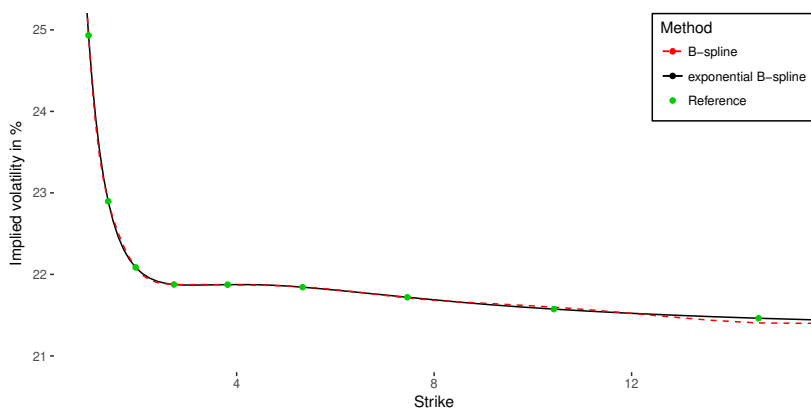
(b) Volatility smile for moneyness larger than one.

Figure 6.7.1: Implied probability density and implied volatility for the spline collocations of the market data of Table 6.A.2 in appendix 6.A.

The optimal implied probability density is relatively smooth, but possesses a few visible modes (Figure 6.7.1a). This makes the monotonic polynomial collocation of chapter 5 ineffective, even when using a high degree polynomial. Polynomials of degree seven

and higher lead to a RMSE larger than one vol point.

Table 6.7.1: Root mean square error (RMSE) of the collocation method implied volatilities against the implied volatilities of Table 6.A.2 in Appendix 6.A.

Method	Regularization	RMSE	Time (ms)
Septic polynomial	none	$1 \cdot 10^{-2}$	230
B-spline	$\lambda = 10^{-12}$	$2 \cdot 10^{-4}$	10
Exponential B-spline	$\lambda = 10^{-7}$	$6 \cdot 10^{-5}$	10
Andreasen-Huge (800 nodes)	none	$1 \cdot 10^{-6}$	25
Andreasen-Huge (3200 nodes)	none	$9 \cdot 10^{-8}$	67
Schumaker convex spline	none	0	0.02

It is possible to obtain a better fit with the B-spline collocation with a better choice of knots, for example, if we compute the knots implied by the calibrated B-spline collocation, and calibrate one more time. In Table 6.7.2, we denote this technique as "Best". It improves significantly the accuracy on the example of Peter Jäckel, but not on the filtered and non filtered TSLA market option quotes, where the different choices for the initial knots lead to a very similar RMSE.

Table 6.7.2: Root mean square error (RMSE) of the collocation method implied volatilities starting the calibration with the Bachelier, the convex, or the "best" initial guess, and using a small regularization constant.

Market data	Collocation method	Bachelier	Convex	Best
Peter Jäckel	B-spline	0.00063	0.00025	0.00001
	Exponential B-spline	0.00016	0.00006	0.00003
TSLA raw	B-spline	0.00330	0.00326	0.00322
	Exponential B-spline	0.00343	0.00345	0.00343
TSLA convex	B-spline	0.00054	0.00042	0.00034
	Exponential B-spline	0.00108	0.00118	0.00108

On Peter Jäckel's example, the optimal implied probability density is relatively smooth everywhere, and especially for strike moneyness larger than one. Figure 6.7.2 shows however that the probability density implied by technique of Andreasen and Huge exhibits a staircase shape when zoomed-in. This is due to the interpolation in between the finite difference grid nodes. In contrast, the probability density implied by the (exponential) B-spline collocation stays very smooth, and is continuous by construction.

6.8. CONCLUSION

The monotonic B-spline and exponential B-spline collocations allow a more flexible arbitrage-free representation as compared to the monotonic polynomial collocation. They can capture multi-modal distributions well. In practice, when the goal is to fit market option prices, we have shown that is important to add a regularization during the
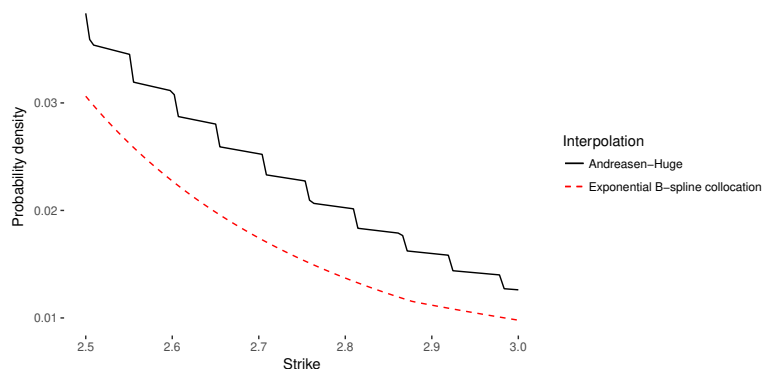
Figure 6.7.2: Implied probability density for the exponential B-spline collocation and Andreasen-Huge techniques, for strike moneyness $K \in [2.5, 3.0]$, calibrated to the market data of Table 6.A.2 in Appendix 6.A. The B-spline has a knot located at $K = 2.679$.

optimization in order to stabilize the calibration and produce a smooth implied probability density, and we have described which regularization is appropriate.

We have also presented a simple non-parametric technique to de-arbitrage a set of option prices, which may be used independently of the B-spline collocation method.

In some specific cases, such as the example from Jäckel [109], the outcome of the B-spline calibration may be dependent on the choice of the initial fixed knots. On the latter example, the exponential B-spline collocation behaved better however.

On actual market options quotes, corresponding to various equity or equity indices, we did not observe this strong dependence on the choice of initial knots. We observed a quality of fit in terms of implied volatilities similar to or better than the best non-parametric arbitrage-free methods such as the technique of Andreasen and Huge [12]. Compared to the latter, the spline collocation has the advantage of providing a natural continuous interpolation and extrapolation. The technique from Andreasen and Huge is based on a fine discretization of the problem, and requires an additional careful arbitrage-free interpolation scheme to compute the prices for option strikes not placed on the discretization grid. The B-spline collocation is also less computationally intensive, as the Andreasen and Huge technique mainly works well on a dense grid, typically composed of thousand points or more.

An additional interesting property of the exponential B-spline representation is the simple analytical expression we obtain for the price of a variance swap. The latter is a linear combination of the B-spline parameters. This allows to include the market prices of variance swaps very easily into the calibration and thus to obtain a better representation of the wings of the implied volatility.

Finally, the B-spline and exponential B-spline collocations can be used directly to price exotic derivatives within the collocated local volatility model of Grzelak and Oosterlee [77].

We leave for further research the definition of an algorithm for an automatic selection of the best B-spline knots, as well as an extension to B-splines of order four.

6.A. MARKET DATA

Table 6.A.1: Implied volatilities against strikes K for TSLA options expiring on January 17, 2020 as of June 15, 2018. This corresponds to a maturity $T = 1.59178$ and the forward is $f = 356.73$.

Strike	Implied volatility	Strike	Implied volatility
20	1.21745	330	0.50712
25	1.15297	335	0.50429
50	1.00135	340	0.50140
55	1.00870	350	0.49619
75	0.90559	360	0.49145
100	0.81965	370	0.48571
120	0.77970	380	0.48210
125	0.75393	390	0.47766
140	0.72553	400	0.46823
150	0.70370	410	0.46913
160	0.68709	420	0.46520
175	0.66315	430	0.46210
180	0.65428	440	0.45970
195	0.63100	450	0.45614
200	0.62320	460	0.45418
210	0.61545	470	0.45155
230	0.58662	480	0.44542
240	0.57838	490	0.44528
250	0.56250	500	0.44304
255	0.56255	510	0.43939
260	0.55723	520	0.44132
270	0.54852	550	0.43363
275	0.54561	580	0.42971
280	0.54006	590	0.42844
285	0.53848	600	0.42411
290	0.53253	650	0.42227
300	0.52224	670	0.42034
310	0.52024	680	0.41934
315	0.51684	690	0.41935
320	0.51274	700	0.41759
325	0.51004		

Table 6.A.2: Implied volatilities against moneyness $\frac{K}{F}$ for an option of maturity $T = 5.0722$, example 1 of Jäckel [109].

Moneyness	Implied volatility
0.035 12	0.642 41
0.049 10	0.621 68
0.068 62	0.590 58
0.095 92	0.553 14
0.134 08	0.511 40
0.187 41	0.466 70
0.261 96	0.420 23
0.366 17	0.373 30
0.511 82	0.327 56
0.715 42	0.285 11
1	0.249 33
1.397 78	0.228 97
1.953 80	0.220 86
2.730 99	0.218 76
3.817 33	0.218 74
5.335 80	0.218 43
7.458 29	0.217 20
10.425 07	0.215 74
14.572 00	0.214 62
20.368 49	0.214 11
28.470 74	0.214 58

AN ADAPTIVE FILON QUADRATURE FOR STOCHASTIC VOLATILITY MODELS

The valuation of European options under the Heston model, or under other stochastic volatility models where the characteristic function is known analytically, involves the computation of a Fourier transform type of numerical integration. This chapter describes adaptive Filon and adaptive Flinn quadrature to calculate this integral efficiently in accordance with a user-defined accuracy. It continues with a comparison in terms of accuracy and performance with quadrature rules commonly used for this problem such as the Lord and Kahl optimal alpha method. Finally, it concludes with the concrete case of model calibration on different market data.

7.1. INTRODUCTION

The valuation of European options under the Heston model, or under other stochastic volatility models where the characteristic function is known analytically, involves the computation of a Fourier transform type of numerical integration. Many variations exist. Heston derived the initial valuation formula from a probabilistic interpretation in [91], while Carr and Madan developed a more direct Fourier transform approach, which enabled the use of the fast Fourier transform (FFT) algorithm in [32]. Their damping parameter α also spun off a family of alternative valuation formulas, with better convergence properties than the original Heston formula. The Lewis formula, corresponding to $\alpha = -\frac{1}{2}$ is particularly popular as it is simple to evaluate, is well-defined everywhere and has quadratic denominator [139]. We should also mention the choice $\alpha = -1$ proposed by Attari, which requires special treatment around zero, and the choice $\alpha = 0$ studied by Joshi and Yang [115]. Joshi and Yang combined this specific choice of α along with matching the value and first derivative of the characteristic function at $z = -i$ with a Black-Scholes control variate[1], which they found was improving the efficiency of real-time calibration. A procedure to find the optimal (strike and maturity dependent) α, leading to the ability of pricing extremely out-of-the-money options, including those whose prices are beyond machine epsilon, is described in [145].

---

[1]The value of the characteristic function at the integration boundary $z = -i$ always matches with the choice $\alpha = 0$, independently of the parameters.

In terms of integration, Kilin [119] showed that the FFT method was not competitive against a simple quadrature with cached characteristic function values. There is however no real consensus on the quadrature to be used. Andersen and Piterbarg advocate for the simplest trapezoidal method with a good truncation [9]. Kahl and Jaeckel, as well as Lord and Kahl propose the adaptive Gauss-Lobatto of Gander and Gautschi combined with a log-transform [117], while Joshi and Yang use the Gauss-Laguerre quadrature.

The Filon quadrature is particularly suited to the computation of Fourier integrals [61, 191]. A generalisation of this method has been applied to the problem of pricing options under the displaced lognormal Heston model in [49]. Their proposed algorithm however involves many specific choices of parameters. In this chapter, we will look at a particularly simple and effective adaptive Filon method, where the adaptive integration points are reusable across strikes, for a given maturity. A similar technique has been used in seismology in [87] and in finance the context of volatility swap pricing in [128]. We will evaluate its behavior against popular Heston integration methods on challenging Heston parameters. Finally, we will take a look at the full volatility surface calibration performance and stability.

While this chapter focuses on the Heston stochastic volatility model, the proposed technique is more general and can be applied other models with closed form characteristic functions like Bates [20], Schöbel-Zhu [178], or Double-Heston [36].

7.2. CHARACTERISTIC FUNCTIONS

The Heston stochastic volatility model for an asset F is described by the following system of stochastic differential equations [91]:

$$dF = \sqrt{v}F dW_F, \tag{7.1}$$
$$dv = \kappa(\theta - v)dt + \sigma\sqrt{v}dW_v, \tag{7.2}$$

with $dW_F dW_v = \rho dt$. For an equity of spot price S, and maturity T, F represents the forward to maturity $F(t) = S(t)e^{(r-q)(T-t)}$, with r the relevant interest rate, and q the dividend yield.

In order to avoid complex discontinuities, we rely on Jim Gatheral's formulation of the normalized Heston characteristic function [144]:

$$\psi(z) = e^{\frac{v_0}{\sigma^2}\frac{1-e^{-DT}}{1-Ge^{-DT}}(\kappa-i\rho\sigma z-D)+\frac{\kappa\theta}{\sigma^2}\left((\kappa-i\rho\sigma z-D)T-2\ln(\frac{1-Ge^{-DT}}{1-G})\right)}, \tag{7.3}$$

with

$$D = \sqrt{(\kappa-i\rho\sigma z)^2 + (z^2+iz)\sigma^2}, \tag{7.4}$$
$$G = \frac{\kappa-i\rho\sigma z - D}{\kappa-i\rho\sigma z + D}. \tag{7.5}$$

The standard characteristic function is then just $\mathbb{E}[e^{iz\ln(F(T))}] = e^{iz\ln(F(0))}\psi(z)$.

In the Black-Scholes model, the asset F follows $dF = \sigma_B F dW$ and the normalized Black-Scholes characteristic function with volatility σ_B is given by

$$\psi_B(z) = e^{-\frac{1}{2}\sigma_B^2 T(z^2+iz)}. \tag{7.6}$$

We will see, that it can be used as a control variate for stochastic volatility models.

7.3. PRICING FORMULAS

Originally, Heston proposed a Black-Scholes like formula in [91]. The vanilla call option price can be expressed as [32]:

$$V_{\text{call}}(F,K,T) = Fe^{-rT}\left[\frac{1}{2} + \frac{1}{\pi}\int_0^\infty \Re\left(\frac{e^{-iuk}\psi(u-i)}{iu\psi(-i)}\right)du\right] + Ke^{-rT}\left[\frac{1}{2} + \frac{1}{\pi}\int_0^\infty \Re\left(\frac{e^{-iuk}\psi(u)}{iu}\right)du\right],$$

$$(7.7)$$

where $k = \ln(K)$. In order to obtain a square-integrable function based on the Call price, Carr and Madan [32] propose[2] a formula based on a damped option price:

$$V_{\text{call}}(F,K,T) = R_\alpha(F,K) + F\frac{e^{-\alpha x}e^{-rT}}{\pi}\int_0^\infty \Re\left(e^{-iux}\frac{\psi(u-(\alpha+1)i)}{(\alpha+iu)(\alpha+1+iu)}\right)du, \qquad (7.8)$$

where α is a damping parameter, $x = \ln(\frac{K}{F})$, and

$$R_\alpha(F,K) = e^{-rT}\left[F\cdot 1_{\alpha\leq 0} - K\cdot 1_{\alpha\leq -1} - \frac{1}{2}\left(F\cdot 1_{\alpha=0} - K\cdot 1_{\alpha=-1}\right)\right].$$

A method to find the optimal α, allowing to price extremely out-of-the-money options is described in [145]. For put options, one can just use the same formula, but with $\alpha < -1$.

A popular alternative formulation with a quadratic denominator was found by [139]:

$$V_{\text{call}}(F,K,T) = Fe^{-rT} - \frac{\sqrt{FK}e^{-rT}}{\pi}\int_0^\infty \frac{\Re\left(e^{-iux}\psi(u-\frac{i}{2})\right)}{u^2 + \frac{1}{4}}du. \qquad (7.9)$$

This is equivalent to taking $\alpha = -\frac{1}{2}$ in Carr-Madan formula. It is a method of choice in [9], where they introduce a Black-Scholes control variate to significantly improve convergence:

$$V_{\text{call}}(F,K,T) = \text{BS}(F,K,T,\sqrt{v_0}) + \frac{\sqrt{FK}e^{-rT}}{\pi}\int_0^\infty \Re\left(e^{-iux}\frac{\psi_B(u-\frac{i}{2}) - \psi(u-\frac{i}{2})}{u^2 + \frac{1}{4}}\right)du.$$

$$(7.10)$$

Put options can be priced with the same formula but using the Black-Scholes put option price instead of the call option price. Finally, a recent formula with Black-Scholes control-variate is studied in [115].

$$V_{\text{call}}(F,K,T) = \text{BS}(F,K,T,\sigma_B) + \frac{e^{-rT}}{\pi}\int_0^\infty \Re\left(e^{-iux}\frac{\psi_B(u-i) - \psi(u-i)}{u(u-i)}\right)du, \qquad (7.11)$$

where BS represents the option price obtained by the Black-Scholes formula for an asset of spot price F, strike price K, maturity T and volatility σ_B. This is similar to taking $\alpha = 0$ in Carr-Madan formula. The authors also find that the optimal choice of volatility σ_B used in the control variate corresponds to $\psi_B'(-i) = \psi'(-i)$. Without this choice of control variate, the formula would require special treatment at 0.

---

[2]This is not strictly the Carr-Madan formula: it is scaled by the forward.

7.3.1. TRUNCATION OF THE INTEGRATION RANGE

A DOMAIN TRANSFORMATION

One immediate issue with the integration is the infinity of the range of integration. A possibility is to use a log transform $z(u)$ as proposed in [117, 145] combined with some adaptive integration algorithm, for example the adaptive Gauss-Lobatto quadrature of [69]. Defining:

$$u(z) = -\frac{\ln(z)}{C_\infty}, \tag{7.12}$$

the Lewis pricing formula (Equation 7.9) can be rewritten as

$$\int_0^\infty \frac{\Re\left(e^{-iux}\psi(u - \frac{i}{2})\right)}{u^2 + \frac{1}{4}}\,du = \int_0^1 \frac{\Re\left(e^{-iu(z)x}\psi(u(z) - \frac{i}{2})\right)}{(u(z)^2 + \frac{1}{4})(u(z)C_\infty)}\,dz. \tag{7.13}$$

The constant C_∞ is chosen so that the transformed variable $z(u)$ has same asymptotic behavior as the characteristic function at ∞:

$$\lim_{u\to+\infty} \frac{1}{u}\ln(\psi(u - (\alpha+1)i) - \psi_B(u - (\alpha+1)i)) = -(C_\infty + iD_\infty), \tag{7.14}$$

with

$$C_\infty = \frac{v_0 + \kappa\theta T}{\sigma}\sqrt{1-\rho^2}, \tag{7.15}$$

$$D_\infty = \frac{v_0 + \kappa\theta T}{\sigma}\rho. \tag{7.16}$$

This can be applied to any of the formulas.

ANDERSEN-PITERBARG APPROACH TO LEWIS FORMULA

Another possibility is to find a good truncation and integrate directly, as proposed in [9], relying on the following approximation when $u_{\max}$ is sufficiently large:

$$\int_{u_{max}}^\infty \left|\frac{\psi(u - \frac{i}{2}) - \psi_B(u - \frac{i}{2})}{u^2 + \frac{1}{4}}\right|\,du \le e^{-C_\infty u_{\max}}\int_{u_{\max}}^\infty \frac{du}{u^2}. \tag{7.17}$$

Both methods actually rely on the same number C_∞. For a relative tolerance of ϵ_u, the truncation limit $u_{\max}$ is found by solving:

$$\frac{e^{-C_\infty u_{\max}}}{u_{\max}} = \epsilon_u, \tag{7.18}$$

or, to avoid numerical overflow:

$$-C_\infty u_{\max} - \ln(u_{\max}) = \ln(\epsilon_u). \tag{7.19}$$

Short expiries

The truncation can be invalid for short expiries ($T < 0.1$) as, then, $e^{-D(u_{\max})T} \not\ll 1$. A Taylor expansion around $T = 0$ gives the Black-Scholes like characteristic function:

$$\ln(\psi(u)) = -\frac{1}{2}v_0 T(u^2 + iu) + \mathcal{O}(T^2).$$

Then, our approximation for short expiries is $\hat{u}_{\max}$ that solves:

$$-\frac{1}{2}v_0 T \hat{u}_{\max}^2 - \ln(\hat{u}_{\max}) = \ln(\epsilon_u). \qquad (7.20)$$

We found that a good practical rule for the full range of expiries is just to use

$$\hat{u}_{\max} = \max(u_{\max}, \hat{u}_{\max}).$$

Similarly, the log-transform is not always well-behaved for short expiries. While the integrand is well-behaved around $z = 0$, this is not always true around $z = 1$ as the characteristic function becomes Black-Scholes like for short expiries. In practice, an adaptive quadrature might require the evaluation of the integrand at very closely spaced points near $z = 1$, sometimes of distance smaller than the machine epsilon. As a work-around, we can use the transform of Lord and Kahl [145] for the Black-Scholes characteristic function and cap C_∞ to

$$\bar{C}_\infty = \sqrt{\frac{v_0 T}{2}}. \qquad (7.21)$$

Let us illustrate the importance of our modifications for the short expiries with the Heston parameters $v_0 = 0.826, \kappa = 0.254, \theta = 0.320, \sigma = 0.344, \rho = -0.557$ on an option of maturity $T = 0.0182$ with forward and strike $F = 1000, K = 1400$. Table 7.3.1 shows that without the adjustment to the truncation, the price is just wrong. The adjustment to C_∞ is particularly important for the non-adaptive quadrature schemes: a Simpson quadrature with 10000 points has a huge error (of around 40% of the reference price). The adaptive Gauss-Lobatto quadrature of Espelid [58] still works with the non capped C_∞ but requires many more points (almost 10000).

Table 7.3.1: Price with the Lewis formula and Black-Scholes control variate of volatility $\sigma_B = \sqrt{v_0}$ with the following Heston parameters: $v_0 = 0.826, \kappa = 0.254, \theta = 0.320, \sigma = 0.344, \rho = -0.557$ on an option of maturity $T = 0.0182$ with forward and strike $F = 1000, K = 1400$.

Quadrature	Points	Truncation	Price
Simpson	10000	$u_{\max} = 12.69$	0.0651248
Simpson	10000	$\hat{u}_{\max} = 56.04$	0.1073414
Simpson	10000	None / $C_\infty = 1.998$	0.0685957
Simpson	10000	None / $\bar{C}_\infty = 0.086$	0.1073414
Gauss-Lobatto	1487 (Adaptive)	$\hat{u}_{\max} = 56.04$	0.1073414
Gauss-Lobatto	9107 (Adaptive)	None / $C_\infty = 1.998$	0.1073414
Gauss-Lobatto	5087 (Adaptive)	None / $\bar{C}_\infty = 0.086$	0.1073414

This is a key weakness of the domain transformation. While our fix improves the behaviour in general, it is not clear if it stays always well-behaved near $z = 0$, and our choice of applying the cap for $T < 0.1$ is somewhat arbitrary.

Interestingly, on this example, the non-transformed, truncated integral is much faster to evaluate with the Gauss-Lobatto quadrature than the log-transformed equivalent. We found this to be generally the case for short expiries, while for longer expiries, the log transform was more beneficial.

7.4. The Filon quadrature

7.4.1. Definition
The Filon quadrature is commonly used to evaluate integrals containing a trigonometrical form such as

$$I_c = \int_a^b f(p)\cos(xp)\,dp, \quad I_s = \int_a^b f(p)\sin(xp)\,dp, \tag{7.22}$$

where $f(p)$ is a known function of p. When x is not small, the rapid oscillations of the trigonometric function are particularly challenging for ordinary quadrature formulas, such as Simpson's rule, which require a division of the range of integration into such small steps that the associated computational cost is prohibitive. The idea of Filon is to fit f by a parabola at three equidistant points, as in Simpson's method, but to integrate exactly the terms in $p^k \cos(xp)$, $p^k \sin(xp)$. Applied to a subdivision in $2n$ parts of the original interval $[a, b]$ this results in the following formula:

$$I_c = h\left\{\alpha\left[f(b)\sin(xb) - f(a)\sin(xa)\right] + \beta C_{ce} + \gamma C_{co}\right\}, \tag{7.23}$$
$$I_s = h\left\{-\alpha\left[f(b)\cos(xb) - f(a)\cos(xa)\right] + \beta C_{se} + \gamma C_{so}\right\}, \tag{7.24}$$

where $h = \frac{b-a}{2n}$, and C_{ce} is the sum of even ordinates of $f(p)\cos(px)$ minus half the end ordinates

$$C_{ce} = \frac{1}{2}\left(f(a)\cos(pa) + f(b)\cos(pb)\right) + \sum_{j=1}^{n-1} f\left(a + 2jh\right)\cos\left(pa + 2jph\right),$$

and C_{co} is the sum of odd ordinates of $f(p)\cos(px)$:

$$C_{co} = \sum_{j=0}^{n-1} f\left(a + (2j+1)h\right)\cos\left(pa + (2j+1)ph\right).$$

Similarly, C_{se} is the sum of even ordinates of $f(p)\sin(px)$ minus half the end ordinates, C_{so} is the sum of odd ordinates of $f(p)\sin(px)$. Finally, the variables α, β, γ are defined as follows

$$\theta^3\alpha = \theta^2 + \theta\sin\theta\cos\theta - 2\sin^2\theta, \tag{7.25}$$
$$\theta^3\beta = 2\left[\theta\left(1 + \cos^2\theta\right) - 2\sin\theta\cos\theta\right], \tag{7.26}$$
$$\theta^3\gamma = 4\left[\sin\theta - \theta\cos\theta\right], \tag{7.27}$$

with $\theta = hx$.

Chase and Fosdick [34] derived a robust numerical algorithm taking special care of the case where θ is small. A more thorough description of the Filon quadrature is presented in [189].

7.4.2. LOCAL ERROR

Let us analyze the error on a single panel $[u_i, u_{i+1}]$. In order to keep the equations simple, we reduce the problem to the interval $[0, 2h]$ with $h = \frac{u_{i+1} - u_i}{2}$ through the translation $g(t) = u_i + t$. Stirling's interpolation formula on the points $\{0, h, 2h\}$ gives:

$$f(p+h) = f(h) + \delta_h^1 p + \delta_h^2 \frac{p^2}{2} + \delta_h^3 \frac{p(p^2 - h^2)}{6} + \delta_h^4 \frac{p^2(p^2 - h^2)}{24} + \delta_h^5 \frac{p(p^2 - h^2)(p^2 - 4h^2)}{120} + \dots$$
(7.28)

where δ_h^i is the i-th central difference of the function f around h.

Filon's formula corresponds to the integration of the first three terms from $-h$ to h. The next omitted terms lead to

$$E_3 = \delta_h^3 \int_{-h}^{h} \frac{p(p^2 - h^2)}{6} \cos\left(x(p + h + u_i)\right) dp$$

$$= \delta_h^3 \cos(xh + xu_i) \int_{-h}^{h} \frac{p(p^2 - h^2)}{6} \cos(xp) dp - \delta_h^3 \sin(xh + xu_i) \int_{-h}^{h} \frac{p(p^2 - h^2)}{6} \sin(xp) dp$$

$$= 0 - \delta_h^3 \sin(xh + xu_i) h^4 \frac{(2h^2 x^2 - 6) \sin(hx) + 6hx \cos(hx)}{3x^4 h^4} .$$

When $h \to 0$, a Taylor expansion gives

$$E_3 = \delta_h^3 \frac{2xh^5}{45} \sin(xu_i + xh) + O(h^7).$$
(7.29)

Contrary to the Simpson formula (case $x = 0$), it is not zero in general. The next term of the series is of the same order:

$$E_4 = \delta_h^4 \int_{-h}^{h} \frac{p^2(p^2 - h^2)}{24} \cos\left(x(p + h + u_i)\right) dp$$

$$= \delta_h^4 \cos(hx + u_i x) \int_{-h}^{h} \frac{p^2(p^2 - h^2)}{24} \cos(px) dp - \delta_h^4 \sin(hx + u_i x) \int_{-h}^{h} \frac{p^2(p^2 - h^2)}{24} \sin(px) dp$$

$$= -\delta_h^4 \cos(hx + u_i x) h^5 \frac{(10h^2 x^2 - 24) \sin(hx) + (24hx - 2h^3 x^3) \cos(hx)}{12h^5 x^5} - 0.$$

When $h \to 0$, a Taylor expansion gives

$$E_4 = -\delta_h^4 \frac{h^5}{90} \cos(xu_i) + O(h^7).$$
(7.30)

When $h \to 0$, the local error is of the same order as the one of Simpson's rule, but is larger in general due to the term in δ_h^3.

As suggested by Linz [143], a Richardson extrapolation between the original panel $[u_i, u_i + 2h]$ and the two half-width panels $[u_i, u_i + h]$ and $[u_i + h, u_i + 2h]$ can be used

to remove the error due to δ_h^3. Let ρ be the ratio between the δ_h^3 related error e_1 of the Filon quadrature on the full panel I_1 and the δ_h^3 related error e_2 on the two panels I_2, the extrapolation consists in using I_R defined by

$$I_R = I_2 + \frac{I_2 - I_1}{\rho - 1}, \tag{7.31}$$

where

$$\rho = \frac{\delta_h^3 \int_{-h}^{h} \frac{p(p^2 - h^2)}{6} \cos\left(x(p + h + u_i)\right) dp}{\delta_h^3 \int_{-\frac{h}{2}}^{\frac{h}{2}} \frac{p\left(p^2 - \left(\frac{h}{2}\right)^2\right)}{6} \cos\left(x\left(p + \frac{h}{2} + u_i\right)\right) dp + \delta_h^3 \int_{-\frac{h}{2}}^{\frac{h}{2}} \frac{p\left(p^2 - \left(\frac{h}{2}\right)^2\right)}{6} \cos\left(x\left(p + \frac{3h}{2} + u_i\right)\right) dp}.$$

Using the trigonometric identity $\cos(a + b) = \cos(a)\cos(b) - \sin(a)\sin(b)$ and noticing that the cosine term is zero for the numerator due to symmetry and cancels out in the denominator, we obtain

$$\rho = \frac{\delta_h^3 \sin(xh + xu_i) \int_{-h}^{h} \frac{p(p^2 - h^2)}{6} \sin(xp) dp}{2\delta_h^3 \sin(xh + xu_i) \int_{-\frac{h}{2}}^{\frac{h}{2}} \frac{p\left(p^2 - \left(\frac{h}{2}\right)^2\right)}{6} \sin(xp - \frac{xh}{2}) dp},$$

which simplifies to

$$\rho = \frac{\left(4h^2 x^2 - 12\right)\sin(hx) + 12hx\cos(hx)}{\left(h^2 x^2 - 12\right)\sin(hx) + 6hx\cos(hx) + 6hx}. \tag{7.32}$$

This will cancel out E_3 completely, making the integration of cubic polynomials exact[3], but will not cancel out E_4.

When $hx \to 0$, $\rho \to 16$, as expected from an error in $O(h^5)$. This is the same ratio as with the Simpson quadrature. Using $\rho = 16$ will be effective on both error terms E_3 and E_4 when h is small.

7.4.3. FILON QUADRATURE FOR THE LEWIS FORMULA

The Lewis formula (Equation 7.9) can be rewritten as:

$$V_{\text{call}}(F, K, T) = Fe^{-rT} - \frac{\sqrt{FK}e^{-rT}}{\pi} \int_0^{\infty} \frac{\Re\left(\psi(u - \frac{i}{2})\right)}{u^2 + \frac{1}{4}} \cos(ux) + \frac{\Im\left(\psi(u - \frac{i}{2})\right)}{u^2 + \frac{1}{4}} \sin(ux) du. \tag{7.33}$$

To compute the vanilla option price, we can therefore apply the cosine and sine Filon quadrature formulas respectively to the functions

$$f(u) = \frac{\Re\left(\psi(u - \frac{i}{2})\right)}{u^2 + \frac{1}{4}}, \quad g(u) = \frac{\Im\left(\psi(u - \frac{i}{2})\right)}{u^2 + \frac{1}{4}}. \tag{7.34}$$

A significant property of the functions $f(u)$ and $g(u)$ is that they are not dependent on the log-moneyness x.

---

[3]a numerical implementation of the extrapolation will benefit from the use of a Taylor expansion of ρ around zero to ensure numerical stability.

7.5. FLINN'S IMPROVEMENT

7.5.1. DEFINITION

Instead of fitting a quadratic polynomial as in Filon's quadrature, Flinn [62] uses a fifth-order polynomial to fit the middle and end point values and first derivatives, resulting not only in a higher-order quadrature, but also in one that works better on larger intervals. The resulting formula is not much more complicated:

$$
\begin{aligned}
I_c = h\{S\left[f(b)\sin(xb) - f(a)\sin(xa)\right] + hP\left[f'(b)\cos(xb) - f'(a)\cos(xa)\right] \\
+ RC_{ce} + hQC'_{se} + NC_{co} + hMC'_{so}\},
\end{aligned}
\tag{7.35}
$$

$$
\begin{aligned}
I_s = h\{-S\left[f(b)\cos(xb) - f(a)\cos(xa)\right] + hP\left[f'(b)\sin(xb) - f'(a)\sin(xa)\right] \\
+ RC_{se} - hQC'_{ce} + NC_{so} - hMC'_{co}\},
\end{aligned}
\tag{7.36}
$$

where C'_{ce} is the sum of even ordinates of $f'(p)\cos(px)$ minus half the end ordinates, C'_{co} is the sum of odd ordinates of $f'(p)\cos(px)$, C'_{se} is the sum of even ordinates of $f'(p)\sin(px)$ minus half the end ordinates, C'_{so} is the sum of odd ordinates of $f'(p)\sin(px)$. We refer the reader to Flinn's paper [62] for the specific values of the constants M, N, P, Q, R, S. It also provides expansions useful for the case where θ is small.

7.5.2. LOCAL ERROR

Flinn's approximation corresponds to a Hermite interpolation of f on three points. The Hermite polynomial on $x_1, x_2, ..., x_N$ is given by

$$
H(x) = \sum_{i=1}^{N} l_i^2(x)\left[\left(1 - 2l'_i(x_i)(x - x_i)\right)f(x_i) + (x - x_i)f'(x_i)\right],
\tag{7.37}
$$

where l_i are the Lagrange polynomials $l_i(x) = \Pi_{i=1, i\neq j}^{N} \frac{x - x_j}{x_i - x_j}$. The quintic Hermite quadrature on the panel $[u_i, u_i + 2h]$ is:

$$
I_H = \frac{h}{15}\left[7f(u_i) + 16f(u_i + h) + 7f(u_i + 2h) + h\left(f'(u_i) - f'(u_i + 2h)\right)\right],
\tag{7.38}
$$

and the error in Hermite interpolation is

$$
f(x) - H(x) = \frac{f^{(2N)}(\xi)}{(2N)!}\Pi_{i=1}^{N}(x - x_i)^2,
\tag{7.39}
$$

where ξ belong to the smallest interval containing $(x_i)_{i=1,...,N}$ and x. The error in the Hermite quadrature on a single panel of width $2h$ using $N = 3$ points at $\{u_i, u_i + h, u_i + 2h\}$ is thus

$$
E_H = \int_{-h}^{h} \frac{f^{(6)}(\xi(p + u_i + h))}{6!}(p - h)^2 p^2 (p + h)^2 dp = \frac{f^{(6)}(\xi_i)}{4725}h^7,
\tag{7.40}
$$

where the second equality comes from the use of the first mean value theorem for integrals as $(p - h)^2 p^2 (p + h)^2 \geq 0$, and $\xi_i \in [u_i, u_i + 2h]$. For the Flinn quadrature, this becomes

$$
\begin{aligned}
E_F &= \int_{-h}^{h} \frac{f^{(6)}(\xi(p + u_i + h))}{6!}(p - h)^2 p^2 (p + h)^2 \cos\left(x(p + u_i + h)\right)dp \\
&= \frac{f^{(6)}(\xi_i)\cos(x\lambda_i)}{4725}h^7,
\end{aligned}
\tag{7.41}
$$

where $\lambda_i \in [u_i, u_i + 2h]$. In particular, if $f^{(6)}$ does not vary much on the interval, we have $|E_F| \leq |E_H|$.

In similar fashion as with the Filon quadrature, we could derive an extrapolation scheme that makes the integration of sextic polynomials exact. It would lead to a ratio $\rho = 64$ for $h \to 0$. Numerical tests however did not show any strong improvement of the accuracy with this extrapolation in cases of practical interest.

7.5.3. Flinn quadrature for the Lewis formula

It is not much more costly to evaluate both the characteristic function ψ and its derivative ψ'. The first derivative can be computed at the same time by simple analytical differentiation, reusing most of the costly intermediate variables.

To compute the vanilla option price, we can therefore apply the cosine and sine Flinn quadrature, respectively, to the functions

$$f(u) = \frac{\Re\left(\psi(u - \frac{i}{2})\right)}{u^2 + \frac{1}{4}} \,,\, f'(u) = \frac{\Re\left(\psi'(u - \frac{i}{2})\right)}{u^2 + \frac{1}{4}} - 2\frac{\Re\left(\psi(u - \frac{i}{2})\right)}{\left(u^2 + \frac{1}{4}\right)^2}u, \qquad (7.42)$$

and

$$g(u) = \frac{\Im\left(\psi(u - \frac{i}{2})\right)}{u^2 + \frac{1}{4}} \,,\, g'(u) = \frac{\Im\left(\psi'(u - \frac{i}{2})\right)}{u^2 + \frac{1}{4}} - 2\frac{\Im\left(\psi(u - \frac{i}{2})\right)}{\left(u^2 + \frac{1}{4}\right)^2}u. \qquad (7.43)$$

7.5.4. Making it adaptive

The similarity between Simpson's and Filon's methods suggests to apply the same adaptive technique as for Simpson's rule. We simply apply the adaptive Simpson algorithm to the computation of the two integrals

$$\bar{I}_c = \int_0^{u_{\max}} f(u)\,du \,,\, \bar{I}_s = \int_0^{u_{\max}} g(u)\,du \qquad (7.44)$$

and record the abscissae u_i and function values (f_i, g_i) (eventually along with the derivative values) in a map structure. We then sort the values by abscissa and use the Filon or the Flinn quadrature to the intervals defined by the abscissae, three points by three points. In practice, the Filon constants α, β, γ in Equations (7.25), (7.26), (7.27) can be reused across adjacent intervals, unless the step size has changed. The cost of evaluating the trigonometric functions can be further reduced by taking advantage of the identities $\cos(u+\theta) = \cos(u)\cos(\theta) - \sin(u)\sin(\theta)$, $\sin(u+\theta) = \cos(u)\sin(\theta) + \sin(u)\cos(\theta)$ and evaluating the cos and sin integrals together.

The underlying assumption is that an adaptive Simpson algorithm is going to approximate f and g well enough so that the Filon or the Flinn quadrature on the same points is accurate enough. The two integrals of Equation (7.44) correspond to the Lewis formula at-the-money, that is, where $x = 0$.

There are various adaptive Simpson algorithms. A somewhat popular one, `squank`, is based on [147, 148], which refines the Simpson method with a Richardson extrapolation and uses interval bisection. Gander and Gautschi [69] propose an alternative algorithm `adaptsim` with a different local error control relying on an initial estimate of the integral by a five points Monte-Carlo integration. Espelid [58] wrote a more recent algorithm

`modsim` using directly a five points Newton-Cotes formula (which is equivalent to the extrapolated Simpson formula) with refined local error control based on Null rules. This later algorithm can be transformed to a globally adaptive algorithm the same way the author transforms its locally adaptive `coteda` to the globally adaptive `coteglob`.

While, in practice, the choice of adaptive algorithm matters little for the stability of the overall adaptive Filon method, we found that Gander and Gautchi's `adaptsim` was in general failing much more than the `squank` or `modsim` algorithms, when applied directly to the Lewis formula instead of the Filon reduction. This is mostly due to a bad initial estimate of the integral. Furthermore the `modsim` algorithm was in general faster than `squank` (requiring less points), even more so with global error control. Finally, `adaptquin` is a modification of the Gander and Gautchi `adaptsim` algorithm that uses the Hermite quintic quadrature instead of the Simpson quadrature, and extrapolates with $\rho = 64$ instead of $\rho = 16$.

The precomputed abscissae and function values can be reused to value options at different strike prices. In contrast with the standard adaptive quadrature methods applied directly to the Lewis formula, the adaptivity is independent of the strike price here.

7.6. Numerical results

7.6.1. Challenging Heston parameters

Medium maturity

We consider an option of maturity $T = 1$ and strike price $K = 0.25$ on an asset following the Heston stochastic volatility model with parameters $v_0 = 0.0225, \kappa = 0.1, \theta = 0.01, \sigma = 2.0, \rho = 0.5, F = 1$. The option is therefore very out of the money. We have set the truncation level at 10^{-8}, and use the same accuracy for the various adaptive quadrature schemes considered. Except for the Cos method of Fang and Oosterlee [59], and the Lord-Kahl optimal α method, we rely on the Lewis formula with Black-Scholes control variate of volatility $\sigma_B = \sqrt{v_0}$.

Under those settings, Table 7.6.1 shows that the doubly adaptive Newton-Cotes quadrature `coteda` of Espelid [58] has a very high error, well above the tolerance for a tolerance of 10^{-8} (but is fine with a tolerance of 10^{-7} or 10^{-9}). The adaptive Gauss-Lobatto `modlob` has no such issue but requires a large number of points (over 10000). The Cos method requires a truncation at $L = 30$ to achieve a reasonable accuracy with 1000 points, well above the recommended $L = 8$ of their paper. The Flinn method requires 485 points with the globally adaptive Simpson quadrature and only 121 points with the adaptive quintic Hermite quadrature `adaptquin` to achieve an accuracy of 10^{-10} per unit notional, which is as accurate as the direct `modlob` with more than 10000 points. Even with the use of Lord and Kahl optimal-α, oscillations remain in the integrand on this example[4], and the number of quadrature points used does not decrease significantly compared to the use of the Lewis formula with a control variate.

Interestingly, using the adaptive Simpson `modsim` directly on the Lewis formula requires many more points than our adaptive Flinn method (close to 9000) for a lower overall accuracy.

---

[4]The optimal α usually helps, especially to compute very small prices of out-of-the-money options, because of the scaling, but it does not always remove oscillations.

Table 7.6.1: 1Y put option of notional 100,000 and strike price 25% with Heston parameters $v_0 = 0.0225, \kappa = 0.1, \theta = 0.01, \sigma = 2.0, \rho = 0.5$ under various numerical methods.

Method	Tolerance	Points	Price
modlob Lord-Kahl	1e-8	7947	119.385327
coteda	1e-8	1361	99.666129
modlob	1e-8	10987	119.385324
modlob Log	1e-8	9527	119.385347
modsim	1e-8	8853	119.324143
modsim Filon	1e-8	733	119.385917
globsim Flinn	1e-8	485	119.385352
adaptquin Flinn	1e-8	121	119.385406
Cos	L=12	1000	0.0
Cos	L=16	1000	123.033165
Cos	L=30	1000	119.387924

SHORT MATURITY

We use here the same parameters as in Table 7.3.1 but set the tolerance at 10^{-8} instead of 10^{-12}. The Gauss-Lobatto quadrature requires much fewer points with this tolerance level. For the same accuracy, the adaptive Flinn method needs only a quarter of the number of points used by the direct modlob (see Table 7.6.2).

Table 7.6.2: Call option of maturity $T = 0.0182$ with forward and strike price $F = 1000, K = 1400$ and Heston parameters $v_0 = 0.826, \kappa = 0.254, \theta = 0.320, \sigma = 0.344, \rho = -0.557$ under various numerical methods with error tolerance 10^{-8}.

Method	Points	Price
modlob Lord-Kahl	257	0.107341448
modsim	645	0.107341552
modsim Filon	329	0.107341554
globsim Flinn	125	0.107341551
adaptquin Flinn	49	0.107341552

On options of longer maturities the number of points used by modlob and by our adaptive Flinn quadrature is similar.

7.6.2. PERFORMANCE

Let us look at the performance and accuracy of the various quadrature schemes, using the Lewis formula with the Black-Scholes control variate of volatility $\sigma_B = \sqrt{v_0}$. We use an accuracy of 10^{-6} for the adaptive quadrature schemes while the truncation is done for a relative tolerance of 10^{-9}. The reference is the Lord-Kahl method, with an adaptive quadrature of accuracy 10^{-10}.

We price hundred put options of different strike prices but same maturity with realistic Heston parameters for an equity. Table 7.6.3 shows that the adaptive Flinn method is

up to twenty times faster than a direct adaptive Gauss-Lobatto quadrature. This should not be too surprising since the adaptivity is independent of the strike price with the Flinn method, but not with the direct approach.

Table 7.6.3: Performance and Accuracy of the various integrations to price 100 put options of strike prices between 0.4 and 1.6 with the following Heston parameters: $\kappa = 1.0, \theta = 0.1, \sigma = 1.0, v_0 = 0.1, \rho = -0.9$.

Method	RMSE	Total Time(ms)
	Maturity of 2 weeks	
`modlob` Lord-Kahl	4.53E-06	17.0
`modlob` Log	1.74E-11	20.3
`modlob`	2.91E-11	13.8
`modsim` Filon	1.82E-10	3.6
`globsim` Flinn	4.15E-12	1.6
`adaptquin` Flinn	1.57E-10	0.4
	Maturity of 2 years	
`modlob` Lord-Kahl	6.46E-06	23.7
`modlob` Log	2.27E-09	9.9
`modlob`	4.45E-12	7.3
`modsim` Filon	7.89E-12	4.0
`globsim` Flinn	6.57E-12	2.6
`adaptquin` Flinn	1.19E-08	0.4

In the Lord-Kahl method, the optimal alpha is strike-dependent, and thus any caching the characteristic function will be useless. This is why their method tends to be the slowest. Furthermore the accuracy is now relative to the scaling by the optimal alpha. This explains the higher (absolute) root mean square error with the Lord-Kahl method on this test.

7.6.3. HESTON CALIBRATION

ERROR MEASURE

The calibration of the Heston model consists in minimizing the difference between the market implied volatilities (or option prices) and the model implied volatilities (or option prices).

Our implied volatility error measure will simply be the weighted root mean square error in the implied volatilities M_σ described in Section 5.3.5, Equation (5.17) with equal weights $w_{\sigma_i} = 1$.

An alternative is to use the root mean square error in the option prices M_V of Equation (5.18). For the Heston calibration, equal weights in the measure M_V result in a significantly low quality of fit for shorter maturities as option prices increase with the maturity. We will instead use the equivalent weights given by Equation (5.20) with a vega floor at $v_{\min} = 10^{-3}F$, where F is the forward price corresponding to the option maturity.

A SMART INITIAL GUESS

From five well-chosen option implied volatilities, corresponding to the shortest-expiry at-the-money volatility, 2 calendar spreads between t_1 and t_2 of log-moneyness $-x_0$ and x_0, Forde and Jacquier [64] show how to find the Heston parameters by solving a simple linear system for a Heston small-time expansion that passes exactly through those points. Their expansion of the Black implied volatility σ_B in terms of the log-moneyness x reads

$$\sigma_B^2(x,t) = v_0 \left(1 + \frac{\rho\sigma x}{2v_0} + \left(1 - \frac{7}{4}\rho^2 \right) \frac{\sigma^2 x^2}{12 v_0^2} \right) + \frac{t}{2} \left(\frac{\rho\sigma v_0}{2} - \frac{\sigma^2}{6} + \frac{\rho^2\sigma^2}{24} + \alpha - \kappa v_0 \right)$$
$$+ \frac{\rho\sigma x t}{24 v_0} \left(\sigma^2 - \sigma^2\rho^2 + \rho\sigma v_0 - 2\alpha - 2\kappa v_0 \right)$$
$$+ \frac{\sigma^2 x^2 t}{7680 v_0^2} \left(\sigma^2 \left(176 - 712\rho^2 + 521\rho^4 \right) + 40\sigma\rho^3 v_0 + 80\alpha(13\rho^2 - 6) - 80\kappa\rho^2 v_0 \right)$$

$$(7.45)$$

with $\alpha = \kappa\theta$.

Chosen option strikes and maturities can make a big difference on the initial guess. A good rule is +/- 20% (and sometimes +/- 5%) around the money and discard the first maturities. In practice, we found that taking the best guess of the two log-moneyness +/-5% and +/-20% was successful as initial guess on a wide variety of implied volatility surfaces. When the options are chosen closer to at-the-money, we noticed that a virtual butterfly spread arbitrage could arise, modifying the formula to ensure the value of the butterfly (noted C in [64, p. 8]) is positive was enough to make the algorithm robust.

We can then apply a Levenberg-Marquardt minimizer [156] with our choice of error measure to find the optimal Heston parameters for given market option prices.

An alternative would be to rely on the differential evolution algorithm [184] to find a good initial guess. This has however the risk to be less stable and is much slower than the smart initial guess that was found to work well in general in [126].

CALIBRATION TRAPS

Cui et al. [41] notice that the Heston calibration problem intrinsically does not have multiple local minima and advocate the use of an analytical gradient. The use of analytical gradients is commendable, but it really helps to avoid falling into the numerical finite difference trap: the finite difference step size needs to be chosen in accordance with the numerical quadrature accuracy as described in [106] and [160, p. 196]. This explains why the use of adaptive quadrature schemes, where the tolerance level can be set, is particularly important. In their paper, Cui et al. test quadrature schemes with a fixed number of points and must then rely on analytical gradients.

Analytical gradients for the Heston characteristic function and the Lewis pricing formula calculated with the Filon quadrature are trivial to compute using forward automatic[5] differentiation [169], even when manually applying the technique.

Another source of calibration problems is the parameters space. For example, a straightforward implementation of the characteristic function will not be reliable for

---

[5]A simple implementation based on (vectorized) dual numbers is efficient.

very low vol-of-vol parameter due to numerical noise, a Taylor expansion must then be used. In a similar fashion, very large (exploding) parameters will be a source of numerical errors and can even lead in some cases to prices beyond the range of machine representable numbers. Furthermore, the correlation must obey $\rho \in [-1, 1]$. The Levenberg-Marquardt minimizer does not allow box constraints. A common practice is to use a domain transformation from $\mathbb{R}$ to an interval $[a, b]$ (closed or open) such as a hyperbolic transformation $h(x) = a + \frac{b-a}{1+e^{-x}}$ or a cosine transformation $h(x) = \frac{a+b}{2} + \frac{a-b}{2} \cos(x)$. Unfortunately, transformations have side-effects. For example, it is possible that in the first Levenberg-Marquardt iterations, the correlation parameter moves close to the boundary at -1, because it is optimal considering the value of the other parameters at that point. In later iterations, with the hyperbolic transformation, it will be almost impossible to move back from the boundary as the derivative of the transformation is extremely small close to the boundary. The calibration is then stuck on one of the boundaries.

The cosine transformation behaves much better in this regard, but can still lead to nearly local minima. For example, in the flat region of Figure 7.6.1, the vol-of-vol parameter σ changes of only 10^{-4} between each iteration. The calibration then needs a quadrature that ensures a good accuracy of the gradient. It will also require a large number of iterations to converge, in this case, 484. On this specific calibration example, the Levenberg-Marquardt minimizer can easily move towards high κ and σ as the RMSE near $\nu_0 = 0.0001, \theta = 0.0215, \rho = -0.620$ is smallest there, when the other parameters are kept fixed (Figure 7.6.2). This behavior is typical for a small initial variance ν_0.
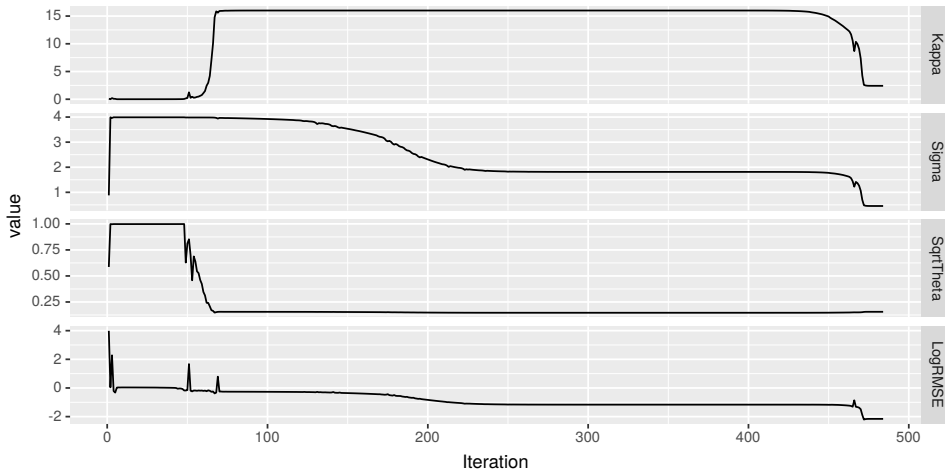
Figure 7.6.1: Heston parameters and RMSE per iteration of the Levenberg-Marquardt minimization of SPX500 options from Kahale [116] under the inverse vega weighted price error measure M_ν using the cosine transformation with initial guess $\nu_0 = 0.98, \kappa = 0.088, \theta = 0.34, \sigma = 0.88, \rho = -0.82$.

When the initial guess is far from the minimum, an unconstrained calibration will very quickly be pushed towards the infeasible region, possibly at the first iteration as in the example of Table 7.6.4.

With the smart initial guess, the minimizer will take only small steps towards the

Figure 7.6.2: Inverse vega weighted price error measure M_v using $v_0 = 0.0001$, $\theta = 0.0215$, $\rho = -0.620$ and varying κ and σ on the market data from Kahale [116].

Table 7.6.4: Unconstrained Levenberg-Marquardt calibration with the price error measure and analytical gradient on the market data from Kahale [116].

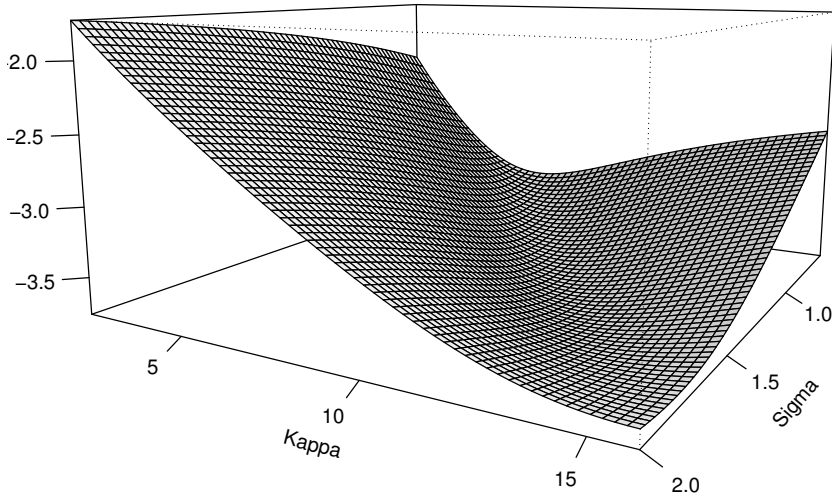|	V_0	κ	θ	σ	ρ
Guess	0.5655	3.8982	0.7010	0.9823	0.8414
Iteration 1	-0.3516	27.0406	-0.1825	16.3636	-8.8685

minimum, as it is never too far off. The problem of extreme parameters and boundaries disappears.

RESULTS

We first consider the market data of Kahale [116], $r = 0.06$. We use a relative tolerance of 10^{-6} for the adaptive quadrature schemes, and a truncation tolerance of 10^{-9}. We remove the options of price (normalized by the spot) lower than the quadrature tolerance from the data. On this data, this corresponds to a single point of expiry $T = 0.175$ and strike $K = 826$. This cleaning step is particularly important to ensure the stability of the calibration using the volatility error measure.

The calibration of the Heston model using the volatility error measure M_σ is not slower than the calibration using the inverse vega weighted price error measure M_V (Table 7.6.5 vs Table 7.6.6). It could actually be faster when the initial guess is not as good. But it is also less stable: slightly different Heston parameters (especially v_0 and κ) can lead to a very similar error measure and as a consequence, the calibrated parameters can fluctuate depending on the method or its tolerance level, this is especially true if small option prices are not filtered out. In [126] it was found necessary to add more weight to

near-the-money options in order to stabilise the calibration.

Table 7.6.5: Heston calibration under the volatility error measure for the option data of Kahale [116].

Method	v_0	κ	θ	σ	ρ	RMSE	Time(ms)
Smart guess	0.0128	1.581	0.0329	0.381	-0.400	0.018551	0.065
simpson	0.0158	1.357	0.0251	0.357	-0.557	0.007511	329
Cos L=12, M=128	0.0139	2.521	0.0240	0.510	-0.596	0.023186	110
modlob	0.0095	5.441	0.0232	0.932	-0.584	0.005199	346
modlob Log	0.0095	5.448	0.0232	0.933	-0.584	0.005199	605
modlob Lord-Kahl	0.0095	5.442	0.0232	0.932	-0.584	0.005199	490
modsim Filon	0.0095	5.444	0.0232	0.933	-0.584	0.005199	174
globsim Flinn	0.0095	5.435	0.0232	0.932	-0.584	0.005199	107
adaptquin Flinn	0.0095	5.449	0.0232	0.933	-0.584	0.005199	44

The calibration using the weighted price error measure is much more stable, we found that changing the weights to increase the importance of near-the-money options did not change much the outcome of the calibration.

Table 7.6.6: Heston calibration under the weighted price error measure for the option data of Kahale [116].

Method	v_0	κ	θ	σ	ρ	RMSE	Time(ms)
Smart guess	0.0128	1.581	0.0329	0.381	-0.400	0.11152	0.06
simpson	0.0132	2.310	0.0243	0.438	-0.645	0.01460	69
Cos L=12, M=128	0.0132	2.332	0.0243	0.442	-0.645	0.01463	43
modlob	0.0131	2.420	0.0242	0.454	-0.644	0.01445	377
modlob Log	0.0131	2.420	0.0242	0.454	-0.644	0.01445	689
modlob Lord-Kahl	0.0131	2.420	0.0242	0.454	-0.644	0.01445	525
modsim Filon	0.0131	2.420	0.0242	0.454	-0.644	0.01445	230
globsim Flinn	0.0131	2.420	0.0242	0.454	-0.644	0.01445	144
adaptquin Flinn	0.0131	2.420	0.0242	0.454	-0.644	0.01445	35

On a 2.5Ghz Intel Core i5-3210M with Go 1.9, the calibration with the adaptive Flinn method is around ten times faster than the modlob or Lord-Kahl methods. It is also faster than the Simpson 3/8 rule with 101 points and cached characteristic function evaluations and faster than the Cos method with $M = 128$ points and a truncation level $L = 12$. Both Simpson and Cos methods are not accurate enough to converge to the correct minimum under the volatility error measure (Table 7.6.5).

In order to obtain a better calibration with the Cos method, more quotes would need to be filtered out[6], or a higher truncation level $L = 24$ and a larger number of points $M = 256$ need to be used. The doubling of the number of points translates to a doubling of the time required to price an option.

---

[6] If we filter out more quotes, we could also relax the tolerance of the adaptive quadrature schemes.

In appendix 7.A, we also consider SPX500 options as of October 2010. The relative performance of each pricing method is similar as on the example of Kahale [116].

7.7. CONCLUSION

We have described a simple adaptive Filon method with better performance against accuracy behavior than popular alternatives to price options under the Heston model. It is particularly interesting in the context of model calibration, where many options of different strike prices but same maturity are priced.

Being adaptive, it does not suffer from having to choose a non-obvious parameter value, typically the number of points of non-adaptive quadrature schemes, or the truncation level for the Cos method.

The technique can easily be transposed to any stochastic volatility model that possesses an analytical characteristic function.

7

7.A. HESTON CALIBRATION FOR OPTIONS ON SPX500 FROM OCTOBER 2010

On SPX500 options from October 2010, the calibration on equally weighted volatilities would be even more unstable without removing too small option prices from the data. With the cleaning up procedure, the calibration results are very stable and slightly faster than the calibration on the weighted price error measure (Table 7.A.1 against Table 7.A.2).

Table 7.A.1: Heston calibration under the volatility error measure for options on SPX500 in October 2010.

Method	ν_0	κ	θ	σ	ρ	RMSE	Time(ms)
Smart guess	0.0736	0.450	0.100	0.208	-0.756	0.01770	0.05
simpson	0.0718	1.430	0.080	0.569	-0.372	0.00503	128
modlob	0.0718	1.430	0.080	0.569	-0.372	0.00503	435
modlob Log	0.0718	1.430	0.080	0.569	-0.372	0.00503	810
modlob Lord-Kahl	0.0718	1.430	0.080	0.569	-0.372	0.00503	550
modsim Filon	0.0718	1.430	0.080	0.569	-0.372	0.00503	260
adaptquin Flinn	0.0718	1.430	0.080	0.569	-0.372	0.00503	53

Again, the price error measure makes the problem better behaved (we could even not filter out any option if desired as the inverse vega cap is going to minimize the impact of very small option prices in the calibration).

Table 7.A.2: Heston calibration under the price error measure for options on SPX500 from October 2010.

Method	ν_0	κ	θ	σ	ρ	RMSE	Time(ms)
Smart guess	0.0736	0.450	0.100	0.208	-0.756	0.14384	0.06
simpson	0.0715	1.053	0.082	0.484	-0.382	0.04321	130
modlob	0.0715	1.053	0.082	0.484	-0.382	0.04321	485
modlob Log	0.0715	1.053	0.082	0.484	-0.382	0.04321	920
modlob Lord-Kahl	0.0715	1.053	0.082	0.484	-0.382	0.04319	601
modsim Filon	0.0715	1.053	0.082	0.484	-0.382	0.04321	284
adaptquin Flinn	0.0715	1.053	0.082	0.484	-0.382	0.04321	50

8

NUMERICAL TECHNIQUES FOR THE HESTON COLLOCATING VOLATILITY MODEL

In the collocating volatility model (CLV), the stochastic collocation technique is used as a convenient representation of the terminal distribution of the market option prices. A specific dynamic is added in the form of a stochastic driver process, which allows more control over the prices of forward starting options. This is reminiscent of the Markov functional models. Grzelak uses a single factor Ornstein-Uhlenbeck process as the driver for the CLV model, and Fries a single factor Wiener process with time-dependent volatility in his equity Markov functional model. Van der Stoep et al. consider a Heston stochastic volatility driver process and show it offers more flexibility to capture the forward smile in the context of foreign exchange options. In this chapter, we discuss all aspects of derivative pricing under the Heston-CLV model: calibration with an efficient Fourier method, a Monte-Carlo simulation with second-order convergence and accurate PDE pricing through implicit and explicit finite difference methods.

8.1. INTRODUCTION

In the standard Black-Scholes model, the underlying asset follows a geometrical Brownian motion [24]. The model is typically applied to obtain the prices and hedges of financial derivative contracts, such as options on a foreign exchange rate, a stock price or a swap rate. For a given maturity date, the market price of a vanilla option for each quoted strike price does not match the assumption of a constant Black-Scholes volatility. The volatilities implied by the market exhibit a smile. This is also true in the maturity dimension, where the market implies a particular term-structure of volatilities. Furthermore, the implied volatilities vary in time.

In order to solve this discrepancy, Dupire [55] proposed a model where the volatility is made local: it is a function of the asset price and a particular time. This model however requires a smooth and continuous arbitrage-free Black-Scholes implied volatility representation across the time and asset price dimensions. Finding a good representation is the principal challenge of this model. The local volatility model also suffers from an unrealistic dynamic of the smile in time [85]. In practice this means that forward starting options are mispriced under the local volatility model.

This chapter is based on the article 'Numerical techniques for the Heston collocated volatility model', submitted for publication in *Journal of Computational Finance*, 2019 [133].

A different approach is to assume that the volatility is stochastic. Several stochastic volatility models that retain some analytical and numerical tractability have been explored over the years, the most popular being the model from Heston [91]. They all suffer from similar issues: they don't allow to match the implied volatility smile for short maturities very well and they may be challenging to calibrate properly. A fix for the former issue is to mix stochastic and local volatilities together [2] at the cost of increasing the computational complexity, which involves either an iterative partial differential equation technique as in [175] or the particle method for Monte-Carlo simulation[80]. A good local volatility representation is a prerequisite for the stochastic local volatility model.

Grzelak [77] proposes another alternative with the collocated volatility model (CLV), where the model prices are calibrated to the market options with the stochastic collocation technique, used as a convenient representation of the terminal distribution. A specific dynamic is added in the form of a stochastic driver process, which allows more control over the prices of forward starting options. This is reminiscent of the Markov functional model of Hunt and Kennedy [98], initially derived for interest rate models and extended to equity models in [66]. Grzelak [77] uses a single factor Ornstein-Uhlenbeck process as the driver, and Fries [66] a single factor Wiener process (with time-dependent volatility). Van der Stoep et al. [194] consider a Heston stochastic volatility driver process and show it offers more flexibility to capture the forward smile in the context of foreign exchange options. How to implement this model for equity derivatives in practice? How to calibrate it in a stable manner? Which numerical schemes are most appropriate? What are the model's limitations? We aim in this chapter to discuss all aspects of derivative pricing under the Heston-CLV model: calibration with a Fourier method, Monte-Carlo simulation and accurate partial differential equation (PDE) pricing.

8

The outline of the chapter is as follows. Section 8.2 introduces the CLV model with a Heston driver process and explains its relationship with the Markov functional model. Section 8.3 derives efficient pricing formulas for the calibration of the Heston-CLV model to the market prices of vanilla options. We also propose an extension of the collocation technique to assets that can not move below a boundary. For example, a stock price must stay positive. This is particularly important as many equity derivative contracts are written on a future performance. Section 8.4 applies the second-order discretization scheme of Lenkšas and Mackevičius [135] for the Monte-Carlo simulation of the Heston-CLV model. We put in evidence some flaws of the original scheme, propose a simple modification to resolve those and compare the convergence of the new scheme to the one of the quadratic exponential scheme of Andersen [6]. In Section 8.5, we discretize the Heston-CLV PDE with several finite difference methods, including the recent Runge-Kutta-Legendre scheme of Meyer [154], and compare their convergence in the context of barrier options.

8.2. Collocated volatility model with a Heston driver process

As in [194], we consider a dynamic model where an asset S follows

$$S(t) = g(t, X(t)), \tag{8.1a}$$

$$dX(t) = (r(t) - q(t))X(t)dt + \sqrt{V(t)}X(t)\,dW_X(t), \tag{8.1b}$$

$$dV(t) = \kappa(\theta - V(t)) + \sigma\sqrt{V(t)}\,dW_V(t), \tag{8.1c}$$

with W_X and W_V being two Brownian motions with correlation ρ, r, q the instantaneous growth and dividend rates, and $g(t, x)$ a collocation function. Furthermore, we will choose $X(0) = S(0)$, so that X and S work on the same scale. According to Equations (8.1b) and (8.1c), the driver process X follows the Heston stochastic volatility model [91]. We thus name this model the Heston-CLV model. The collocation function g is typically a polynomial or a spline, which will be calibrated to the market using the stochastic collocation technique, as described in Section 8.3.

The underlying idea is not entirely new. Jäckel [108] and Brockhaus [30] derive the functional g from the risk-neutral density, without specifying a way to imply this risk-neutral density, and use a single factor arithmetic Wiener process with time-dependent volatility as the driver. This is often referred to as the Markov functional model, initially derived for interest rate models [98] and extended to equity models in [66]. Note that the equity Markov functional model uses the equity as the numeraire, so it is not strictly the same. In contrast, in the CLV model, the functional is directly calibrated to the market via the stochastic collocation technique. This allows the use of a more complex driver process, thus enabling a more refined forward smile representation. While we consider a Heston process as the driver, the technique presented here may also be applied to other processes with a known characteristic function, such as a Schöbel-Zhu process [178], a stochastic volatility process with jumps [20], or a double Heston process [36].

The flexibility of the Heston-CLV model is evocative of the stochastic local volatility models [3, 175], where a local volatility function is added to a specific stochastic volatility model. Local stochastic volatility models involve the solution of a two-dimensional Fokker-Planck partial differential equation along with a standard Monte-Carlo simulation or, alternatively, the use of the particle Monte-Carlo method [80] to price and hedge exotic financial derivative contracts. We will see that the Heston-CLV model is simpler to simulate.

The Heston-CLV backward partial differential equation (PDE) results from a direct application of the multi-dimensional Feynman-Kac theorem:

$$\frac{\partial u}{\partial t} = \frac{v x^2}{2}\frac{\partial^2 u}{\partial x^2} + \rho\sigma x v \frac{\partial^2 u}{\partial x \partial v} + \frac{\sigma^2 v}{2}\frac{\partial^2 u}{\partial v^2} + (r-q)x\frac{\partial u}{\partial x} + \kappa(\theta - v)\frac{\partial u}{\partial v} - r u, \tag{8.2}$$

for $0 \le t \le T$, $x > 0$, $v > 0$.

For a European option with payoff $h(S)$ at maturity T on $s = g(T - t, x)$, the initial condition is

$$u(x, v, 0) = h\left(g(T, x)\right). \tag{8.3}$$

In particular, $h(s) = \max(s - K, 0)$ for a call option and $h(s) = \max(K - s, 0)$ for a put option of strike K. The only difference with the Heston PDE lies in the transformed initial condition.

The PDE approach is really interesting to price exotic options, with some path-dependency, such as barrier options, or American options. In the next section, we will present a much more efficient way to price vanilla European options under the Heston-CLV model.

8.3. CALIBRATION TO MARKET VANILLA OPTIONS

The problem of calibrating the Heston stochastic volatility model to market option prices has been studied in depth [10, 130]. Here, we wish to calibrate the Heston-CLV model (more specifically, its collocation function g) to market option prices, for a given set of Heston parameters $\kappa, \theta, \rho, \nu, V(0)$.

In a preliminary step, we calibrate the stochastic collocation functions g_l to the terminal risk-neutral distribution at each market option maturity T_l for $l = 1, ..., M$. We then interpolate linearly in time the g_i to form the Heston-CLV collocation function g. For $t > 0$, let l be the index such that $T_l \leq t < T_{l+1}$,

$$g(t, x) = \frac{T_{l+1} - t}{T_{l+1} - T_l} g_l(x) + \frac{t - T_l}{T_{l+1} - T_l} g_{l+1}(x). \tag{8.4}$$

For $t_0 = 0$, we let $g_0(x) = S(0)$.

In the next sections, we detail the calibration towards options of a single maturity $t = T_l$.

8.3.1. VANILLA OPTION PRICE BY STOCHASTIC COLLOCATION TOWARDS THE HESTON DISTRIBUTION

Let ϕ_Y, Φ_Y be the market implied probability and cumulative probability density functions, ϕ_X, Φ_X be the probability and cumulative probability density functions for the Heston model, and let us recall the main pricing formula (Equation 5.1) for a vanilla call option of strike price K and maturity T_l, where the function $x \to \Phi_Y^{-1}(1 - \Phi_X(x))$ is approximated by the collocation function g_l,

$$\begin{aligned} V_{\text{call}}(K) &\approx \int_0^\infty |g_l(x) - K|^+ \phi_X(x) dx \\ &= \int_{x_K}^\infty (g_l(x) - K) \phi_X(x) dx, \end{aligned} \tag{8.5}$$

with

$$x_K = g_l^{-1}(K).$$

The integral in Equation (8.5) is not always well-defined if g_l is a polynomial of degree equal or higher than two. Indeed, the (lognormal) Heston model suffers from moment explosions. The moment $\mathbb{E}[X(t)^m]$ for $m \geq 1$ may become infinite after some finite time. According to Friz and Ressel [67], a sufficient condition for the explosion is $D^2(-im) < 0$, where D is defined in Equation (8.75) from Appendix 8.A. In terms of the Heston param-

eters, a necessary and sufficient condition is [8]:

$$\rho \leq -\sqrt{\frac{m-1}{m}} + \frac{\kappa}{\sigma m}. \tag{8.6}$$

When $m = 1$, the condition reduces to $\rho < \frac{\kappa}{\sigma}$. In practice, when the Heston model is calibrated to market options, this will always be verified. When m becomes larger, for example $m = 5$ for a quintic polynomial, the condition becomes quite restrictive and the valid space of parameters may not lead to a good fit of the market option prices anymore.

A possible fix is to extrapolate the polynomial g_l linearly after a cut-off strike, for example, beyond the last market option strike price. In some practical cases, however, a high degree (typically $m \geq 9$) is required to fit the market option prices reasonably well (see Section 8.3.2). Instead, we prefer to consider a monotonic quadratic spline with linear extrapolation for g_l. A spline allows to represent more complex shapes. This is particularly relevant in the CLV model, where the collocation variable X is distributed according to a calibrated Heston model.

EFFICIENT PRICING WITH AN ADAPTIVE FILON/FLINN QUADRATURE

In the following, we denote by $F(0, t)$ the forward price of the asset S to maturity t defined by $F(0, t) = \mathbb{E}_{\mathbb{Q}}[S(t)|S(0)]$. For a given maturity, we consider a quadratic spline as the collocation function. In order to compute the price of a put option, we will use the Fourier transform of the following quadratic payoff restricted to the interval $[K_j, K]$, where K_j corresponds to a spline knot and K may be arbitrary for now:

$$w_j(K, S) = \left[a_j + b_j(S - K_j) + c_j \left(S^2 - K_j^2 \right) \right] 1_{K_j \leq S < K}. \tag{8.7}$$

The corresponding Fourier transform is

$$\begin{aligned}
\hat{w}_j(K, z) &= \int_{\ln K_j}^{\ln K} e^{\mathrm{i}zx} \left(a_j + b_j(e^x - K_j) + c_j \left(e^{2x} - K_j^2 \right) \right) dx \\
&= \tilde{a}_j \frac{K^{\mathrm{i}z} - K_j^{\mathrm{i}z}}{\mathrm{i}z} + \tilde{b}_j \frac{K^{\mathrm{i}z+1} - K_j^{\mathrm{i}z+1}}{\mathrm{i}z+1} + c_j \frac{K^{\mathrm{i}z+2} - K_j^{\mathrm{i}z+2}}{\mathrm{i}z+2},
\end{aligned} \tag{8.8}$$

with z being a complex-valued number and $\tilde{a}_j = a_j - b_j K_j + c_j K_j^2$, $\tilde{b}_j = b_j - 2c_j K_j$.

Let ψ_X denote the Heston characteristic function (see Appendix 8.A). The undiscounted price $W_j(K)$ of the derivative paying $w_j(K, S)$ at maturity is then given by integrating over a specific contour [139],

$$W_j(K) = -\frac{1}{2\pi} \int_{\mathrm{i}z_i-\infty}^{\mathrm{i}z_i+\infty} e^{-\mathrm{i}z \ln F(0, T_l)} \psi_X(-z) \hat{w}_j(K, z) dz$$

We then apply Equation (8.8), with $x_j = \ln \frac{K_j}{F(0,T_l)}$ and $k = \ln \frac{K}{F(0,T_l)}$. This leads to

$$
\begin{aligned}
W_j(K) &= \frac{1}{2\pi} \int_{iz_i-\infty}^{iz_i+\infty} \psi_X(-z) e^{ix_j z} \left[\frac{\tilde{a}_j}{iz} + \frac{\tilde{b}_j}{iz+1} K_j + \frac{c_j}{iz+2} K_j^2 \right] dz \\
&\quad - \frac{1}{2\pi} \int_{iz_i-\infty}^{iz_i+\infty} \psi_X(-z) e^{ikz} \left[\frac{\tilde{a}_j}{iz} + \frac{\tilde{b}_j}{iz+1} K + \frac{c_j}{iz+2} K^2 \right] dz \\
&= \tilde{a}_j \left[M_0(x_j) - M_0(k) \right] + \tilde{b}_j \left[M_1(x_j)K_j - M_1(k)K \right] + c_j \left[M_2(x_j)K_j^2 - M_2(k)K^2 \right],
\end{aligned}
$$

(8.9)

with

$$
M_s(x) = \frac{1}{2\pi} \int_{iz_i-\infty}^{iz_i+\infty} \frac{\psi_X(-z)}{iz+s} e^{ixz}.
$$

(8.10)

We will use the contour $z_i = \frac{1}{2}$. We will ignore the residue R_s as the residues of the integrals $M_s(x_j)$ and $M_s(k)$ cancel out, and obtain

$$
M_s(x) = R_s(x) + \tilde{M}_s(x),
$$

(8.11)

with

$$
\begin{aligned}
\tilde{M}_s(x) &= \frac{1}{2\pi\sqrt{e^x}} \int_{-\infty}^{\infty} e^{ixu} \frac{\psi_X\left(-u-\frac{i}{2}\right)}{s-\frac{1}{2}+iu} du \\
&= \frac{1}{\pi\sqrt{e^x}} \int_0^{\infty} \Re\left\{ e^{-ixu} \frac{\psi_X\left(u-\frac{i}{2}\right)}{s-\frac{1}{2}-iu} \right\} du \\
&= \frac{1}{\pi\sqrt{e^x}} \int_0^{\infty} \Re\left\{ \frac{\psi_X\left(u-\frac{i}{2}\right)}{s-\frac{1}{2}-iu} \right\} \cos(xu) + \Im\left\{ \frac{\psi_X\left(u-\frac{i}{2}\right)}{s-\frac{1}{2}-iu} \right\} \sin(xu) du.
\end{aligned}
$$

(8.12)

The integrals in $M_s(x)$ may be computed with the adaptive Filon (or Flinn) quadrature of Chapter 7. In practice, the underlying adaptive Simpson (respectively adaptive quintic Hermite) quadrature, which defines the Filon integration nodes, may only be applied to the integrand of M_0, that is, to the real and imaginary parts of the function $\frac{\psi_X\left(u-\frac{i}{2}\right)}{-\frac{1}{2}-iu}$. As the variations of M_1 and M_2 are similar, the integration nodes obtained via the integrand of M_0 are good enough to be reused for M_1 and M_2. For any x, the Heston characteristic function will be evaluated only at those fixed nodes, independently of x. The value of $M_s(x)$ is then a simple sum over those nodes and its computational cost is directly proportional to the number of quadrature nodes and to the cost of evaluating the cosine and sine functions.

Let us now consider the quadratic spline payoff with linear extrapolation defined by

$$
w(K,S) = |K - g_l(S)|^+,
$$

(8.13)

with

$$
g_l(S) = \begin{cases} \sum_{j=1}^n w_j(K_{j+1},S) & \text{for } K_1 < S < K_{n+1}, \\ b_0(S-K_1) + K_1 & \text{for } S \le K_1, \\ b_{n+1}(S-K_{n+1}) + K_{n+1} & \text{for } K_{n+1} \le S. \end{cases}
$$

(8.14)

For $K < K_1$, only the left extrapolation plays a role in the price $V_{\text{put}}(K)$ of the financial derivative paying $w(K, S)$ at maturity. $V_{\text{put}}(K)$ corresponds to the price of a vanilla put option of maturity T_l in the Heston-CLV model when a quadratic spline is used as collocation function. Using the same contour $z_i = \frac{1}{2}$ as in Equations (8.9), (8.12), we have

$$V_{\text{put}}(K) = (K - K_1(1 - b_0)) + (K - K_1(1 - b_0))\tilde{M}_0(k) - b_0 K \tilde{M}_1(k), \quad \text{for } K < K_1 \quad (8.15)$$

The first term corresponds to the residue at $z = 0$. For $K_1 \leq K$, let j_K be the index such that $K_{j_K} \leq K < K_{j_K+1}$. According to Equation (8.9), we have

$$
\begin{aligned}
V_{\text{put}}(K) = {}& (K - K_1(1 - b_0)) + (K - K_1(1 - b_0))\tilde{M}_0(x_1) - b_0 K_1 \tilde{M}_1(x_1) \\
& + \sum_{j=1}^{j_K-1} (K - \tilde{a}_j)\left[\tilde{M}_0(x_{j+1}) - \sum_{j=1}^{j_K-1} \tilde{M}_0(x_j)\right] \\
& - \sum_{j=1}^{j_K-1} \tilde{b}_j\left[\tilde{M}_1(x_{j+1})K_{j+1} - \tilde{M}_1(x_j)K_j\right] + c_j\left[\tilde{M}_2(x_{j+1})K_{j+1}^2 - \tilde{M}_2(x_j)K_j^2\right] \\
& + (K - \tilde{a}_{j_K})\left[\tilde{M}_0(k) - \tilde{M}_0(x_{j_K})\right] - \tilde{b}_{j_K}\left[\tilde{M}_1(k)K - \tilde{M}_1(x_{j_K})K_{j_K}\right] - c_{j_K}\left[\tilde{M}_2(k)K^2 - \tilde{M}_2(x_{j_K})K_{j_K}^2\right].
\end{aligned}
$$
$$(8.16)$$

If $K > K_{n+1}$, we let $j_K = n+1$ and use the convention $\tilde{a}_{n+1} = K_{n+1}(1 - b_{n+1})$, $\tilde{b}_{n+1} = b_{n+1}$, $\tilde{c}_{n+1} = 0$.

The values of the s-th moment $M_s(x_j)$ for $j = 1, ..., n+1$, and $s \in \{0, 1, 2\}$ can be pre-computed for a given set of spline knots $(K_j)_{j=1,...,n+1}$ and a given set of Heston parameters. And then, for any spline coefficients $(a_j, b_j, c_j)_{j=1,...,n+1}$ and any given strike K, only $M_0(k), M_1(k), M_2(k)$ need to be computed. Furthermore, with the adaptive Filon quadrature of Chapter 7, the computational cost for $M_s(k)$ corresponds to the cost of evaluating d times the cosine and sine functions and d multiplications, where d is the number of quadrature nodes.

The first moment[1] of the market implied distribution V_1 will also be useful in the calibration, in order to preserve its value exactly. By definition,

$$
\begin{aligned}
V_1(t) &= \mathbb{E}_{\mathbb{Q}}[S(t)] \\
&= \int_0^\infty g(t, x)\phi_X(x)\,dx. \quad (8.17)
\end{aligned}
$$

Following the same approach as with the put option price $V_{\text{put}}(K)$ in Equation (8.16), we obtain

$$
\begin{aligned}
V_1 = {}& K_1(1 - b_0) + K_1(1 - b_0)\tilde{M}_0(x_1) + b_0 K_1 \tilde{M}_1(x_1) \\
& + \sum_{j=1}^n \tilde{a}_j\left[\tilde{M}_0(x_{j+1}) - \tilde{M}_0(x_j)\right] + \tilde{b}_j\left[\tilde{M}_1(x_{j+1})K_{j+1} - \tilde{M}_1(x_j)K_j\right] + c_j\left[\tilde{M}_2(x_{j+1})K_{j+1}^2 - \tilde{M}_2(x_j)K_j^2\right] \\
& + b_{n+1}F(0, t) - K_{n+1}(1 - b_{n+1})\tilde{M}_0(x_{n+1}) - b_{n+1}K_{n+1}\tilde{M}_1(x_{n+1}) \quad (8.18)
\end{aligned}
$$

---

[1] Not to be confused with the Heston moment M_1.

The term $b_{n+1}F(0,t)$ stems from the residue at $z = i$ in the integral of the right extrapolation.

The call price may be obtained by the put-call parity relation $V_{\text{call}}(K) - V_{\text{put}}(K) = V_1(t) - K$. When the first moment is preserved, we have $V_1(t) = F(0,t)$.

We have thus obtained an efficient pricing formula for European options under the Heston-CLV model with a quadratic B-spline collocation function. This will allow a quick calibration of the B-spline coefficients towards vanilla market option prices.

A CONTROL VARIATE FOR THE PRICE

In order to further improve the efficiency, we add a Black-Scholes control variate in a similar fashion as is proposed by Andersen and Piterbarg [10] for a vanilla option. In the Black-Scholes model, the asset forward $F(t, T_l)$ follows $dF = \sigma_B F dW(t)$ and the normalized Black-Scholes characteristic function with volatility σ_B reads

$$\psi_B(z) = e^{-\frac{1}{2}\sigma_B^2 T_l(z^2 + iz)}, \tag{8.19}$$

where T_l is the time to maturity.

In the Black-Scholes model, the values of $M_0(x), M_1(x), M_2(x)$ are directly linked to the moments of a lognormal distribution and can thus be obtained in closed-form. We have

$$M_0^B(x) = -\Phi\left(\frac{-x - \frac{\sigma_B^2 T_l}{2}}{\sqrt{\sigma_B^2 T_l}}\right), \tag{8.20}$$

$$M_1^B(x) = e^{-x}\Phi\left(\frac{x - \frac{\sigma_B^2 T_l}{2}}{\sqrt{\sigma_B^2 T_l}}\right), \tag{8.21}$$

$$M_2^B(x) = e^{-2x + \sigma_B^2 T}\Phi\left(\frac{x - \frac{3\sigma_B^2 T_l}{2}}{\sqrt{\sigma_B^2 T_l}}\right). \tag{8.22}$$

where Φ is the cumulative normal distribution function.

The control variate approach consists in using, in Equation (8.12), $\psi_X = \psi_H - \psi_B$ instead of $\psi_X = \psi_H$, where ψ_H represents the normalized Heston characteristic function. At the same time, we adjust the values of $M_0(x), M_1(x), M_2(x)$ by adding respectively $M_0^B(x), M_1^B(x), M_2^B(x)$, in order to cancel out the contribution of the Black-Scholes model. We use the initial variance of the Heston model as Black-Scholes volatility: $\sigma_B = \sqrt{V_0}$. Other choices, described in [115], are possible, but we did not notice any significant improvement with those in practice.

TRUNCATION RANGE

In Equation (8.12), the range of integration in infinite. We follow chapter 7 to define the truncation of the interval of integration such that the adaptive Filon quadrature (or another quadrature) can be applied. In our case, the payoff is slightly different. If we want to define a relative error tolerance in terms of the option price, we only need an error bound for the moments $\bar{M}_s$ for $s = 0,1,2$, according to Equation (8.16).

The asymptotic behavior of the Heston characteristic function at ∞ reads [117]

$$\lim_{u \to +\infty} \frac{1}{u} \ln\left(\psi\left(u - \frac{i}{2}\right) - \psi_B\left(u - \frac{i}{2}\right)\right) = -(C_\infty + i D_\infty), \tag{8.23}$$

with

$$C_\infty = \frac{V_0 + \kappa\theta T}{\sigma}\sqrt{1 - \rho^2}, \quad D_\infty = \frac{V_0 + \kappa\theta T}{\sigma}\rho. \tag{8.24}$$

For $u_{\max}$ sufficiently large, we thus have

$$\left|\int_{u_{\max}}^{\infty} \frac{\psi\left(u - \frac{i}{2}\right)}{s - \frac{1}{2} - iu} du\right| \leq \int_{u_{\max}}^{\infty} \left|\frac{e^{-C_\infty u}}{u}\right| du.$$

We integrate by parts to obtain

$$\int_{u_{\max}}^{\infty} \left|\frac{e^{-C_\infty u}}{u}\right| du = \frac{e^{-C_\infty u_{\max}}}{C_\infty u_{\max}} - \int_{u_{\max}}^{\infty} \frac{e^{-C_\infty u}}{C_\infty u^2} du$$
$$\leq \frac{e^{-C_\infty u_{\max}}}{C_\infty u_{\max}}$$

We thus may bound the relative error in price by ϵ by truncation at $u_{\max}$ such that

$$\frac{e^{-C_\infty u_{\max}}}{C_\infty u_{\max}} = \epsilon \tag{8.25}$$

The equation may be solved numerically using Newton's method or any other univariate root solver. The truncation may however become invalid for short expiries ($T < 0.1$) as, then, $u_{\max} T \gg 1$. A Taylor expansion around $T = 0$ gives the Black-Scholes like characteristic function:

$$\ln(\psi(u)) = -\frac{1}{2}V_0 T(u^2 + iu) + \mathcal{O}(T^2).$$

An approximation for short expiries is $\hat{u}_{\max}$ that solves:

$$\Phi\left(-\frac{1}{2}V_0 T\hat{u}_{\max}\right) = \frac{1}{2}V_0 T\epsilon\hat{u}_{\max}. \tag{8.26}$$

We found that a good practical rule for the full range of expiries is just to use $\max(u_{\max}, \hat{u}_{\max})$.

8.3.2. CALIBRATION OF THE TERMINAL COLLOCATION FUNCTION

For a given maturity, in Chapter 5, we describe a method to calibrate a quadratic spline to market options in the case where the stochastic collocation is towards a Gaussian distribution. In particular, the method relies on a B-spline formulation to ensure that the optimal collocation spline is monotonic and preserves the first moment exactly.

The optimal collocation spline is chosen so as to minimize the weighted least squares error in market prices E_V or equivalently in market volatilities E_σ. Let us detail the two error measures. The volatility error measure reads

$$E_\sigma = \frac{\sqrt{\sum_{i=0}^m \mu_i^2 \left(\sigma(\xi, K_i) - \sigma_i \right)^2}}{\sqrt{\sum_{i=0}^m \mu_i^2}}, \tag{8.27}$$

where $\sigma(\xi, K_i)$ is the Black-Scholes implied volatility[2] obtained from the specific model considered, with parameters ξ. For each i, σ_i is the market implied volatility and μ_i is the weight associated to the implied volatility σ_i. In our numerical examples, we will choose $\mu_i = 1$. In practice, it is typically set as the inverse of the bid-ask spread.

The price error measure reads

$$E_V = \frac{\sqrt{\sum_{i=0}^m \omega_i^2 \left(V_{\mathsf{call}}(\xi, K_i) - c_i \right)^2}}{\sqrt{\sum_{i=0}^m \omega_i^2}}, \tag{8.28}$$

where $V_{\mathsf{call}}(\xi, K_i)$ is the model option price and c_i is the market option price at strike K_i. In the case of the stochastic collocation, ξ corresponds to the coefficients of the collocating B-spline. We can find a weight ω_i that makes the solution similar to the one under the measure E_σ by matching the gradients of each problem.

The calibration of the terminal collocation function g_l to a set of market options of maturity T_l is almost the same when the collocation is towards a Heston distribution as when it is towards a Gaussian distribution, with the two following differences:

- the model option price is given in the Heston case by the application of the adaptive Filon quadrature (Equation 8.16).

- the preservation of the first moment is given by Equation (8.18) in the Heston case. In both cases, the spline coefficients will be shifted in parallel so that the first moment relation holds exactly.

In particular, we consider a quadratic B-spline representation, that is, B-splines of order $k = 3$. The B-spline representation of g_l on $N + 1 + k$ knots reads [43]

$$g_l(x) = \sum_{i=0}^N \alpha_i B_{i,3}(x). \tag{8.29}$$

We use the nearly optimal B-spline knots $\tau_{i+3} = \frac{x_{i+1} + x_{i+2}}{2}$ for $i = 0, ..., N-3$ according to [43, p. 193] with the boundary knots $\tau_0 = \tau_1 = \tau_2 = x_0$ and $\tau_{N+1} = \tau_{N+2} = \tau_{N+3} = x_N$, where $(x_i)_{i=0,...,N}$ are the collocation points corresponding to the market option strikes. This choice of knots ensures that g_l is in the class C^1 on $[x_0, x_N]$. The $(x_i)_{i=0,...,N}$ may correspond to a subset of the market option strikes we will calibrate against. The B-spline representation can be easily converted to a more classical piecewise polynomial representation as explained in [134], so that we can use Equation (8.16) to price a put option under the Heston-CLV model.

---

[2]Fast and robust algorithms to obtain the implied volatility from an option price are given in [110, 140]. When no implied volatility corresponds to the model option price, which may happen because of numerical error, we just fix the implied volatility to zero.

Because the derivative of the equivalent piecewise polynomial representation is linear between two distinct knots, g_l will be monotonically increasing on an interval $[\tau_{i-1}, \tau_i]$ if and only if the derivative at the endpoints is positive. And thus, g_l will be monotonically increasing on the interval $[x_0, x_N]$ if and only if $\alpha_i - \alpha_{i-1} > 0$ for $i = 1, ..., N$ in Equation (8.29).

In order to ensure the monotonicity in a Levenberg-Marquardt optimizer, which we use to minimize the error measure E_V or E_σ, we rely on the following mapping:

$$z_i = \alpha_1 - \alpha_{i-1}, \text{ for } i > 0.$$

We enforce $z_i \geq 0$ as box constraints in the least-squares minimization. Box constraints may be added in a relatively straightforward manner to any Levenberg-Marquardt algorithm, such as the one of Klare and Miller [120], by means of the projection technique described in [118]. We do not optimize z_0 but choose $z_0 = 0$ and then correct its value through the first moment preservation relation.

The same kind of initial guess, based on a rough estimate of the market survival density for the maturity T_l, may be used as in Chapter 6. It is however much simpler to use the identity function as initial guess. This corresponds to starting from the standard Heston model and worked well on our examples.

In Figure 8.3.1a, we calibrated the Heston model to options on the Tesla stock (ticker TSLA) of maturities 1, 7 and 19 months as of June 18, 2018. This results in the Heston parameters $V_0 = 0.23$, $\kappa = 0.16$, $\theta = 3.82$, $\sigma = 3.26$, $\rho = -0.43$. We then calibrated the Heston-CLV model using firstly a quintic polynomial, and secondly a B-spline composed of 15 knots. We did not attempt to preserve the forward price when calibrating the Heston-CLV with a quintic polynomial collocation, as the second moment of the Heston model already explodes for maturities $T > 0.623$ with the stated parameters. The first moment preservation has very little impact on the quality of fit towards vanilla options. For the shortest maturity, when compared to the standard Heston model, the quintic polynomial collocation improves the fit in the wings. But it fails to improve around the money (that is for option strikes near 1.0). In general, in the Heston-CLV model, a quintic polynomial is not flexible enough to capture the projection of the implied cumulative density towards the Heston variable. A higher polynomial degree would be better, but even with a ninth degree polynomial, the error in implied volatilities would still be noticeable at-the-money. The B-spline collocation has no such issue, and its corresponding fit in terms of the implied volatilities is very good.

In Figure 8.3.1b, we cap σ and θ during the Heston calibration, in order to avoid a fifth moment explosion. This results in the parameters $V_0 = 0.34$, $\kappa = 0.50$, $\theta = 0.45$, $\sigma = 0.90$, $\rho = -0.84$ and the corresponding fit of the Heston model in terms of implied volatility is poor. Here, the Heston-CLV with quintic polynomial collocation allows to fit the market implied volatilities well however.

Let us take a look at the plots of the collocation function in both cases, in order to understand better why the quintic polynomial fits well in one case but not in the other. In Figures 8.3.2a and 8.3.2b, we plot the estimate of the collocation variable x for each market strike y based on a discrete estimate of the market implied cumulative density (see Chapter 6) along with the collocation function, which is here the quintic polynomial mapping x to y, for the two sets of Heston parameters.

8

(a) Well calibrated Heston model, but with exploding second moment.
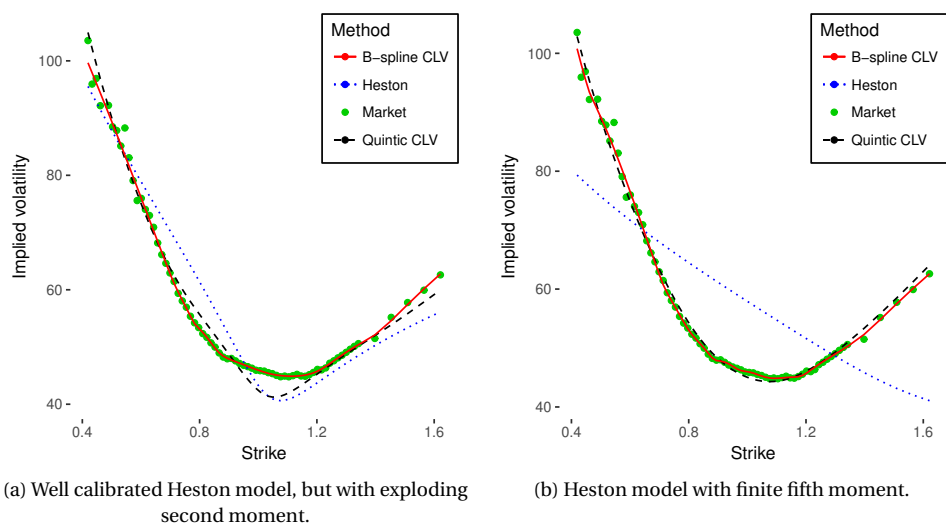
(b) Heston model with finite fifth moment.

Figure 8.3.1: Black-Scholes volatility implied by the Heston model, and the Heston-CLV model for the options of maturity 1 month, calibrated to TSLA options of maturities 1, 7 and 19 months as of June 18, 2018. The strike indicated is relative towards the forward price.
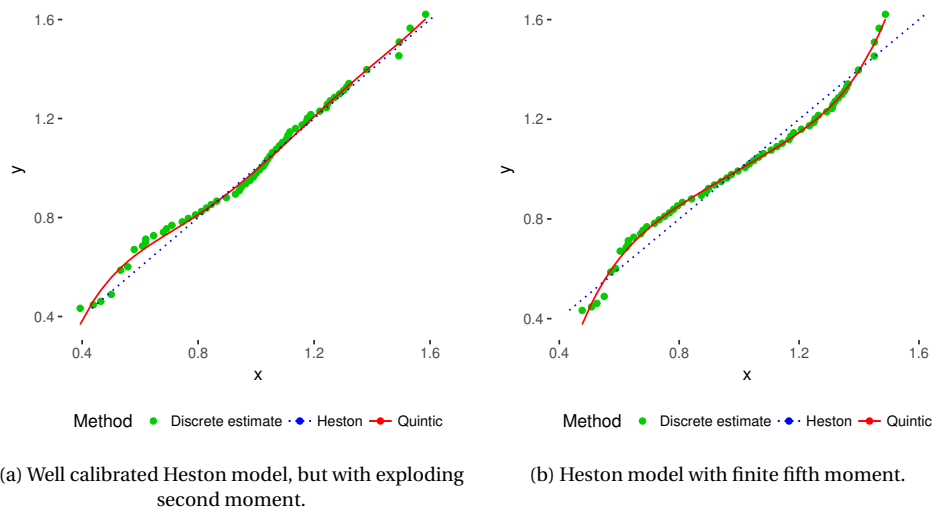

(a) Well calibrated Heston model, but with exploding second moment.

(b) Heston model with finite fifth moment.

Figure 8.3.2: Collocation function for TSLA options of maturity 1 month based on two different sets of Heston parameters.

In the case where the Heston model is well-calibrated to the market (and the second moment explodes), a polynomial has difficulties to capture the oscillating smaller-order

corrections around the Heston model.

8.3.3. Absorption in the CLV model

With the collocation method, there is no guarantee, a priori, that $g_l(x) > 0, \forall x > 0$. If there exists some $x > 0$ such that $g_l(x) \leq 0$, we will not theoretically be able to compute the present value of any payoff depending on the performance, the simplest one being

$$V_{\text{Performance}}(T_l, T) = \mathbb{E}_{\mathbb{Q}}\left[\frac{S(T)}{S(T_l)} \mid S(0)\right], \qquad (8.30)$$

where $T > T_l > 0$. Indeed, the above expectation is only well-defined if $S(T_l)$ is guaranteed to be strictly positive or strictly negative. In practice, it may not always be an issue. For example if the probability of hitting a negative value is extremely small, we may simply truncate g to x_ϵ where $g(t, x_\epsilon) = \epsilon$ for a small $\epsilon > 0$. We define

$$\bar{g}(t, x) = \begin{cases} \epsilon & \text{for } x < x_\epsilon, \\ g(t, x) & \text{for } x \geq x_\epsilon, \end{cases} \qquad (8.31)$$

as proposed in [79] and use $\bar{g}$ instead of g in the collocation.

With the collocation function g, if the probability of $S(T_l)$ being negative is not negligible, the simple fix above will not work well anymore. For many paths, we may end up with $S(T_l) = \epsilon$, but $S(T) \gg \epsilon$. In theory, if, on the same path, the stock has been absorbed at T_l, it should also be absorbed at $T > T_l$. This is not necessarily the case in the CLV model as both T_l and T are simulated from a terminal distribution. We give an example, based on the market data for TSLA options in Table 8.4.1.

Inspired by the handling of absorption in the Bachelier (or normal) model described in Appendix 8.B, where the *reflection* method [113, p. 220] is used in order to obtain a solution in closed-form, we consider the probability density on $[\epsilon, \infty)$ defined by

$$\bar{\phi}_Y(y) = \phi_Y(y) - \phi_Y(2\epsilon - y). \qquad (8.32)$$

The probability of absorption is given by

$$P_a = 1 - \int_\epsilon^\infty \phi_Y(y) - \phi_Y(2\epsilon - y)\,dy = 2\Phi_Y(\epsilon). \qquad (8.33)$$

This leads to the put option price

$$\begin{aligned}
V_{\text{put}}(K) &= (K - \epsilon)P_a + \int_\epsilon^{+\infty} |K - y|^+ \phi_Y(y)\,dy - \int_\epsilon^{+\infty} |K - y|^+ \phi_Y(2\epsilon - y)\,dy \\
&= 2(K - \epsilon)\Phi_Y(\epsilon) + \int_\epsilon^K (K - y)\phi_Y(y)\,dy - \int_\epsilon^{2\epsilon - K} (2\epsilon - K - y)\phi_Y(y)\,dy \\
&= \int_0^K (K - y)\phi_Y(y)\,dy - \int_0^{2\epsilon - K} (2\epsilon - K - y)\phi_Y(y)\,dy \\
&\approx \int_0^{x_K} (K - g_l(x))\phi_X(x)\,dx - \int_0^{x_{2\epsilon - K}} (2\epsilon - K - g_l(x))\phi_X(x)\,dx, \qquad (8.34)
\end{aligned}$$

where $x_{2\epsilon-K} = |g_l^{-1}(2\epsilon - K)|^+$. Similarly, the call option price reads

$$
\begin{aligned}
V_{\text{call}}(K) &= \int_\epsilon^{+\infty} |y - K|^+ \phi_Y(y)\,dy - \int_\epsilon^{+\infty} |y - K|^+ \phi_Y(2\epsilon - y)\,dy \\
&= \int_K^\infty (K - y)\phi_Y(y)\,dy - \int_{-\infty}^{2\epsilon-K} (2\epsilon - y - K)\phi_Y(y)\,dy \\
&\approx \int_{x_K}^\infty (g_l(x) - K)\phi_X(x)\,dx - \int_0^{x_{2\epsilon-K}} (2\epsilon - g_l(x) - K)\phi_X(x)\,dx,
\end{aligned}
\tag{8.35}
$$

and the same put-call parity relation still holds: $V_{\text{call}}(K) - V_{\text{put}}(K) = V_1 - K$ where V_1 is defined in Equation (8.18).

8.4. MONTE-CARLO SIMULATION OF THE HESTON-CLV MODEL

The Monte-Carlo simulation of the Heston-CLV model is straightforward: we use a good discretization scheme for the Heston model in order to discretize the X process, which is a standard Heston process; then we obtain the value of S on each path by applying directly the collocation function to each path of X (Equation 8.1a). Unlike the case of the stochastic local volatility model, there is no need to use very small time steps. The discretization error is entirely due to the Heston process discretization.

8.4.1. A SECOND-ORDER DISCRETIZATION SCHEME

The quadratic exponential (QE) scheme of Andersen and Piterbarg [6] is widely used to discretize the Heston process. Its convergence properties are however not known. Instead, we will present a scheme derived from the DVSS2 scheme of Lenkšas and Mackevičius [135], which has a proven second-order convergence, and stays computationally efficient. The algorithm we propose consists in the following steps:

1. Apply the first deterministic split step:

$$
\dot z = Z(t) - \frac{1}{4}\theta \Delta t + \frac{1}{2\kappa}\left(1 - e^{-\kappa \frac{\Delta t}{2}}\right)(\theta - V(t)),
\tag{8.36}
$$

$$
\dot v = V(t)e^{-\kappa \frac{\Delta t}{2}} + \theta\left(1 - e^{-\kappa \frac{\Delta t}{2}}\right)
\tag{8.37}
$$

where $Z(t) = \ln X(t) - \int_0^t (r(\tau) - q(\tau))\,d\tau$, $Z(0) = \ln X(0)$ and $V(t = 0) = V_0$. The values $\dot z$ and $\dot v$ correspond to the deterministic part of respectively the log-asset Z and variance V at $t + \frac{\Delta t}{2}$.

2. Normalize the stochastic step

$$
\bar z = \frac{\dot z \sigma - \dot v \rho}{\sigma^2 \sqrt{1 - \rho^2}},
\tag{8.38}
$$

$$
\bar v = \frac{\dot v}{\sigma^2}.
\tag{8.39}
$$

3. Draw two uniform random floating point numbers U_1, U_2 in the interval $(0,1)$.

4. Generate the normally distributed variable $\xi = \Phi^{-1}(U_1)$, where Φ^{-1} is the inverse cumulative normal distribution, which can be efficiently computed by the algorithm of Wichura [196].

5. Generate a random variable $\hat{V}$ taking the values v_1, v_2, v_0 with probabilities p_1, p_2 and $p_0 = 1 - p_1 - p_2$:

$$\hat{V} = \begin{cases} v_1 & \text{if } U_2 < p_1\,, \\ v_2 & \text{if } U_2 > 1 - p_2\,, \\ v_0 & \text{otherwise .} \end{cases}$$

6. Calculate the random variable

$$\hat{Z} = \bar{z} + \xi\sqrt{\frac{1}{2}(\bar{v} + \hat{V})\Delta t}\,. \tag{8.40}$$

7. Denormalize the stochastic variables

$$\tilde{Z} = \sigma\left(\sqrt{1 - \rho^2}\hat{Z} + \rho\hat{V}\right), \tag{8.41}$$

$$\tilde{V} = \sigma^2\hat{V}\,. \tag{8.42}$$

8. Finally, apply the second split step:

$$Z(t + \Delta t) = \tilde{Z} - \frac{1}{4}\theta\Delta t + \frac{1}{2\kappa}\left(1 - e^{-\kappa\frac{\Delta t}{2}}\right)(\theta - \tilde{V})\,, \tag{8.43}$$

$$V(t + \Delta t) = \tilde{V}e^{-\kappa\frac{\Delta t}{2}} + \theta\left(1 - e^{-\kappa\frac{\Delta t}{2}}\right). \tag{8.44}$$

The probabilities p_1, p_2 and values v_1, v_2, v_0 are defined as follows:

8

- if $\bar{v} \geq 2\Delta t$,

$$v_1 = \bar{v} + \frac{s - d}{2}\,, \quad v_2 = \bar{v} + \frac{s + d}{2}\,, \quad v_0 = \bar{v}\,,$$

$$p_1 = \frac{2\bar{v}\Delta t}{d(d - s)}\,, \quad p_2 = \frac{2\bar{v}\Delta t}{d(d + s)}\,,$$

with $s = \frac{3\Delta t}{2}$ and $d^2 = \frac{21}{4}(\Delta t)^2 + 12\bar{v}\Delta t$.

- if $0 < \bar{v} < 2\Delta t$,

$$v_1 = \frac{s - d}{2}\,, \quad v_2 = \frac{s + d}{2}\,, \quad v_0 = 0\,,$$

$$p_1 = \bar{v}\frac{2\bar{v} + 2\Delta t - s - d}{d(d - s)}\,, \quad p_2 = \bar{v}\frac{2\bar{v} + 2\Delta t - s + d}{d(d + s)}\,,$$

with $s = \frac{4\bar{v}^2 + 9\bar{v}\Delta t + 3(\Delta t)^2}{2\bar{v} + \Delta t}$ and $d^2 = \Delta t\frac{16\bar{v}^3 + 33\bar{v}^2\Delta t + 18\bar{v}(\Delta t)^2 + 3(\Delta t)^3}{(2\bar{v} + \Delta t)^2}$.

Our algorithm differs from the original DVSS2 scheme only in step 4. Lenkšas and Mackevičius [135] use for ξ a discrete random variable which matches the first five moments of the normal distribution, for reasons of computational efficiency (and because it is enough to prove the second-order convergence), while we use a standard floating point normally distributed random variable. Thus the second-order convergence is still valid in our scheme. From now on, we will refer to our scheme as DVSS2X. Let us clarify why we have made this change.

One assumption for the second-order convergence with a discrete random variable matching the first five moments of the normal distribution is that the integrand f is smooth. Denis Talay presupposes that f and its derivatives up to order 6 are continuous in [187]. Unfortunately, in finance, it is quite common to have discontinuities. A typical example is the digital option which pays 1 if the asset price at maturity is larger than a given strike price. This digital feature is often present in exotic derivatives.

A good illustration of this effect is to take a vol-of-vol parameter σ small, so that the Heston model resembles the Black-Scholes model. In Figure 8.4.1a, we pick $\theta = v_0 = 0.09, \sigma = 0.01, \rho = 0, \kappa = 1$ and price a digital call option of 3 months maturity. Even though the time step size $\Delta t = \frac{1}{32}$ is relatively small (8 intermediate time steps in our digital option example), the error due to the discrete sampling is large, and we clearly see discrete steps in the staircase like price, which will be detrimental to compute the greeks Δ or Γ. Note that when the vol-of-vol parameter is taken to the usual levels for equities, DVSS2 behaves well, and this effect is not visible in digital options.

(a) Heston, low vol-of-vol parameter, $\Delta t = \frac{1}{32}$.

(b) Black, $\Delta t = 0.01$. "Five" stands for the discrete variable matching 5 moments, "AS241" for the continuous inverse cumulative distribution, "-BB" for Brownian Bridge path construction.
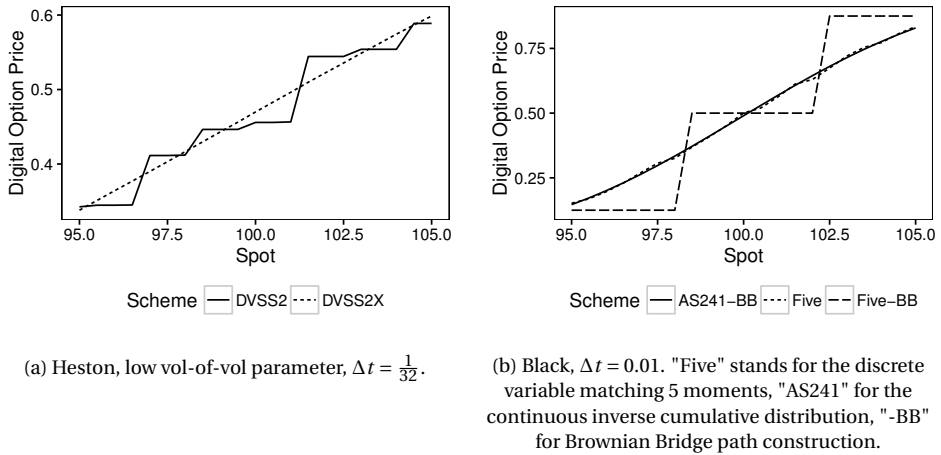
Figure 8.4.1: Monte-Carlo price of a digital call option under the Heston and Black-Scholes models with or without discrete random variable. Each simulation runs on 10^7 paths.

Another side-effect of discrete sampling is that the Brownian-bridge technique is not applicable. Indeed, in the Brownian-bridge path construction, the last point of the path, corresponding to the maturity date, is sampled first, and the other path points inside are then computed from the first and last points in a recursive manner. But any non-

path dependent option, such as a digital option, depends only on the value of the path at maturity, that is, on this last point. As the latter point follows a discrete distribution, the price of the digital option is a staircase function with only a few steps (at most 4 with DVSS2 choice for ξ). This is quite far from the theoretical digital option price, which corresponds to the cumulative distribution function (see Figure 8.4.1b).

In contrast, for the incremental path construction, each point is computed from the previous point. The last point will thus include the variation of all points in the path, which will be very close to normal, even with a discrete distribution per point.

Our proposed change solves the two issues raised above. Furthermore, we also noticed that the continuous sampling in DVSS2X improved the accuracy of the prices of forward start options.

DVSS2X CONVERGENCE EXAMPLE

In order to assess the convergence of the DVSS2X scheme for the Heston-CLV model, we first calibrate the model to the Eurostoxx 50 index (ticker SX5E) options of as of February 26, 2016. The Heston parameters are $V_0 = 0.133$, $\kappa = 0.350$, $\theta = 0.321$, $\sigma = 1.388$, $\rho = -0.630$. We then run a Monte-Carlo simulation for vanilla call options with forward moneyness $\frac{K}{F(0,t)}$ 1.0 and 1.4, and a put option with forward moneyness 0.7, of maturity $t = 0.5$, and using 2^{16} paths. The reference price is obtained by the adaptive Filon method. The large number of paths guarantees that the Monte-Carlo sampling error is small enough (respectively $15 \cdot 10^{-6}$, $3 \cdot 10^{-6}$ and $8 \cdot 10^{-6}$), so that we can deduce the convergence order by estimating the slope of the log-log plot of the error against the time step size (Figure 8.4.2a). The overall order of convergence of the DVSS2X scheme, over the three options is 2.12.

In Figure 8.4.2b, we perform the same experiment with the quadratic exponential (QE) scheme of Andersen and Piterbarg [6], widely used in the financial industry. This scheme has however no proven convergence order. Here, we obtain an overall convergence order over the three options of 1.55.

The DVSS2X scheme exhibits not only a higher order of convergence, our implementation is also around 25% faster than the QE scheme for a given time step size. We wrote both schemes in the Google Go language, making sure to cache any data constant across paths, and used otherwise the same methods to generate random numbers (MELG19937-64 from [90]) and to sample from a normal distribution [196].

ABSORPTION IN THE MONTE-CARLO METHOD

The reflection method described in Section 8.3.3 may also be applied in the Monte-Carlo simulation. Let $X_1, ..., X_m$ be a path of the Heston driver process X defined by Equation (8.1b), corresponding to the dates $t_1, ..., t_m$. When we compute the path of the asset S from X, we record the reflections:

- If $g(t_i, X_i) \geq \epsilon$, we let $S_i = g(t_i, X_i)$ and $P_i = 1$.

- Else, we let $S_i = g(t_i, X_i) - 2\epsilon$ and $P_i = -1$.

We take the reflections into account when the payoff is evaluated on each path. Let $\mathsf{CF}\left(t_i, (S_j)_{j=1,...,i}\right)$ be the cash flow at time t_i. The corresponding undiscounted value for the path considered is set to $\left(\prod_{j=1}^{i} P_j\right) \mathsf{CF}\left(t_i, (S_j)_{j=1,...,i}\right)$.
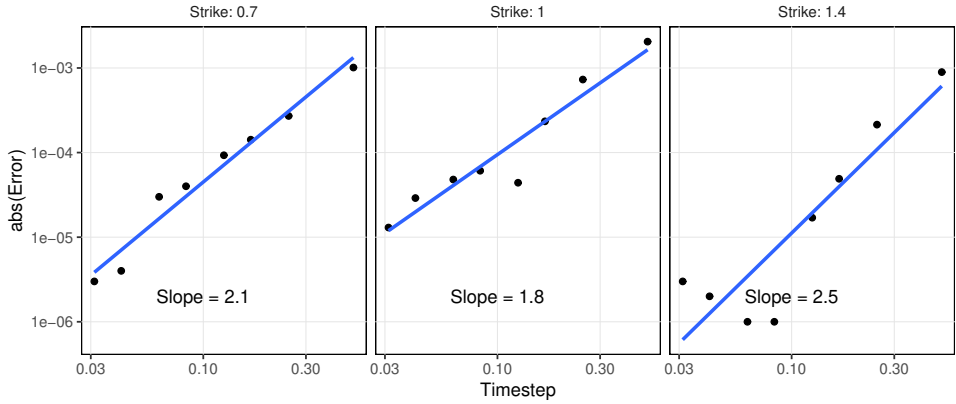
(a) DVSS2X scheme.
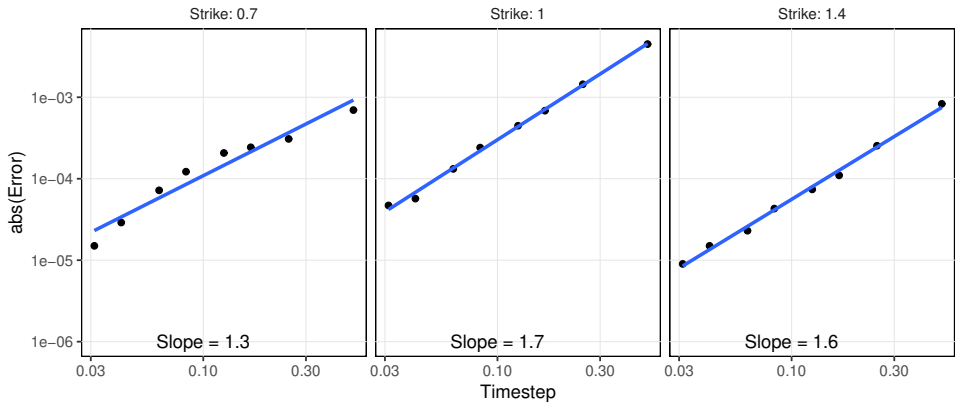
(b) QE scheme.

Figure 8.4.2: Error in the price obtained by the Monte-Carlo simulation of out-the-money vanilla options with forward moneyness 0.7, 1.0, 1.4 and maturity 6 months as a function of the time step size. The Heston-CLV model is calibrated to SX5E options of as of February 26, 2016.

In Table 8.4.1, we calibrate the Heston-CLV model to TSLA options as of June 18, 2018, and price the performance payoff (Equation 8.30) with the Monte-Carlo method described in Section 8.4 between the maturities January 18th, 2019 and January 17th, 2020. In this example, we remove any interest rate effect by considering only the artificial case where $r = q = 0$. While the absorption does not play a role for the price of an at-the-money option in this example, the error in the performance contract price is at least one order of magnitude lower with the reflection method. Truncation also leads to a larger standard error in the Monte-Carlo simulation, because the number of paths where $S(t_1) = \epsilon$ and $S(t_2) \gg \epsilon$ is not negligible, where t_1, t_2 correspond respectively to the maturities January 18th, 2019 and January 17th, 2020. This example also seems to

indicate that the martingale property holds[3] with the reflection method. We will analyze this in more detail in Section 8.4.2.

Table 8.4.1: Price of an at-the-money call option and a future performance contract obtained by a Monte-Carlo simulation using 1 million paths and 32 time steps per year, where the Heston-CLV model is calibrated to TSLA options as of June 18, 2018. The forward prices are normalized so that the theoretical price of the future performance contract is 1. The Heston parameters are $V_0 = 0.23$, $\kappa = 0.163$, $\theta = 3.82$, $\sigma = 3.26$, $\rho = -0.43$.

Method	Price	Error	Standard Error
	At-the-money call option		
No absorption	0.243491	-0.000709	0.000548
Absorption at $\epsilon = 1\%$ by truncation	0.243492	-0.000709	0.000549
Absorption at $\epsilon = 1\%$ by reflection	0.243491	-0.000709	0.000548
	Contract on future performance		
No absorption	1.041000	0.041000	0.011730
Absorption at $\epsilon = 0.1\%$ by truncation	1.058137	0.058137	0.005290
Absorption at $\epsilon = 0.1\%$ reflection	1.004069	0.004069	0.002532
Absorption at $\epsilon = 1\%$ by truncation	1.021739	0.021739	0.001337
Absorption at $\epsilon = 1\%$ reflection	1.000288	0.000288	0.001053

8.4.2. THE MARTINGALE PROPERTY IN PRACTICE

A known deficiency of Markov functional models is that they do not respect the martingale property [30, 108]. The Heston-CLV model is similar to a Markov functional model: the collocation function only captures the terminal distribution at each maturity date and is then applied at different dates independently, without taking into account any joint distribution between the dates. Yet, the driver is a calibrated Heston model, whose joint distribution is close to the market distribution. We may thus expect the collocation function to provide a second-order correction and the martingale property to be reasonably well preserved.

The martingale property can be measured by pricing a contract on the future performance. Under deterministic interest rates and in the absence of arbitrage, the following identity must hold:

$$\mathbb{E}_{\mathbb{Q}}\left[\frac{S(t_j)}{S(t_i)}\,|S(0)\right] = \frac{F(0, t_j)}{F(0, t_i)}, \quad \text{for } 0 \le t_i < t_j, \tag{8.45}$$

where F denotes here the forward price of the asset S at time $t = 0$ so that $F(0, t_i) = \mathbb{E}_{\mathbb{Q}}[S(t_i)]$.

When $t_i = 0$, the identity holds exactly, since the first moment is preserved exactly during the calibration of the collocation function g. When $t_i > 0$, the identity almost

---

[3]This is with the default κ where the performance price with the shortest maturity is around 0.998. If we adjust the κ so that the martingale property is slightly better across the three maturities considered, the same conclusion would remain: the performance price is biased with truncation. Absorption does not play a role in the shortest maturity.

holds in the case of the market data for TSLA options as of June 18th, 2018. The maximum numerical error in the price of the future performance contract between the different maturities is of around 0.3%. While this particular example is challenging because of the absorption implied by the market option prices, it only consists of three option maturities and is thus not representative of market data that the financial industry typically uses to price exotic derivatives.

In Table 8.4.2, we measure the undiscounted future performance for all the pairs of distinct maturities, where the Heston-CLV model is calibrated to SX5E options as of February 26, 2016. It consists of 14 option maturities from two weeks to five years, a standard range for this equity index. On this data, we do not observe any significant implied probability of absorption. The Heston-CLV model fits the market very well (Figure 8.4.3b), and we observe a similar drift of up to 0.3%, when we choose a mean reversion parameter κ, which minimizes the overall drift. Interestingly, this κ is very close to the unconstrained calibrated Heston κ (0.350 vs 0.386). With the latter, the drift increases to up to 0.5%, which is still much milder than the drift of around 5% from the typical Markov functional model [30].

In the Monte-Carlo simulation, the 95% interval of confidence corresponds to three times the standard error. For one million paths, it is ±0.3%, comparable to the measured drift.

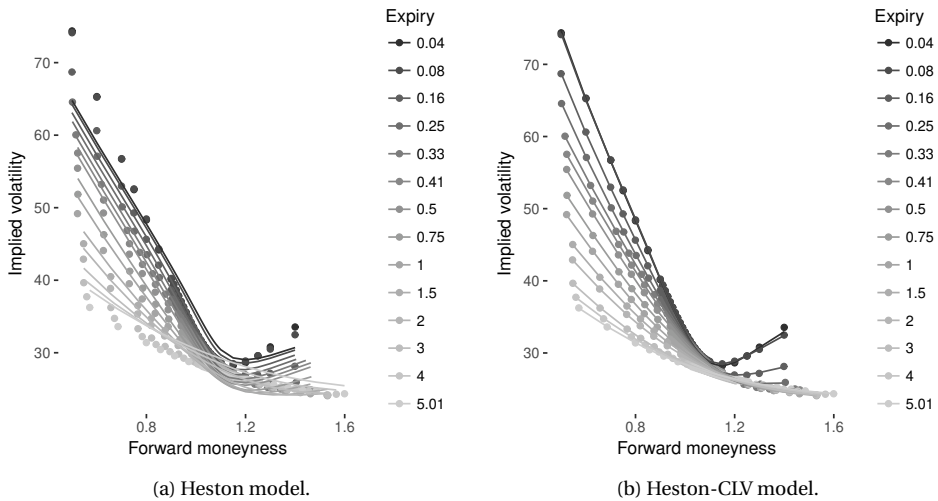(a) Heston model.   (b) Heston-CLV model.

Figure 8.4.3: Black-Scholes volatility implied by the Heston model, and the Heston-CLV model calibrated to SX5E options of as of February 26, 2016. The forward moneyness is defined as $\frac{K}{F(0,t_i)}$ for the expiry t_i.

8.5. THE HESTON-CLV PARTIAL DIFFERENTIAL EQUATION

For vanilla European options, the Fourier-based approach is very efficient. It becomes interesting to numerically solve the PDE (8.2) in order to price exotic options, with some path-dependency, such as barrier options. In practice, the PDE approach may be used

Table 8.4.2: Error in the price of a future contract on performance, expressed in %, for each pair of distinct maturities, obtained by a Monte-Carlo simulation using 1 million paths and 32 time steps per year, when the Heston-CLV model is calibrated to SX5E options as of February 26, 2016. The Monte-Carlo standard error is less than 0.09% and the Heston parameters are $V_0 = 0.133$, $\kappa = 0.350$, $\theta = 0.321$, $\sigma = 1.388$, $\rho = -0.630$.

Maturity	0.04	0.08	0.16	0.25	0.33	0.41	0.50	0.75	1.00	1.50	2.00	3.00	4.00
0.08	-0.02												
0.16	-0.01	0.01											
0.25	-0.02	-0.01	0.02										
0.33	-0.06	-0.05	-0.02	0.02									
0.41	-0.06	-0.02	-0.03	0.04	0.01								
0.50	-0.05	-0.06	-0.02	0.06	0.06	0.09							
0.75	-0.02	-0.05	-0.06	-0.02	-0.00	0.03	-0.03						
1.00	-0.13	-0.10	-0.12	-0.06	-0.09	-0.04	-0.10	-0.00					
1.50	-0.08	-0.10	-0.14	-0.14	-0.18	-0.16	-0.22	-0.21	-0.28				
2.00	-0.05	-0.20	-0.03	-0.12	-0.08	-0.09	-0.20	-0.22	-0.31	-0.14			
3.00	0.01	-0.02	0.03	0.07	0.03	0.04	-0.01	-0.04	-0.20	-0.06	0.16		
4.00	0.01	-0.04	0.10	0.14	0.12	0.14	0.06	0.04	-0.13	-0.10	0.11	-0.30	
5.01	0.04	0.13	0.09	0.10	0.16	0.13	0.07	0.10	-0.06	0.00	0.05	-0.11	0.31

to include market prices of barrier options in the calibration of the CLV model.

Let us consider, for illustration purposes, the specific case of a down-and-out put option. The buyer of a down-and-out put barrier option of strike price K will receive $\max(K - S, 0)$ at maturity T, if the asset S stays above a fixed barrier level b, at all times $t \le T$.

In terms of the Heston driver variable X, the barrier is not constant, but follows the curve $x(t, b)$ defined by

$$g(t, x(t, b)) = b,$$

where g is the collocation function. The problem of discretizing efficiently an implicitly defined, time-varying barrier, while keeping a second-order convergence, is not easily solved.
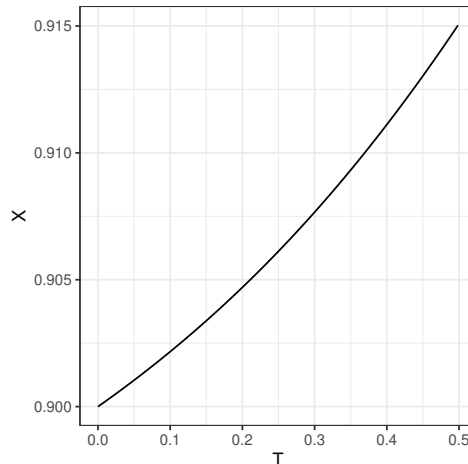

Figure 8.5.1: Barrier profile $x(t, b)$ with b=0.9 and the collocation function defined in Table 8.5.1.

In contrast, if we solve a PDE in the variable S, the barrier corresponds exactly to a Dirichlet boundary, which actually simplifies the problem, compared to a regular Eu-

ropean option without barrier. The PDE coefficients become however time-dependent. The price of a derivative contract u on (s, v) is given by

$$\frac{\partial u}{\partial t} + \dot{g}\frac{\partial u}{\partial s} = \frac{vx^2}{2}g'\frac{\partial}{\partial s}\left(g'\frac{\partial u}{\partial s}\right) + \rho\sigma xvg'\frac{\partial^2 u}{\partial s\partial v} + \frac{\sigma^2 v}{2}\frac{\partial^2 u}{\partial v^2}$$

$$+ (r-q)xg'\frac{\partial u}{\partial s} + \kappa(\theta - v)\frac{\partial u}{\partial v} - ru, \tag{8.46}$$

with

$$g'(t, s) = \frac{\partial g}{\partial x}(t, x(t, s)),$$

$$\dot{g}(t, s) = \frac{\partial g}{\partial t}(t, x(t, s)),$$

and initial condition

$$u(s, v, 0) = h(s). \tag{8.47}$$

The Heston model is recovered with $g(t, s) = s$, $\dot{g} = 0$, $g'(t, s) = 1$.

8.5.1. BOUNDARY CONDITIONS
The PDE will be solved on a truncated domain $[s_{min}, s_{max}] \times [v_{min}, v_{max}]$. We will typically truncate the s domain to four standard deviations. A simple approximation is given by

$$s_{min} = 0, \quad s_{max} = Ke^{+4\sqrt{\theta T}}.$$

where K is the option strike price. For the v domain, let $\Phi_\chi(y, d_\chi, \lambda_\chi)$ be the cumulative distribution for the non-central chi-square distribution with d_χ degrees of freedom and non-centrality parameter λ_χ. The distribution of the variance process $V(T)$ conditional on $V(0)$ is known [6, 39], and thus we may choose

$$v_{min} = 0, \quad v_{max} = \Phi_\chi^{-1}(1 - \epsilon_v, d_\chi, v_0 n_\chi)\frac{e^{-\kappa T}}{n_\chi},$$

with $d_\chi = 4\frac{\kappa\theta}{\sigma^2}$, $n_\chi = 4\kappa\frac{e^{-\kappa T}}{\sigma^2(1-e^{-\kappa T})}$, and $\epsilon_v = 10^{-4}$.

At $s = s_{min}$ and $s = s_{max}$ the Dirichlet boundary conditions for a vanilla option correspond to the discounted intrinsic value

$$u(s, v, t) = e^{-r(T-t)}h\left(se^{(r-q)(T-t)}\right), \tag{8.48}$$

for $v \in [v_{min}, v_{max}]$ and $s \in \{s_{min}, s_{max}\}$. In particular, we will have $u(s_{min}, v, t) = 0$ for a call option in practice.

At $v = v_{max}$, we follow [10, p. 385-386] and let the price to be linear in the variance dimension:

$$\frac{\partial^2 u}{\partial v^2}(x, v, t) = \frac{\partial^2 u}{\partial x\partial v}(x, v, t) = 0, \tag{8.49}$$

for $s \in (s_{min}, s_{max})$. A priori, it is not guaranteed that Equation (8.49) is a sufficiently accurate approximation at the lower boundary v_{min}. When $v_{min} = 0$, the exact boundary

condition at $v = v_{min} = 0$ corresponds to the PDE obtained by setting $v = 0$ and is preferable in practice. With the choice $v_{min} = 0$, the two conditions are equivalent.

An alternative to the Dirichlet boundary conditions is to consider that the value is linear along s, which leads to

$$\frac{\partial^2 u}{\partial s^2}(s, v, t) = \frac{\partial u}{\partial v}(s, v, t) = 0, \tag{8.50}$$

for $v \in [v_{min}, v_{max}]$ and $s \in \{s_{min}, s_{max}\}$.

The Dirichlet boundaries are convenient for theoretical stability analysis, while the linear boundaries are often more accurate in practice.

In a knock-out barrier option, the option becomes worthless as soon as the underlying price is above (up-and-out) or below (down-and-out) a given barrier level b. For a down-and-out option, we set $s_{min} = b$ and use a Dirichet boundary $u(b, v, t) = 0$.

8.5.2. PDE TRANSFORMATIONS

In the case of the PDE (8.2) in the variable x, a change of variable $y = \ln x$ simplifies the PDE as it removes the dependence of its coefficients on x. As evidenced in [188, p. 158-159], in the case of the Black-Scholes PDE (corresponding to setting $\sigma = \kappa = 0$), the difference between the largest and the smallest eigenvalue of the discretization matrix is much smaller with the logarithmic transformation. As a consequence, if we are using an explicit scheme, we will be able to use a larger time-step for a given spatial discretization. If we are using an implicit scheme such as Crank-Nicolson, the oscillations will be reduced with the transformation, and the accuracy may improve. However, the logarithmic transformation will also distort significantly the option payoff, which may result in a significant loss of accuracy as many more points are effectively used in the grid near the lower boundary, instead of where it matters physically (typically around the option strike price). Instead of applying directly such a transformation, we therefore follow [188] and express the variable s as a function of a new variable η, so that η can be discretized uniformly in its interval. We wish to concentrate points where the payoff is not smooth, that is $s = K$ for a vanilla or a barrier option. Regarding the variable v, we are interested in the value of the option price u at $v = V_0$. It makes thus sense to concentrate points around V_0 by expressing v in terms of a new coordinate ξ. This leads to

$$\frac{\partial u}{\partial t} + \frac{\dot{g}}{J^S}\frac{\partial u}{\partial \eta} = \frac{v(\xi)x^2}{2}\frac{g'}{J^S}\frac{\partial}{\partial \eta}\left(\frac{g'}{J^S}\frac{\partial u}{\partial \eta}\right) + \rho\sigma x \frac{v(\xi)g'}{J^V J^S}\frac{\partial^2 u}{\partial \eta \partial \xi} + \frac{\sigma^2 v(\xi)}{2J^V}\frac{\partial}{\partial \xi}\left(\frac{1}{J^V}\frac{\partial u}{\partial \xi}\right)$$
$$+ (r-q)x\frac{g'}{J^S}\frac{\partial u}{\partial \eta} + \frac{\kappa(\theta - v(\xi))}{J^V}\frac{\partial u}{\partial \xi} - ru, \tag{8.51}$$

where

$$J^S(\eta) = \frac{\partial s}{\partial \eta}(\eta), \quad J^V(\xi) = \frac{\partial v}{\partial \xi}(\xi) \tag{8.52}$$

are the respective Jacobians of each transformation. The linear boundary condition in s (Equation 8.50) translates to

$$\frac{\partial}{\partial \eta}\left(\frac{1}{J^S(\eta)}\frac{\partial u}{\partial \eta}\right) = 0 = \frac{\partial u}{\partial \xi},$$

for $v(\xi) \in [v_{\min}, v_{\max}]$ and $s(\eta) \in \{s_{\min}, s_{\max}\}$. Furthermore, when g is a quadratic spline with linear extrapolation, we have $\frac{\partial^2 g}{\partial x^2}(t, x(t, s)) = 0$, assuming that the extrapolation starts at some $s < s_{\min}$ as well as at some $s_{\max} < s$.

We will use the hyperbolic sine function as smooth transformation that concentrates points [188]

$$S(\eta) = K + \lambda_S \sinh((c_2 - c_1)\eta + c_1), \tag{8.53}$$

$$J^S(\eta) = \lambda_S(c_2 - c_1)\cosh((c_2 - c_1)\eta + c_1), \tag{8.54}$$

with $c_1 = \sinh^{-1}\left(\frac{S_{\min} - K}{\lambda_S}\right)$, $c_2 = \sinh^{-1}\left(\frac{S_{\max} - K}{\lambda_S}\right)$. In our numerical examples, we will choose $\lambda_S = \frac{K}{4}$, with η uniform in $[0, 1]$ (see Figure 8.5.2). The transformation of the variable v reads

$$v(\xi) = V_0 + \lambda_v \sinh((\tilde{c}_2 - \tilde{c}_1)\xi + \tilde{c}_1), \tag{8.55}$$

$$J^V(\xi) = \lambda_v(\tilde{c}_2 - \tilde{c}_1)\cosh((\tilde{c}_2 - \tilde{c}_1)\xi + c_1), \tag{8.56}$$

with $\tilde{c}_1 = \sinh^{-1}\left(\frac{v_{\min} - V_0}{\lambda_v}\right)$, $\tilde{c}_2 = \sinh^{-1}\left(\frac{v_{\max} - V_0}{\lambda_v}\right)$. For a uniform $\xi \in [0, 1]$, a large scaling parameter λ_v will lead to a uniform $V \in [v_{\min}, v_{\max}]$ whereas V will be highly non-uniform for small values of λ_v. A good choice for the scaling parameter is $\lambda_v = 2V_0$.
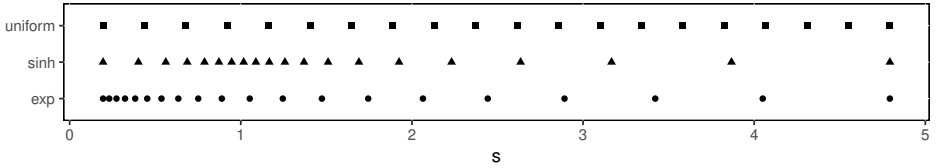

Figure 8.5.2: Discretization of the variable s with different transformations, as implied by the Heston parameters $V_0 = 0.133$, $\kappa = 0.350$, $\theta = 0.321$, $\sigma = 1.388$, $\rho = -0.630$ and $T = 0.49863$, for $M = 20$, $K = 1$.

8.5.3. FINITE DIFFERENCE DISCRETIZATION OF ORDER-2 IN SPACE

Let us define a uniform grid in the coordinates η, ξ of Equation (8.51), for $j = 1, ..., L$, for $i = 1, ... M$,

$$\xi_j = (j - 1)\Delta\xi, \quad \Delta\xi = \frac{1}{L - 1}, \tag{8.57}$$

$$\eta_i = (i - 1)\Delta\eta, \quad \Delta\eta = \frac{1}{M - 1}. \tag{8.58}$$

There is no need to consider the case of a non-uniform grid since the coordinate transformations $s(\eta)$ and $v(\xi)$ already give us the flexibility we need in the grid geometry.

For $j = 1, ..., L$ and $i = 1, ... M$, let

$$x_i(t) = x(t, s(\eta_i)), \quad v_j = v(\xi_j),$$
$$J_i^S = J^S(\eta_i), \quad J_j^V = J^V(\xi_j),$$
$$g_i'(t) = g'(t, x_i(t)), \quad \dot{g}_i(t) = \dot{g}(t, x_i(t)),$$
$$u_{i,j}(t) = u(s(\eta_i), v(\xi_j), t).$$

On this grid, we define the discrete operator $\mathcal{L}_{i,j} = \mathcal{L}_{i,j}^\eta + \mathcal{L}_{i,j}^\xi + \mathcal{L}_{i,j}^{\eta,\xi} + \mathcal{L}_{i,j}^r$, where

$$\mathcal{L}_{i,j}^\eta(t, u) = \frac{\beta_{i,j}^S v_j x_i^2}{2\Delta\eta} \frac{g_i'}{J_i^S} \left(g_{i+\frac{1}{2}}' \frac{u_{i+1,j} - u_{i,j}}{J_{i+\frac{1}{2}}^S \Delta\eta} - g_{i-\frac{1}{2}}' \frac{u_{i,j} - u_{i-1,j}}{J_{i-\frac{1}{2}}^S \Delta\eta} \right)$$
$$+ \frac{(r-q)x_i g_i' - \dot{g}_i}{J_i^S} \frac{u_{i+1,j} - u_{i-1,j}}{2\Delta\eta}, \tag{8.59}$$

$$\mathcal{L}_{i,j}^{\eta,\xi}(t, u) = \rho\sigma \frac{x_i v_j g_i'}{J_i^S J_j^V} \frac{u_{i+1,j+1} - u_{i-1,j+1} - u_{i+1,j-1} + u_{i-1,j-1}}{4\Delta\eta\Delta\xi}, \tag{8.60}$$

$$\mathcal{L}_{i,j}^\xi(t, u) = \frac{\beta_j^V \sigma^2 v_j}{2J_j^V \Delta\xi} \left(\frac{u_{i,j+1} - u_{i,j}}{J_{j+\frac{1}{2}}^V \Delta\xi} - \frac{u_{i,j} - u_{i,j-1}}{J_{j-\frac{1}{2}}^V \Delta\xi} \right) + \frac{\kappa(\theta - v_j)}{J_j^V} \frac{u_{i,j+1} - u_{i,j-1}}{2\Delta\xi}, \tag{8.61}$$

$$\mathcal{L}_{i,j}^r(t, u) = -r u_{i,j}, \tag{8.62}$$

for $i = 2, ..., M-1$ and $j = 2, ..., L-1$, with

$$J_{i\pm\frac{1}{2}}^S = J^S\left(\eta_i \pm \frac{1}{2}\Delta\eta\right), \quad J_{j\pm\frac{1}{2}}^V = J^V\left(\xi_j \pm \frac{1}{2}\Delta\xi\right)$$

and $\beta_{i,j}^S = \beta_j^V = 1$. It corresponds to a second-order central discretization in the variables η, ξ of the right-hand side of PDE (8.51).

The Peclet number corresponding to each dimension is

$$P_{i,j}^S = 2\Delta\eta \frac{J_i^S}{g_i' v_j x_i}\left(r - q - \frac{\dot{g}_i}{x_i}\right), \quad P_j^V = 2\Delta\xi \frac{\kappa(\theta - v_j)J_j^V}{\sigma^2 v_j}. \tag{8.63}$$

The Peclet conditions $P_{i,j}^S < 2$ and $P_j^V < 2$ do not necessary hold with typical values for the Heston parameters. This happens when v_j is very small, which is generally the case for the first few indices j. When the Peclet condition does not hold, the stability of the finite difference scheme is not guaranteed anymore: the solution may explode. In order to ensure that the Peclet conditions hold, we will use the exponential fitting technique [5, 102] when $P_{i,j}^S \geq 2$ as well as when $P_j^V \geq 2$. It consists in using the coefficients

$$\beta_{i,j}^S = \frac{P_{i,j}^S}{2\tanh\left(\frac{P_{i,j}^S}{2}\right)}, \quad \beta_j^V = \frac{P_j^V}{2\tanh\left(\frac{P_j^V}{2}\right)}, \tag{8.64}$$

instead of $\beta_{i,j}^S = \beta_j^V = 1$.

The linear boundary conditions are discretized with order-1 forward and backward differences as

$$\mathcal{L}_{i,1}^\eta(t,u) = \frac{\beta_{i,1}^S v_1 x_i^2}{2\Delta\eta} \frac{g_i'}{J_i^S} \left(g_{i+\frac{1}{2}}' \frac{u_{i+1,1} - u_{i,1}}{J_{i+\frac{1}{2}}^S \Delta\eta} - g_{i-\frac{1}{2}}' \frac{u_{i,1} - u_{i-1,1}}{J_{i-\frac{1}{2}}^S \Delta\eta} \right)$$
$$+ \frac{(r-q) x_i g_i' - \dot{g}_i}{J_i^S} \frac{u_{i+1,1} - u_{i-1,1}}{2\Delta\eta},$$

$$\mathcal{L}_{i,1}^{\eta,\xi}(t,u) = 0, \quad \mathcal{L}_{i,1}^r(t,u) = -r u_{i,1}, \quad \mathcal{L}_{i,1}^\xi(t,u) = \frac{\kappa(\theta - v_1)}{J_{1+\frac{1}{2}}^V} \frac{u_{i,2} - u_{i,1}}{\Delta\xi},$$

$$\mathcal{L}_{i,L}^\eta(t,u) = \frac{\beta_{i,L}^S v_L x_i^2}{2\Delta\eta} \frac{g_i'}{J_i^S} \left(g_{i+\frac{1}{2}}' \frac{u_{i+1,L} - u_{i,L}}{J_{i+\frac{1}{2}}^S \Delta\eta} - g_{i-\frac{1}{2}}' \frac{u_{i,L} - u_{i-1,L}}{J_{i-\frac{1}{2}}^S \Delta\eta} \right)$$
$$+ \frac{(r-q) x_i g_i' - \dot{g}_i}{J_i^S} \frac{u_{i+1,L} - u_{i-1,L}}{2\Delta\eta},$$

$$\mathcal{L}_{i,L}^{\eta,\xi}(t,u) = 0, \quad \mathcal{L}_{i,L}^r(t,u) = -r u_{i,L}, \quad \mathcal{L}_{i,L}^\xi(t,u) = \frac{\kappa(\theta - v_L)}{J_{L-\frac{1}{2}}^V} \frac{u_{i,L} - u_{i,L-1}}{\Delta\xi},$$

for $i = 2, ..., M-1$, and

$$\mathcal{L}_{1,j}^\eta(t,u) = \frac{(r-q) x_1 g_1' - \dot{g}_1}{J_{1+\frac{1}{2}}^S} \frac{u_{2,j} - u_{1,j}}{\Delta\eta},$$

$$\mathcal{L}_{1,j}^{\eta,\xi}(t,u) = \mathcal{L}_{1,j}^\xi(t,u) = 0, \quad \mathcal{L}_{1,j}^r(t,u) = -r u_{1,j},$$

$$\mathcal{L}_{M,1}^\eta = \frac{(r-q) x_1 g_M' - \dot{g}_M}{J_{M-\frac{1}{2}}^S} \frac{u_{M,j} - u_{M-1,j}}{\Delta\eta},$$

$$\mathcal{L}_{M,j}^{\eta,\xi}(t,u) = \mathcal{L}_{M,j}^\xi(t,u) = 0, \quad \mathcal{L}_{M,j}^r(t,u) = -r u_{M,j},$$

for $j = 1, ..., L$.

In the case of a Dirichlet boundary in the variable s, for example in the context of barrier options, we have $\mathcal{L}_{i,j} = 0$ for $j = 1, ..., L$ and $i = 1$ or $i = L$ for respectively the lower and upper boundaries.

8.5.4. FINITE DIFFERENCE SCHEMES
We will now analyze a number of discretization schemes on their stability and accuracy properties.

LAWSON-SWAYNE SCHEME
The Lawson-Swayne scheme is an L-stable, and second-order in time finite difference scheme [125]. The L-stability property is particularly interesting since it guarantees that rapid transients in the solution will be damped in a single time step [138]. In contrast,

the Crank-Nicolson scheme is only A-stable, and requires smoothing steps around discontinuities [73], in order to avoid spurious oscillations, which may degrade the overall convergence.

The Lawson-Swayne scheme applied to the Heston-CLV PDE (8.46) in the variable s then reads

$$u_{i,j}(t_{k+\gamma}) - u_{i,j}(t_k) = \gamma \Delta t_k \mathcal{L}_{i,j}\left(t_{k+\gamma}, u(s,v,t_{k+\gamma})\right), \tag{8.65a}$$

$$u_{i,j}(t_{k+2\gamma}) - u_{i,j}(t_{k+\gamma}) = \gamma \Delta t_k \mathcal{L}_{i,j}\left(t_{k+2\gamma}, u(s,v,t_{k+2\gamma})\right), \tag{8.65b}$$

$$u_{i,j}(t_{k+1}) = (\sqrt{2}+1)u_{i,j}(t_{k+2\gamma}) - \sqrt{2}u_{i,j}(t_{k+\gamma}), \tag{8.65c}$$

for $i = 1, ..., L$, $j = 1, ..., M$ and $k = 0, ..., N-1$, with $\gamma = 1 - \frac{\sqrt{2}}{2}$, $\Delta t_k = t_{k+1} - t_k$. In our numerical examples, we use a constant time step $\Delta t_k = \frac{T}{N}$ where T is the option maturity.

For each point of the grid with indices (i, j), $\mathcal{L}_{i,j} u$ defines 9 corresponding coefficients for the indices $(i+1, j+1)$, $(i+1, j)$, $(i, j+1)$, (i, j), $(i-1, j)$, $(i, j-1)$, $(i-1, j-1)$, $(i+1, j-1)$, $(i-1, j+1)$, for $i = 2, ..., M-1$ and $j = 2, ..., M-1$. Let A be the matrix of size (LM, LM) with elements verifying

$$\mathcal{L}_{i,j}(t, u) = \sum_{r=1}^{M}\sum_{s=1}^{L} A_{i+jM,r+sM} u_{r,s}, \tag{8.66}$$

for $i = 1, ..., L$, $j = 1, ..., M$. The elements $A_{j+iM,s+rM}$ correspond to the nine points stencil at (i, j). Let $B = I - \gamma \Delta t A$. Each step of the Lawson-Swayne scheme consists in solving B twice. In the case of the pure Heston model, the matrix B is constant across time and may thus be factorized in an initialization step. Furthermore, B is sparse and contains at most 9 non zero entry per row and per column (Figure 8.5.3). A numerical implementation will thus benefit from a fast direct sparse LU solver, such as UMFPACK [42] or SuperLU [141].
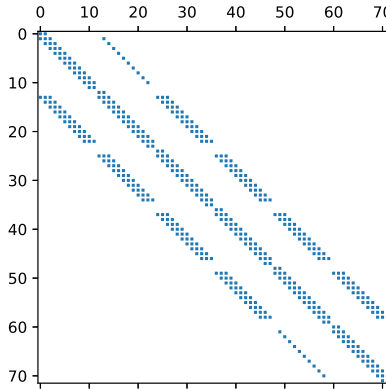

Figure 8.5.3: Structure of the sparse matrix A, with $L = 6$, $M = 12$. Each dot corresponds to a non-zero element.

Unfortunately, in the CLV model, B is time-dependent and thus needs to be decomposed at each stage for every time step. This increases significantly the computational

cost. The use of an iterative solver such as the successive over-relaxation method (SOR) or the biconjugate gradient stabilized method (BICGSTAB) is then recommended.

AN ALTERNATING DIRECTION EXPLICIT (ADE) DISCRETIZATION

Leung and Osher [136] propose to split the matrix A into strictly lower diagonal A_L, strictly upper diagonal A_U and diagonal A_D and solve

$$\left[I - \Delta t \left(\frac{1}{2} A_D + A_L \right) \right] u^0 = \left[I + \Delta t \left(\frac{1}{2} A_D + A_U \right) \right] u(t_k), \tag{8.67a}$$

$$\left[I - \Delta t \left(\frac{1}{2} A_D + A_U \right) \right] u^1 = \left[I + \Delta t \left(\frac{1}{2} A_D + A_L \right) \right] u(t_k), \tag{8.67b}$$

$$u(t_{k+1}) = \frac{u^1 + u^0}{2}, \tag{8.67c}$$

where $u_{i,j}^m = u^m(s(\eta_i), v(\xi_j), t_k)$ represents the option price at an intermediate stage m. The matrix A is time-dependent. In order to keep the second-order accuracy, we evaluate it at the mid-point $t = \frac{t_k + t_{k+1}}{2}$.

In the ADE scheme, each stage is independent and consists then in the solution of one sparse triangular system, which requires only $5LM$ multiplications in the case of the Heston CLV PDE discretization. The performance is the main appeal of this method. The first stage evaluates the system in a left-down towards right-up manner, while the second stage evaluates the system in the opposite direction, hence the name alternating direction explicit. Duffy [53, 54] applied ADE schemes to price options in the one-factor Black-Scholes model.

The stability of the scheme is guaranteed only if the matrix A is symmetric negative definite, which is not the case for our discretization of the Heston-CLV PDE. In fact, we find that such a scheme may explode when the time step Δt is too large compared to the number of steps in the dimension of the asset price S (in our numerical example, for $N \leq 128$ with $M = 1024$ and $L = 128$).

EXPLICIT RUNGE-KUTTA-LEGENDRE DISCRETIZATION

Applied to the Heston-CLV PDE, the explicit Euler method is very simple to implement. It does not require to solve any linear system. Furthermore, with a sparse system (the matrix A described by Equation (8.66)), the matrix-vector multiplications involved are fast ($9LM$ multiplications for the matrix A). The explicit Euler method is however only first-order in time. This can easily be remedied by the use of a predictor-corrector scheme, or of the second-order explicit Runge-Kutta scheme (RK2). The bigger issue is the limitation on the time step size imposed by the stability condition. The latter implies that time step size Δt follows a square relationship with the asset and variance step sizes ΔS and ΔV. For practical grid geometries, more than 10000 time steps may be required for the explicit scheme to be stable.

Super time stepping methods, typically based on the boundedness of Chebyshev polynomial, allow to circumvent the time step size limitation for parabolic (mildly stiff) problems. OŚullivan [164] applied the super time stepping of Alexiades [4] to the pricing of American options in the Black-Scholes model, using a Richardson extrapolation to attain second-order accuracy. In't Hout and Foulon [103] applied the second-order

Runge-Kutta-Chebyshev solver of Sommeijer [182] to compute the price of European and barrier options under the Heston model. Here, we consider a more recent development with increased stability properties due to Meyer [154], where a Legendre polynomial defines the recursion of the super time stepping method. Their approach does not require to define and guess an extra damping parameter and is directly second-order. The Runge-Kutta-Legendre scheme of order-2 (RKL2), with γ stages, reads

$$u_{i,j}^0 = u_{i,j}(t_k), \tag{8.68a}$$

$$u_{i,j}^1 = +\tilde{\mu}_1 \Delta t_k \mathcal{L}_{i,j}\left(t_k, u^0\right), \tag{8.68b}$$

$$u_{i,j}^m = \mu_m u_{i,j}^{m-1} + \nu_m u_{i,j}^{m-2} + (1 - \mu_m - \nu_m) u^0$$
$$\quad + \tilde{\mu}_m \Delta t_k \mathcal{L}_{i,j}\left(t_k^{m-1}, u^{m-1}\right) + \tilde{\gamma}_m \Delta t_k \mathcal{L}_{i,j}\left(t_k, u^0\right), \quad \text{for } 2 \le m \le s, \tag{8.68c}$$

$$u_{i,j}(t_{k+1}) = u_{i,j}^\gamma, \tag{8.68d}$$

with the parameters

$$\mu_m = \frac{2m-1}{m}\frac{b_m}{b_{m-1}}, \quad \nu_m = -\frac{m-1}{m}\frac{b_m}{b_{m-2}},$$

$$\tilde{\mu}_m = \mu_m w_1, \quad \tilde{\gamma}_m = -(1 - b_{m-1})\tilde{\mu}_m,$$

$$b_m = \frac{m^2 + m - 2}{2m(m+1)}, \quad t_k^m = t_k + \frac{m^2 + m - 2}{\gamma^2 + \gamma - 2}\Delta t_k,$$

for $2 \le m \le \gamma$ and $b_0 = b_1 = b_2 = \frac{1}{3}$, $w_1 = \frac{4}{\gamma^2 + \gamma - 2}$, $\tilde{\mu}_1 = b_1 w_1$ and $t_k^1 = t_k + \tilde{\mu}_1 \Delta t_k$.

The γ stages are explicit. The scheme is stable as long as

$$\Delta t_k \le \frac{\Delta t_{\text{explicit}}}{4}\left(\gamma^2 + \gamma - 2\right) \tag{8.69}$$

where $\Delta t_{\text{explicit}}$ is the maximum time step size allowed by the explicit Euler method. A simple, conservative, upper bound for the explicit time step size is $\frac{1}{\max|A_{i,i}|}$, where the matrix A is defined in equation (8.66), and we assumed its diagonal to be dominant. Equation (8.69) gives us a method to automatically determine the minimum number of stages γ for a given time step size Δt_k. In particular, we notice that this number of stages γ is proportional to the inverse square root of $\Delta t_{\text{explicit}}$, and thus, the RKL2 scheme should be more efficient than the classic explicit Euler scheme. In our numerical examples, we will take the first odd integer larger than, or equal to, the minimum number of stages allowed.

The construction of the sparse matrix at different steps is the most time-consuming part of the overall algorithm as it is time-dependent. If we implement the Equations (8.68b)-(8.68d) in straightforward fashion, the matrix A needs to be computed at each intermediate stage. A simple optimization is to use the matrix at the mid-point $\frac{t_k + t_{k+1}}{2}$ for all stages. The method will still be of second-order. In our implementation, this optimization increased the performance by a factor three and did not impact the accuracy of the method.

ALTERNATING DIRECTION IMPLICIT DISCRETIZATIONS

A different approach to speed up the solution of multi-dimensional PDEs consists in splitting the systems across each dimension of the problem. Let us explore a few alternative direction implicit (ADI) schemes that are second-order in time. The first ADI scheme [168] does not consider any mixed-derivative terms in the PDE. In order to achieve second-order accuracy in time, with mixed-derivatives terms, Craig and Sneyd [40] derive an iterative scheme. In't Hout and Welfert [105] propose an extension of the Craig-Sneyd scheme, with one additional correction stage, so that the second-order convergence stays valid for any choice of the internal parameter θ. Hundsdorfer and Verwer [94, 195] describe a different second-order discretization scheme with free parameter θ. In't Hout and Foulon [103] have however observed it to have a slightly inferior convergence when applied to the Heston PDE. We have noticed the same on the Heston-CLV PDE. Furthermore, we noticed a worse damping than with the modified Craig-Sneyd scheme, using the recommended parameters for each scheme, respectively $\theta = \frac{1}{2} + \frac{\sqrt{3}}{6}$ and $\theta = \frac{1}{3}$. As the two schemes have essentially the same computational cost, we will not consider the Hundsdorfer-Verwer scheme further. Instead, we will consider the more recent two-steps BDF2-type scheme called SC2B, which belongs to the class of stabilizing correction multistep methods developed by [95].

Modified Craig-Sneyd.   Applied to PDE (8.46), we obtain

$$u_{i,j}^0 - u_{i,j}(t_k) = \Delta t_k \mathscr{L}_{i,j}\left(t_k, u(s(\eta), v(\xi), t_k)\right), \tag{8.70a}$$

$$u_{i,j}^1 - u_{i,j}^0 = \theta \Delta t_k \left[\mathscr{L}_{i,j}^\eta\left(t_{k+1}, u^1\right) - \mathscr{L}_{i,j}^\eta\left(t_k, u(s, v, t_k)\right)\right], \tag{8.70b}$$

$$u_{i,j}^2 - u_{i,j}^1 = \theta \Delta t_k \left[\mathscr{L}_{i,j}^\xi\left(t_{k+1}, u^2\right) - \mathscr{L}_{i,j}^\xi\left(t_k, u(s, v, t_k)\right)\right], \tag{8.70c}$$

$$u_{i,j}^3 - u_{i,j}^0 = \theta \Delta t_k \left[\mathscr{L}_{i,j}^{\eta,\xi}\left(t_{k+1}, u^2\right) - \mathscr{L}_{i,j}^{\eta,\xi}\left(t_k, u(s, v, t_k)\right)\right], \tag{8.70d}$$

$$u_{i,j}^4 - u_{i,j}^3 = \left(\frac{1}{2} - \theta\right)\Delta t_k \left[\mathscr{L}_{i,j}\left(t_{k+1}, u^2\right) - \mathscr{L}_{i,j}\left(t_k, u(s, v, t_k)\right)\right], \tag{8.70e}$$

$$u_{i,j}^5 - u_{i,j}^4 = \theta \Delta t_k \left[\mathscr{L}_{i,j}^\eta\left(t_{k+1}, u^5\right) - \mathscr{L}_{i,j}^\eta\left(t_k, u(s, v, t_k)\right)\right], \tag{8.70f}$$

$$u_{i,j}(t_{k+1}) - u_{i,j}^5 = \theta \Delta t_k \left[\mathscr{L}_{i,j}^\xi\left(t_{k+1}, u(s, v, t_{k+1})\right) - \mathscr{L}_{i,j}^\xi\left(t_k, u(s, v, t_k)\right)\right], \tag{8.70g}$$

where $u_{i,j}^m = u^m(s(\eta_i), v(\xi_j), t_k)$ represents the option price at an intermediate stage m. The first, fourth and fifth stages are explicit. The four other stages involve the solution of two tridiagonal matrices, one for each dimension. The first three stages correspond to the Douglas-Rachford scheme. The last four stages are effectively corrector stages on the Douglas-Rachford scheme. The standard Craig-Sneyd scheme corresponds to the specific choice $\theta = \frac{1}{2}$, which makes the fifth stage vanish. Compared to the standard Craig-Sneyd scheme, the additional stage of the modified scheme (Equation 8.70e) is explicit, and thus does not increase significantly the overall computational effort.

According to [104], the scheme is stable for $\theta \geq \max\left(\frac{1}{4}, \frac{|\rho|+1}{6}\right)$. In our numerical experiments, will make the choice $\theta = \frac{1}{3}$ so that stability is guaranteed for any choice of the correlation ρ.

The scheme may also be written with the operators $\mathcal{L}^\eta$ and $\mathcal{L}^\xi$ reversed. The choice does not really impact the accuracy in practice. With linear boundary conditions, finishing with $\mathcal{L}^\eta$ may be more appropriate, since the operator $\mathcal{L}^\xi$ does not capture the linear boundary in S.

Stabilizing correction multistep methods SC2A and SC2B. Applied to PDE (8.46), we obtain

$$
u_{i,j}^0 - a_0 u_{i,j}(t_k) - a_1 u_{i,j}(t_{k-1}) = \sum_{m=0}^1 \Delta t_{k-m} \hat{b}_m \mathcal{L}_{i,j}^{\eta,\xi} \left(t_{k-m}, u(s(\eta), v(\xi), t_{k-m}) \right)
$$
$$
+ \sum_{m=0}^1 \Delta t_{k-m} \check{b}_m \left[\mathcal{L}_{i,j}^\eta + \mathcal{L}_{i,j}^\xi \right] \left(t_{k-m}, u(s(\eta), v(\xi), t_{k-m}) \right),
$$
$$
\tag{8.71a}
$$
$$
u_{i,j}^1 - u_{i,j}^0 = \theta \Delta t_k \left[\mathcal{L}_{i,j}^\eta \left(t_{k+1}, u^1 \right) - \mathcal{L}_{i,j}^\eta (t_k, u(s, v, t_k)) \right], \tag{8.71b}
$$
$$
u_{i,j}(t_{k+1}) - u_{i,j}^1 = \theta \Delta t_k \left[\mathcal{L}_{i,j}^\xi (t_{k+1}, u(s, v, t_{k+1})) - \mathcal{L}_{i,j}^\xi (t_k, u(s, v, t_k)) \right], \tag{8.71c}
$$

with coefficients $(a_0, a_1) = \left(\frac{4}{3}, -\frac{1}{3}\right)$, $(\hat{b}_0, \hat{b}_1) = \left(\frac{4}{3}, -\frac{2}{3}\right)$ and $(\check{b}_0, \check{b}_1) = \left(\frac{4}{3} - \theta, -\frac{2}{3} + \theta\right)$. As recommended in [95], we choose the parameter $\theta = \frac{2}{3}$, which constitutes a reasonable compromise between stability properties and error constants. This set of coefficients defines the BDF2 type scheme SC2B. The first stage is explicit, and involves u at the times t_k and t_{k-1}. The two other stages are implicit and correspond to the two implicit stages of the Douglas-Rachford scheme, with a specific choice of θ.

The two-steps Adams-type scheme SC2A corresponds to $(a_0, a_1) = (1, 0)$, $(\hat{b}_0, \hat{b}_1) = \left(\frac{3}{2}, -\frac{1}{2}\right)$ and $(\check{b}_0, \check{b}_1) = \left(\frac{3}{2} - \theta, -\frac{1}{2} + \theta\right)$, with $\theta = \frac{3}{4}$.

In order to start the multistep method, we use the Douglas-Rachford scheme for the first time step, with $\theta = 1$. Although the latter scheme is only first-order in time, we found it to lead to more accurate results than the Craig-Sneyd or modified Craig-Sneyd schemes applied to the first time step only.

DAMPING AND SMOOTHING.

It is well-known that the Crank-Nicolson scheme leads to spurious oscillations in the solution in the presence of non-smooth initial conditions [73]. Most financial derivative contracts define non-smooth initial conditions. A remedy consists in replacing, at each time of non-smooth condition, the first time step by two half-steps of the implicit Euler scheme, as first proposed by Rannacher [173]. If, in the Craig-Sneyd scheme, we consider the case $\mathcal{L}_{i,j}^\xi = \mathcal{L}_{i,j}^{\eta,\xi} = 0$, we obtain the Crank-Nicolson scheme. We may thus expect the Craig-Sneyd scheme to suffer from the same oscillation deficiencies as the Crank-Nicolson scheme.

The damping procedure described above requires to solve twice a large sparse matrix. While this may be an acceptable trade-off, a less computationally intensive approach is to split the Euler scheme across dimensions. Haentjens and In't Hout [81]

suggest to use the Douglas-Rachford ADI scheme (Equations 8.70a, 8.70b, 8.70c) with parameter $\theta = 1$. As a note of caution, the latter scheme does not always have strong damping properties, as evidenced on a system of two advection-reaction equations in [97, p. 378]. On the Heston-CLV PDE, we observed significant damping with the Douglas-Rachford ADI scheme, albeit slightly smaller than with the implicit Euler scheme.

In order to illustrate the importance of smoothing, we consider the Heston-CLV model, calibrated to SX5E options as of February 26, 2016, as described in Section (8.4.1). The corresponding Heston parameters are $V_0 = 0.133$, $\kappa = 0.350$, $\theta = 0.321$, $\sigma = 1.388$, $\rho = -0.630$.

We then compute the gamma in the PDE coordinate s for a vanilla put option of maturity $T = 0.5$, that is $\frac{\partial^2 u}{\partial s^2}$, at the nodes of the finite difference grid, for $v = V_0$. In order to show clearly the oscillations that may appear in the gamma, we use a large number of steps $M = 2048$ for the asset dimension η, $L = 32$ steps for the variance dimension ξ, along with a relatively small number of time steps $N = 16$. The observations would not change with a higher L. Figure 8.5.4 shows large oscillations in the gamma, when the Craig-Sneyd scheme is used. Two half-steps of the implicit Euler scheme are enough
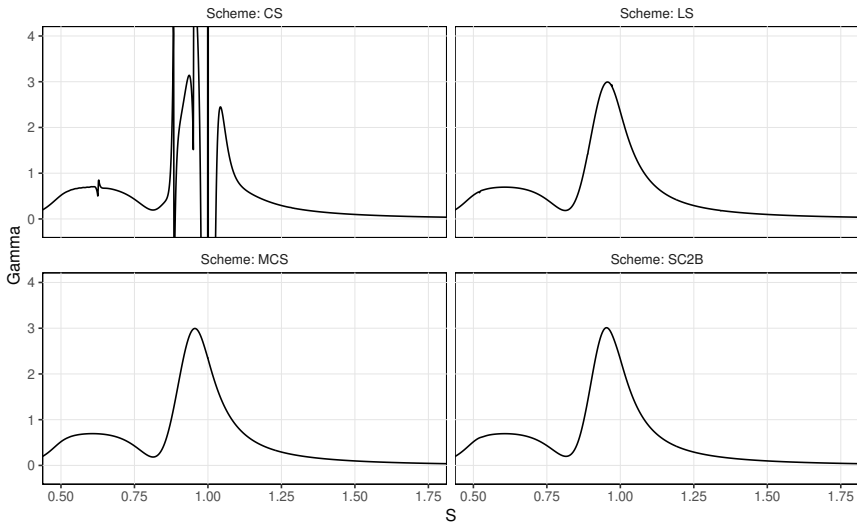

Figure 8.5.4: Gamma from various finite difference schemes. CS stand for the Craig-Sneyd scheme, MCS for the modified Craig-Sneyd scheme, SC2B for the stabilizing correction multistep method of BDF2-type, LS for the Lawson-Swayne scheme.

to completely remove the oscillations. If, instead of the implicit Euler scheme, we use the Douglas-Rachford scheme with $\theta = 1$, a small oscillation remains around $s = 1$. The modified Craig-Sneyd scheme results in no visible oscillation at all. Oscillations appear if we reduce the number of time steps, in our case with $N = 8$. With the Lawson-Swayne scheme, even with $N = 8$, oscillations are barely visible due to its *L-stability* property. Regarding the two-step methods, the SC2A scheme leads to a tiny oscillation around $S = 1$ with $N = 16$, which disappears for $N \geq 20$. The SC2B scheme has stronger damping

properties, and no oscillations were visible for $N = 8$.

We noticed that it was key to split first in the variance dimension v (or ξ) and then in the asset dimension s (or η). If we do the opposite, not only is the gamma inaccurate very close to the lower boundary s_{min}, but some oscillations are still present in the Craig-Sneyd scheme solution, even after applying the damping steps.

In Figure 8.5.5 we plot the gamma obtained by the explicit schemes. The ADE scheme explodes for $N \leq 256$, and we thus used a much larger number of time steps than with the other schemes to look for oscillations. Oscillations are visible for $N = 512$ and disappear for $N \geq 1024$. The gamma still has a large error for $N = 1024$, as its peak is noticeably higher. The gamma obtained by the RKL2 scheme exhibits oscillations for $N = 16$, which
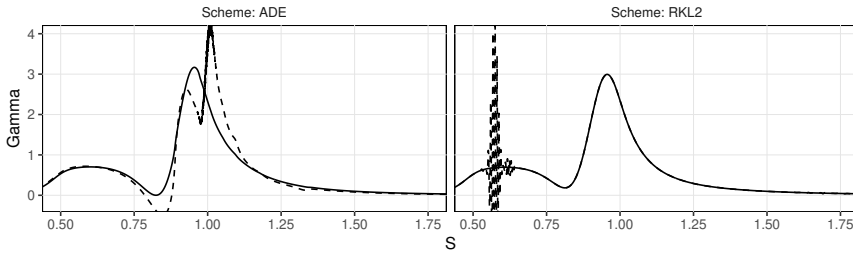
Figure 8.5.5: Gamma from the ADE and RKL2 explicit finite difference schemes. For the ADE scheme the number of time steps is $N = 1024$ (solid line), and $N = 512$ (dashed line). For the RKL2 scheme, $N = 64$ (solid line) and $N = 16$ (dashed line).

disappear for $N = 64$. The corresponding number of stages is respectively $\gamma = 1113$ and $\gamma = 557$. These oscillations are likely related to eigenvalues with a large real part, which push the scheme towards its instability region. Indeed, we noticed that the scheme may diverge for an option with barrier $B = 0.9$ and $M = 4096$ steps in the asset dimension, that is, a very high density of points. The stability region becomes narrower as the number of stages increases.

The issue is more pronounced in the Heston-CLV model than in the pure Heston model. In the Heston model, the RKL2 scheme stayed stable with Heston parameters $\kappa = 3, \theta = 0.12, \sigma = 0.04, \rho = 0.6, r = 0.01, q = 0.04, T = 1$, which corresponds to case 2 of [103]. In the latter paper, the authors observe that the Runge-Kutta-Chebyshev scheme diverges for large time step sizes because of the high advection resulting from those parameters. We however don't have a clear[4] explanation as to why the RKL2 scheme appears more stable.

An additional technique to improve the accuracy of the result is to smooth out the initial condition. A common practice [73, 188] is to use the average value of the initial

---

[4]It is found in [154, Figure 11], that the region of stability of the RKL2 scheme is wider along the imaginary axis than the region of the Runge-Kutta-Chebyshev scheme with a damping factor $\epsilon = \frac{2}{13}$. Foulon and In't Hout however uses a much larger $\epsilon = 10$ to increase the width of the region of stability because of the relatively high advection present in the Heston PDE. The number of internal stages will increase in accordance with the increased damping factor. With such a large parameter, the region of stability was similar with both schemes. The geometry of the region of stability thus does not offer a conclusive explanation.

condition h at the node of index i closest to the strike level (location of the discontinuity):

$$\bar{h}(s_i) = \frac{2}{s_{i+1} - s_{i-1}} \int_{\frac{s_{i-1}+s_i}{2}}^{\frac{s_i+s_{i+1}}{2}} h(s)ds, \quad s_i \le K < s_{i+1}, \tag{8.72}$$

$\bar{h}$ is then the effective initial condition of the finite difference method.

Kreiss et al. [121] propose a more general smoothing, that guarantees the preservation of second-order accuracy in the general case of parabolic equations. On our problem, the Kreiss smoothing reads

$$\bar{h}(s_i) = \frac{1}{s_{i+1} - s_i} \int_{s_i}^{s_{i+1}} \left(1 + \frac{s - s_i}{s_{i+1} - s_i}\right) h(s)ds$$
$$+ \frac{1}{s_i - s_{i-1}} \int_{s_{i-1}}^{s_i} \left(1 - \frac{s_i - s}{s_i - s_{i-1}}\right) h(s)ds, \tag{8.73}$$

for i verifying $s_{i-1} \le K < s_{i+1}$. For a call or a put option of strike K, two points are smoothed.

8.5.5. DELTA HEDGING AND THE PDE DELTA

In the previous section, we plotted the gamma $\frac{\partial^2 u}{\partial s^2}(s)$ directly obtained from the finite difference grid points. While it is useful to show evidence of oscillations due to a finite difference scheme, it should not be used for trading purposes. Indeed, the raw delta (or gamma) at s_i, is computed from the price at the points (s_{i-1}, s_i, s_{i+1}), but the first moment (or equivalently the forward price) is only preserved at s_i.

The issue is obvious in Figure 8.5.6a, where we plot the raw delta of a short forward contract. We would expect the delta to be -1. Instead, it oscillates between -0.2 and -0.9
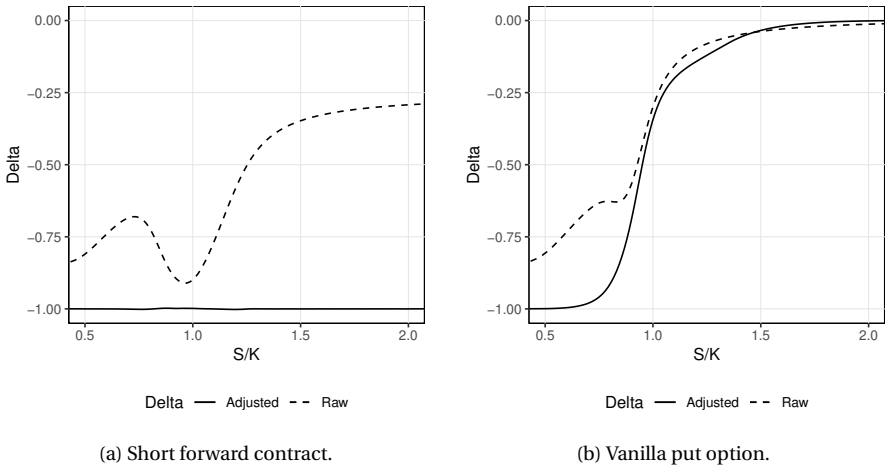

(a) Short forward contract.   (b) Vanilla put option.

Figure 8.5.6: Raw delta and adjusted delta in the Heston-CLV model.

(the end points correspond to the slope of the collocation function g at the boundaries).

In reality, the collocation function g needs to be adjusted for each spot price s_i considered in the plot, so that the first moment is preserved, for each point. In Figures 8.5.6a and 8.5.6b, we recompute the first B-spline coefficient α_0, which is equivalent to a parallel translation of the collocation function (see Section 8.3.2), and we solve the resulting PDE using the modified Craig-Sneyd scheme with Euler damping steps, for each point of the plot. Another approach would be to fully recalibrate the function against each market option quote, taking the Black-Scholes volatility of each option constant, in a similar fashion as practitioners do for the local volatility model.

With the proposed adjustment, the delta of a short forward contract becomes -1, by construction, and the delta of a vanilla put option moves monotonically from -1 to 0, as would be expected.

8.5.6. NUMERICAL EXAMPLES

In order to measure the error due to the discretization in time for each finite difference scheme, we compute the error in the price obtained with various numbers of time steps towards a reference price obtained with a second-order Runge-Kutta scheme with 40000 time steps, using $M = L = 128$ steps for the discretization in s and v. As the asset and variance dimensions are kept constant, we measure here only the error related to the discretization in time.

We apply two half-steps of implicit Euler for the Craig-Sneyd and modified Craig-Sneyd schemes. Without those, the convergence of the initial steps is erratic because of spurious oscillations introduced by the discontinuity in the terminal condition derivatives.

In the figures and tables, we will use the abbreviations *ADE* for Alternating direction explicit, *CS* for Craig-Sneyd, *MCS* for modified Craig-Sneyd, *LS* for Lawson-Swayne, *RKL2* for Runge-Kutta-Legendre of order-2, *SC2B* for stabilizing correction multistep method of BDF2-type.

In Figure 8.5.7, we plot the error in the price of a barrier option of level 0.9 and 6-months maturity, for each finite difference scheme against the number of time steps, when the Heston-CLV model is calibrated to SX5E options of as of February 26, 2016. At maturity, the collocation function g is the quadratic spline whose coefficients are detailed in Table 8.5.1, with a linear extrapolation of left slope $s_L = 0.83293$ and right slope $s_R = 0.26688$. Before maturity, g is the linear interpolation of the identity function and the quadratic spline at maturity. On this data, the maximum diagonal element of the operator matrix A (defined by Equation 8.66) is around 74019. This means that the explicit Euler finite difference scheme will be stable theoretically for $N \geq 36908$ to price options of maturity $T = 0.49863$ years. Second-order convergence corresponds to a linear regression slope of -2 on the log-log plot of the temporal error against the number of time steps. On this example, the modified Craig-Sneyd and SC2B schemes have a slightly lower order of convergence of around 1.5. The other schemes are close to second-order, except for RKL2 which is above second-order here. Although the ADE scheme exhibits a second-order convergence, the absolute error in the price of the barrier option is higher by a factor of thousand than with the other schemes, for a given number of time steps. Consequently, we will not consider the ADE scheme further.

In Figure 8.5.8, we plot the measured order of convergence for a range of barrier lev-

8

Table 8.5.1: Coefficients of the quadratic spline for the collocation function
$g(x) = g_i(x) = a_i + b_i(x - x_i) + c_i(x - x_i)^2 + d_i(x - x_i)^3$ for $x \in [x_i, x_{i+1}]$ at maturity $T = 0.49863$, rounded to the fifth decimal for the Heston parameters $\kappa = 0.35$, $\theta = 0.321$, $\sigma = 1.388$, $\rho = -0.63$ and an initial variance $v_0 = 0.133$.

x_j	a_j	b_j	c_j
0.51712	0.62668	0.83293	-0.38181
0.88945	0.88387	0.54862	3.20097
0.97218	0.95117	1.07831	0.83772
1.01355	0.99722	1.14762	0.31401
1.05492	1.04523	1.17360	-0.31901
1.09629	1.09324	1.14721	-1.38348
1.17903	1.17868	0.91827	-1.96822
1.34451	1.27674	N/A	N/A

els. The order of the RKL2 scheme is consistently above 2.0. The order of the modified Craig-Sneyd scheme is the lowest: 1.6 on average (Table 8.5.2). The order of the other schemes is very close to 2.0.

Table 8.5.2: Order of temporal convergence for vanilla and barrier options. For barrier options, we compute the mean of the measured log-log regression slope, for a range of barrier levels between 0.5 and 0.9.

Scheme	Vanilla	Barrier (mean)
CS	1.9	1.9
MCS	2.0	1.6
LS	2.0	2.0
RKL2	2.1	2.2
SC2B	2.0	1.8

In terms of computational time, the Craig-Sneyd and modified Craig-Sneyd schemes are very similar, and are five times faster than the Lawson-Swayne scheme (Table 8.5.3), where we used a BICGSTAB solver with incomplete-LU preconditioning for the Lawson-Swayne scheme, and a specialized tridiagonal solver for the ADI schemes. The SC2B scheme is twice as fast as the Craig-Sneyd scheme, for a four times larger error. For a given accuracy, the two schemes perform thus similarly. The timing stems from a Julia language implementation, running Julia 1.1 on an AMD Ryzen 1700 CPU.

The performance of a scheme is strongly dependent on the grid geometry. The choice $M = L = 128$ is relatively favorable to the RKL2 scheme. If, on the contrary, we use a very fine grid in the asset dimension, for example $M = 1024$, the stability condition of RKL2 scheme implies the use of many more stages, especially when the number of time steps N is relatively small. Even if the RKL2 scheme would still be an order of magnitude faster than a second-order explicit scheme, it would be less competitive against ADI schemes. Similarly, a higher concentration of points (through a smaller λ_S in Equation (8.53)) requires more stages in the RKL2 scheme, as the maximum eigenvalue is then larger. Note that by choosing $\lambda_S = \frac{K}{4}$, the points are highly concentrated, and thus our example is not
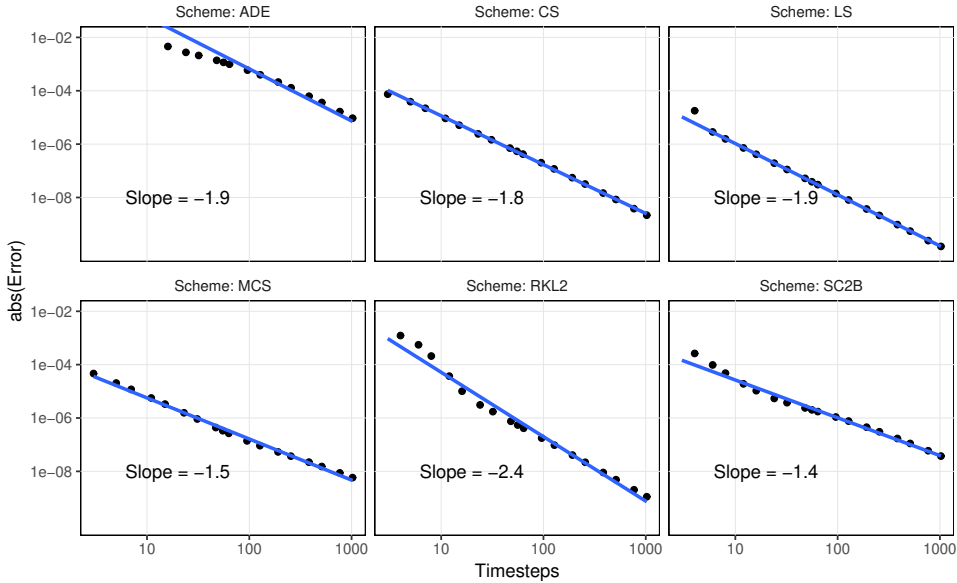
Figure 8.5.7: Convergence of the barrier option price with a barrier level at 0.9, for different finite difference discretization schemes applied to the Heston CLV PDE when the Heston-CLV model is calibrated to SX5E options of as of February 26, 2016.

so favorable to the RKL2 scheme after all. On the other side, when many time steps are used, then the RKL2 scheme becomes even more efficient since less stages are required.

In Table 8.5.4, we rank the finite difference methods according to a few criteria:

- stability: will the scheme diverge in some cases? Does it damp discontinuities well?

- accuracy: how is the accuracy for a moderate number of time steps?

- performance: how slow is it to compute on a standard grid? on a more concentrated grid?

- ease of implementation: how difficult is it to code? ADI schemes are more involved than direct schemes. Two-steps schemes usually require an additional restart procedure after each discontinuity in time, for example, in the case of daily or weekly monitored barrier options.

Overall, we find that the modified Craig-Sneyd scheme strikes a good balance between stability, good damping properties, accuracy and computational cost. The SC2B scheme is also attractive, but, it requires a restart procedure at each payoff discontinuity in time. In a similar fashion, the Craig-Sneyd scheme will also require new damping steps at each payoff discontinuity. In terms of ease of implementation, the RKL2 scheme
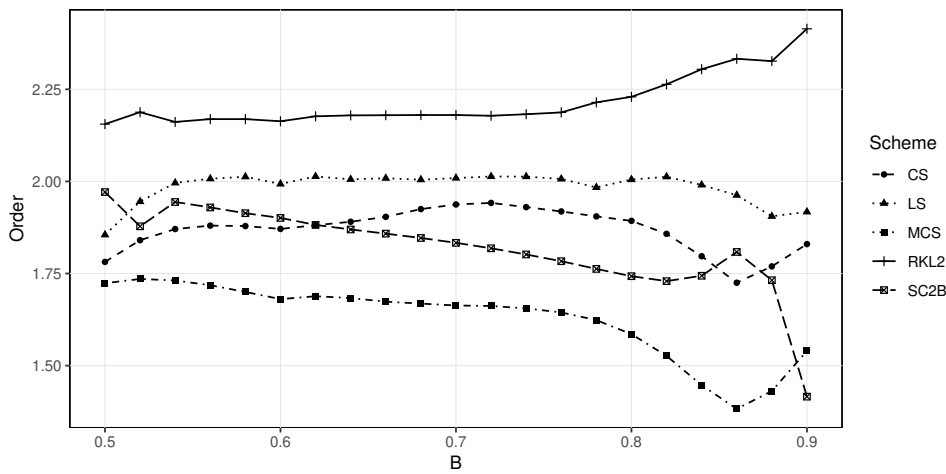
Figure 8.5.8: Measured order of convergence for different barrier levels, with different finite difference discretization schemes applied to the Heston CLV PDE when the Heston-CLV model is calibrated to SX5E options of as of February 26, 2016.

Table 8.5.3: Root mean square error in the price of a barrier option, along with the computational time, using a fixed grid size $L = 128$, $M = 128$ and different number of time steps, for a barrier $B = 0.8$. The reference is the price obtained by the second-order Runge-Kutta scheme using $N = 40000$, which takes 41s.

Scheme	64 time steps		256 time steps	
	Error	Time (s)	Error	Time (s)
LS	$3.2 \cdot 10^{-7}$	2.42	$2.0 \cdot 10^{-8}$	8.60
CS with damping	$8.7 \cdot 10^{-7}$	0.45	$5.7 \cdot 10^{-8}$	1.41
MCS	$8.9 \cdot 10^{-7}$	0.30	$1.1 \cdot 10^{-7}$	1.22
MCS with damping	$1.3 \cdot 10^{-6}$	0.45	$1.2 \cdot 10^{-7}$	1.43
RKL2	$2.0 \cdot 10^{-6}$	0.25	$1.1 \cdot 10^{-7}$	0.56
SC2B	$3.9 \cdot 10^{-6}$	0.17	$4.3 \cdot 10^{-7}$	0.69
ADE	$1.5 \cdot 10^{-3}$	0.55	$1.3 \cdot 10^{-4}$	2.17

Table 8.5.4: Adequacy of each finite difference scheme, when applied to the Heston-CLV PDE.

Scheme	Stability	Accuracy	Performance	Ease-of-implementation
CS with damping	++	+	+	- -
LS	++	++	- -	++
MCS	+	+	++	-
RKL2	-	+	+	++
SC2B	++	+	++	- -

is particularly attractive. It may easily be applied to higher-order space discretizations while preserving a very good performance, since it is fully explicit.

8.6. CONCLUSION

In this chapter, we have focused on different important aspects of the so-called Heston-CLV model. We have presented a fast and flexible calibration of the Heston-CLV model, through a specific B-spline parameterization, and a custom adaptive Filon quadrature. A minor modification of the DVSS2 scheme of Lenkšas and Mackevičius [135] allows the pricing of *exotic* options under Monte-Carlo with proven second-order convergence. We noticed that the non-martingality, inherent to the class of Markov functional models, is very mild when the model is calibrated to market vanilla option prices. The drift is much smaller than with one-dimensional Markov functional models.

Finally, we derived the PDE followed by the price of financial derivatives under the Heston-CLV model, in terms of the asset price and variance variables. In those coordinates, barrier options (and other path-dependent options) may be priced by alternating direction implicit methods (ADI), while preserving their order of convergence.

If we consider only stability and ease-of-implementation, the Lawson-Swayne scheme is particularly relevant, because of its *L*-stability. But this is at the cost of performance. If we add performance as an important criterion, the modified Craig-Sneyd ADI scheme becomes the most relevant scheme for the Heston-CLV PDE. Multisteps ADI schemes have the advantage of possessing stronger damping properties, but a restart procedure is necessary as soon as there is a discontinuity in time in the financial derivative payoff. If there are many discontinuities, such as in the case of a daily monitored barrier option, the restart procedure may affect the overall order of convergence of the scheme. We leave for further research the investigation of which restart procedure is the most appropriate.

The second-order Runge-Kutta-Legendre explicit scheme is an interesting simpler alternative that performs well, sometimes better than ADI methods, depending on the finite difference grid geometry. Furthermore, being explicit, higher-order space discretizations may easily be handled. In contrast, ADI methods will require a more complex, slower, sparse matrix solver. In cases where advection is particularly large, the Runge-Kutta-Legendre scheme may diverge as its stability region is bounded on the imaginary axis.

While we studied the Heston-CLV model in particular, our analysis of the Monte-Carlo schemes and the finite difference schemes is also relevant to stochastic local volatility models, which also involve a two-factor SDE (respectively a PDE) with time and asset dependent coefficients. In the context of a stochastic-local volatility model, the Dupire local volatility corresponding to a term-structure of collocation functions with an appropriate interpolation in time can be computed exactly, without any numerical discretization error, as shown in Appendix 8.C.

8

8.A. The Heston characteristic function

In order to avoid complex discontinuities, we rely on Gatheral's formulation for the normalized Heston characteristic function [144]:

$$\psi(z) = e^{\frac{v_0}{\sigma^2}\frac{1-e^{-D(z)T}}{1-Ge^{-D(z)T}}(\kappa-\mathrm{i}\rho\sigma z-D(z))+\frac{\kappa\theta}{\sigma^2}\left((\kappa-\mathrm{i}\rho\sigma z-D(z))T-2\ln\left(\frac{1-Ge^{-D(z)T}}{1-G(z)}\right)\right)} \tag{8.74}$$

with

$$D(z) = \sqrt{(\kappa-\mathrm{i}\rho\sigma z)^2+(z^2+\mathrm{i}z)\sigma^2}, \tag{8.75}$$

$$G(z) = \frac{\kappa-\mathrm{i}\rho\sigma z-D(z)}{\kappa-\mathrm{i}\rho\sigma z+D(z)}. \tag{8.76}$$

The standard characteristic function is $\mathbb{E}[e^{\mathrm{i}z\ln(F(T,T))}] = e^{\mathrm{i}z\ln(F(0,T))}\psi(z)$.

8.B. Bachelier model with absorption

In the classical Bachelier (or normal) model, the asset $F(t, T)$ follows the stochastic differential equation

$$dF(t) = \sigma\,dW(t) \tag{8.77}$$

where W is a Brownian motion and the initial value is $F(0, T) = f$. The asset has a non-zero probability of being negative. In many applications, it is important that the asset stays above a threshold. For example, stocks must be positive, or interest rates are bounded below by a negative rate. The non-negativity becomes particularly important when the asset is to be used as a numeraire.

In the Bachelier model with absorption, once the asset reaches the threshold level L, it sticks there. This model has been previously explored in [107], but many of the equations in his paper contains errors. Absorption is relatively common in many stochastic models, such as the constant elasticity of variance (CEV) with an exponent $\beta \in \left(0, \frac{1}{2}\right)$, or the related SABR model [84]. The evolution of the asset may also be modelized as a partial differential equation (PDE). The probability density p follows the Fokker-Planck PDE:

$$\frac{\partial p}{\partial t}(F, t) = \frac{1}{2}\sigma^2\frac{\partial^2 p}{\partial F^2}(F, t), \tag{8.78}$$

with initial condition $p(F, 0) = \delta(F - f)$, for $F > L$ and boundary $p(L, t) = 0$.

We use the method of reflection to solve this equation [113, p. 220]: we continue $p(S)$ to the real line and define $\bar{p}$ the solution of Equation (8.78) on the real line with initial condition $\bar{p}(F, 0) = \delta(F - f) - \delta(F + f - 2L)$. $\bar{p}$ satisfies the initial condition $\bar{p}(F, 0) = \delta(F - f)$, for $F > L$. It also satisfies $\bar{p}(L, t) = 0$ since $\bar{p}(2L - F) + \bar{p}(F)$ is a bounded solution of Equation (8.78) with initial value 0 and hence stays at 0 for all t by the uniqueness theorem.

By linearity, the solution is

$$p(F, t) = \phi\left(\frac{F - f}{\sigma\sqrt{t}}\right) - \phi\left(\frac{F + f - 2L}{\sigma\sqrt{t}}\right), \tag{8.79}$$

where ϕ is the normal probability density function, $\phi(x) = \frac{1}{\sqrt{2\pi}}e^{-\frac{1}{2}x^2}$.

The conservation of the probability over $[L, +\infty)$ means that the probability of absorption P_a at $F = L$ is:

$$\begin{aligned}
P_a(t) &= 1 - \int_L^\infty \phi\left(\frac{F - f}{\sigma\sqrt{t}}\right) - \phi\left(\frac{F + f - 2L}{\sigma\sqrt{t}}\right) dF \\
&= 1 - \left[1 - \Phi\left(\frac{L - f}{\sigma\sqrt{t}}\right) - 1 + \Phi\left(\frac{f - L}{\sigma\sqrt{t}}\right)\right] \\
&= 2\Phi\left(\frac{L - f}{\sigma\sqrt{t}}\right).
\end{aligned} \tag{8.80}$$

Undiscounted vanilla option prices can then be computed through the Breeden-Litzenberger formula [28] for $K > L$,

$$V_{\text{call}}(K, T) = \int_K^\infty (F - K) p(T, F) dF, \tag{8.81}$$

$$V_{\text{put}}(K, T) = (K - L) P_a(T) + \int_L^K (K - F) p(T, F) dF. \tag{8.82}$$

We obtain

$$\begin{aligned}
V_{\text{call}}(K, T) =& \sigma\sqrt{T}\phi\left(\frac{f - K}{\sigma\sqrt{T}}\right) + (f - K)\Phi\left(\frac{f - K}{\sigma\sqrt{T}}\right) \\
& - \sigma\sqrt{T}\phi\left(\frac{2L - f - K}{\sigma\sqrt{T}}\right) - (2L - f - K)\Phi\left(\frac{2L - f - K}{\sigma\sqrt{T}}\right),
\end{aligned} \tag{8.83}$$

and

$$\begin{aligned}
V_{\text{put}}(K, T) =& \sigma\sqrt{T}\phi\left(\frac{K - f}{\sigma\sqrt{T}}\right) + (K - f)\Phi\left(\frac{K - f}{\sigma\sqrt{T}}\right) \\
& - \sigma\sqrt{T}\phi\left(\frac{K + f - 2L}{\sigma\sqrt{T}}\right) - (2L - f - K)\Phi\left(\frac{2L - f - K}{\sigma\sqrt{T}}\right).
\end{aligned} \tag{8.84}$$

In particular, the undiscounted prices obey the standard put-call parity relationship $V_{\text{call}} - V_{\text{put}} = F - K$ and the martingale property is preserved in this model.

8.C. LOCAL VOLATILITY FOR A TERM-STRUCTURE OF COLLOCATED SMILES

The discrete version of the calendar spread no-arbitrage condition reads [71]

$$\frac{V_{\text{call}}(K_2, T_2)}{K_2} \geq \frac{V_{\text{call}}(K_1, T_1)}{K_1}, \tag{8.85}$$

for $T_2 \geq T_1$, where V_{call} is the undiscounted call option price and the strikes K_2, K_1 are chosen so that the forward moneyness is constant:

$$\frac{K_1}{F(0,T_1)} = \frac{K_2}{F(0,T_2)} .$$

The relation can be derived from Jensen inequality in the absence of cash dividends (proportional dividends or a continuous dividends yield are acceptable), knowing that the process $\frac{S(t)}{F(0,t)}$ is a martingale. This discrete arbitrage-free inequality can be used to define a continuous arbitrage-free interpolation in time assuming that the inequality holds at two expiries t_1 and t_2. For example, we can define the prices at time $t_1 < t < t_2$ by

$$V_{\text{call}}(K,t) = \frac{t-t_1}{t_2-t_1} \frac{F(0,t)}{F(0,t_2)} V_{\text{call}}\left(\frac{KF(0,t_2)}{F(0,t)}, t_2\right) + \frac{t_2-t}{t_2-t_1} \frac{F(0,t)}{F(0,t_1)} V_{\text{call}}\left(\frac{KF(0,t_1)}{F(0,t)}, t_1\right).$$

(8.86)

Dupire [55] expresses the local volatility σ_L as

$$\sigma_L^2(K,T) = 2\frac{\frac{\partial V_{\text{call}}^0}{\partial T}}{K^2 \frac{\partial^2 V_{\text{call}}^0}{\partial K^2}},$$

(8.87)

where $V_{\text{call}}^0(K,T)$ is the undiscounted call option price on a *fixed* forward $F(0,T)$. With the collocation method, the Dupire local volatility has a closed form expression with the above interpolation of Call prices in time.

$$\frac{\partial V_{\text{call}}^0}{\partial T}(K,t) = \frac{K}{t_2-t_1}\left(\frac{V_{\text{call}}(K_2,t_2)}{K_2} - \frac{V_{\text{call}}(K_1,t_1)}{K_1}\right)$$

(8.88)

for $\frac{K}{F(0,t)} = \frac{K_1}{F(0,T_1)} = \frac{K_2}{F(0,T_2)}$.

$$\frac{\partial^2 V_{\text{call}}^0}{\partial K^2}(K,t) = \frac{t-t_1}{t_2-t_1} \frac{K_2}{K} \frac{\partial^2 V_{\text{call}}}{\partial K^2}(K_2,t_2) + \frac{t_2-t}{t_2-t_1} \frac{K_1}{K} \frac{\partial^2 V_{\text{call}}}{\partial K^2}(K_1,t_1).$$

(8.89)

When the call option prices are determined by the collocation method with a function g_l for the maturity T_l, we have

$$\frac{\partial V_{\text{call}}}{\partial K}(K_i) = -\Phi(-c_{K_i}), \quad \frac{\partial^2 V_{\text{call}}}{\partial K^2}(K_i) = \frac{\phi(c_{K_i})}{g_i{}'(c_{K_i})},$$

(8.90)

with $c_{K_i} = g_i^{-1}(K_i)$. For $t_1 < t < t_2$, the Dupire equation becomes

$$\sigma_L(K,t) = 2K^2 \frac{\frac{V_{\text{call}}(K_2,t_2)}{K_2} - \frac{V_{\text{call}}(K_1,t_1)}{K_1}}{(t-t_1)K_2 \frac{\phi(c_{K_2})}{g_2{}'(c_{K_2})} + (t_2-t)K_1 \frac{\phi(c_{K_1})}{g_1{}'(c_{K_1})}} .$$

(8.91)

In particular, there will be no numerical discretization error when computing Dupire local volatility σ_L.

9

CONCLUSIONS AND OUTLOOK

9.1. CONCLUSIONS

In this thesis, we solved one-dimensional and two-dimensional, linear and non-linear PDEs arising in finance with stable and efficient finite difference methods. We also proposed a new Fourier method to price European options under stochastic volatility models possessing a known characteristic function, and a variation of a second-order Monte-Carlo method to price exotic options under the Heston stochastic volatility model and its associated models, such as the Heston collocated volatility model and the Heston stochastic local volatility model.

In Chapter 2, we have shown how the TR-BDF2 scheme can be applied, firstly to the non-linear PDE corresponding to the pricing of American options under the (extended) Black-Scholes model, and secondly to the HJB PDE arising from the uncertain volatility model. The scheme does not suffer from the Crank-Nicolson oscillations problem, particularly visible in the option greeks. It is more resilient to the grid geometry and to the underlying PDE in general. A common fix for the Crank-Nicolson scheme is the Rannacher smoothing steps. The latter allow to damp the oscillations significantly for European options, but not always for American options.

Chapter 3 develops an analysis for the positivity of a finite difference scheme on the simple problem of a diffusion equation with constant volatility and a Dirac delta initial condition. Our analysis is similar to a von Neumann stability analysis. We are however not interested in the amplification factor relating the L2-norm of the solution at subsequent time steps, but we focus on the discrete probability density values at the Dirac location, and whether they stay positive, or whether they oscillate. It is found that the BDF2, Lawson-Morris and BDF1 Richardson extrapolation schemes preserve the positivity of the density at the spike at every time step, for any time step size. The Lawson-Swayne and TR-BDF2 schemes preserve the positivity from the second time step onwards, for any time step size. Finally, the Rannacher smoothing also preserves positivity with an initialization of two half time steps of BDF1, but requires four half time steps of BDF1 to overcome the oscillations at the spike. This is particularly relevant in Chapter 4, where we apply a variety of finite difference schemes to the arbitrage-free SABR PDE for the marginal probability density. We find that it is possible to accurately compute option prices under the arbitrage-free SABR model with very few time steps, even for long maturities. The Rannacher smoothing steps are a particularly simple way to improve accuracy significantly of the Crank-Nicolson scheme on this problem. However, as the number of time steps decreases, the lower convergence of the Euler smoothing steps becomes more apparent. The simpler BDF2 scheme is more efficient on this problem. Other less known

schemes such as TR-BDF2 or Lawson-Swayne further increase the efficiency. Thus, with a careful choice of finite difference scheme, the arbitrage-free PDE of Hagan et al. [84] is particularly competitive to the one-step finite difference approach of Andreasen and Huge [13].

In Chapters 5 and 6, we apply the stochastic collocation technique directly to market options quotes in order to produce a smooth and accurate interpolation and extrapolation of the option prices, even on challenging equity or equity index option examples. Specific parameterizations, which ensure the monotonicity of the collocation polynomial or the collocation B-spline, as well as the conservation of the zero-th and first moments of the risk-neutral distribution transparently during the optimization, guarantee the absence of arbitrage. This results in closed-form formula for CMS convexity adjustments, which can thus be efficiently calibrated jointly with interest rate swaptions. Similarly, an exponential B-spline representation results in a simple analytical expression for the price of a variance swap. Furthermore, the latter price being a linear combination of the B-spline parameters, the market prices of variance swaps may be integrated in the calibration of the B-spline at a minimal additional computational cost in order to obtain a better representation of the wings (or tails) of the implied volatility, to which the variance swap is particularly sensitive. We have also presented a simple non-parametric technique to de-arbitrage a set of option prices, which may be used independently of the B-spline collocation method.

Chapter 7 describes a new adaptive Filon quadrature to price options under the Heston model. It has better performance than popular alternatives and is particularly interesting in the context of model calibration where many options of different strike but same maturity are priced. Being adaptive, it does not suffer from having to choose a non-obvious parameter value, typically the number of points of non-adaptive quadratures, or the truncation level for the Cos method.

In chapter 8, we apply the B-spline collocation technique of chapter 6 along with the adaptive Filon quadrature of chapter 7 to calibrate the Heston collocated local volatility model of Grzelak [77] to market option prices. We propose a modification of the DVSS2 scheme of Lenkšas and Mackevičius [135] in order to more accurately price forward starting options, and put in evidence the second-order convergence of the scheme, when applied to the Heston-CLV model. Finally, we apply several finite difference schemes to the corresponding Heston-CLV PDE, with a focus on pricing barrier options. If we consider only stability and ease-of-implementation, the Lawson-Swayne scheme is found to be particularly relevant, because of its L-stability. But this is at the cost of performance. If we add performance as a criterion, the modified Craig-Sneyd ADI scheme becomes the most relevant scheme for the Heston-CLV PDE. Multi-step ADI schemes have the advantage of possessing stronger damping properties, but a restart procedure is necessary as soon as there is a discontinuity in time in the financial derivative payoff. If there are many discontinuities, such as in the case of a daily monitored barrier option, the restart procedure may affect the overall order of convergence of the scheme. The second-order Runge-Kutta-Legendre explicit scheme is an interesting simpler alternative that performs well, sometimes better than ADI methods, depending on the finite difference grid geometry. Furthermore, being explicit, higher-order space discretizations may easily be handled. In contrast, ADI methods will require a more complex, slower, sparse

matrix solver. In cases where advection is particularly large, the Runge-Kutta-Legendre scheme may diverge as its stability region is bounded on the imaginary axis.

Regarding the Heston-CLV model, we notice that the price of a contract on a future performance is reasonably in line with the theoretical price, despite the lack of martingality of the model, when the Heston driver process is calibrated to the market vanilla options. We put in evidence that the delta and gamma greeks should however not be computed directly from the finite difference grid. While we propose a fix to obtain meaningful greeks, this makes the interpretation of the solution of the Heston-CLV PDE for a given exotic option not so obvious. Furthermore, we find that the numerical techniques are not necessarily much simpler than those of the more standard stochastic local volatility models: there is the problem of absorption to eventually deal with in the Monte-Carlo simulation as well as in the B-spline calibration and the PDE is of similar complexity. In fact, while we studied the Heston-CLV model in particular, our analysis of the Monte-Carlo schemes and the finite difference schemes is relevant to stochastic local volatility models, which also involve a two-factor SDE (respectively a two-dimensional PDE) with time- and asset-dependent coefficients. In the context of a stochastic-local volatility model, the stochastic collocation technique may still be used to capture the terminal distribution at each market option maturity in an arbitrage-free manner, as we show that the Dupire local volatility corresponding to a term-structure of collocation functions with an appropriate interpolation in time can be computed exactly, without any numerical discretization error.

9.2. Outlook

Our analysis of the TR-BDF2 scheme in the context of American option pricing may be enhanced with a proof of an L^2-error estimate for the one-dimensional diffusion with an obstacle term, in a similar fashion as Bokanowski and Debrabant [26] do for the BDF2 scheme.

Our analysis of the positivity of a finite difference scheme on the simple problem of a diffusion with constant volatility and Dirac initial condition may be generalized to cover all points of the finite difference grid, and not only the line corresponding to the Dirac location. Appendices 3.A and 3.B may serve as a starting point.

In [60], Filipovic et al. study the application of polynomial processes for energy prices. The collocated volatility model with a polynomial collocation function is similar to the application of a polynomial map onto the driver process. It would be interesting to formalize the link between polynomial processes and the collocated volatility model, as it may offer new applications for the collocated volatility model and new insights into polynomial processes.

Finally, the application of multi-step ADI methods of Hundsdorfer and In't Hout [95] for the pricing of general exotic derivatives, which may have discontinuities in time, would benefit from an investigation of which restart procedure is the most appropriate to keep the second-order convergence in practice.

9

REFERENCES

[1] G. E. Alefeld, F. A. Potra, and Y. Shi. Algorithm 748: enclosing zeros of continuous functions. *ACM Transactions on Mathematical Software (TOMS)*, 21(3):327–344, 1995.

[2] C. Alexander and L. Nogueira. Hedging with stochastic and local volatility. Technical report, Henley Business School, Reading University, 2004.

[3] C. Alexander, L. Nogueira, et al. Stochastic local volatility. Technical report, Henley Business School, Reading University, 2008.

[4] V. Alexiades, G. Amiez, and P.-A. Gremaud. Super-time-stepping acceleration of explicit schemes for parabolic problems. *Communications in numerical methods in engineering*, 12(1):31–42, 1996.

[5] D. N. d. G. Allen and R. V. Southwell. Relaxation methods applied to determine the motion, in two dimensions, of a viscous fluid past a fixed cylinder. *The Quarterly Journal of Mechanics and Applied Mathematics*, 8(2):129–145, 1955.

[6] L. B. G. Andersen. Efficient simulation of the Heston stochastic volatility model. *Available at SSRN 946405*, 2007.

[7] L. B. G. Andersen and R. Brotherton-Ratcliffe. The equity option volatility smile: a finite difference approach. *Journal of Computational Finance*, 1(2):5–38, 1998.

[8] L. B. G. Andersen and V. V. Piterbarg. Moment explosions in stochastic volatility models. *Finance and Stochastics*, 11(1):29–50, 2007.

[9] L. B. G. Andersen and V. V. Piterbarg. Interest rate modeling–volume iii: Products and risk management. *Atlantic Financial Press*, 1:702–708, 2010.

[10] L. B. G. Andersen and V. V. Piterbarg. *Interest Rate Modeling, Volume I: Foundations and Vanilla Models*. Atlantic Financial Press London, 2010.

[11] M. Andersen, J. Dahl, and L. Vandenberghe. Cvxopt: A python package for convex optimization. *abel. ee. ucla. edu/cvxopt*, 2013.

[12] J. Andreasen and B. N. Huge. Volatility interpolation. *Risk*, 24(3):76, 2011.

[13] J. Andreasen and B. N. Huge. Zabr–expansions for the masses. *Available at SSRN 1980726*, 2011.

[14] A. Antonov, M. Konikov, and M. Spector. The free boundary sabr: Natural extension to negative rates. *Available at SSRN 2557046*, 2015.

[15] J. Arneric, Z. Aljinović, and T. Poklepović. Extraction of market expectations from risk-neutral density. 33:235–256, 2015.

[16] R. C. Aster, B. Borchers, and C. H. Thurber. *Parameter estimation and inverse problems*. Elsevier, 2018.

[17] M. Avellaneda, A. Levy, and A. Paras. Pricing and hedging derivative securities in markets with uncertain volatilities. *Applied Mathematical Finance*, 2(2):73–88, 1995.

[18] B. Bahra. Implied risk-neutral probability density functions from option prices: a central bank perspective1. In *Forecasting Volatility in the Financial Markets (Third Edition)*, pages 201–226. Elsevier, 2007.

[19] R. Bank, W. Coughran, W. Fichtner, E. Grosse, D. Rose, and R. Smith. Transient simulation of silicon devices and circuits. *IEEE Transactions on Computer-Aided Design of Integrated Circuits and Systems*, 4(4):436–451, 1985.

[20] D. S. Bates. Jumps and stochastic volatility: Exchange rate processes implicit in deutsche mark options. *Review of financial studies*, 9(1):69–107, 1996.

[21] K. J. Bathe. Conserving energy and momentum in nonlinear dynamics: A simple implicit time integration scheme. *Computers & Structures*, 85(7-8):437–445, 2007.

[22] K.-J. Bathe and M. M. I. Baig. On a composite implicit time integration procedure for nonlinear dynamics. *Computers & Structures*, 83(31):2513–2524, 2005.

[23] S. Benaim, M. Dodgson, and D. Kainth. An arbitrage-free method for smile extrapolation. *Royal Bank of Scotland, Technical report*, 2008.

[24] F. Black and M. Scholes. The pricing of options and corporate liabilities. *Journal of political economy*, 81(3):637–654, 1973.

[25] R. R. Bliss and N. Panigirtzoglou. Option-implied risk aversion estimates. *The journal of finance*, 59(1):407–446, 2004.

[26] O. Bokanowski and K. Debrabant. High order finite difference schemes for some nonlinear diffusion equations with an obstacle term. *arXiv preprint arXiv:1802.05681*, 2018.

[27] C. Bolley and M. Crouzeix. Conservation de la positivité lors de la discrétisation des problèmes d'évolution paraboliques. *ESAIM: Mathematical Modelling and Numerical Analysis-Modélisation Mathématique et Analyse Numérique*, 12(3):237–245, 1978.

[28] D. T. Breeden and R. H. Litzenberger. Prices of state-contingent claims implicit in option prices. *Journal of business*, pages 621–651, 1978.

[29] M. J. Brennan and E. S. Schwartz. The valuation of American put options. *Journal of Finance*, 32(2):449–462, 1977.

[30] O. Brockhaus. Implied sampling: Properties and pitfalls. Commerzbank, 2006.

[31] P. Carr and R. Lee. Robust replication of volatility derivatives. *preprint*, 2008.

[32] P. Carr and D. Madan. Option valuation using the fast fourier transform. *Journal of Computational Finance*, 2(4):61–73, 1999.

[33] P. Carr and D. Madan. Towards a theory of volatility trading. *Option Pricing, Interest Rates and Risk Management, Handbooks in Mathematical Finance*, pages 458–476, 2001.

[34] S. M. Chase and L. D. Fosdick. An algorithm for filon quadrature. *Communications of the ACM*, 12(8):453–457, 1969.

[35] M. K. C. Cheng. A new framework to estimate the risk-neutral probability density functions embedded in options prices. (10-181), 2010.

[36] P. Christoffersen, S. Heston, and K. Jacobs. The shape and term structure of the index option smirk: Why multifactor stochastic volatility models work so well. *Management Science*, 55(12):1914–1932, 2009.

[37] S. Conte and C. de Boor. Elementary numerical analysis—an algorithmic approach, 1972, 1980.

[38] S. Corlay. B-spline techniques for volatility modeling. *Journal of Computational Finance*, 19(3), 2016.

[39] J. C. Cox, J. E. Ingersoll Jr, and S. A. Ross. A theory of the term structure of interest rates. *Econometrica*, 53(2):385–408, 1985.

[40] I. J. Craig and A. D. Sneyd. An alternating-direction implicit scheme for parabolic equations with mixed derivatives. *Computers & Mathematics with Applications*, 16(4):341–350, 1988.

[41] Y. Cui, S. del Baño Rollin, and G. Germano. Full and fast calibration of the Heston stochastic volatility model. *European Journal of Operational Research*, 2017.

[42] T. A. Davis. Algorithm 832: Umfpack v4. 3—an unsymmetric-pattern multifrontal method. *ACM Transactions on Mathematical Software (TOMS)*, 30(2):196–199, 2004.

[43] C. De Boor, C. De Boor, C. De Boor, and C. De Boor. *A practical guide to splines*, volume 27. Springer-Verlag New York, 1978.

[44] N. Deguillaume, R. Rebonato, and A. Pogudin. The nature of the dependence of the magnitude of rate moves on the rates levels: a universal relationship. *Quantitative Finance*, 13(3):351–367, 2013.

[45] K. Demeterfi, E. Derman, M. Kamal, and J. Zou. More than you ever wanted to know about volatility swaps. *Goldman Sachs quantitative strategies research notes*, 41, 1999.

9

[46] Y. D'Halluin, P. Forsyth, K. Vetzal, and G. Labahn. A numerical PDE approach for pricing callable bonds. *Applied Mathematical Finance*, 8(1):49–77, 2001.

[47] S. Dharmaraja. An analysis of the tr-bdf2 integration scheme. *Thesis (S.M.) - Massachusetts Institute of Technology*, pages 31–35, 2007.

[48] S. Dharmaraja, Y. Wang, and G. Strang. Optimal stability for trapezoidal-backward difference split-steps. *IMA Journal of Numerical Analysis*, 2009.

[49] A. S. Dickinson. Numerical approximation of option premia in displaced-lognormal Heston models. *Available at SSRN 1833438*, 2011.

[50] R. L. Dougherty, A. S. Edelman, and J. M. Hyman. Nonnegativity-, monotonicity-, or convexity-preserving cubic and quintic hermite interpolation. *Mathematics of Computation*, 52(186):471–494, 1989.

[51] P. Doust. No-arbitrage sabr. *The Journal of Computational Finance*, 15(3):3, 2012.

[52] D. J. Duffy. A critique of the crank nicolson scheme strengths and weaknesses for financial instrument pricing. *Wilmott Magazine*, 2004.

[53] D. J. Duffy. Unconditionally stable and second-order accurate explicit finite difference schemes using domain transformation: part i one-factor equity problems. *Available at SSRN 1552926*, 2009.

[54] D. J. Duffy and A. Germani. *C# for Financial Markets*. John Wiley & Sons, 2013.

[55] B. Dupire et al. Pricing with a smile. *Risk*, 7(1):18–20, 1994.

[56] B. L. Ehle. *On Pade Approximations to the Exponential Function and A-stable Methods for the Numerical Solution of Initial Value Problems*. PhD thesis, University of Waterloo, 1969.

[57] P. H. Eilers and B. D. Marx. Flexible smoothing with b-splines and penalties. *Statistical science*, pages 89–102, 1996.

[58] T. O. Espelid. Doubly adaptive quadrature routines based on newton–cotes rules. *BIT Numerical Mathematics*, 43(2):319–337, 2003.

[59] F. Fang and C. W. Oosterlee. A novel pricing method for european options based on fourier-cosine series expansions. *SIAM Journal on Scientific Computing*, 31(2):826–848, 2008.

[60] D. Filipović, M. Larsson, and T. Ware. Polynomial processes for power prices. *Swiss Finance Institute Research Paper*, (18-34), 2018.

[61] L. N. G. Filon. On a quadrature formula for trigonometric integrals. *Proceedings of the Royal Society of Edinburgh*, 49:38–47, 1928.

[62] E. Flinn. A modification of filon's method of numerical integration. *Journal of the ACM (JACM)*, 7(2):181–184, 1960.

[63] E. Flint and E. Maré. Estimating option-implied distributions in illiquid markets and implementing the ross recovery theorem. *South African Actuarial Journal*, 17(1):1–28, 2017.

[64] M. Forde, A. Jacquier, and R. Lee. The small-time smile and term structure of implied volatility under the Heston model. *SIAM Journal on Financial Mathematics*, 3(1):690–708, 2012.

[65] P. Forsyth and K. Vetzal. Quadratic convergence for valuing american options using a penalty method. *SIAM Journal on Scientific Computing*, 23(6):2095–2122, 2002.

[66] C. P. Fries. Markov functional modeling of equity, commodity and other assets. 2006.

[67] P. K. Friz and M. K. Ressel. Moment explosions. *Encyclopedia of Quantitative Finance*, 2010.

[68] W. Gander. On halley's iteration method. *American Mathematical Monthly*, pages 131–134, 1985.

[69] W. Gander and W. Gautschi. Adaptive quadrature revisited. *BIT Numerical Mathematics*, 40(1):84–101, 2000.

[70] C. Gardner, W. Nonner, and R. S. Eisenberg. Electrodiffusion model simulation of ionic channels: 1D simulations. *Journal of Computational Electronics*, 3(1):25–31, 2004.

[71] J. Gatheral and A. Jacquier. Arbitrage-free SVI volatility surfaces. *Quantitative Finance*, 14(1):59–71, 2014.

[72] J. Gatheral and M. Lynch. Lecture 1: Stochastic volatility and local volatility. *Case Studies in Financial Modeling Notes, Courant Institute of Mathematical Sciences*, 2004.

[73] M. Giles and R. Carter. Convergence analysis of crank-nicolson and rannacher time-marching. *Journal of Computational Finance*, 9(4):89, 2006.

[74] J. Glass. Smooth-curve interpolation: A generalized spline-fit procedure. *BIT Numerical Mathematics*, 6(4):277–293, 1966.

[75] I. Good. The colleague matrix, a chebyshev analogue of the companion matrix. *The Quarterly Journal of Mathematics*, 12(1):61–68, 1961.

[76] A. Gourlay and J. L. Morris. The extrapolation of first order methods for parabolic partial differential equations, ii. *SIAM Journal on Numerical Analysis*, 17(5):641–655, 1980.

[77] L. A. Grzelak. The collocating local volatility framework – a fresh look at efficient pricing with smile. *International Journal of Computer Mathematics*, 0(0):1–20, 2018.

9

[78] L. A. Grzelak and C. W. Oosterlee. From arbitrage to arbitrage-free implied volatilities. *Journal of Computational Finance*, 20(3):31–49, 2017.

[79] L. A. Grzelak, J. A. S. Witteveen, M. Suarez-Taboada, and C. W. Oosterlee. The stochastic collocation Monte-Carlo sampler: highly efficient sampling from 'expensive'distributions. *Quantitative Finance*, pages 1–18, 2018.

[80] J. Guyon and P. Henry-Labordere. The smile calibration problem solved. *Available at SSRN 1885032*, 2011.

[81] T. Haentjens and K. J. In't Hout. Alternating direction implicit finite difference schemes for the Heston-Hull-White partial differential equation. *The Journal of Computational Finance*, 16(1):83, 2012.

[82] P. S. Hagan. Convexity conundrums: Pricing cms swaps, caps, and floors. *The Best of Wilmott*, page 305, 2005.

[83] P. S. Hagan. Change of variables and conservative numerical schemes. *Not published*, 2013.

[84] P. S. Hagan, D. Kumar, A. Lesniewski, and D. Woodward. Arbitrage-free sabr. *Wilmott*, 2014(69):60–75, 2014.

[85] P. S. Hagan, D. Kumar, A. S. Lesniewski, and D. E. Woodward. Managing smile risk. *Wilmott magazine*, 2002.

[86] P. S. Hagan, D. Kumar, A. S. Lesniewski, and D. E. Woodward. Universal smiles. *Wilmott*, 2016(84):40–55, 2016.

[87] Z. Hai-Ming and C. Xiao-Fei. Self-adaptive filon's integration method and its application to computing synthetic seismograms. *Chinese Physics Letters*, 18(3):313, 2001.

[88] P. C. Hansen. Analysis of discrete ill-posed problems by means of the l-curve. *SIAM review*, 34(4):561–580, 1992.

[89] P. C. Hansen and D. P. O'Leary. The use of the l-curve in the regularization of discrete ill-posed problems. *SIAM Journal on Scientific Computing*, 14(6):1487–1503, 1993.

[90] S. Harase and T. Kimoto. Implementing 64-bit maximally equidistributed f 2-linear generators with mersenne prime period. *ACM Transactions on Mathematical Software (TOMS)*, 44(3):30, 2018.

[91] S. L. Heston. A closed-form solution for options with stochastic volatility with applications to bond and currency options. *Review of financial studies*, 6(2):327–343, 1993.

[92] Z. Hu, J. Kerkhof, P. McCloud, and J. Wackertapp. Cutting edges using domain integration. *Risk*, 19(11):95, 2006.

9

[93] J. Hull and A. White. A generalized procedure for building trees for the short rate and its application to determining market implied volatility functions. *Quantitative Finance*, pages 1–12, 2014.

[94] W. Hundsdorfer. Accuracy and stability of splitting with stabilizing corrections. *Applied Numerical Mathematics*, 42(1-3):213–233, 2002.

[95] W. Hundsdorfer and K. J. in't Hout. On multistep stabilizing correction splitting methods with applications to the Heston model. *SIAM Journal on Scientific Computing*, 40(3):A1408–A1429, 2018.

[96] W. Hundsdorfer and J. G. Verwer. Numerical solution of advection-diffusion-reaction equations. *CWI Report NMN9603, Centrum voor Wiskunde en Informatica, Amsterdam*, 1996.

[97] W. Hundsdorfer and J. G. Verwer. *Numerical solution of time-dependent advection-diffusion-reaction equations*, volume 33. Springer Science & Business Media, 2013.

[98] P. Hunt and J. Kennedy. *Financial derivatives in theory and practice*. John Wiley & Sons, 2004.

[99] H. T. Huynh. Accurate monotone cubic interpolation. *SIAM Journal on Numerical Analysis*, 30(1):57–100, 1993.

[100] J. M. Hyman. Accurate monotonicity preserving cubic interpolation. *SIAM Journal on Scientific and Statistical Computing*, 4(4):645–654, 1983.

[101] S. Ikonen and J. Toivanen. Operator splitting methods for American option pricing. *Applied Mathematics Letters*, 17(7):809–814, 2004.

[102] A. M. Il'in. Differencing scheme for a differential equation with a small parameter affecting the highest derivative. *Mathematical Notes of the Academy of Sciences of the USSR*, 6(2):596–602, 1969.

[103] K. J. In't Hout and S. Foulon. Adi finite difference schemes for option pricing in the Heston model with correlation. *International Journal of Numerical Analysis & Modeling*, 7(2), 2010.

[104] K. J. In't Hout and C. Mishra. Stability of adi schemes for multidimensional diffusion equations with mixed derivative terms. *Applied Numerical Mathematics*, 74:83–94, 2013.

[105] K. J. In't Hout and B. Welfert. Unconditional stability of second-order adi schemes applied to multi-dimensional diffusion equations with mixed derivative terms. *Applied Numerical Mathematics*, 59(3-4):677–692, 2009.

[106] J. Iott, R. T. Haftka, and H. M. Adelman. Selecting step sizes in sensitivity analysis by finite differences. *NASA Technical Report*, 1985.

9

[107] K. Iwasawa. Analytic formula for the european normal black scholes formula. *unpublished, available at https://pdfs.semanticscholar.org/d49a/c0e3e363b8f9b23963c76ac1aafe4cc8bc2d.pdf*, 2001.

[108] P. Jäckel. A practical method for the valuation of a variety of hybrid products. In *ICBI conference slides*, 2005.

[109] P. Jäckel. Clamping down on arbitrage. *Wilmott*, 2014(71):54–69, 2014.

[110] P. Jäckel. Let's be rational, 2015.

[111] P. Jaillet, D. Lamberton, and B. Lapeyre. Variational inequalities and the pricing of American options. *Acta Applicandae Mathematicae*, 21(3):263–289, 1990.

[112] M. A. Jenkins. Algorithm 493: Zeros of a real polynomial [c2]. *ACM Transactions on Mathematical Software (TOMS)*, 1(2):178–189, 1975.

[113] F. John. Partial differential equations, volume 1 of applied mathematical sciences, 1982.

[114] S. Johnson and B. Nonas. Arbitrage-free construction of the swaption cube. *Wilmott Journal*, 1(3):137–143, 2009.

[115] M. Joshi and C. Yang. Fourier transforms, option pricing and controls. *Option Pricing and Controls (October 9, 2011)*, 2011.

[116] N. Kahalé. An arbitrage-free interpolation of volatilities. *Risk*, 17(5):102–106, 2004.

[117] C. Kahl and P. Jäckel. Not-so-complex logarithms in the Heston model. *Wilmott magazine*, 19(9):94–103, 2005.

[118] C. Kanzow, N. Yamashita, and M. Fukushima. Levenberg-marquardt methods for constrained nonlinear equations with strong local convergence properties. *Journal of Computational and Applied Mathematics*, 172:375–397, 2004.

[119] F. Kilin. Accelerating the calibration of stochastic volatility models. Technical report, CPQF Working Paper Series, 2007.

[120] K. Klare and G. Miller. Gn–a simple and effective nonlinear least-squares algorithm for the open source literature. 2013.

[121] H.-O. Kreiss, V. Thomée, and O. Widlund. Smoothing of initial data and rates of convergence for parabolic difference equations. *Communications on Pure and Applied Mathematics*, 23(2):241–259, 1970.

[122] D. Lamberton and B. Lapeyre. *Introduction to Stochastic Calculus Applied to Finance*. Chapman and Hall, 1996.

[123] J. Lamperti et al. A simple construction of certain diffusion processes. *Journal of Mathematics of Kyoto University*, 4(1):161–170, 1964.

9

[124] J. D. Lawson and J. L. Morris. The extrapolation of first order methods for parabolic partial differential equations. i. *SIAM Journal on Numerical Analysis*, 15(6):1212–1224, 1978.

[125] J. D. Lawson and D. A. Swayne. A simple efficient algorithm for the solution of heat conduction problems. In *Proceedings of the 6th Manitoba Conference on Numerical Mathematics*, pages 239–250, 1976.

[126] F. Le Floc'h. Fourier integration and stochastic volatility calibration. *Available at SSRN 2362968 http://ssrn.com/abstract=2362968*, 2014.

[127] F. Le Floc'h. Tr-bdf2 for fast stable american option pricing. *Journal of Computational Finance*, 17(3):31–56, 2014.

[128] F. Le Floc'h. Volatility derivatives practical notes. *Available at SSRN 2620166*, 2015.

[129] F. Le Floc'h. Fast and accurate analytic basis point volatility. *SSRN 2420757*, 2016.

[130] F. Le Floc'h. An adaptive filon quadrature for stochastic volatility models. *Journal of Computational Finance*, 22(3), 2018.

[131] F. Le Floc'h and G. Kennedy. Finite difference techniques for arbitrage-free sabr. *Journal of Computational Finance*, 20(3), 2017.

[132] F. Le Floc'h and C. W. Oosterlee. Model-free stochastic collocation for an arbitrage-free implied volatility: Part i. *Decisions in Economics and Finance*, Feb 2019.

[133] F. Le Floc'h and C. W. Oosterlee. Numerical techniques for the Heston collocating volatility model. *submitted for publication in the Journal of Computational Finance*, 2019.

[134] F. Le Floc'h and C. W. Oosterlee. Model-free stochastic collocation for an arbitrage-free implied volatility, part ii. *Risks*, 7(1):30, 2019.

[135] A. Lenkšas and V. Mackevičius. A second-order weak approximation of Heston model by discrete random variables. *Lithuanian Mathematical Journal*, 55(4):555–572, 2015.

[136] S. Leung and S. Osher. An alternating direction explicit (ade) scheme for time-dependent evolution equations. *Preprint UCLA June*, 9:2005, 2005.

[137] R. J. LeVeque. *Finite Difference Methods for Ordinary and Partial Differential Equations*. Society for Industrial and Applied Mathematics (SIAM), 2007.

[138] R. J. LeVeque. *Finite difference methods for ordinary and partial differential equations: steady-state and time-dependent problems*, volume 98. SIAM, 2007.

[139] A. Lewis. A simple option formula for general jump-diffusion and other exponential lévy processes. *Available at SSRN 282110*, 2001.

9

[140] M. Li and K. Lee. An adaptive successive over-relaxation method for computing the black–scholes implied volatility. *Quantitative Finance*, 11(8):1245–1269, 2011.

[141] X. S. Li. An overview of SuperLU: Algorithms, implementation, and user interface. *ACM Trans. Math. Softw.*, 31(3):302–325, September 2005.

[142] L. P. Lilleore and A. Wojt. Eur rates, a liquidity roadmap revisited. presentation from Nordea, October 6 2014, p. 11, 2014.

[143] P. Linz. Algorithm 427: Fourier cosine integral. *Communications of the ACM*, 15(5):358–360, 1972.

[144] R. Lord and C. Kahl. Why the rotation count algorithm works. *Available at SSRN 921335*, 2006.

[145] R. Lord and C. Kahl. Optimal fourier inversion in semi-analytical option pricing. *SSRN papers.ssrn.com/abstract=921336*, 2007.

[146] G. Lorentz and K. Zeller. Degree of approximation by monotone polynomials i. *Journal of Approximation Theory*, 1(4):501–504, 1968.

[147] J. N. Lyness. Notes on the adaptive simpson quadrature routine. *Journal of the ACM (JACM)*, 16(3):483–495, 1969.

[148] J. N. Lyness. Algorithm 379: Squank (simpson quadrature used adaptivity—noise killed). *Communications of the ACM*, 13(4):260–262, 1970.

[149] K. Malhotra Jogesh et al. Stiffness-tolerant methods for transient analysis of stiff Markov chains. *Microelectronics and Reliability*, 34(11):1825–1841, 1994.

[150] A. M. Malz. A simple and reliable way to compute option-based risk-neutral distributions. 06 2014.

[151] L. Mathelin and M. Y. Hussaini. A stochastic collocation algorithm for uncertainty analysis. *NASA*, CR-2003-212153, 2003.

[152] F. Mercurio and A. Pallavicini. Swaption skews and convexity adjustments. 2005.

[153] F. Mercurio and A. Pallavicini. Smiling at convexity: bridging swaption skews and cms adjustments. 2006.

[154] C. D. Meyer, D. S. Balsara, and T. D. Aslam. A stabilized runge–kutta–legendre method for explicit super-time-stepping of parabolic and mixed equations. *Journal of Computational Physics*, 257:594–626, 2014.

[155] C. Moler. Cleve's corner: Roots-of polynomials, that is. *The MathWorks Newsletter*, 5(1):8–9, 1991.

[156] J. J. Moré. The levenberg-marquardt algorithm: implementation and theory. In *Numerical analysis*, pages 105–116. Springer, 1978.

9

[157] K. W. Morton and D. F. Mayers. *Numerical solution of partial differential equations: an introduction.* Cambridge university press, 2005.

[158] K. Murray, S. Müller, and B. Turlach. Fast and flexible methods for monotone polynomial fitting. *Journal of Statistical Computation and Simulation*, 86(15):2946–2966, 2016.

[159] B. F. Nielsen, O. Skavhaug, and A. Tveito. Penalty and front-fixing methods for the numerical solution of American option problems. *Journal of Computational Finance*, 5(4):69–98, 2002.

[160] J. Nocedal and S. Wright. *Numerical optimization.* Springer Science & Business Media, 2006.

[161] T. R. Nonweiler. Algorithms: Algorithm 326: Roots of low-order polynomial equations. *Communications of the ACM*, 11(4):269 – 270, 1968.

[162] J. Oblój. Fine-tune your smile: Correction to hagan et al. *Wilmott Magazine*, May/June, 2008.

[163] C. W. Oosterlee, C. C. W. Leentvaar, and X. Huang. Accurate american option pricing by grid stretching and high order finite differences. Technical report, Working papers, DIAM, Delft University of Technology, the Netherlands, 2005.

[164] S. O'Sullivan and C. O'Sullivan. On the acceleration of explicit finite difference methods for option pricing. *Quantitative Finance*, 1469-7696, 2009.

[165] K. Pantazopoulos, E. Houstis, and S. Kortesis. Front-tracking finite difference methods for the valuation of american options. *Computational Economics*, 12(3):255–273, 1998.

[166] E. Passow and J. A. Roulier. Monotone and convex spline interpolation. *SIAM Journal on Numerical Analysis*, 14(5):904–909, 1977.

[167] L. Paulot. Asymptotic implied volatility at the second order with application to the sabr model. *Available at SSRN 1413649*, 2009.

[168] D. W. Peaceman and H. H. Rachford, Jr. The numerical solution of parabolic and elliptic differential equations. *Journal of the Society for industrial and Applied Mathematics*, 3(1):28–41, 1955.

[169] D. Piponi. Automatic differentiation, c++ templates, and photogrammetry. *Journal of Graphics Tools*, 9(4):41–55, 2004.

[170] V. Piterbarg. Derivatives pricing-funding beyond discounting: Collateral agreements and derivatives pricing. *Risk*, 23(2):97, 2010.

[171] D. Pooley, P. Forsyth, and K. Vetzal. Numerical convergence properties of option pricing PDEs with uncertain volatility. *IMA Journal of Numerical Analysis*, 23(2):241–267, 2003.

9

[172] D. M. Pooley, K. R. Vetzal, and P. A. Forsyth. Convergence remedies for non-smooth payoffs in option pricing. *Journal of Computational Finance*, 6(4):25–40, 2003.

[173] R. Rannacher. Finite element solution of diffusion problems with irregular data. *Numerische Mathematik*, 43(2):309–327, 1984.

[174] C. Reisinger and A. Whitley. The impact of a natural time change on the convergence of the Crank-Nicolson scheme. *ArXiv e-prints*, Oct. 2012.

[175] Y. Ren, D. Madan, and M. Q. Qian. Calibrating and pricing with embedded local volatility models. *RISK-LONDON-RISK MAGAZINE LIMITED-*, 20(9):138, 2007.

[176] B. Reznick. Some concrete aspects of hilbert's 17th problem. *Contemporary mathematics*, 253:251–272, 2000.

[177] L. F. Richardson. The approximate arithmetical solution by finite differences of physical problems involving differential equations, with an application to the stresses in a masonry dam. *Philosophical Transactions of the Royal Society of London. Series A, Containing Papers of a Mathematical or Physical Character*, 210:307–357, 1911.

[178] R. Schöbel and J. Zhu. Stochastic volatility with an ornstein–uhlenbeck process: an extension. *European Finance Review*, 3(1):23–46, 1999.

[179] L. I. Schumaker. On shape preserving quadratic spline interpolation. *SIAM Journal on Numerical Analysis*, 20(4):854–864, 1983.

[180] S. E. Shreve. *Stochastic Calculus For Finance II, Continuous-Time Models*. Springer Finance, 2004.

[181] A. Sokol. A simple and accurate model for yield curve dynamics with mean reversion skew. presented at the WBS interest rate conference, London, on the March 19 2015, p. 68, 2015.

[182] B. P. Sommeijer, L. F. Shampine, and J. G. Verwer. RKC: an explicit solver for parabolic PDEs. *Journal of Computational and Applied Mathematics*, 88(2):315–326, 1998.

[183] B. Stellato, G. Banjac, P. Goulart, A. Bemporad, and S. Boyd. OSQP: An operator splitting solver for quadratic programs. *ArXiv e-prints*, Nov. 2017.

[184] R. Storn and K. Price. Differential evolution–a simple and efficient heuristic for global optimization over continuous spaces. *Journal of global optimization*, 11(4):341–359, 1997.

[185] J. C. Strikwerda. *Finite difference schemes and partial differential equations*. Society for Industrial and Applied Mathematics (SIAM), 2004.

[186] S. A. Syrdal. A study of implied risk-neutral density functions in the norwegian option market. 2002.

9

[187] D. Talay. Efficient numerical schemes for the approximation of expectations of functionals of the solution of a SDE, and applications. In *Filtering and control of random processes*, pages 294–313. Springer, 1984.

[188] D. Tavella and C. Randall. *Pricing Financial Instruments - The Finite Difference Method.* John Wiley & Sons, 2000.

[189] C. J. Tranter. Integral transforms in mathematical physics. 1951.

[190] L. N. Trefethen. Six myths of polynomial interpolation and quadrature. Technical report, Mathematics Today, 2011.

[191] E. Tuck. A simple filon-trapezoidal rule. *Mathematics of Computation*, 21(98):239–241, 1967.

[192] B. A. Turlach and A. Weingessel. quadprog: Functions to solve quadratic programming problems. *CRAN-Package quadprog*, 2007.

[193] R. Tyson, L. Stern, and R. J. LeVeque. Fractional step methods applied to a chemotaxis model. *Journal of Mathematical Biology*, 41(5):455–475, 2000.

[194] A. van der Stoep, L. A. Grzelak, and C. W. Oosterlee. Collocating local volatility: A competitive alternative to stochastic local volatility models. *Available at SSRN 3251912*, 2018.

[195] J. G. Verwer, E. J. Spee, J. G. Blom, and W. Hundsdorfer. A second-order rosenbrock method applied to photochemical dispersion problems. *SIAM Journal on Scientific Computing*, 20(4):1456–1480, 1999.

[196] M. J. Wichura. Algorithm as 241: The percentage points of the normal distribution. *Applied Statistics*, pages 477–484, 1988.

[197] P. Wild. On the stability of time discretisations for the semiconductor equations. *COMPEL: The International Journal for Computation and Mathematics in Electrical and Electronic Engineering*, 10(1):11–25, 1993.

[198] P. Wilmott, J. Dewynne, and S. Howison. *Option Pricing: Mathematical Models and Computation.* Oxford Financial Press, 1993.

[199] H. Windcliff, P. Forsyth, and K. Vetzal. Shout options: A framework for pricing contracts which can be modified by the investor. *Journal of Computational and Applied Mathematics*, 134(1-2):213–241, 2001.

[200] H. Windcliff, P. Forsyth, and K. Vetzal. Analysis of the stability of the linear boundary condition for the Black-Scholes equation. *Journal of Computational Finance*, 8:65–92, 2004.

[201] W. Wolibner. Sur un polynôme d'interpolation. *Colloquium Mathematicae*, 2(2):136–137, 1951.

[202] U. Wystup. *FX options and structured products.* John Wiley & Sons, 2015.

9

[203] Zeliade Systems. Quasi-Explicit Calibration of Gatheral's SVI model. Technical report, Zeliade White Paper, Zeliade Systems, 2009.

ACKNOWLEDGEMENTS

Fabien LE FLOC'H

1975   Born in Fontenay-sous-bois, France.

EDUCATION

1993–1996   Mathematics and physics preparatory classes (math sup and spé M')
Lycée Marcelin Berthelot, Saint-Maur, France

1996–1999   Master of science in semi-conductor physics
École supérieure d'électricité (CentraleSupélec), Gif-sur-Yvette, France

2018–2020   PhD. Applied mathematics
Delft University of Technology, Delft, the Netherlands
Thesis: Advanced and accurate discretization schemes for relevant PDEs in finance
Promotor: Prof. dr. ir. C.W. Oosterlee

AWARDS

1999   Osram Sylvania individual achievement award

WORK EXPERIENCE

1999–2000   Software consultant
Alcatel/Nextenso, Paris, France.

2000–2004   Software consultant
One 0 development, San Francisco and Los Angeles, U.S.A.

2004–2007   Software engineer and architect
Prima solutions/Edifixio/Horizon software/Darty, Paris, France

2007–present   Principal financial engineer
Calypso Technology, Paris, France

8. **F. Le Floc'h** and **C.W. Oosterlee**, Numerical techniques for the Heston collocated volatility model, working paper, submitted for publication, 2019.

7. **F. Le Floc'h**, More stochastic expansions for the pricing of vanilla options with cash dividends, working paper, submitted for publication, 2019.

6. **F. Le Floc'h** and **C. W. Oosterlee**, Model-free stochastic collocation for an arbitrage-free implied volatility, part ii, *Risks,* 7(1), 2019.

5. **F. Le Floc'h** and **C. W. Oosterlee**, Model-free stochastic collocation for an arbitrage-free implied volatility, part i, *Decisions in Economics and Finance,* 2019.

4. **F. Le Floc'h**, An adaptive Filon quadrature for stochastic volatility models, *Journal of Computational Finance,* 22(3), 2018.

3. **F. Le Floc'h**, Variance swap replication: discrete or continuous?, *Journal of Risk and Financial Management,* 11(1), 11, 2018.

2. **F. Le Floc'h** and **G.J. Kennedy**, Finite difference techniques for arbitrage-free SABR, *Journal of Computational Finance,* 20(3), 2017.

1. **F. Le Floc'h**, TR-BDF2 for fast stable American option pricing, *Journal of Computational Finance,* 17(3), 2014.

PREPRINTS

8. **F. Le Floc'h**, Pitfalls of exponential fitting on the Black-Scholes PDE, Available at SSRN: http://ssrn.com/abstract=2711720, 2016.

7. **F. Le Floc'h**, Volatility derivatives practical notes, Available at SSRN: http://ssrn.com/abstract=2620166, 2015.

6. **F. Le Floc'h** and **G. J. Kennedy**, Explicit SABR calibration through simple expansions, Available at SSRN: http://ssrn.com/abstract=2467231, 2014.

5. **F. Le Floc'h**, Fast and accurate analytic basis point volatility, Available at SSRN: http://ssrn.com/abstract=2420757, 2014.

4. **F. Le Floc'h** and **A. Prüll**, Barrier options under negative rates in Black-Scholes, Available at SSRN: http://ssrn.com/abstract=2501907, 2014.

3. **F. Le Floc'h**, Arbitrages in the volatility surface interpolation and extrapolation, Available at SSRN: http://ssrn.com/abstract=2175001, 2012

2. **F. Le Floc'h**, Stable interpolation of the yield curve, Available at SSRN: http://ssrn.com/abstract=2175002, 2012

1. **F. Le Floc'h**, Issues of nelder-mead simplex optimisation with constraints, Available at SSRN: http://ssrn.com/abstract=2097904, 2012

LIST OF ATTENDED CONFERENCES WITH PRESENTATION

Presentations:

2. International conference of computational finance, A Coruna, Spain, July 2019.

1. Workshop on models and numerics in financial mathematics at the Lorentz center, Leiden, the Netherlands, May 2015.